

**LOUGHBOROUGH  
UNIVERSITY OF TECHNOLOGY  
LIBRARY**

AUTHOR/FILING TITLE

WILLIAMS, R. A.

ACCESSION/COPY NO.

040090920

VOL. NO.

CLASS MARK

T

*date due:-*

~~3 NOV 1994~~

~~LOAN 3 WKS. + 3  
UNLESS RECALLED~~

~~For use in the  
library only.~~

~~PLYMOUTH~~

28 APR 1995

LOAN COPY - 3 APR 2000

13 DEC 1995      26 JUN 2000

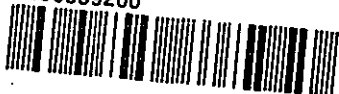
27 JUN 1997

26 JUN 1998

25 JUN 1999

14 JAN 2000

0400909200



COMPARISON OF CLASSICAL AND OPTIMAL ACTIVE  
SUSPENSION CONTROL SYSTEMS

by

R.A. WILLIAMS ©1986

A DOCTORAL THESIS

Submitted in partial fulfilment of the requirements for the  
award of Doctor of Philosophy of Loughborough University  
of Technology

Loughborough University of Technology Library	
Date	May 94
Class	
Acc. No.	040090920

67185385

COMPARISON OF CLASSICAL AND OPTIMAL  
ACTIVE SUSPENSION CONTROL SYSTEMS

Synopsis

British Rail has been designing active suspensions for some 16 years, starting with tilt systems for the Advanced Passenger train. These have been designed using classical control techniques requiring a combination of experience, intuition and frequency response stability techniques, such as Nichols' plots. In order to see if a more systematic approach to control system design could produce improvements in performance and implementation the current investigation was instigated in which controllers designed using classical techniques are compared with controllers designed using linear optimal control theory.

The active suspension used for the investigation was an Electro Magnetic active vertical suspension fitted to a service MkIII coach. Design of the actuators is described in the thesis along with the design of analogue and digital control systems.

Two classical control systems were designed, a simple "Sky Hook" damper control system and a more sophisticated position control system developed from British Rail's experience with Maglev suspensions. A regulator designed using linear optimal control theory was found to give very good results in theory. However to implement the regulator it was necessary to design a system observer. In order to achieve a practically realisable observer considerable rationalisation of the vehicle model was required, which drew heavily on experience gained designing classical control systems.

The classical control systems proved to be much easier to commission than the optimal controllers as they were designed with implementation in mind. During track testing problems of interaction between vehicles were encountered, as a result the biggest improvements in ride were obtained with the simple Sky Hook damper, as it was less specific to the vehicle than the other configurations.

With further development one of the optimal control systems considered will probably turn out to be the most effective as it draws on the attributes of both classical and optimal design techniques.

## CONTENTS

	Page
Synopsis	2
Symbols	8
Chapter 1. History of Active Suspensions	19
-1.1 Definition of an Active Suspension	19
-1.2 Justification for Active Suspensions	19
1.3 Active Suspensions at British Rail	23
-1.4 Active Suspension Research World Wide	24
1.4.1 Railway Systems	24
1.4.2 Maglev	25
-1.4.3 Automotive Applications	26
1.5 Aims of the Project	27
Chapter 2. Methods of Analysis	30
2.1 State Space Equations	30
2.2 Eigen-Values	32
2.3 Frequency Responses	33
2.3.1 Track Input Spectra	34
2.3.2 Weighted RMS Accelerations	36
2.3.3 Power Consumption	38
2.3.4 Using the Frequency Response Program	40
2.4 Linear Optimal Control	40
2.4.1 Optimal Regulator	41
2.4.2 Solution of the Matrix Riccati Equation	42
2.4.3 Optimal Observer	45
2.4.4 Optimal Observer with Uncorrelated State Excitation and Observer Noise	47
2.5 Response of a System to a Random Disturbance	48
2.5.1 Relationship between Track Spectrum Roughness Factor and Track Covariance	50
2.5.2 Correlated Inputs	51
2.5.3 Lyapunov Equation in Practice	53

		Page
Chapter	3. Mk III Coach Passive Suspension	56
	3.1 Mk III Coach Passive Suspension	56
	3.2 Air Spring Model	56
	3.2.1 Pneumatic Damping	61
	3.3 Flexible Body Modes	65
	3.4 Passive Suspension Dynamic Performance	67
Chapter	4. Electro Magnetic Actuators	69
	4.1 Electro Magnetic Actuators	69
	4.1.1 Double Acting Actuators	69
	4.2 Power Supply	71
	4.3 Magnet Performance	73
	4.4 Actuator Heating	78
	4.5 Actuator Design	79
	4.6 Eddy Currents	83
	4.7 Linearisation of Actuator Characteristics	85
Chapter	5. Classical Control System Design	89
	5.1 Force Control Loop	89
	5.2 Main Control Loops	92
	5.2.1 Absolute (Sky Hook) Damping	92
	5.2.2 Position Control	98
	5.2.3 Flexible Body Mode	105
	5.2.4 Position Control Eigen-Values	110
	5.3 Response to a Random Track Input	111

		Page
Chapter	6. Optimal Control Systems	116
	6.1 Optimal Regulator Design	117
	6.1.1 Track Inputs	118
	6.1.2 Weighting Functions	119
	6.1.3 Regulators	122
	6.2 Optimal Observers	123
	6.2.1 Full Size Observer	124
	6.2.2 Small Model Regulator	125
	6.2.3 Small Model Observer	126
	6.3 Experimental Observers	137
	6.3.1 Experimental Regulator	137
	6.3.2 Small Model Observer	138
	6.4 Modal Observers	139
	6.4.1 Modal State Equations	139
	6.4.2 Modal Observers	143
	6.5 Comparison of Classical and Optimal Controllers	144
	6.6 Time Delayed Inputs	150
Chapter	7 Train Modes	152
Chapter	8. Control System Electronics	159
	8.1 Power Electronics	159
	8.1.1 Power Supply Unit	161
	8.2 Instrumentation	163
	8.3 Classical Control System Layouts	166
	8.3.1 Position Control System	166
	8.3.2 Absolute Damping	168
	8.4 Control Circuits	170
	8.4.1 Matrix Boards	170
	8.4.2 Actuator Control Unit	170
	8.4.3 Position Control Filter Module	174
	8.4.4 Position Control Phase Advance Module	176
	8.4.5 Absolute Damping Circuit	178
	8.4.6 Absolute Damping Notch Filter Circuit	180
	8.5 Small Model Observer	180
	8.5.1 Actuator Control	183

	Page	
8.5.2	Acceleration Error Board	184
8.5.3	Relative Displacement Error Board	184
8.5.4	Current Error Board	187
8.5.5	Optimal Control Matrix Board	189
8.5.6	Output Matrix and Notch Filters	191
8.6	Modal Observer	193
8.7	Card Frame	195
Chapter 9.	Commissioning and Testing	197
9.1	System Commissioning	198
9.1.1	Sky Hook Damping Static Performance	199
9.1.2	Position Control Static Performance	199
9.1.3	Small Model Observer Commissioning	204
9.1.4	Modal Observers Static Performance	205
9.2	Power Supply	209
9.3	Track Tests	212
9.3.1	Sky Hook Damper Experimental Results	214
9.3.2	Position Control Measured Performance	217
9.3.3	Modal Optimal Control Measured Performance	222
9.4	Comparative Performance	226
9.5	Position Control Revisited	228
Chapter 10.	Digital Controllers	229
10.1	Classical Control System Design and Analysis	229
10.1.1	Complex Frequency Response Program	230
10.1.2	Classical Controller Performance	233
10.2	Optimal Control System Design and Analysis	238
10.2.1	Digital Regulator Design	238
10.2.2	Digital Observer Design	242
10.2.3	Analysis of Optimal Controllers	243
10.2.4	Optimal Regulator	244
10.2.5	Optimal Observers	247
10.3	Resolution	248
10.4	Why Digital?	250



	Page
Chapter 11. A Computer Aided Design Method	251
11.1 Summary of the Design Technique	251
11.2 System Description	253
11.2.1 British Rail Equations	253
11.2.2 DFVLR Equations	253
11.2.3 Position Control Small Model	255
11.2.4 Revised Equations	259
11.2.5 Specification of Performance Indices	259
11.3 Trials of the Design Technique	261
11.4 Conclusions	262
Chapter 12. Conclusions and Future Work	267
12.1 Conclusions	267
12.2 Future Work	269
12.3 Acknowledgements	269
References	271
Appendix A (Chapter 2)	278
Appendix B (Chapter 3)	279
Appendix C (Chapter 5)	283
Appendix D (Chapter 6)	291
Appendix E (Chapter 7)	297
Appendix F (Chapter 10)	300
Appendix G (Chapter 11)	309

## SYMBOLS

## Chapter 1

C	damping rate (Ns/m)
K	spring stiffness (N/m)
s	Laplace operator
Z	vertical displacement (m)
$Z_t$	track displacement (m)
$\omega$	angular frequency (rad/s)
$\omega_o$	characteristic frequency (rad/s)

## Chapter 2

A	state matrix
$a_o, a_1, a_2$	track spectrum constants
B	control input matrix
C	output matrix
c	damping rate (Ns/m)
D	control output matrix
E	input matrix
e	error vector
F	regulator feedback matrix
f	frequency (Hz)
$f_s$	spatial frequency (m/cycle)
G	input output matrix
H	input power spectrum
I	unit matrix
Im	imaginary part of eigen value
J	performance index
K	observer feedback matrix
$K_s, K_d$	spring rates (N/m)
M	mass (kg)
N	controlled variable matrix
P	solution of the regulator Riccati equation
p	adjoint variable
Q	solution of the observer Riccati equation
q	input vector
$q_1, q_2$	observer variables
$R_1, R_2, R_3$	weighting matrices
Re	real part of eigen value

s	Laplace operator
T	track roughness factor (m.cycle)
t	time(s)
U	transformation matrix
u	control vector
$V_1, V_2, V_3$	noise intensities
v	velocity (m/s)
W	similarity transform matrix
$W_F$	frequency weighting factor
$W_P$	power consumption (w)
$w_1, w_2$	white noise vectors
X	covariance matrix
$X_h$	psd of state variable
x	state vector
Y	output power spectrum
y	output vector
$y_w$	weighted output vector
Z	canonical matrix
z	controlled variable
$z_1$	suspension displacement (m)
$z_b$	body displacement (m)
$z_t$	track displacement (m)
$\delta$	time delay (s)
$\Lambda$	matrix of eigen-values
$\lambda$	eigen-value
$\xi$	damping ratio
$\Phi$	transition matrix
$\omega$	angular frequency (rad/s)

Note the subscript I denotes the imaginary component of a vector and the subscript R the real part.

### Chapter 3

A	spring area ( $m^2$ )
a	displacement of a bending beam (m)
$C_D$	aerodynamic discharge coefficient
$C_P$	specific heat at constant pressure (J/kg)
$C_q$	non-linear damping coefficient ( $Ns^2/m^2$ )

$C_r$	damping coefficient (Ns/m)
$C_v$	specific heat at constant volume (J/kg)
$F$	Air spring force (N)
$g$	acceleration due to gravity ( $m/s^2$ )
$H$	enthalpy (J)
$I$	inertia of bending beam (kg m/s)
$KE$	kinetic energy (J)
$KE_x$	kinetic energy of an element length $\delta x$ (J)
$K_r$	reservoir stiffness (N/m)
$K_s$	spring stiffness (N/m)
$l$	length of vehicle (m)
$M$	mass of air (kg)
$M_v$	mass of vehicle (kg)
$m$	mass per unit length of vehicle (kg)
$m_f$	mass flow (kg/s)
$m_r$	mass flow out of reservoir (kg/s)
$m_s$	mass flow out of air spring (kg/s)
$P$	absolute pressure (Pa)
$P_o$	static pressure (Pa)
$P_s$	spring pressure (Pa)
$P_r$	reservoir pressure (Pa)
$Q$	Heat (J)
$Q_v$	volume flow ( $m^3/s$ )
$R$	gas constant ( $kg\ m^2/s^2/^\circ K$ )
$s$	Laplace operator
$T$	absolute temperature ( $^\circ K$ )
$t$	time (s)
$U$	internal energy (J)
$V$	volume ( $m^3$ )
$V_r$	reservoir volume ( $m^3$ )
$V_s$	spring volume ( $m^3$ )
$x$	displacement along flexible beam (m)
$z$	vehicle displacement (m)
$z_b$	bogie displacement (m)
$z_f$	flexible mode displacement (m)
$z_{fx}$	flexible mode displacement at point $x$ (m)
$\gamma$	ratio of specific heats
$\rho$	air density ( $kg/m^3$ )

## Chapter 4

A	area ( $m^2$ )
$A_{eff}$	effective pole area of magnet ( $m^2$ )
$A_s$	surface area of magnet ( $m^2$ )
a	width of outer magnet pole (m)
B	magnetic flux density (T)
$B_m$	amplitude of modulated flux density (T)
d	depth of slot (m)
F	magnet force (N)
$F_p$	peak force (N)
$F_{rms}$	rms force (N)
G	air gap between magnet poles (m)
H	magnet field strength (A/m)
I	current (A)
K	force constant ( $Nm/A^2$ )
$K_d$	heat dissipation coefficient ( $w/m^2/^\circ K$ )
$K_g$	negative stiffness (N/m)
$K_I$	linear current constant (N/A)
$K_{I2}$	non-linear current constant ( $N/A^2$ )
$K_T$	temperature coefficient of conductor (ohms/ $^\circ K$ )
$L_L$	leakage inductance (H)
$L_M$	mutual inductance (H)
N	number of turns
NI	magneto-motive-force (A)
P	magnetic permeance (A/m)
$P_d$	power dissipation (w)
$P_e$	eddy current power loss (w)
$P_p$	pole permeance (A/m)
$P_s$	slot permeance (A/m)
q	half slot width (m)
R	radial distance from centre of magnet (m)
$R_1$	radius of inner pole (m)
$R_2$	radius of outer pole (m)
$R_s$	resistance of conductor (ohms)
r	radius of element in centre pole (m)
$r_e$	resistance of element of core (ohms)
$\mu_o$	permeability of free space (H/m)
$\rho$	resistivity of conductor (ohms/m)
$\rho_s$	resistivity of core (ohms/m)

$\Phi_L$	leakage flux (Wb)
$\Phi_M$	mutual flux (Wb)
$\Phi_T$	total flux (Wb)

## Chapter 5

C	damper rate (kN s/m)
$C_f$	flexible body damping (kN s/m)
F	actuator force (N)
$F_a$	force due to four actuators (N)
$F_D$	force demand (N)
$G_a$	amplifier gain
$G_B$	bounce gain
$G_P$	pitch gain
$\epsilon_{fi}$	relative displacement of flexible body mode at the position of the actuators.
$\epsilon_{fo}$	relative displacement of flexible body mode at the accelerometers.
$\epsilon_{fx}$	relative displacement of flexible body mode at position x
HP	high pass filter
K	spring stiffness (kN/m)
$K_a$	area change stiffness (kN/m)
$K_F$	force feedback gain (V/A)
$K_f$	flexible body stiffness (kN/m)
$K_I$	force constant (N/A)
$L_L$	leakage inductance (H)
$L_M$	mutual inductance (H)
LP	lowpass filter
l	half suspension spacing (m)
M	mass (kg)
$M_f$	effective mass of flexible body mode (kg)
s	Laplace operator
$T_1, T_2, \text{ etc}$	time constants (s)
z	rigid body displacement (m)
$z_b$	bogie displacement (m)
$z_m$	measured body displacement (m)
$z_t$	track displacement (m)
$z_x$	displacement of flexible mode at position x
$z_{fx}$	flexible body displacement

$\zeta$	damping ratio
$\phi$	pitch displacement (rad)
$\phi_b$	input pitch displacement (rad)
$\omega_B$	bounce loop frequency (rad/s)
$\omega_p$	pitch loop frequency (rad/s)
$\omega_{max}$	frequency of maximum phase of phase advance network (rad/s)
$\omega_{nf}$	centre frequency of notch filter (rad/s)
$\omega_1$	lead frequency of phase advance network (rad/s)
$\omega_2$	lag frequency of phase advance network (rad/s)

## Chapter 6

A	state matrix
a	acceleration weighting factor
B	control input matrix
b	relative displacement weighting factor
C	measurement matrix
c	current weighting factor
E	input vector
F	regulator feedback matrix
F <sub>a</sub>	actuator force (N)
G <sub>a</sub>	amplifier gain
I	current (A)
I <sub>1</sub>	current at leading end of vehicle (A)
I <sub>2</sub>	current at trailing end of vehicle (A)
J	performance index
K	observer gain matrix
K <sub>s</sub>	negative stiffness (N/m)
K <sub>I</sub>	force constant (N/A)
L <sub>L</sub>	leakage inductance (H)
L <sub>m</sub>	mutual inductance (H)
l	distance (m)
N	controlled variable matrix
Q	solution of the observer Riccati equation
R	magnet resistance (ohms)
R <sub>1</sub> , R <sub>2</sub>	weighting matrices
s	Laplace operator
t	time (s)
u	control vector

v	noise intensity
v	velocity (m/s)
w	white noise vector
x	state vector
y	output vector
z	controlled vector
$z_B$	in-phase track input (m)
$z_P$	anti-phase track input (m)
$z_l$	displacement over leading bogie (m)
$z_b$	displacement over trailing bogie (m)
$z_{b1}$	leading bogie displacement (m)
$z_{b2}$	trailing bogie displacement (m)
$\delta$	time delay (s)
$\lambda$	input weighting
$\omega$	angular frequency (rad/s)

## Chapter 8

A	state matrix
$A_n$	amplifier n
C	measurement matrix
$C_n$	capacitance n (F)
$D_n$	force demand n
$F_P$	peak force (N)
$I_n$	current n
$I_{1E}, I_{2E}$	current error
$K_{I2}$	non-linear force constant
L	inductance
P	rate of change of flux
$R_n$	resistance (ohms)
s	Laplace operator
$V_n$	voltage n (V)
X	multiplier
x	state vector
y	output vector
z	vertical displacement (m)
$z_t$	track displacement
$z_{1E}, z_{2E}$	acceleration error
$z_{R1E}, z_{R2E}$	relative displacement error
$\Phi$	pitch displacement (rad)
$\phi$	flux (wb)
$\omega$	angular frequency (rad/s)



## Chapter 10

A	Continuous state matrix
A <sub>i</sub>	Imaginary part of polynomial numerator
A <sub>r</sub>	Real part of polynomial numerator
a <sub>0</sub> , a <sub>1</sub> , a <sub>2</sub>	Polynomial coefficients
B	Continuous input matrix
B <sub>i</sub>	Imaginary part of polynomial denominator
B <sub>r</sub>	Real part of polynomial denominator
b <sub>0</sub> , b <sub>1</sub> , b <sub>2</sub>	Polynomial coefficients
C	Discrete regulator feedback matrix
D	Discrete weighting matrix
E	Discrete weighting matrix
G	Digital to Analogue matrix
H	Measurement matrix
H <sub>mn</sub>	Polynomial elements of system matrix
I	Unit matrix
Im	Imaginary part of eigenvalue
J	Performance index
K	Digital observer gain matrix
M	Solution of the discrete observer equation
N	Number of samples
P	System matrix
P <sub>i</sub>	Imaginary part of P
P <sub>c</sub>	Continuous system matrix
P <sub>r</sub>	Real part of P
P <sub>s</sub>	Sampled system matrix
Q <sub>c</sub>	Sampled to continuous coupling matrix
Q <sub>d</sub>	Input noise variance
Q <sub>s</sub>	Continuous to sampled coupling matrix
R	Input matrix
R <sub>c</sub>	Continuous input matrix
R <sub>d</sub>	Measurement noise

$R_e$	Real part of eigenvalue
$R_I$	Imaginary part of R
$R_R$	Real part of R
$R_s$	Sampled input matrix
$s$	Laplace operator
$t$	time
$T$	Sample period
$u$	Input vector
$u_I$	Imaginary part of input vector
$u_R$	Real part of input vector
$u_i$	Discrete input vector
$V$	Velocity
$X_Z$	Matrix of variable eigenvectors inside unit circle
$X_E$	Matrix of variable eigenvectors outside unit circle
$x$	State vector
$x_c$	Continuous state vector
$x_i$	Discrete state vector
$x_s$	Sampled state vector
$\hat{x}_i$	Observed state vector
$y_i$	Discrete measurement vector
$\hat{y}_i$	Observed measurement vector
$z$	Sampled data operator
$\alpha_0, \alpha_1, \alpha_2$	Discrete polynomial coefficients
$\beta$	Discrete input matrix
$\beta_0, \beta_1, \beta_2$	Discrete polynomial coefficients
$\Gamma$	Analogue to digital matrix
$\theta$	Adjoint variable
$\Lambda_E$	Matrix of adjoint variable eigenvectors outside unit circle
$\Lambda_Z$	Matrix of adjoint variable eigenvectors inside unit circle
$\tau$	time(s)
$\phi$	Transition matrix
$\omega$	Angular frequency (rad/s)
$\omega_s$	Sampled angular frequency (rad/s)
$\omega_l$	Warped angular frequency (rad/s)

## Chapter 11

A	Plant matrix
$A_r$	Controller state matrix
B	Control input matrix
$B_r$	Controller input matrix
C	State output matrix
$\underline{C}$	Target performance vector
$C_m$	Measurement matrix
$C_r$	State control matrix
D	Control output matrix
E	Plant input matrix
$E_r$	Command input matrix
F	Input output matrix
$F_m$	Input measurement matrix
$\underline{G}$	Performance vector elements $G_1 G_2 G_3$ etc
$\underline{k}$	Free control parameters
q	Input vector
r	Command input vector
s	Laplace operator
u	Control vector
x	State vector
$x_r$	Controller state vector
$y_a$	Output vector
$y_m$	Measured variable vector

Note the following convections have been used.

'	denotes the first derivative of a variable
"	denotes the second derivative of a variable
T	denotes a transposed matrix
^	denotes an observed variable

## CHAPTER 1

### HISTORY OF ACTIVE SUSPENSIONS

#### 1.1 Definition of an Active Suspension

Ground transport vehicles are fitted with a suspension to isolate them from the high frequency irregularities of the surface over which they are travelling, thus minimising the accelerations experienced in the vehicle. If the vehicle is guided a lateral suspension is also required to isolate the vehicle from lateral irregularities in the guideway.

Conventional, passive, suspensions are composed of elements which can store energy—springs and the mass of the vehicle, and those which can dissipate energy—dampers (Fig 1.1a). An active suspension contains an actuator which applies a controlled force to the vehicle, and is capable of adding energy to the system as well as storing and dissipating it (Fig 1.1b). The active suspension may contain passive elements in parallel with the active element. This is particularly useful with vertical active suspensions where springs can be used to support the vehicle, reducing power consumption and actuator size.

A limited form of active suspension can be achieved with a controlled element which is only capable of dissipating energy. This is known as a semi-active suspension.

#### 1.2 Justification for Active Suspension

Active suspensions can provide suspension characteristics which cannot be realised with passive components alone. The justification for them has been reviewed by Karnopp (1).

At the simplest level the advantages can be demonstrated by the unicycle models in Fig 1.2, and arise from the way in which the damping is applied. In a simple passive suspension the damping is applied between the vehicle and the track (Fig. 1.2a) and can be described by the transfer function:-

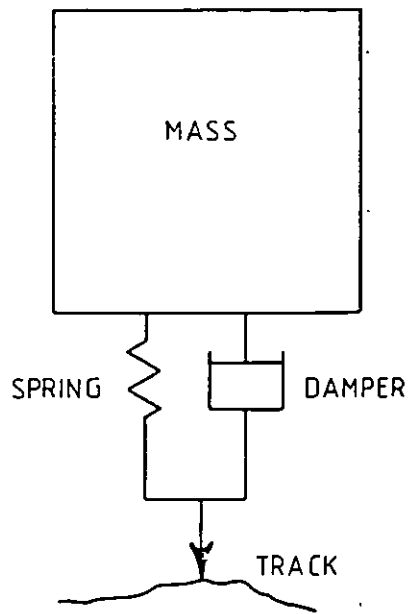


FIG. 1-1a PASSIVE SUSPENSION

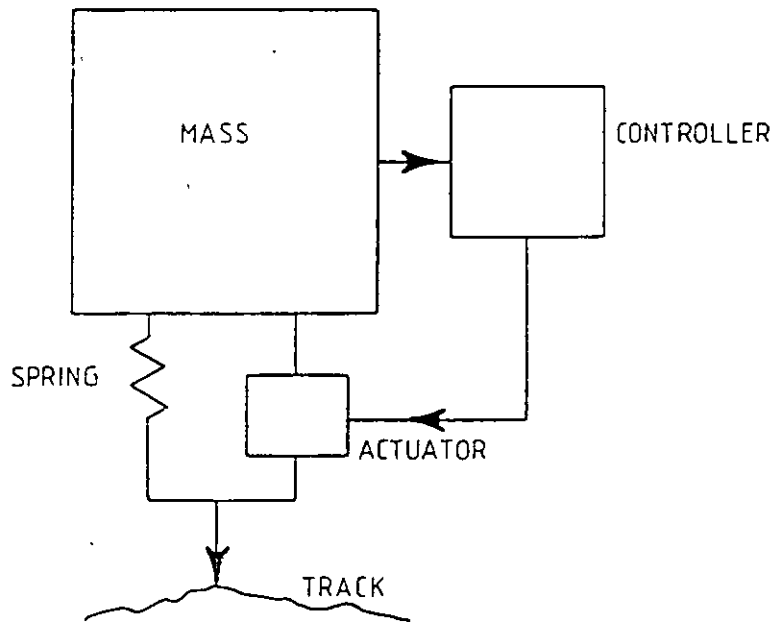


FIG. 1-1b ACTIVE SUSPENSION

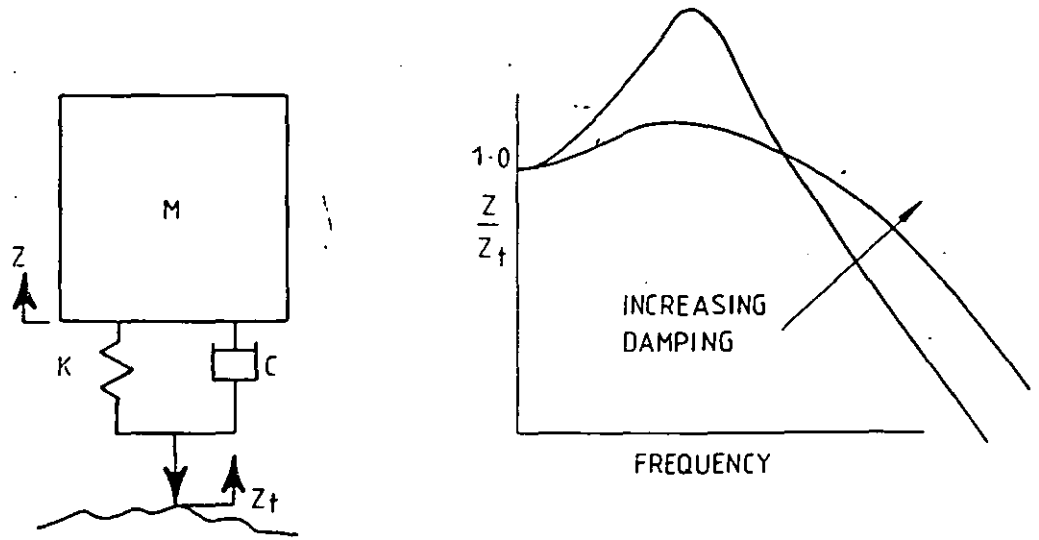


FIG. 1-2a RELATIVE DAMPING

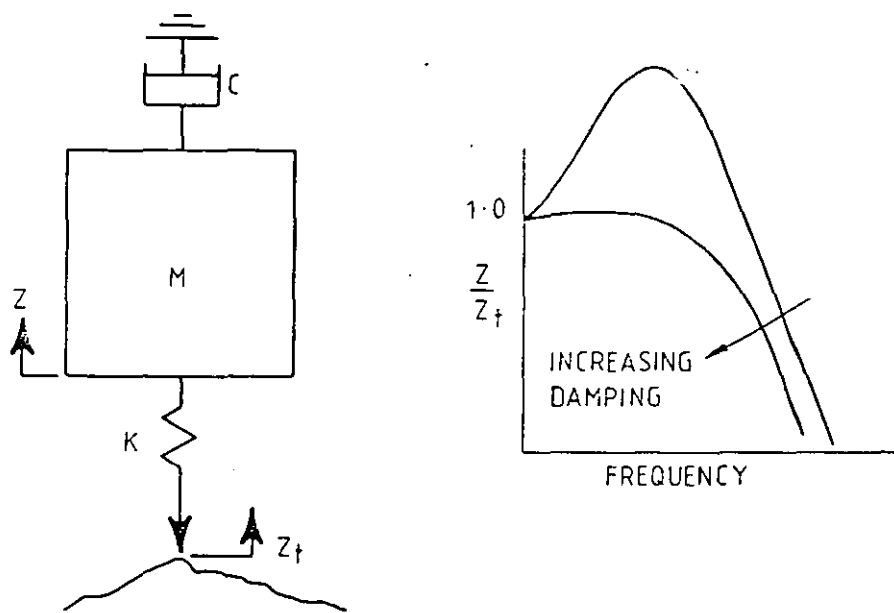


FIG. 1-2b SKY HOOK DAMPING

$$\frac{Z}{Z_t} = \frac{1 + \frac{C}{K}s}{1 + \frac{C}{K}s + \frac{Ms^2}{K}} \quad (1.1)$$

While increased damping reduces the resonance peak, the high frequency transmissibility is also increased.

$$\text{For } \omega \gg \omega_0 \quad \left( \text{where } \omega_0 = \sqrt{\frac{K}{M}} \right) \quad (1.2)$$

$$\frac{Z}{Z_t} \doteq \frac{C}{Ms}$$

Therefore the damping rate is a compromise between minimising the size of the resonant peak and the high frequency transmission. With an active suspension it is possible to realise a "sky hook" damper (Fig. 1.2b) in which the damper is attached to an absolute reference. This is impossible to achieve with purely mechanical components as there is nowhere to anchor the damper. The transfer function for a suspension with a "sky hook" damper is

$$\frac{Z}{Z_t} = \frac{1}{1 + \frac{C}{K}s + \frac{Ms^2}{K}} \quad (1.3)$$

which has a high frequency transmissibility

$$\frac{Z}{Z_t} \doteq \frac{K}{Ms^2} \quad (1.4)$$

Not only is this independent of the damping rate but the attenuation is proportional to  $1/\omega^2$ , compared with  $1/\omega$  for the relative damper.

Active suspensions can also be used to resolve some of the inevitable conflicts which arise in suspension design (2). For instance it must:-

- 1) Support the vehicle weight, provide guidance and react external disturbances, such as load changes and wind gusts, all of which requires a "stiff" suspension.



- 2) Isolate the vehicle from track irregularities to provide the passengers, or freight, with a comfortable ride, which requires a soft suspension.

In conventional railway vehicles the conflict is partially resolved by providing a stiff primary suspension (between the wheels and bogie frames) and a soft secondary suspension (between the bogies and body).

### 1.3 Active Suspensions at British Rail

Work on active suspensions began at British Rail in the late sixties with studies of tilting trains (3, 4). By tilting passenger vehicles while passing through curves the effect of lateral acceleration on the passengers is removed, leading to increased comfort (5) and higher operating speeds. Though it is possible to tilt a vehicle by using pendulum action alone, it is usually necessary to include an active element to achieve sufficient speed of operation. Initially tilt systems were powered by hydraulic actuators, however recent work has shown that there are advantages to be gained by using electric actuators (6).

The second active suspension to be developed was a d.c. electro-magnetic Maglev System suitable for low speed urban transport (7, 8, 9, 10). This work culminated in the worlds first commercial Maglev system (11) at Birmingham airport. The electro magnets in the BR Maglev system operate in attraction and are thus naturally unstable. In order to achieve stable suspension the force exerted by the electro-magnets has to be controlled via the magnet currents. The suspension displacements available to an attractive Maglev suspension are quite small (+15 mm) when compared with typical passive suspensions (+30 mm). However the control used to maintain a stable suspension can also be used to control the ride of the vehicle, and it becomes possible to achieve an acceptable ride with the smaller displacements.

The ride obtained from small suspension displacements with the Maglev suspension encouraged an investigation into the use of active suspensions for conventional railway vehicles (12, 13, 14, 15). The philosophy adopted with these active suspensions was that they would act in parallel with an existing passive suspension. This ensures that the vehicle has an adequate ride in the event of an active suspension failure and, more important, in the case of lateral suspensions where bogie dynamics are influenced by the secondary suspension, the stability is not impaired. With a vertical active suspension putting the actuators in parallel with a passive suspension saves a considerable amount of power as they do not have to carry the static load of the vehicle.

Actuator systems which have been tested so far are:-

- 1) Hydraulic lateral suspension.
- 2) Electro-pneumatic (air pump) vertical suspension.
- 3) Electro-magnetic vertical suspension.
- 4) Electro-mechanical lateral suspension.

Results have shown that reductions in r.m.s. acceleration of up to 50% can be obtained.

#### 1.4 Active Suspension Research World Wide

##### 1.4.1 Railway Systems

Surveys of active suspension research have included application to ground transport vehicles (16, and 17), and a more general survey covering all forms of suspension and guidance (18).

The only railway vehicle active suspensions to have reached the stage of track testing, apart from those on British Rail, have been tilt systems. In Germany and Japan a limited degree of tilt ( $5^\circ$ ) was achieved by differential inflation of the air spring secondary (between body and bogie) suspension (19, 20). In Spain the Talgo train (21) achieves tilt by pendulum action as the air springs are set very high up in the vehicle, however the roll stiffness is regulated by controlling the airflow between the airbags. The Italian Pendolino tilt system (22) uses hydraulic actuators to tilt the vehicle with respect to a non-tilting bolster. In Sweden experiments are being conducted with a hydraulic tilt system which is very similar to BR's APT tilt system (23).

In Japan a 1/5th scale model of a pneumatic vertical active suspension has been built to test control concepts (24). Apart from this most work has concentrated on lateral suspensions where severe conflicts arise between stability of the bogie, its ability to negotiate curves and the ride quality experienced in the vehicle. Most studies to date have concentrated on forces applied between body and bogie (25, 26, 27) and another (27) looking specifically at pneumatic actuation. Also considered has been the use of the longitudinal and lateral forces generated by linear induction motors attached to either the vehicle body or bogie to give stability and ride improvements (28). More direct control of railway vehicle lateral dynamics has been investigated by controlling the torque generated between wheels on the same axle (29, 30).

#### 1.4.2 Maglev

Maglev systems using controlled d.c. electro-magnets represent one of the most highly developed forms of active suspension; as they are inherently unstable some form of active control is essential and most research groups have taken advantage of that control to modify the ride of vehicle. The Federal Republic of Germany is currently testing a high speed system at its Emsland test site capable of speeds of 400 km/h (31), while Japan has tested both high speed and low speed vehicles (32, 33) with the 30 km/h HSSTO3 scheduled to enter service in 1985.

Work on low speed systems, suitable for urban transport was conducted by Sussex University in the UK (43) in the mid 70's. In the Federal Republic of Germany (35) and Romania (36) prototype systems are in advanced states of development. The German system combines a novel combination of suspension and propulsion.

While active suspensions are not essential for other forms of non-contacting suspension they have been proposed for air cushion vehicles (37) and cryogenic Maglev systems (38) as being the only method of achieving an acceptable ride at very high speeds on track of a quality which can be built using current construction techniques.

#### 1.4.3 Automotive Applications

Suspension design in a road vehicle is a compromise between ride and handling as the former requires a soft suspension while the latter requires a stiff suspension. A very successful method of achieving this compromise is shown in (39) using hydraulic actuators controlled by mechanical masses springs and dampers. Servo hydraulic systems, using a combination of analogue and digital control, have been tested in racing cars and saloon cars (40), though little detail has been revealed.

Military vehicles designed for off road use, particularly tanks and armoured personnel carriers, have been the subject of active suspension investigations (41), as it is possible to drive at speeds which the crews would otherwise find intolerable.

The other application of active suspensions in the automotive field is as a guidance system for automatically controlled buses (42).

This brief survey of active suspension research and development is not exhaustive but shows the scope for active suspensions and the level of interest being shown world wide in the subject. At the moment most are in the early stages of development and it is essential if the technology is to prove viable to identify cheap, efficient but above all reliable systems. To this end it is necessary to identify the most effective form of control system.

### 1.5 Aims of the Project

The active suspension which forms the basis of this thesis functions as a ride improver. The design aim is a reduction in r.m.s. acceleration of around 50%, which is impossible to achieve with passive components as it requires spring stiffnesses to be reduced by a factor of four. There are three ways in which this improvement can be justified.

- 1) To improve the ride at current operating speeds. Fig 1.3 shows vertical accelerations measured on the three principal British Rail routes at current operating speeds compared with a proposed international standard. For much of the time the vehicles do not meet the standard.
- 2) Current ride standards can be maintained while increasing operating speed.
- 3) Track maintenance standards can be reduced while maintaining ride standards.

Active suspension development at British Rail has had a common core, and most of the systems which have been tested to date owe their origins to the Maglev suspension (7, 8, 9, 10, 11). This includes the tilt system which, despite pre-dating Maglev, proved amenable to the techniques evolved. The basic technique has even been extended to provide a measure of preview in the tilt system.

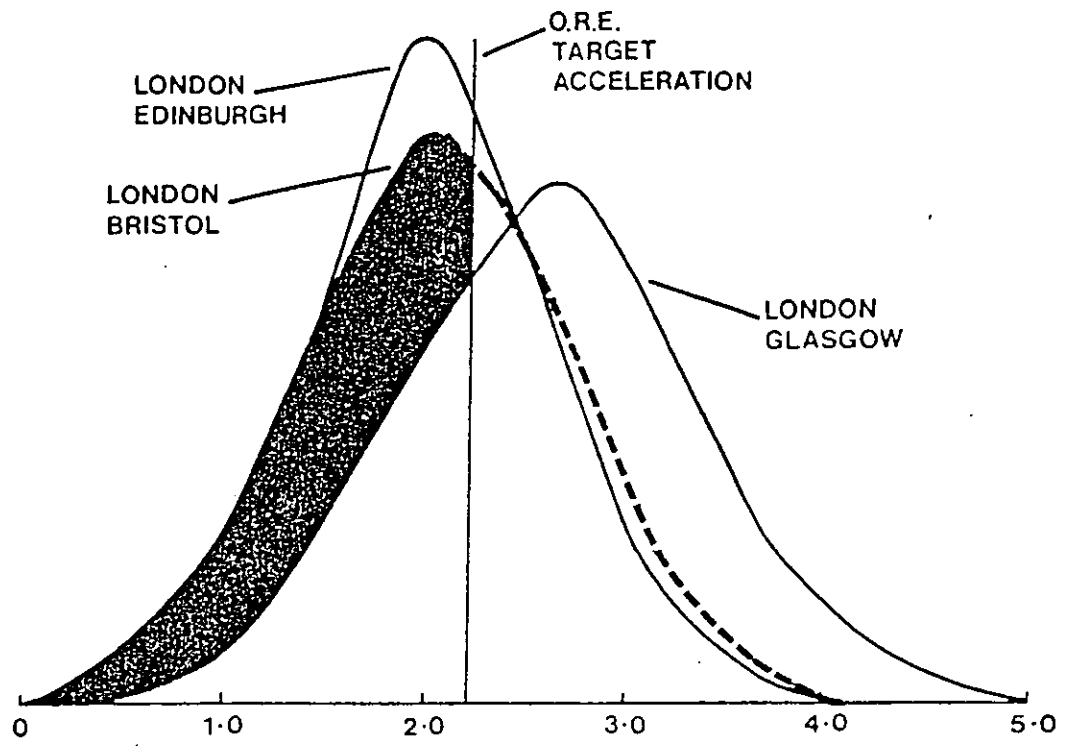


FIG 1.3 VERTICAL WEIGHTED RMS ACCELERATION %g.

A systematic approach to design has been evolved (14), which involves a combination of intuition, experience and classical control system analysis techniques based mainly upon frequency responses. Quite a lot of iteration is required at the design stage to achieve the best control system configuration and there is always the thought that a better configuration may be possible. This provided the first impetus to look at an alternative design technique. The second was that the requirements of an active suspension designed to provide ride control while acting in parallel with a passive suspension, are different from those of Maglev and tilt systems which require precise control of position.

In looking for a different design technique it was found that active suspensions (25, 26, 27, 28, 43, 44) designed using linear optimal control theory (45) provided a recurrent theme and this was the course which was pursued. The object of the exercise was to see if linear optimal control theory could provide improved performance with a practical control system which could be implemented cheaply, simply and reliably. The study concentrates on the design of a control system for an electro-magnetic vertical active suspension which acts in parallel with an airspring passive suspension.

Design studies were made of controllers for the vehicle using both the classical and optimal techniques and the resulting controllers built and tested. A theoretical analysis was also made of digital controllers designed using the two techniques. The thesis assesses the ease of design and implementation of the controllers and their relative merits.

CHAPTER 2METHODS OF ANALYSIS2.1 State Space Equations

Linear Optimal Control Theory (45) requires the system to be controlled to be described by a set of linear first order differential equations of the form:-

$$\dot{x}(t) = A(t) x(t) + B(t) u(t) + E(t) q(t) \quad (2.1)$$

The system output is described by the output equation:-

$$y(t) = C(t) x(t) + D(t) u(t) + G(t) q(t) \quad (2.2)$$

Despite a long history of dynamic analysis at British Rail, at the outset of the project there were no suitable computer programs available for analysing systems described in this manner, or for designing optimal regulators and observers. Consequently a set of computer programs has been written to design optimal control systems and analyse systems described by sets of state space equations. These are:-

- 1) An eigen value and vector program
- 2) A frequency response program
- 3) A program for designing an optimal regulator
- 4) A program for designing an optimal observer.
- 5) A program for computing the response to a random input by solution of the Lyapunov equation.

A common input format was used for all the computer programs facilitating the exchange of data between them.

Because railway vehicles do not vary very much with time, the time invariant form of the state equations was used.



$$\dot{x}(t) = Ax(t) + Bu(t) + Eq(t) \quad (2.3)$$

$$y(t) = Cx(t) + Du(t) + Gq(t) \quad (2.4)$$

Quite often when setting up the state equations the situation arises that a variable is most conveniently described in terms of the derivative of a state. For instance consider the unicycle suspension in Fig. 2.1:-

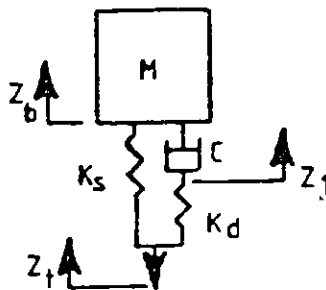


Fig 2.1 UNICYCLE SUSPENSION

The differential equations of the system are most easily described by

$$\ddot{z}_b = \frac{c}{M} (\dot{z}_1 - \dot{z}_b) + \frac{K_s}{M} (z_t - z_b) \quad (2.5)$$

$$\dot{z}_1 = \dot{z}_b + \frac{K_d}{c} (z_t - z_1) \quad (2.6)$$

However there is no state  $\dot{z}_1$  in the state equations, only its derivative and in order to derive the state equations, it is necessary to substitute equation 2.6 into 2.5 yielding the state equations:-

$$\begin{array}{c|ccc|c|c|c} \ddot{z}_b & 0 & -\frac{K_s}{M} & -\frac{K_d}{M} & \dot{z}_b & \frac{K_s + K_d}{M} & z_t \\ \dot{z}_b & 1 & 0 & 0 & z_b & 0 & \\ \dot{z}_1 & 1 & 0 & -\frac{K_d}{c} & z_1 & \frac{K_d}{c} & \end{array} \quad (2.7)$$

With a large system not only is this substitution tedious but the potential for errors (to creep in) is a real problem. A way which was found to alleviate this problem was to introduce a state derivative matrix ( $A_1$ ) which makes the computer do the substitution.

Thus the state equation becomes:

$$\dot{x}(t) = A x(t) + A_1 \dot{x}(t) + Bu(t) + Eq(t) \quad (2.8)$$

$$\dot{x}(t) = (A + A_1.A) x(t) + (B + A_1.B) u(t) + (E + A_1.E) q(t) \quad (2.9)$$

A certain amount of caution must be exercised when using the  $A_1$  matrix to ensure that  $a_{ji} = 0$  when  $x_i$  is being substituted in the equation of  $x_j$ , otherwise the resulting equations will be nonsense as the equations are singular. Equation (2.7) now becomes:

$$\begin{bmatrix} \ddot{z}_b \\ \dot{z}_b \\ \dot{z}_1 \end{bmatrix} = \begin{bmatrix} -c & -K_s & 0 \\ \overline{M} & \overline{M} & \\ 1 & 0 & 0 \\ 1 & 0 & -\frac{K_d}{c} \end{bmatrix} \begin{bmatrix} \dot{z}_b \\ z_b \\ z_1 \end{bmatrix} + \begin{bmatrix} 0 & 0 & c \\ 0 & 0 & 0 \\ 0 & 0 & 0 \end{bmatrix} \begin{bmatrix} \ddot{z}_b \\ \dot{z}_b \\ \dot{z}_1 \end{bmatrix} + \begin{bmatrix} \frac{K_s}{\overline{M}} \\ 0 \\ \frac{K_d}{c} \end{bmatrix} z_t \quad (2.10)$$

## 2.2 Eigen Values

The eigen values and vectors of the state equations

$$\dot{x} = Ax$$

were calculated using NAG subroutine (46) FO2AGF. NAG subroutines were used to perform most of the basic matrix manipulations such as addition, multiplication, inversion, etc. The damping ratio  $\xi$  is calculated from the eigen values as:

$$\xi = \frac{\text{Re}^2}{\sqrt{\text{Re}^2 + \text{Im}^2}} \quad (2.11)$$

where Re and Im are the real and imaginary parts of the eigen values respectively, the undamped natural frequency of the system

$$\omega = \frac{1}{2\pi} \frac{\text{Re}}{\xi} \quad (2.12)$$

Double precision arithmetic was required for all the computer programs.

### 2.3 Frequency Responses

Frequency responses are central to the classical analysis of control systems as they are used to determine stability margins and bandwidths. They can also be used to predict the response of the system to an input spectrum.

The frequency response of equation (2.13)

$$\dot{x}(t) = Ax(t) + Eq(t) \quad (2.13)$$

can be computed by taking the Laplace transform and solving the equation

$$x = (sI - A)^{-1} E q \quad (2.14)$$

While A and E are real, x and y are complex as the frequency response  $x(\omega)$  is computed by substituting  $j\omega$  for s in equation (2.14). Complex arithmetic can be avoided by partitioning the x and y vectors into their real and imaginary parts giving

$$\begin{bmatrix} -sI & | & -A \\ -A & | & sI \end{bmatrix} \begin{bmatrix} x_I \\ x_R \end{bmatrix} = \begin{bmatrix} 0 & | & B \\ B & | & 0 \end{bmatrix} \begin{bmatrix} q_I \\ q_R \end{bmatrix} \quad (2.15)$$

and

$$\begin{bmatrix} x_I \\ x_R \end{bmatrix} = \begin{bmatrix} -sI & | & -A \\ -A & | & sI \end{bmatrix}^{-1} \begin{bmatrix} 0 & | & B \\ B & | & 0 \end{bmatrix} \begin{bmatrix} q_I \\ q_R \end{bmatrix}$$

It will be noted that provided  $\omega \neq 0$  there are no problems of matrix inversion as the leading diagonal is full. Two methods of solving (2.15) were tried. The first used a matrix inversion routine (FO1AAF) to solve the equation (2.16). The second was to use a linear-equation-solving routine (FO4AGF) to solve (2.15) directly. Of the two approaches the second is by far the most efficient as it requires only about 25% of the time to compute a set of frequency responses. Both methods produced identical answers so neither has an advantage on accuracy.

Having computed the response vector  $x(\omega)$  at frequency  $\omega$ , its derivative

$$\dot{x}_I(\omega) = \omega x_R(\omega) \quad (2.17)$$

$$\dot{x}_R(\omega) = -\omega x_I(\omega) \quad (2.18)$$

Hence the output vector is:-

$$y(\omega) = Cx(\omega) + K \dot{x}(\omega) + D u(\omega) + G q(\omega) \quad (2.19)$$

This makes it much easier to formulate the output equations when accelerations are required.

### 2.3.1 Track Input Spectra

Railway track has been shown (47) to follow a filtered Gaussian distribution, Fig (2.2), which produces a spatial power spectrum of the form

$$H(f_s) = \frac{T}{a_0 f_s^2 + a_1 f_s^3 + a_2 f_s^4} \quad \text{m}^2/\text{cycle}/\text{m} \quad (2.20)$$

$f_s$  is the spatial frequency of the track in cycles/m.  $T$ ,  $a_0$ ,  $a_1$  and  $a_2$  are constants. For a vehicle travelling at velocity  $v$  m/s the power spectrum  $H(f)$  in  $\text{m}^2/\text{Hz}$ , where  $f$  is in Hz, is given by:-

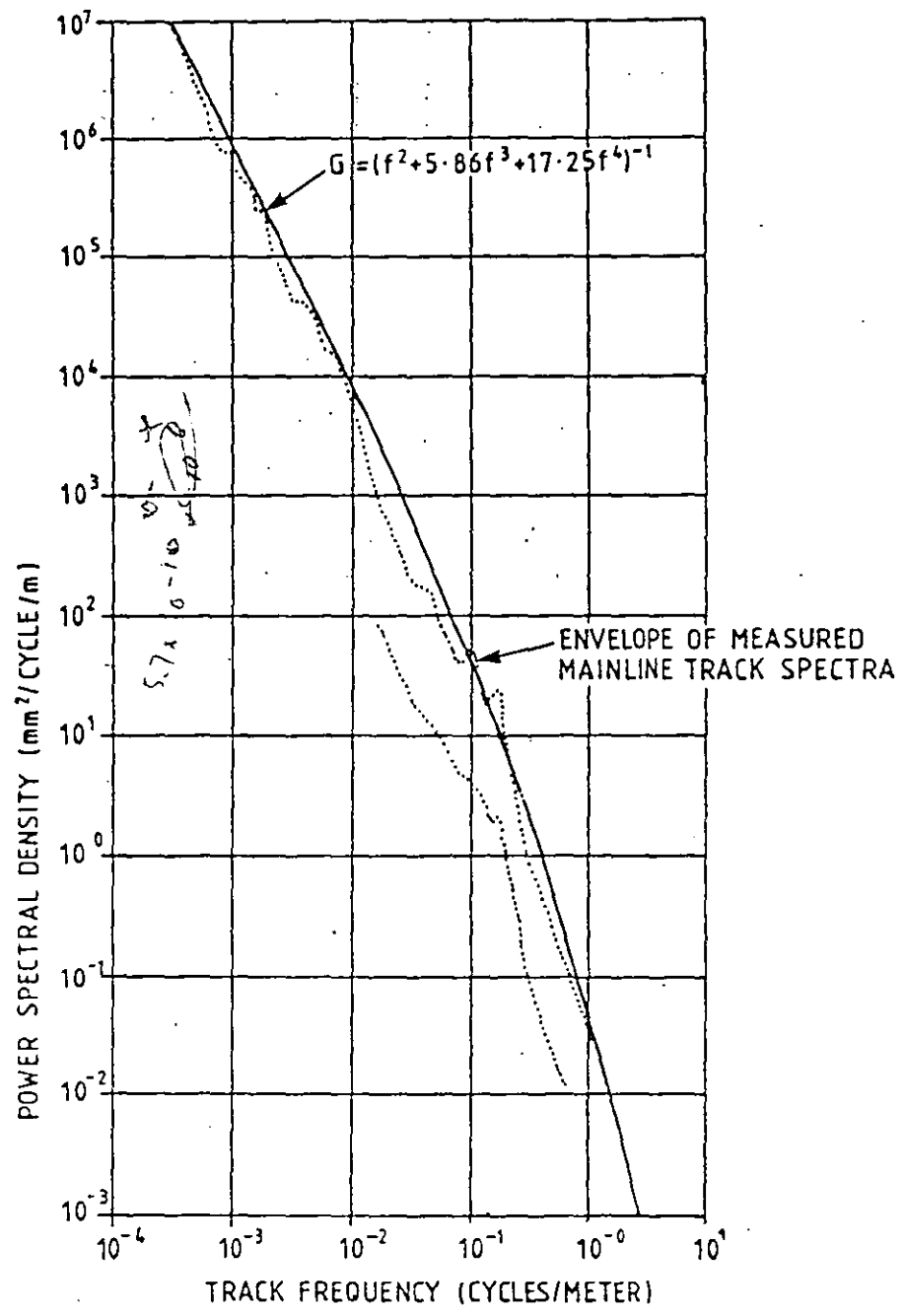


FIG.2.2 POWER SPECTRAL DENSITY DISTRIBUTION OF THE VERTICAL DISPLACEMENTS OF MAIN LINE RAILWAY TRACK

$$H(f) = \frac{Tv}{\frac{a_0 f^2}{v^2} + \frac{a_1 f^3}{v^3} + \frac{a_2 f s^4}{v^4}} \quad \text{m}^2/\text{Hz} \quad (2.21)$$

If the output vector  $(y_I(f), y_R(f))^T$  is computed for a unit input then the power spectrum of the  $i$ th element is given by:

$$Y_i(f) = (y_i(f)_R + j(y_i(f)_I) H(f))((y_i(f)_R - j(y_i(f)_I)) \quad (2.22)$$

$$\text{or} \quad Y_i(f) = ((y_i(f))_R^2 + (y_i(f))_I^2) H(f) \quad (2.23)$$

The mean square response of the system is then computed by

$$y_i^2 = \int_0^\infty Y_i(f) df \quad (2.24)$$

and the r.m.s. response

$$(y_i)_{\text{r.m.s.}} = \sqrt{y_i^2} \quad (2.25)$$

In practice  $Y_i$  is computed between the minimum frequency  $f_{\min}$  and maximum frequency  $f_{\max}$ . A simple numerical trapezoidal integration has been found to give satisfactory results.

$$y_i^2 = \sum_{k=0}^n \frac{[Y_i(k) + Y_i(k+1)] [f(k+1) - f(k)]}{2} \quad (2.26)$$

### 2.3.2 Weighted R.M.S. Accelerations

Human response to vibration is frequency dependent and the ISO (48) have produced a set of sensitivity curves, shown in figure 2.3, to vertical and lateral vibration. These take account of the varying susceptibility of the human body to vibrations of different frequencies. It will be noted that different parts of the body are susceptible to different frequency ranges.

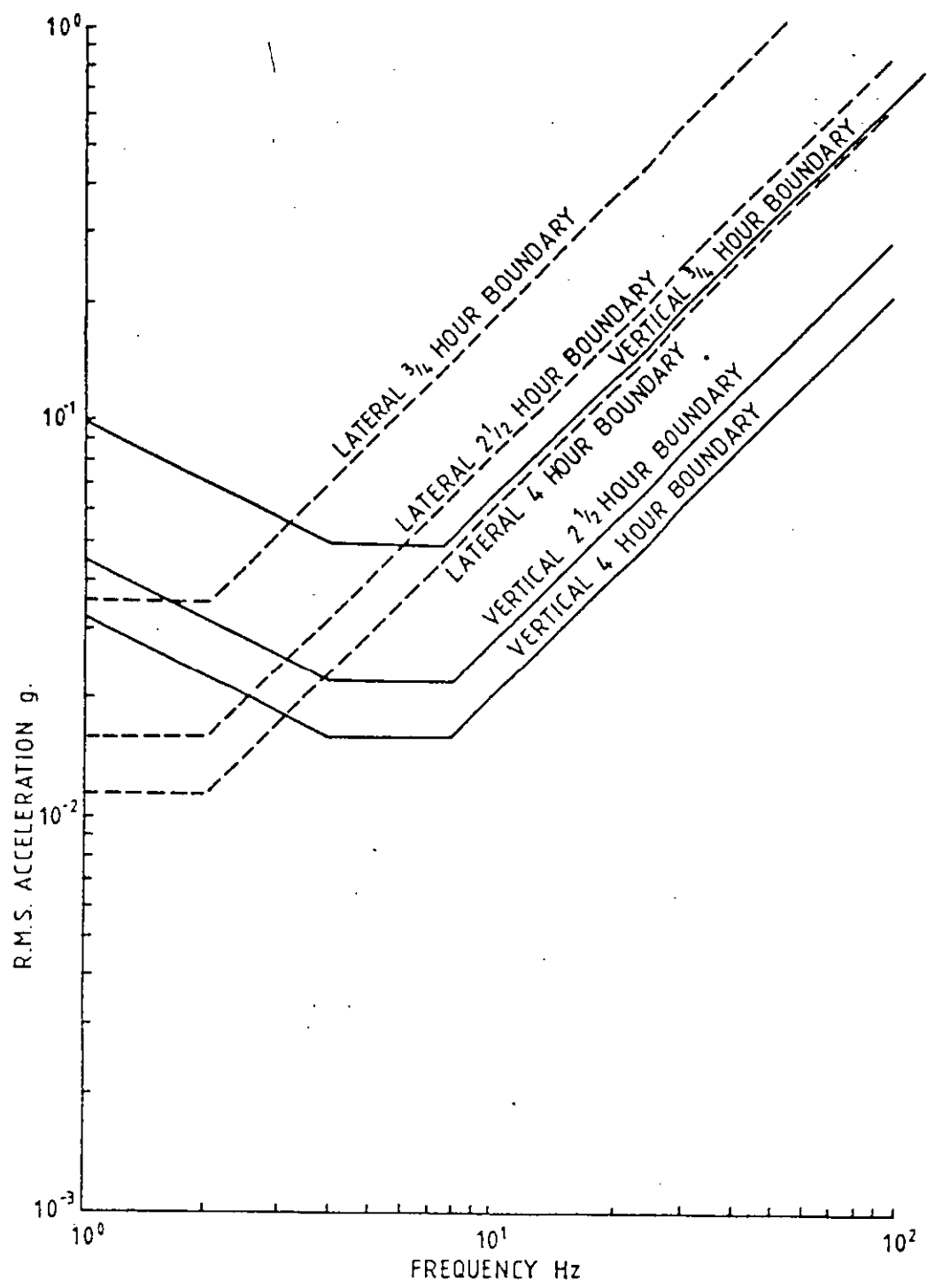


FIG.2.31.S.O. REDUCED COMFORT BOUNDARIES

In order to assess the effect of a suspension on passengers subjected to broadband vibration a weighting function has been derived based on the I.S.O. curves (48). Fig 2.4 shows the vertical and lateral weighting functions, which are in fact the inverse of the sensitivity curves in Fig. 2.3. The weighting factors  $W_f$  are:-

Vertical			Lateral	
f	0 > 0.5 Hz	$W_f = 1.0$		
f	0.5 > 1.0 Hz	$W_f = 0.5/f$	f < 2.0 Hz	$W_f = 1.0$
f	1.0 > 2.0 Hz	$W_f = 0.7$	f > 2.0 Hz	$W_f = 2/f$
f	2.0 > 2.5 Hz	$W_f = 0.18f + 0.34$		
f	2.5 > 8.0 Hz	$W_f = 1$		
f	> 8.0	$W_f = 8/f$		

Weighted r.m.s accelerations ( $y_w$ ) are computed for the output vector  $y$  using the equation

$$y_w^2 = \sum_{k=1}^n \frac{(W_f^2(k) \cdot Y(k) + W_f^2(k+1) \cdot Y(k+1)) (f(k+1) - f(k))}{2} \quad (2.27)$$

$Y(k)$  is the p.c.d. of the vector  $y$  at the  $k^{\text{th}}$  frequency.

Since the project which is the basis of this thesis, was started, new work (49) has suggested that an amended weighting function be adopted. As this is not due to come into general use until the end of 1985 the older weighting function has been used.

### 2.3.3. Power Consumption

It is necessary to determine the power consumption of the active suspension. This can usually be found by taking the scalar product of two variables for instance volts. current or force. velocity. This is quite easy if the outputs which form the power product are in polar form. Given the two variables as  $R_1\theta_1$  and  $R_2\theta_2$  then the power

$$W_p = \int_0^{\infty} R_1(f) \cdot R_2(f) \cos(\theta_1(f) - \theta_2(f)) df \quad (2.28)$$



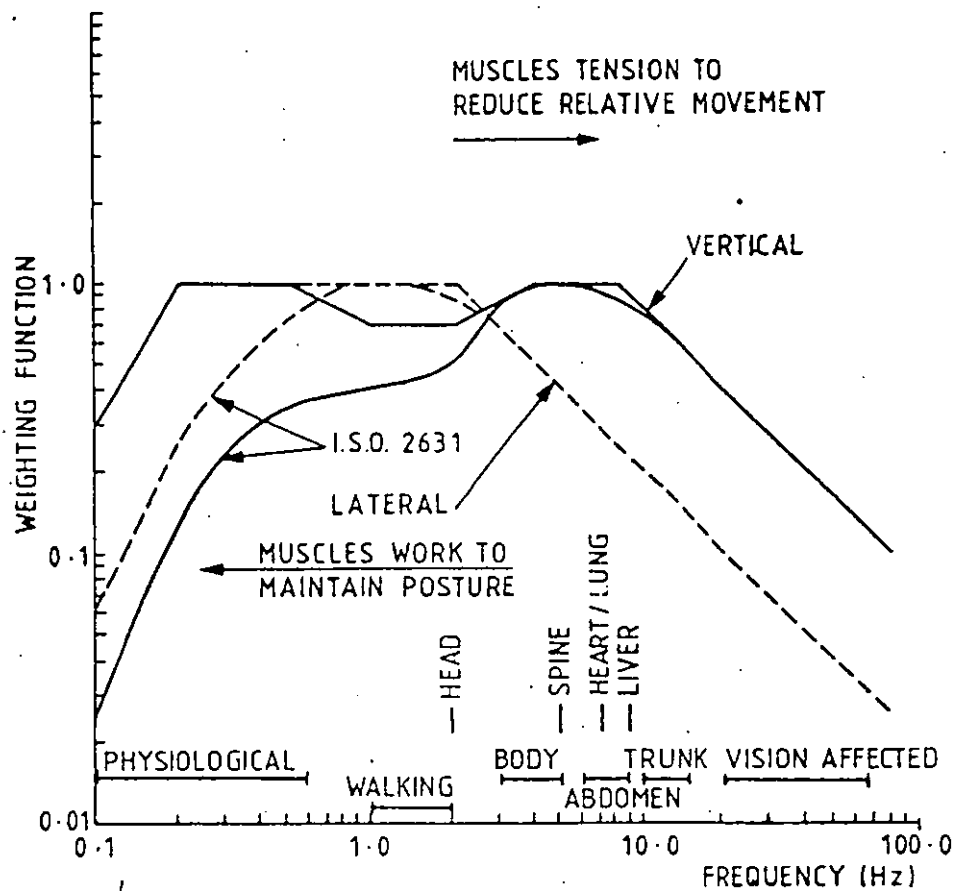


FIG.2.4 WEIGHTING FUNCTIONS FOR LATERAL AND VERTICAL ACCELERATION ASSESSMENTS

Again a trapezoidal numerical integration is performed to calculate  $W_p$ .

#### 2.3.4 Using the Frequency Response Program

The computer program calculates the frequency response of the system for a predetermined range of frequencies  $f_{\min}$  to  $f_{\max}$ . The incremental range can be either logarithmic or linear. For each frequency  $f$ , the track spectrum  $H(f)$  is computed and for the vectors  $x(f)$ ,  $\dot{x}(f)$  and  $y(f)$  the output is given in rectangular form, and in polar form with gain as expressed as a ratio and in dB's. The p.s.d. of each variable  $X_h(f)$ ,  $\dot{X}_h(f)$  and  $Y_h(f)$  are also computed.

After the specified range of frequencies has been covered  $x_{\text{rms}}$  and  $\dot{x}_{\text{rms}}$  are computed. For the  $y$  vector  $y_{\text{rms}}$  and  $y_w$  are computed. Power dissipations which have been specified are also computed.

#### 2.4 Linear Optimal Control

Linear optimal control theory (45) assumes that all the states of the system to be controlled are available as feedbacks. Thus if the uncontrolled system is described by the state equation

$$\dot{x}(t) = A x(t) + B u(t) \quad (2.29)$$

it is possible to determine a feedback matrix  $F$  by which all the elements of the state variable  $x(t)$  can influence the input variables  $u(t)$ .

$$u(t) = -F x(t) \quad (2.30)$$

The closed loop system is described by equation (2.31) and shown diagrammatically in Fig 2.5.

$$\dot{x}(t) = (A - BF) x(t) \quad (2.31)$$

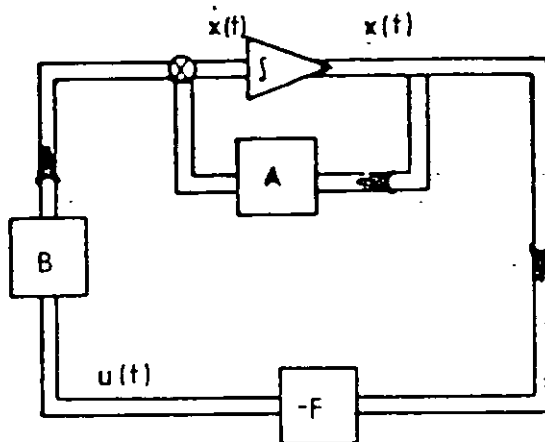


Fig 2.5 CLOSED LOOP SYSTEM WITH STATE FEEDBACK

#### 2.4.1 Optimal Regulator

An optimal regulator is a state feedback matrix  $F$  which minimises a quadratic performance index of the form

$$J = \int_0^{\infty} (x^T(t) R_1 x(t) + u^T(t) R_2 u(t)) dt \quad (2.32)$$

where  $R_1$  and  $R_2$  are weighting matrices.

An alternative form of equation (2.32) is

$$J = \int_0^{\infty} (z^T(t) R_3 z(t) + u^T(t) R_2 u(t)) dt \quad (2.33)$$

where  $z(t) = Nx(t)$  and  $R_1 = N^T R_3 N$

The advantage of 2.33 is that weighted variables can be selected which are linear combinations of  $x(t)$  and have a single weighting factor applied. Thus  $R_3$  can be a diagonal matrix.

The matrices  $R_1$  and  $R_3$  are semipositive definite i.e.  
 $x^T R_1 x \geq 0$  and  $z^T R_3 z \geq 0$

$R_2$  must be positive definite  
 i.e.  $u^T R_2 u > 0$

The optimal feedback matrix is given by

$$F = R_2^{-1} B^T P \quad (2.34)$$

where  $P$  comes from the matrix differential equation

$$\dot{P} = PBR_2^{-1}B^TP - R_1 - A^TP - PA \quad (2.35)$$

Equation (2.35) is the Matrix Riccati equation. References (45) and (50) show how the Matrix Riccati equation is derived, with (45) in particular showing several different methods of derivation.

#### 2.4.2 Solution of the Matrix Riccati Equation

The method used to solve the Matrix Riccati equation was the eigen vector decomposition technique suggested by MacFarlane (51) and Potter (52). This requires that the Matrix Riccati equation is reformulated in the canonical form. The adjoint variable  $p(t)$  is defined as

$$p(t) = P(t) x(t) \quad (2.36)$$

$$\text{and } \dot{p}(t) = \dot{P}(t) x(t) + P(t)\dot{x}(t) \quad (2.37)$$

Combining equations (2.29), (2.30), (2.34), (2.35), (2.36) and (2.37) gives the partitioned equation

$$\begin{bmatrix} \dot{x} \\ \dot{p} \end{bmatrix} = \begin{bmatrix} A & -BR_2^{-1}B^T \\ -R_1 & -A^T \end{bmatrix} \begin{bmatrix} x \\ p \end{bmatrix} \quad (2.38)$$

$$Z = \begin{bmatrix} A & -BR_2^{-1}B^T \\ -R_1 & -A^T \end{bmatrix}$$

The canonical matrix  $Z$  has eigen values which are spaced symmetrically in the left and right halves of the  $s$  plane. Using similarity transforms a diagonal matrix can be found such that

$$Z = W \begin{vmatrix} \Lambda & & 0 \\ 0 & & -\Lambda \end{vmatrix} W^{-1} \quad (2.39)$$

Where  $\Lambda$  is a diagonal matrix of the eigen-values of  $Z$ , and  $W$  is a suitable transformation matrix.  $W$  was selected as a matrix of the eigen vectors of  $Z$  (51) and (52). Other transformation matrices such as Schur Vectors (53) can be used. However eigen vectors were chosen because of the ready availability of subroutines for computing eigen vectors.

The columns of  $W$  are made up of the eigen vectors associated with the eigen value in the corresponding column in the diagonal matrix

$$\begin{vmatrix} \Lambda & & 0 \\ 0 & & -\Lambda \end{vmatrix} \quad (2.40)$$

$W$  and  $W^{-1}$  can be partitioned to

$$W = \begin{vmatrix} W_{11} & W_{12} \\ W_{21} & W_{22} \end{vmatrix} \text{ and } W^{-1} = \begin{vmatrix} V_{11} & V_{12} \\ V_{21} & V_{22} \end{vmatrix} \quad (2.41)$$

The solution of (2.38) between time  $t$  and  $t_1$  is

$$\begin{vmatrix} x(t) \\ p(t) \end{vmatrix} = \begin{vmatrix} W_{11} & W_{12} \\ W_{21} & W_{22} \end{vmatrix} \begin{vmatrix} e^{\Lambda(t-t_1)} & 0 \\ 0 & e^{-\Lambda(t-t_1)} \end{vmatrix} \begin{vmatrix} V_{11} & V_{12} \\ V_{21} & V_{22} \end{vmatrix} \begin{vmatrix} x(t_1) \\ p(t_1) \end{vmatrix}$$

$$\text{If } t_1 \gg t \text{ and } t_1 \rightarrow \infty \quad e^{\Lambda(t-t_1)} \rightarrow 0 \quad (2.42)$$

so that

$$x(t) = W_{12} e^{-\Lambda(t-t_0)} (V_{21} x(t_0) + V_{22} p(t_0)) \quad (2.43)$$

$$p(t) = W_{22} e^{-\Lambda(t-t_0)} (V_{21} x(t_0) + V_{22} p(t_0)) \quad (2.44)$$

From (2.36)  $P = px^{-1}$

and combining (2.43) and (2.44) gives

$$P = W_{22} W_{12}^{-1}$$

Thus a solution of the Matrix Riccati Equation is obtained from a matrix of the eigen vectors of the canonical matrix Z.

In most cases  $W_{12}$  and  $W_{22}$  will be complex matrices. However, the use of complex arithmetic can be avoided by the use of a non-singular transform U where

$$\begin{vmatrix} W_{12}^1 \\ W_{22}^1 \end{vmatrix} = \begin{vmatrix} W_{12} \\ W_{22} \end{vmatrix} U \quad (2.45)$$

such that

$$W_{22}^1 (W_{12}^1)^{-1} = (W_{22} U) (W_{12} U)^{-1} = W_{22} W_{12}^{-1} \quad (2.46)$$

As the complex eigen vectors occur in conjugate pairs a suitable transformation is to use the real parts of the eigen vector as one column of  $(W_{12}^1 \ W_{22}^1)^T$  and to use the imaginary parts of one of the conjugate pairs as another column. The whole matrix can now be treated as a real matrix.

A useful side effect of this method is that the eigen values of the Z matrix in the left half of the s plane are in fact the closed loop eigen values of the control system.

Fig 2.6 shows a graphical representation of the Matrix Riccati Equation

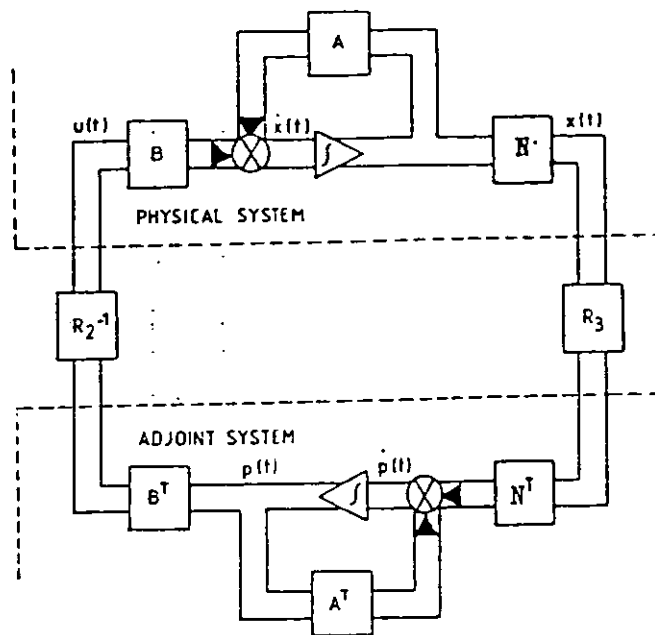


Fig 2.6 MATRIX RICCATI EQUATION

The output of the real system is weighted by the matrix  $R_3$ . The adjoint system then recreates the effect of  $R_3$  on the input. It is then divided by the input weighting matrix  $R_2$  to recreate the optimal feedback, in effect taking the ratio of the output weighting matrix and the control action required to produce it.

### 2.4.3 Optimal Observer

In the previous section it was shown that an optimal control system is required to feedback all the states of the system. In most cases it is not possible to measure all the states of the system. The way round the problem is to recreate the states which cannot be measured by means of an observer.

Given a system described by the state equation

$$\dot{x}(t) = A x(t) + Bu(t) \quad (2.47)$$

with measured output variables

$$y(t) = C x(t) \quad (2.48)$$

the unmeasured states of the system can be recreated by the system shown in Fig. 2.7.

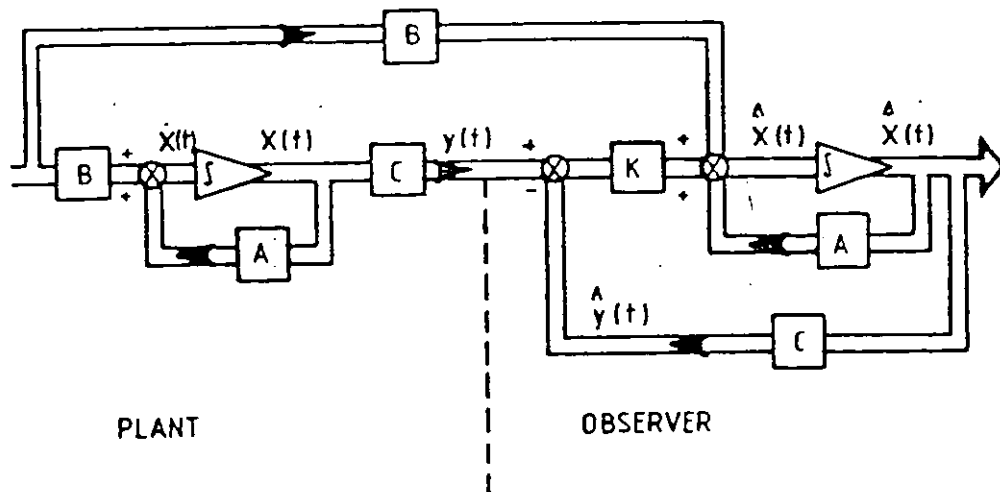


Fig. 2.7 PLANT AND OBSERVER

The observer consists of a model of the plant. The model states  $\hat{x}(t)$  are driven towards the plant states  $x(t)$  by comparing the measured variables  $y(t)$  with the recreated variables  $\hat{y}(t)$  and using the resulting error to drive the model. A matrix  $K$  has to be selected which will ensure that the observer is stable and will follow the plant as closely as possible.

The observer is described by the equation

$$\dot{\hat{x}}(t) = [A - KC] \hat{x}(t) + Bu(t) + Ky(t) \quad (2.49)$$

where  $\hat{x}(t)$  is the observed value of  $x(t)$ . For a simple system, values for the  $K$  matrix can be selected on a trial and error basis to give the required stability and speed of reconstruction. However for a complex system a systematic approach is required. The method selected was the Kalman and Bucy filter (54).



2.4.4 Optimal Observer with Uncorrelated StateExcitation and Observer Noise

If the system to be observed is excited by white noise  $w_1(t)$  and measurements of the output vector corrupted by white noise  $w_2(t)$  the state and observation equations become

$$\dot{x}(t) = Ax(t) + Bu(t) + w_1(t) \quad (2.50)$$

$$y(t) = Cx(t) + w_2(t) \quad (2.51)$$

$w_1(t)$  has intensity  $V_1$  and  $w_2(t)$  intensity  $V_2$

The aim of the observer is to reduce the reconstruction error

$$e(t) = x(t) - \hat{x}(t) \quad (2.52)$$

$$\dot{e}(t) = [A - KC] e(t) + (I, -K) \begin{bmatrix} w_1(t) \\ w_2(t) \end{bmatrix} \quad (2.53)$$

The covariance of the reconstruction error

$$E[e(t), e^T(t)] = Q(t) \quad (2.54)$$

$$Q(t) = [A - KC] Q(t) + Q(t) [A - KC]^T + V_1 + KV_2K^T \quad (2.55)$$

The reconstruction error  $e(t)$  is minimised by a gain matrix

$$K = Q(t) C^T V_2^{-1} \quad (2.56)$$

substituting this into (2.55) gives

$$\dot{Q}(t) = V_1 - Q(t) C^T V_2^{-1} C Q(t) + Q(t) A^T + A Q(t) \quad (2.57)$$

which is essentially the same as the Matrix Riccati equation (2.35) and a steady state solution can be obtained in the same manner by setting the canonical matrix

$$Z = \begin{vmatrix} -A^T & & C^T V_2^{-1} C \\ & I & \\ EV_3 E^T & & A \end{vmatrix} \quad (2.58)$$

where  $EV_3 E^T = V_1$

As the measurement intensity matrix  $V_2$  is inverted it is necessary when designing an observer by this method to assume that noise is present on all the measured variables.

It will be shown in the following section that if  $V_2^{-1}$  is set to zero the canonical matrix (2.58) can be used to compute the covariance of the system. Thus including  $V_2^{-1}$  in effect calculates a gain matrix which is a function of the signal to noise ratio of the observer.

## 2.5 Response of a System to a Random Disturbance

In reference (55) the response of a railway vehicle is calculated to a random input by use of the Lyapunov equation, rather than by integration of the frequency response as shown in Section 2.3.

Given a system described by

$$\dot{x}(t) = A x(t) + E w(t) \quad (2.59)$$

$$y(t) = C x(t) \quad (2.60)$$

$w(t)$  is a white noise vector with intensity  $V(t)$ .

For a single output variable  $y$  the mean square response

$$y^2 = E \left[ cx, x^T c^T \right] \quad (2.61)$$

For a system driven by random noise the expectation value of  $y^2$  is:-

$$(y^2) = CE[x, x^T] C^T \quad (2.62)$$

$[x, x^T]$  is a square symmetric matrix,  $X$ , which is referred to as the covariance matrix

$$X = E[x, x^T] \quad (2.63)$$

$$\dot{X} = E[\dot{x}, x^T] + E[x, \dot{x}^T] \quad (2.64)$$

Substituting equation 2.59 this gives

$$\dot{X} = AX + XA^T + EVE^T$$

As the system is driven by white noise the process is stationary and the value at any instant is uncorrelated with the value at any other instant. Thus the derivative  $\dot{X} \rightarrow 0$  as  $t \rightarrow \infty$  giving the equation

$$0 = AX + XA^T + EVE^T \quad (2.65)$$

This is a Lyapunov equation and, as it is similar in form to the Matrix Riccati equation (2.35), it can be solved by the same computer program. The canonical matrix  $Z$  is rearranged to give:-

$$\begin{array}{c|c} \begin{array}{c} q_1 \\ \vdots \\ q_2 \end{array} & \begin{array}{c|c} -A^T & 0 \\ \hline EVE^T & A \end{array} \end{array} \begin{array}{c} q_1 \\ \vdots \\ q_2 \end{array} \quad (2.66)$$

Note that this is the same form as (2.58) with  $V_2^{-1}$  set to zero the covariance matrix is computed from

$$X = W_{22} W_{12}^{-1} \quad (2.67)$$

The output covariances are computed from

$$E[y, y^T] = CXC^T \quad (2.68)$$

The mean square values of  $y$  are the diagonal elements of the output covariance matrix  $CXC^T$ .

It will be noted that not only does this technique give the mean square responses of the system but the eigen vector solution of the Lyapunov equation also gives the system eigen values as a by-product.

#### 2.5.1 Relationship between Track Spectrum Roughness Factor and Track Covariance

Section 2.3.1 showed that railway track can be described by a spatial power spectrum of the form

$$\frac{T}{a_0 f_s^2 + a_1 f_s^3 + a_2 f_s^4} \quad \text{m}^2/\text{cycle/m} \quad (2.69)$$

A simplified form of this expression is often used

$$\frac{T}{a_0 f_s^2} \quad \text{m}^2/\text{cycle/m} \quad (2.70)$$

For a vehicle travelling at a constant velocity  $v$  this will give rise to a mean square displacement.

$$z_t^2 = \int_0^{\infty} \frac{2Tv}{\omega} d\omega \quad (2.71)$$

The covariance of a system is computed in the frequency domain from the equation.

$$X = \frac{1}{2} \int_{-\infty}^{\infty} (j\omega I - A)^{-1} E V E^T (-j\omega I - A^T)^{-1} d\omega \quad (2.72)$$

Equating equations (2.71) and (2.72) the variance of the track is shown to be

$$V_T = 2\pi^2 T_v$$

It will be noted that the ratio is  $2\pi^2$  not  $4\pi^2$  as 2.71 is evaluated between 0 and  $\infty$ , while (2.72) is equated between  $-\infty$  and  $\infty$

It will be noted that the integral of equation (2.71) is infinite. The problem which this creates is avoided in the frequency response program by not computing a response at 0 Hz. In the solution of the Lyapunov equation the problem is avoided by modelling the track spectrum in the frequency domain as

$$\frac{2 T_v}{\omega_0^2 + \omega^2} \quad (2.73)$$

where  $\omega_0$  is a constant frequency

The state equations for the track input then becomes

$$\dot{z}_t = -\omega_0 z_t + w_t \quad (2.74)$$

### 2.5.2 Correlated Inputs

A railway vehicle travelling along the track is subjected to the same track inputs to each wheel, delayed in time. Thus a two axle vehicle is subjected to two vertical inputs  $z_{t1}(t)$  and  $z_{t2}(t)$  with a delay  $\delta$  between them so that

$$z_{t2}(t) = z_{t1}(t + \delta) \quad (2.75)$$

In the frequency domain this is quite easy to deal with as

$$z_{t2}(\omega) = z_{t1}(\omega)e^{-j\omega\delta} \quad (2.76)$$

Hence the provision of a complex input vector in equation (2.15).

Using the Lyapunov equation the problem is more difficult to deal with as it is necessary to calculate the correlation between the inputs. A method for doing this has been proposed by Hederick and Firouztash (56).

Each wheelset responds independently to the random track irregularities, but is correlated with those wheelsets in front of it. Reference (56) shows how the correlation can be computed from the transition matrix.

The equation

$$\dot{x}(t) = A x(t) \quad (2.77)$$

has a solution between time  $t_0$  and  $t$  of

$$x(t) = \Phi(t, t_0) x(t_0) \quad (2.78)$$

where  $\Phi(t, t_0)$  is the transition matrix and

$$\Phi(t, t_0) = e^{A(t-t_0)} \quad (2.79)$$

Let the track inputs be represented by one column in the E matrix so that  $E_1$  is the input at the first wheelset  $E_2$  the second etc.

$$E(t) = [E_1(t), E_2(t), \dots, E_n(t)] \quad (2.78)$$

Given a 4 axle vehicle, with time delays  $\delta_1$   $\delta_2$   $\delta_3$  between successive wheel sets and intensity of the track input  $V$ , the Lyapunov equation is

$$\begin{aligned}
 \dot{x} = & Ax + xA^T + EVE^T + V [E_2 E_1^T \phi^T(\delta_1) \\
 & + E_3 E_1^T \phi^T(\delta_1 + \delta_2) + E_4 E_1^T \phi^T(\delta_1 + \delta_2 + \delta_3) \\
 & + E_3 E_2^T \phi^T(\delta_2) + E_4 E_2^T \phi^T(\delta_2 + \delta_3) + E_4 E_3^T \phi^T(\delta_3) \\
 & + \phi(\delta_2) E_3^T + \phi(\delta_2 + \delta_3) E_2 E_4^T + \phi(\delta_3) E_3 E_4^T] \quad (2.79)
 \end{aligned}$$

where  $\phi(\delta)$  is the transition matrix from  $t = 0$  to  $t = \delta$

### 2.5.3 Lyapunov Equation in Practice

The usual method of evaluating the transition matrix (2.79) is by a Taylor series

$$e^{A(\delta t)} = I + A\delta t + \frac{(A\delta t)^2}{2!} + \frac{(A\delta t)^3}{3!} + \text{etc} \quad (2.80)$$

where  $\delta t$  is the time  $t-t_0$

Fig 2.8 shows a simple pitch and bounce model of a railway vehicle connected directly to the track input. For the sake of simplicity damping is provided to an absolute reference

Appendix A gives the state equations of the model and the vehicle parameters.

Poor mainline railway track has a roughness factor  $T = 4 \times 10^{-7} \text{ m}^2$ . For a vehicle travelling at 55 m/s the equivalent intensity  $V = .434 \times 10^{-3} \text{ m}^2$ .

Table 2.1 shows the responses computed for the vehicle shown in Fig 2.8 at 55 m/s using the frequency response program and the Lyapunov program. It will be seen that the two techniques produce comparable results.

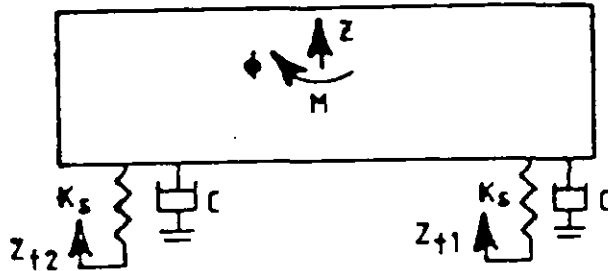


Fig 2.8 PITCH AND BOUNCE MODEL

TABLE 2.1 R.M.S. Responses Calculated for 55 m/s on Poor Track

	Frequency Response Program	Lyapunov Program
"		
z leading	2.5% g	2.6% g
"		
z centre	1.3% g	1.3% g
"		
z trailing	2.7% g	2.8% g
z-zt leading	7.6 mm	7.4 mm
z-zt trailing	7.7 mm	7.5 mm

When the responses of a complete vehicle, including bogies, were computed however, the Lyapunov equation broke down. The problem occurred when computing the transition matrices for equation (2.79). In the model in Fig 2.8 the minimum time constant is 0.13 s, which is comparable with the time delay between the inputs of 0.3 s. Consequently the series (2.80) converges quickly and only 13 elements were required to be computed. When the bogies were included the minimum time constant of the system



was .01 secs which required 73 elements of the Taylor series to be computed for the maximum time delay and the cumulative error generated was unacceptable. The test applied for convergence was that if after computing  $n$  elements of the series;

$$\Phi_n = \sum_{k=1}^n \left[ I + A\delta t + \frac{(A\delta t)^2}{2!} + \text{etc} \frac{(A\delta t)^n}{n!} \right] \quad (2.81)$$

each term in the next element

$$\frac{(A\delta t)^{n+1}}{(n+1)!} (i,n) < (.001) \times \frac{(A\delta t)^{n+1} (i,n)}{(n+1)! \Phi_n (i,n)} \quad (2.82)$$

Because of the unsatisfactory results obtained, this technique was not pursued, though it should be possible to obtain satisfactory results by taking a similarity transformation of the state matrix

$$A = W^{-1} (\Lambda) W \quad (2.83)$$

where  $\Lambda$  is a diagonal matrix of the eigen values of the state equation. Thus

$$e^{A\delta t} = W^{-1} e^{\Lambda\delta t} W \quad (2.84)$$

where  $e^{\Lambda\delta t}$  is a diagonal matrix which can be computed directly without resorting to a Taylor series. Note however, that  $W$  and  $\Lambda$  are both complex. While this is a mathematically elegant method of computing the responses of a system to a random input it does not produce the frequency information of the frequency response methods.

CHAPTER 3MK III COACH PASSIVE SUSPENSION

The active suspension used for the comparative design study was an electromagnetic vertical active suspension fitted to a British Rail Mk III Coach. It acts in parallel with the existing passive, airspring, suspension to reduce power consumption and to enable the vehicle to operate passively when power is removed from the active suspension.

3.1 Mk III Coach Passive Suspension

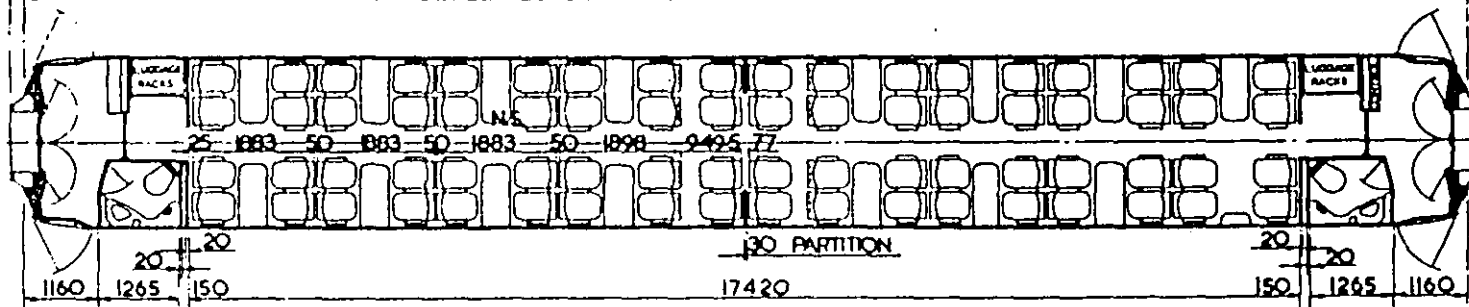
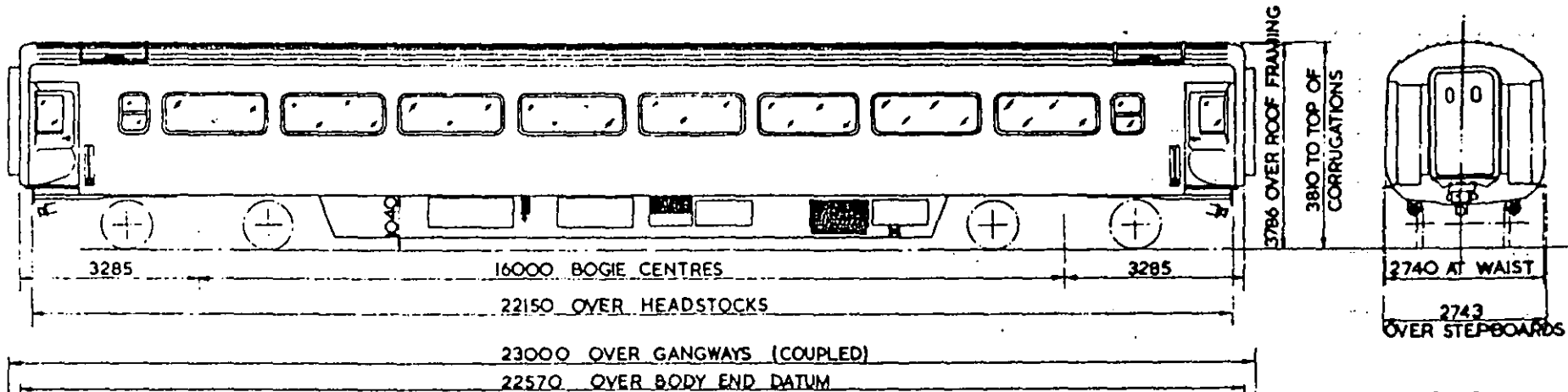
A standard British Rail Mk III TSO, M12094 Fig 3.1, was used for the experimental part of this study, consequently a theoretical model of the vehicle suspension was required. The primary suspension (between the wheels and the bogie frame) has coil springs and hydraulic dampers acting through swinging arms Fig. 3.2. Vertically the secondary suspension (between the vehicle and bogies) has double convolution air springs with damping provided by restricting the airflow between the airsprings and surge reservoirs (Fig. 3.3). Lateral suspension is provided by a swinging bolster. While this is not relevant to the theoretical model it proved particularly useful when it came to physically accommodating the electromagnetic actuators. Vehicle parameters and state equations are given in Appendix B.

3.2 Air Spring Model

Air springs provide a very rudimentary form of active suspension through the low rate integral action of the levelling valves, which give a constant ride height. This overcomes the problems of large static deflections inherent with soft springs and, as the suspension frequency, for a spring with constant height, does not vary very much with load there is a relatively small change in ride between the tare and laden conditions.

OPEN SECOND

B.R. 675



- 2 SALOONS. 72 SEATS
- 2 TOILETS
- 2 LUGGAGE BAYS

TARE		
TONS	CWTS	QRS
33	14	3
LOT	VEHICLE No.	
30882	42003-42083	

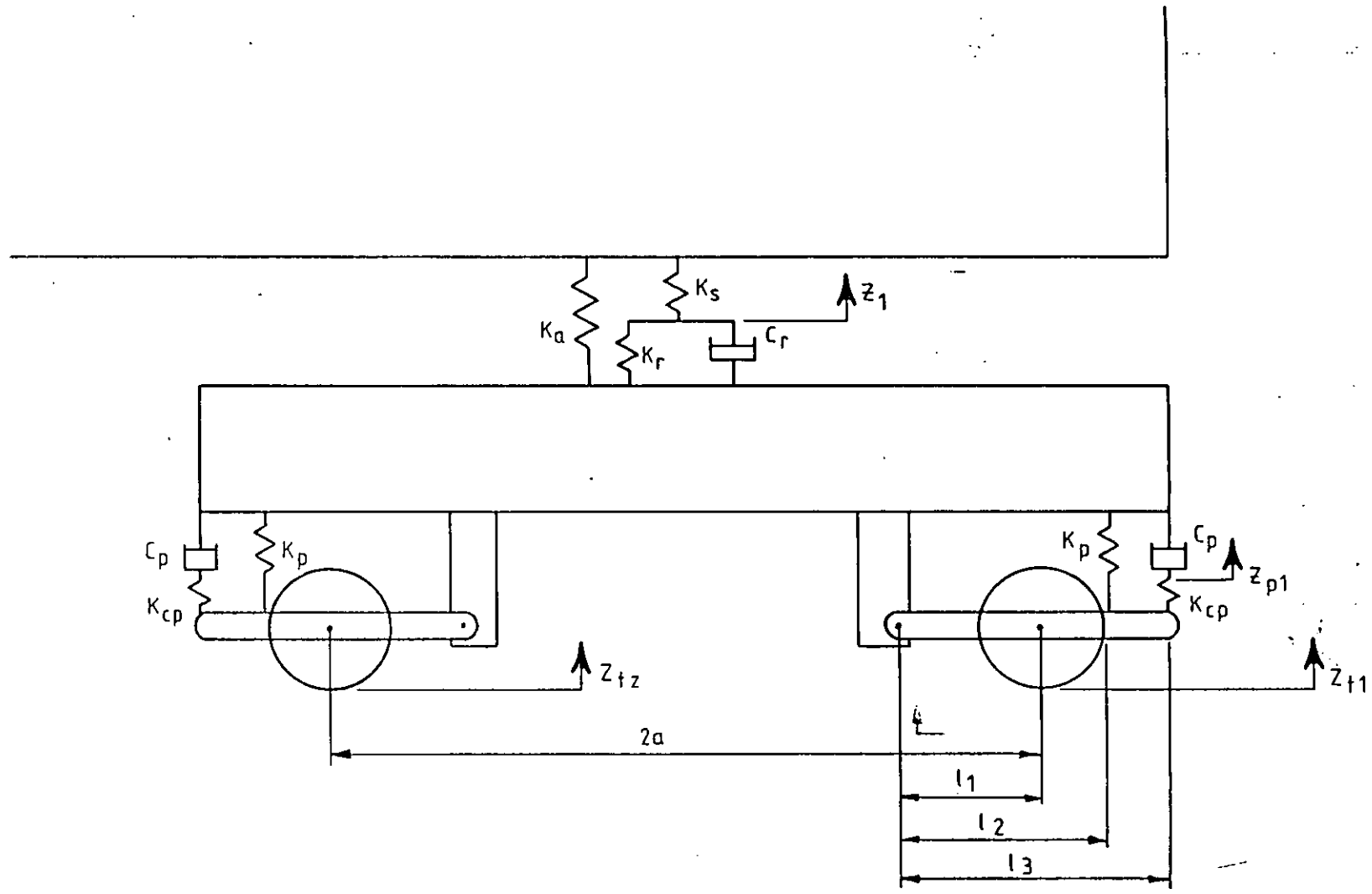


FIG. 3-2 MK III COACH PRIMARY SUSPENSION

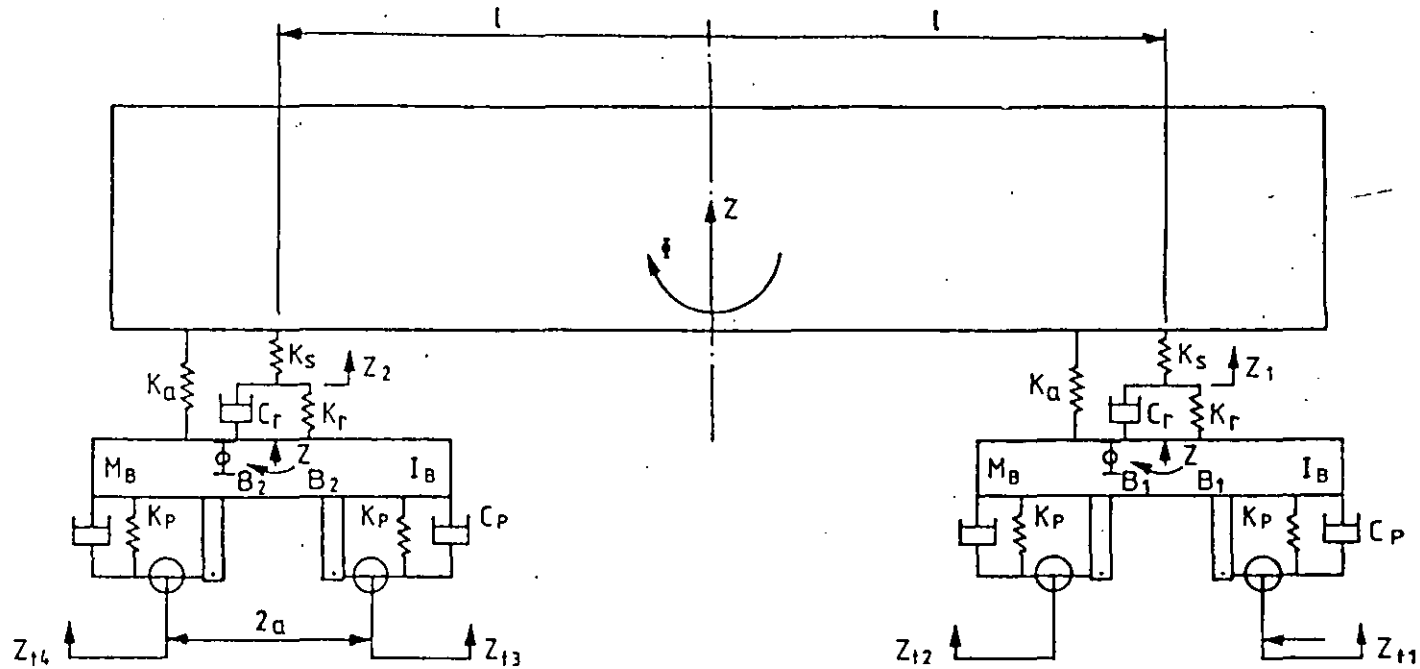
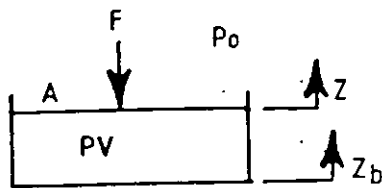


FIG. 3.3 MK III COACH VERTICAL SUSPENSION MODEL



$F$  = Force  
 $A$  = Area  
 $P$  = Absolute Pressure  
 $P_o$  = Static Pressure  
 $V$  = Volume  
 $\gamma$  =  $C_p/C_v$  ratio of  
 specific heats

Fig 3.4 SIMPLE AIR SPRING

Fig 3.4 shows a simple airspring model. At normal suspension frequencies (1.0 Hz to 2.0 Hz) compression and expansion of the spring will be adiabatic.

$$\text{Thus } PV^\gamma = \text{Const} \quad (3.1)$$

$$\text{and } \delta P = -\frac{\gamma P \delta V}{V} \quad (3.2)$$

$$F = (P - P_o) A \quad (3.3)$$

$$\text{and } \delta F = A \delta P + (P - P_o) \delta A \quad (3.4)$$

$$V = (z - z_b) A \quad (3.5)$$

$$\text{Therefore } \delta V = \delta(z - z_b) A + (z - z_b) \delta A \quad (3.6)$$

Thus 3.4 can be re-written as:

$$\delta F = -\frac{\gamma P A^2}{V} \delta(z - z_b) + (P - \gamma P - P_o) \delta A \quad (3.7)$$

The spring stiffness has two components

$$\frac{\delta F}{\delta(z - z_b)} = -\frac{\gamma P A^2}{V} + (P - \gamma P - P_o) \frac{\delta A}{\delta(z - z_b)} \quad (3.8)$$

$$-\frac{\gamma P A^2}{V} = K_s \quad (3.9)$$

where  $K_s$  is the volume stiffness of the spring and

$$(P - \gamma P - P_o) \frac{\delta A}{\delta(z - z_b)} = K_a \quad (3.10)$$

Where  $K_g$  is the area change stiffness which is particularly large with double convolution springs of the type fitted to the Mk III Coach.

### 3.2.1 Pneumatic Damping

The suspension stiffness  $K_g$  (3.9) can be reduced by increasing the volume of the spring  $V$ . This can be done by fitting an auxiliary surge reservoir as shown in Fig. 3.5.

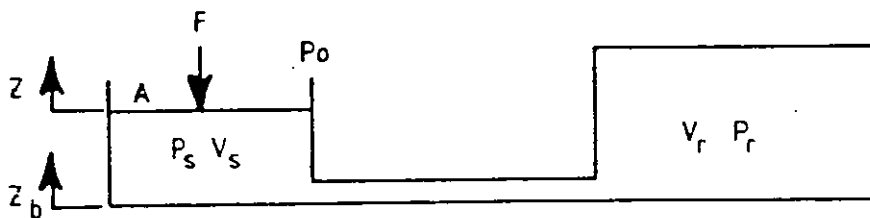


Fig 3.5 AIR SPRING WITH SURGE RESERVOIR

- $P_s$  = Spring Pressure  
 $V_s$  = Spring Volume  
 $P_r$  = Reservoir Pressure  
 $V_r$  = Reservoir Volume

By restricting the airflow between the spring and reservoir it is possible to introduce damping into the system. The enthalpy in the spring is:-

$$H = U + PV \quad (3.11) \quad H = \text{Enthalpy}$$

and the change of heat

$U = \text{Internal Energy}$

$$dQ = dU + PdV$$

$$(3.12) \quad Q = \text{Heat}$$

$M = \text{Mass of air}$

$$\text{so that } \left| \frac{\partial H}{\partial T} \right|_p = \left| \frac{\partial Q}{\partial T} \right|_p = MC_p \quad (3.13) \quad C_p = \text{Specific Heat at Constant Pressure}$$

$$\text{and } \left| \frac{\partial Q}{\partial T} \right|_v = \left| \frac{\partial U}{\partial T} \right|_v = MC_v \quad (3.14) \quad C_v = \text{Specific Heat at Constant Volume}$$

$$\text{giving } H = MC_p T \quad (3.15) \quad R = \text{Gas Constant}$$

$$\text{and } U = MC_v T \quad (3.16) \quad T = \text{Absolute Temperature}$$

The rate of change of enthalpy is

$$\frac{dH}{dt} = \frac{dU}{dt} + \frac{PdV}{dt} + \frac{VdP}{dt} \quad (3.17)$$

or substituting (3.15) and (3.16)

$$\frac{dM}{dt} C_p T = \frac{dM}{dt} C_v T + \frac{PdV}{dt} + \frac{VdP}{dt} \quad (3.18)$$

For the air remaining in the spring the rate of change of enthalpy is:

$$\frac{dH}{dt} = \frac{dQ}{dt} + \frac{VdP}{dt} \quad (3.19)$$

However the compression is adiabatic so that  $\frac{dQ}{dt} = 0$  and the rate of enthalpy of the air leaving the spring is

$$\frac{dM}{dt} C_p T = \frac{dM}{dt} C_v T + \frac{PdV}{dt} \quad (3.20)$$

$$\text{or } m_f C_p T = m_f C_v T + \frac{PdV}{dt} \quad (3.21)$$

where  $m_f$  is the mass flow  $\frac{dM}{dt}$

Taking the gas law

$$PV = MRT \quad (3.22)$$

$$T \frac{dM}{dt} = \frac{1}{R} \frac{dPV}{dt} \quad (3.23)$$

which with (3.21) gives

$$m_f C_p T = \frac{C_v}{R} \left( \frac{VdP}{dt} + \frac{PdV}{dt} \right) + \frac{PdV}{dt} \quad (3.24)$$

because  $C_p - C_v = R$  and  $\gamma = \frac{C_p}{C_v}$

$$m_f = \frac{1}{RT} \left( \frac{VdP}{dt} + \frac{PdV}{dt} \right) \quad (3.25)$$



If a restriction is placed in the surge pipe the volume flow in the pipe

$$Q_v = aC \sqrt{\frac{\Delta P}{\rho}} \quad (3.26)$$

$\Delta P$  is the pressure drop across the restriction  $a$ , the area of the restriction,  $C$  a constant and  $\rho$  the density of the air. Under steady state conditions:-

$$\Delta P = C_D Q_v^2 = C_D \frac{(RTm_r)^2}{(P)} \quad (3.27)$$

Where  $C_D$  is the discharge coefficient and is dependent upon the geometry of the system.

From (3.25) the flow of air into the reservoir

$$m_r = \frac{V_r}{RT} \frac{dP_r}{dt} \text{ as } \frac{dV_r}{dt} = 0 \quad (3.28)$$

If the length of the surge pipe is negligible

$m_s = -m_r$  so that 3.25 and 3.28 can be combined to give

$$\frac{V_s}{\gamma} \frac{dP_s}{dt} + \frac{V_r}{\gamma} \frac{dP_r}{dt} + P \frac{dV_s}{dt} = 0 \quad (3.29)$$

Combining (3.27) and (3.28)

$$P_r = \frac{P_s}{1 + C_q} \left( \frac{d}{dt} \right)^2 \quad \text{where } C = \frac{C_D V_r^2}{\gamma^2 P^2} \quad (3.30)$$

Eliminating  $P_r$  between (3.29) and (3.30) gives

$$\frac{dP_s}{dt} = - \frac{(1 + C_q) \left( \frac{d}{dt} \right)^2}{\frac{V_s}{\gamma} (1 + C_q) \left( \frac{d}{dt} \right)^2 + \frac{V_r}{\gamma}} \quad (3.31)$$

Taking  $dP_s = \frac{dF}{A}$  and  $dV = Adz$  (ie. assuming constant area)

3.31 can be rearranged to give

$$\frac{dF}{dz} = \frac{-(1 + C_q \frac{(d)}{(dt)})^2}{(K_s (1 + C_q \frac{(d)}{(dt)}) + K_r)} \quad (3.32)$$

Where  $K_s = \frac{PA^2}{V_s}$  and  $K_r = \frac{PA^2}{V_r}$  and related to the spring and damper system is fig 3.6.

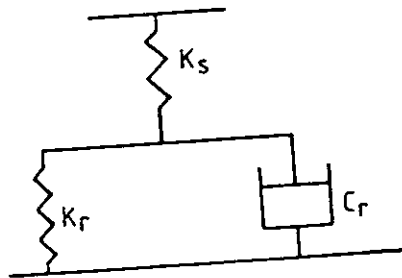


Fig 3.6 SPRING AND DAMPER REPRESENTATION OF AIR SPRING AND RESERVOIR

$$\frac{dF}{dz} = \frac{-(K_s K_r + K_s C_r s)}{(K_r + K_s + C_r s)} \quad (3.33)$$

$s$  is the Laplace operator

$C_r$  is a linearised damping rate derived from the non-linear constant  $C_q$ . Most of the subsequent analysis in the thesis is linear so that a linearisation of  $C_r$  is required. Experience with pneumatic damping over a number of years has shown that the discharge coefficient  $C_D$  is in fact very difficult to determine and has usually to be found by measurement. Thus, while the spring rates are calculated quite easily from the geometry of the system, the damping rate is usually determined empirically.

Note that the spring pressure is a function of the vehicle weight:-

$$\text{ie. } P - P_0 = \frac{Mg}{A} \quad (3.34)$$

For the Mk III coach  $P$  is between  $4 P_0$  and  $5 P_0$  thus  $P \doteq \frac{M_v g}{A}$ , and as the natural frequency of the air spring using (3.9) is

$$f' = \frac{1}{2\pi} \sqrt{\frac{Y P A^2}{V M}} \doteq \frac{1}{2\pi} \sqrt{\frac{Y g A}{V}} \quad (3.35)$$

and, provided the ride height is kept constant the natural frequency of the suspension will remain approximately constant. The reservoir stiffness and damping rate also increase with vehicle weight maintaining a constant dynamic performance.

It will be noted that the area change stiffness  $K_a$  acts in parallel with the spring and reservoir stiffnesses.

### 3.3 Flexible Body Modes

Flexible body modes have proved a problem with active suspensions as they can be stimulated by the control system. The primary bending mode usually provides the most problems, hence it has been included with the passive suspension model.

As the flexible body modes are at a much higher frequency than the rigid body modes they behave as if the vehicle were a freely suspended beam. Over the length of the vehicle the displacement at a point  $x$  due to the bending mode will be.

$$z_{fx} = z_f (\sin(\pi x / l) - a) \quad \text{for } x = 0 \text{ to } x = l \quad (3.36)$$

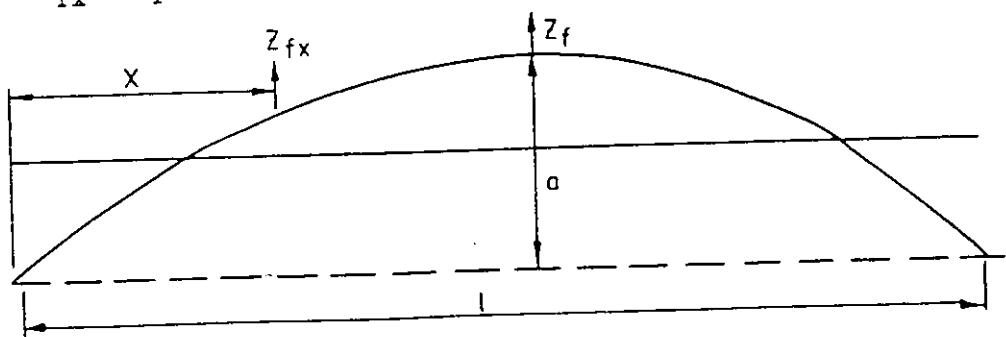


Fig 3.7 PRIMARY BENDING MODE

The vehicle can be considered as a uniformly loaded beam with a mass  $m$  per unit length. For a free bending mode the inertia summed over the length of the vehicle must be zero. Therefore if the momentum of a length  $\delta x$  is

$$I_x = m \dot{z}_{fx} \delta x \quad (3.37)$$

then the total momentum will be

$$I = m \int_0^1 \dot{z}_f (\sin(\pi x/l) - a) dx \quad (3.38)$$

$$= m \dot{z}_f [(-1/\pi) \cos(\pi x/l)]_0^1 - [ax]_0^1 = 0 \quad (3.39)$$

$$\text{Therefore } a = 2/\pi \quad (3.40)$$

$$\text{and } z_{fx} = z_f (\sin(\pi x/l) - 2/\pi) \quad (3.41)$$

In order to include the flexible mode in the suspension model it is necessary to model it as a lumped mass and stiffness. The lumped mass must have a kinetic energy which is equivalent to the kinetic energy of the bending mode. Therefore the kinetic energy at a point  $x$  is

$$KE_x = m \dot{z}_{fx}^2 \delta x/2 \quad (3.42)$$

and the total kinetic energy

$$KE = m/2 \int_0^1 \dot{z}_f^2 (\sin^2(\pi x/l) - \sin(\pi x/l) 4/\pi + 4\pi^2) dx \quad (3.43)$$

$$= \dot{z}_f^2 m/2 ([x/2]_0^1 + [\sin(2\pi x/l) 1/4\pi]_0^1$$

$$+ [\cos(\pi x/l) 4 1/\pi^2]_0^1 + [4 x/\pi^2]_0^1) \quad (3.44)$$

$$= \dot{z}_f^2 ml/2 (1/2 - 4/\pi^2) \quad (3.45)$$

$ml = M_v$  the mass of the vehicle.

If  $z_f$  is taken as unit deflection the kinetic energy of the flexible mode is 10% of the kinetic energy of the bounce mode with unit deflection, thus the effective mass can be taken as 10% of the actual mass.

The flexible body mode was modelled with 2% damping, which is known from resonance testing to be typical for railway vehicle structures.

### 3.4 Passive Suspension Dynamic Performance

Eigen-values were calculated for the passive suspension model in both the tare and laden conditions. They are given in Table 3.1.

Table 3.1 Vertical Eigen-Values Passive Mk III Coach

Mode	Laden		Tare	
	Damping	Frequency	Damping	Frequency
Body Bounce	16%	1.0 Hz	18%	1.0 Hz
	100%	1.7 Hz	100%	1.6 Hz
Body Pitch	19%	1.4 Hz	21%	1.4 Hz
	100%	1.6 Hz	100%	1.5 Hz
Flexible Body	2%	9.0 Hz	2%	10.0 Hz
Mode				
Bogie Bounce	39%	5.8 Hz	42%	5.4 Hz
Bogie Pitch	55%	8.7 Hz	55%	8.7 Hz

The eigen-values do not change very much between the tare and laden conditions. The most noticeable change is the shift in bogie bounce frequency and damping due to stiffening of the secondary air springs.

Vehicle responses were calculated for a track input spectrum with roughness factor  $T = 4 \times 10^{-7} \text{ m}^2$  (see Section 2.3.1) at 55 m/s. This represents poor quality main line railway at the maximum operating speed of the vehicle.

These responses are tabulated in Table 3.2. Note that the accelerations marked RED have had the weighting function, section 2.3.2, applied. The term RED is used within BR to refer to this weighting function and distinguish it from other functions which have been used at other times.

Table 3.2 Passive Suspension Responses 55 m/s On Poor Mainline Track

	(Leading End)			Centre		(Trailing End)		
	r.m.s. (m/s <sup>2</sup> )	Accn RED	Sec Disp mm	r.m.s. (m/s <sup>2</sup> )	Accn RED	r.m.s. (m/s <sup>2</sup> )	Accn RED	Sec Disp mm
Laden	.61	.46	4.8	.30	.24	.79	.57	6.9
Tare	.62	.47	5.7	.32	.24	.80	.59	7.8

It will be noted that the change in ride between the tare and laden conditions is quite small due to the inherent characteristics of the air springs.

CHAPTER 4  
ELECTRO MAGNETIC ACTUATORS

4.1 Electro Magnetic Actuators

The appeal of electromagnets as active suspension actuators lies in their simplicity and lack of moving parts. Against this must be set the fact that the range of operation is strictly limited and that they are only effective in attraction. In order to keep the power consumption of the magnets to reasonable levels the static load of the vehicle is carried on the existing air spring secondary suspension, with the magnetic actuators acting in parallel making them in effect intelligent dampers. This has the added advantage that when the active suspension fails it reverts to a passive state in which it still produces an acceptable ride. By using a vehicle with air springs the range of movement required from the actuators is reduced as they only have to accommodate the dynamic movements of the vehicle and not the change in ride height which would otherwise occur between tare and laden if the vehicle had a coil spring suspension.

In initial laboratory experiments with electromagnets acting in parallel with a passive suspension (58), the problem of magnets only being effective in compression was overcome by using the magnets to generate a preload force in a spring. This form of actuator proved to be unacceptably large if the power consumption was to be kept to reasonable levels. Consequently a double acting actuator was developed for subsequent experiment (59), (60).

4.1.1 Double Acting Actuators

Each actuator is composed of 4 electromagnets, shown in Fig. 4.1 Magnet 1 is attached to the vehicle body. Magnets 2 and 3, which are in fact separate windings in the same core, are attached to the bogie. Magnet 4 is attached to the bolster, which is directly connected to the vehicle body in the vertical plane via the swing links. Energising magnets 1 and 2 pulls the vehicle down while energising 3 and 4 raises it.

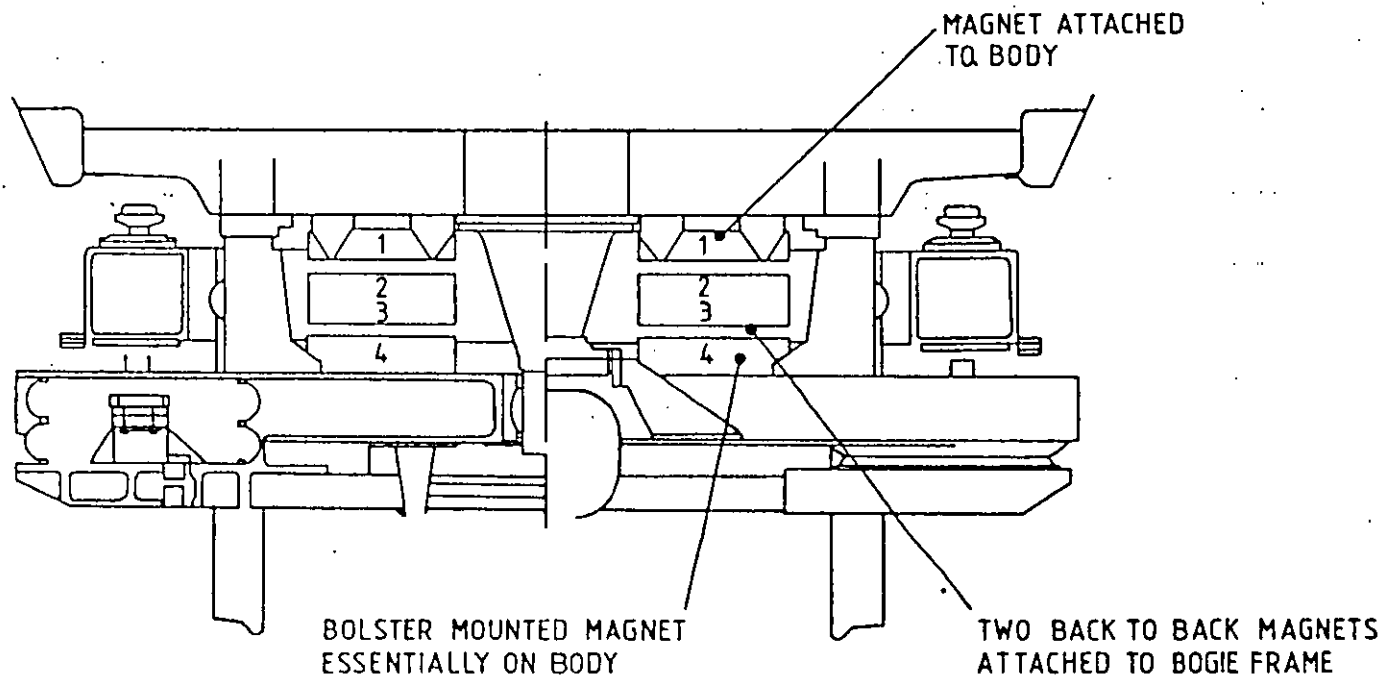


FIG.4.1 ELECTRO - MAGNETIC ACTIVE SUSPENSION



## 4.2 Power Supply

Fig 4.2 shows the power supply to the magnets. The main power source is the 1000 V train heat line. If the train is hauled by an a.c. electric locomotive the train heat supply is a.c. However if the train is hauled by a diesel electric locomotive the train heat supply is d.c. Because of the difficulties of providing a suitable power supply from 1000 V d.c. the system is interlocked to render it inoperative unless 1000 V a.c. is present on the train heat line. This limitation is not too onerous as most of the locomotive hauled Mk III Coaches spend 95% of their time being hauled by electric locomotives.

The 1000 V a.c. supply is transformed to 160 V a.c., which is then input to a step up power supply unit to generate 300 V d.c. A sophisticated power supply is required as the nominal 1000 V varies between 763 V and 964 V with extreme values of 1060 V and 590 V.

Power to the actuators is controlled via 4-quadrant pulse-width-modulated transistor power amplifiers. The amplifiers are capable of accepting energy generated by the magnets.

Blocking diodes in series with each magnet pair ensure that, as the current from the amplifier reverses, it is directed into the appropriate coils to give actuation in both directions.

Flux coils are embedded in the top of the windings of magnets 2 and 3; these are used as sensors in the control system.

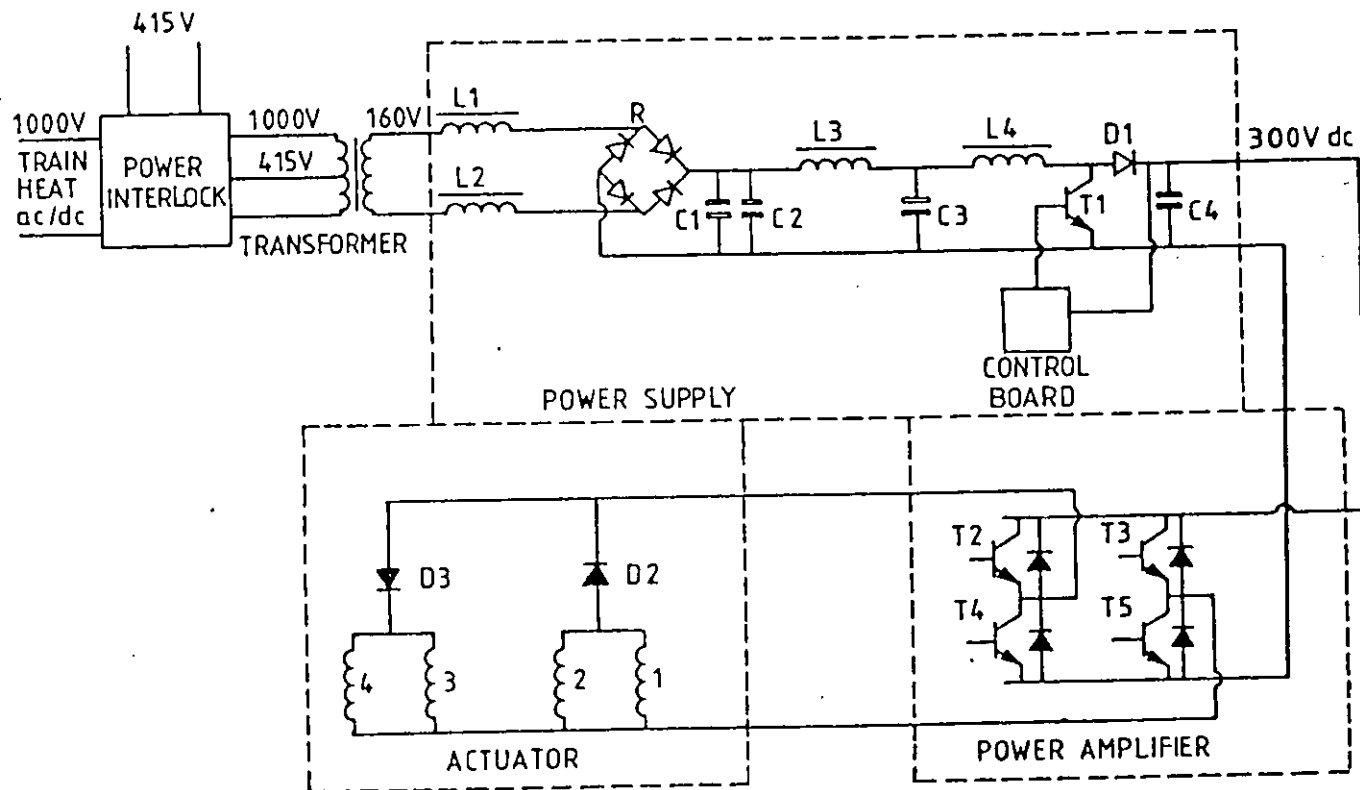


FIG.4.2 POWER ELECTRONICS

## 4.3

Magnet Performance

Pot wound magnets were adopted as they offer a compact and rugged form of construction (Fig. 4.3).

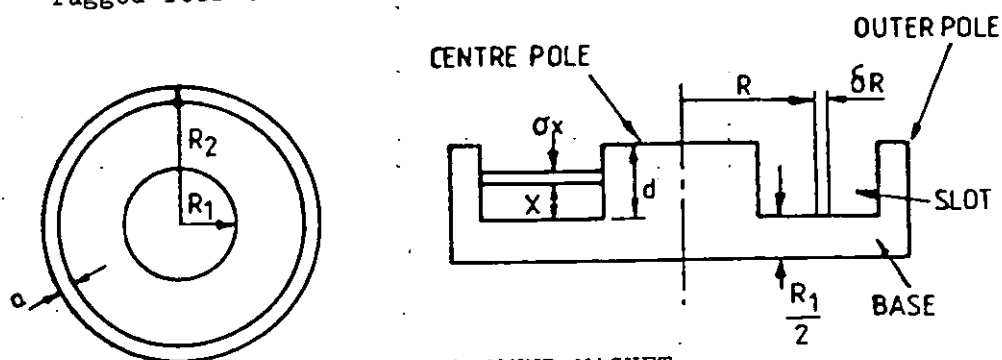


Fig 4.3 POT WOUND MAGNET

$F$  = Magnet Force (N)

$NI$  = Number of Ampere Turns (A) = m.m.f = Magneto Motive Force

$\mu_0$  = Permeability of Free Space =  $4 \times 10^{-7}$  (H/m)

$A$  = Area ( $m^2$ )

$G$  = Air Gap Between Magnets (m)

$B$  = Magnetic Flux Density (T)

$H$  = Magnetic Field Strength (A/m)

$P$  = Magnetic Permanence (A/m)

$l$  = Magnetic Path Length (m)

$NI = \int H dl$

$B = \mu_0 H$  in air

The force generated by a pair of electromagnets is calculated from the magnetic pressure  $BH/2$ .

The force is

$$F = 1/2 BHA \quad (4.1)$$

Assuming that most of the m.m.f drop occurs in the air gap the force generated by a pair of magnets separated by a gap  $G$  is

$$F = \frac{(NI)^2 \mu_0 A_{\text{eff}}}{2 (2G)^2} \quad (4.2)$$

$A_{\text{eff}}$  is the effective pole area of the magnets which is larger than the geometric area as the flux does not flow in straight lines but bellows out at the edges, increasing the dimensions of the pole by a factor  $G/\pi$ , an effect known as fringing. This gives the effective area of the centre pole as

$$A_{\text{ce}} = \pi \left( R_1 + \frac{G}{\pi} \right)^2 \quad (4.3)$$

and of the outer pole

$$A_{\text{oe}} = 2 \pi \left( a + \frac{2G}{\pi} \right) \left( R_2 + \frac{a}{2} \right) \quad (4.4)$$

Thus

$$A_{\text{eff}} = \pi \left( R_1 + \frac{G}{\pi} \right)^2 + 2 \pi \left( a + \frac{2G}{\pi} \right) \left( R_2 + \frac{a}{2} \right) \quad (4.5)$$

The force generated by the magnets can now be calculated. However care must be taken to ensure that the flux in the magnets does not become saturated as this will limit their performance. Saturation occurs first at the base of the centre pole, thus the flux flowing in the centre pole must be calculated.

Note that the thickness of the magnet base is  $R_1/2$  so that the cross sectional area of the base where it joins the centre pole is the same as the cross sectional area of the pole. This prevents saturation occurring in the base of the magnet. The flux in the centre pole has two components:-

1. Mutual flux, which flows between the magnet pair and generates the force between them
2. Leakage flux, which only flows within a single magnet and does not contribute to the force

The total flux

$$\Phi = \Phi_T + \Phi_M + \Phi_L \quad (4.6)$$

Mutual Flux

$$\Phi_M = B \pi R_1^2 = \frac{\mu_0 N I \pi R_1^2}{2G} \quad (4.7)$$

Two flux leakage paths can be identified:-

1. Slot leakage across the slot and
2. Pole leakage between the pole faces

The leakage permeance in free space can be calculated from:-

$$P = \frac{\mu_0 H A}{\int H d l} \quad (4.8)$$

Thus the permeance of an annulus in the slot  $\delta x$  deep and at a radius  $R$  from the centre of the magnet and  $\delta R$  wide is

$$\delta P_s = \frac{\mu_0 2 \pi R \delta x}{\delta R} \quad (4.9)$$

Assuming that the m.m.f is equally distributed along the centre pole the m.m.f at height  $x$

$$\text{mmf}_x = \frac{N I x}{d} \quad (4.10)$$

Thus the slot leakage flux

$$\Phi_s = N I P_s = \frac{\mu_0 N I 2 \pi \int_0^d x dx}{d \int_{R_1}^{R_2} \frac{dR}{R}} \quad (4.11)$$

Giving

$$P_s = \frac{\mu_0 \pi d}{\ln(R_2/R_1)} \quad (4.12)$$

To simplify the calculation of pole leakage the magnet can be approximated to a pair of parallel poles of width  $a$  and length  $2\pi R_2$  (Fig 4.4)

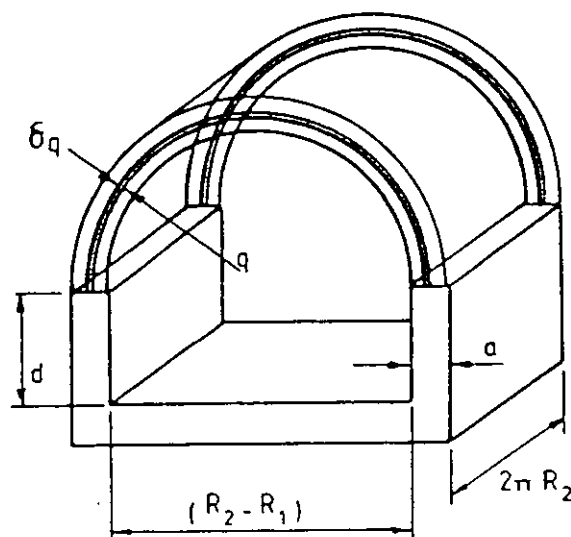


Fig 4.4 POLE LEAKAGE FLUX

The permeance of a small element of flux  $\delta q$  thick is

$$\delta P_p = \frac{\mu_0 2 \pi R_2 \delta q}{\pi q} \quad (4.13)$$

so that

$$P_p = 2 \mu_0 \int_{Q_1}^{Q_2} \frac{dq}{q} \quad (4.14)$$

$$\text{Where } Q_1 = \frac{R_2 - R_1}{2} \quad (4.15)$$

$$\text{and } Q_2 = \frac{R_2 - R_1}{2} + a \quad (4.16)$$

Thus

$$P_p = 2 \mu_0 R_2 \ln \left( 1 + \frac{2a}{(R_2 - R_1)} \right) \quad (4.17)$$

and the total leakage flux is

$$\Phi_L = NI \mu_0 \left[ \frac{d}{\ln(R_2/R_1)} + 2R_2 \ln \left( 1 + \frac{2a}{(R_2 - R_1)} \right) \right] \quad (4.18)$$

The total flux at the bottom of the centre pole can be found by adding 4.7 and 4.18 and the maximum flux density.

$$B_{\text{Max}} = \frac{\Phi_T}{\pi R_1^2} \quad (4.19)$$

If  $B_{\max}$  is less than  $2T$  this linear analysis is valid as most of the m.m.f drop occurs in the air gap. However as  $B_{\max}$  approaches  $2T$  the flux generated is reduced because of saturation effects in the magnet core.

The actuator inductance can be broken into two components  
mutual inductance  $L_m = \frac{N \Phi_M}{I}$  (4.20)

and leakage inductance  $L_L = \frac{N \Phi_L}{I}$  (4.21)

#### 4.4 Actuator Heating

Assuming that the slot is totally filled with conductor the resistance of an element  $\delta R$  wide and  $d$  deep at a radius  $R$  from the centre of the magnet is

$$R_s = \frac{2 \pi \rho R}{\int_{R_1}^{R_2} 2d \delta R} \quad (4.22)$$

$\rho$  is the resistivity of the conductor.

The total resistance is

$$R_s = \frac{2 \pi \rho}{d \ln (R_2/R_1)} \quad (4.23)$$

and the power dissipated in the magnets

$$P_d = \frac{(NI)^2}{d \ln (R_2/R_1)} \frac{2 \pi \rho}{d \ln (R_2/R_1)} \quad (4.24)$$

Aluminium foil or copper wire can be used for the windings. In a production actuator aluminium would probably be preferable on grounds of cost and weight. However for a single vehicle copper wire was used as it was more readily available in the quantities required. As the slot is not completely filled with conductor a packing factor is required in the calculation of resistance and power, which experience has shown to be .75.



A dissipation constant  $K_d$  of 20 watts/m<sup>2</sup>/°K, under forced convection was measured in (59) for a pair of experimental magnets. Therefore the temperature rise in the magnets can be calculated from

$$\Delta T = \frac{P_d}{K_d A_s} \quad (4.25)$$

However as the resistivity of the copper increases with temperature.

$$\Delta T = \frac{P_d}{K_d A_s - K_T P_d} \quad (4.26)$$

$P_d$  is the power dissipation at the nominal temperature and  $K_T$  the temperature coefficient of the conductor.

#### 4.5 Actuator Design

Actuator design is constrained by practical considerations such as:-

1. The space envelope available
2. Power dissipation
3. The practical V.A. rating of power electronics
4. Maximum temperature of the actuator coils.

The space envelope constrained the actuators to a maximum height of 350 mm and a maximum diameter of 300 mm.

A continuous power dissipation of 3.5 kW for the four actuators was aimed for as representing 10% of the installed auxiliary power of 35 kW for the Mk III Coach.

Actuator current and voltage ratings were chosen to suit an existing power amplifier of proven reliability. The V.A. rating is higher than may be expected from the theoretical investigation owing to shortcomings encountered with the prototype system running out of forcing voltage (60). See Section 8.1.

The actuators were designed to generate a peak force of 10 kN (at 50 amps) from experience with other active suspension systems. The actuator parameters are given in Table 4.1. and Fig. 4.5 shows a cross section of the actuator.

Table 4.1 Actuator Parameters

Overall Height	350 mm
Diameter	300 mm
Centre Pole Diameter	160 mm
Slot Width	70 mm
Slot Depth	48 mm
Nominal Air Gap	30 mm
No of Turns/Coil	700
Resistance (20°C) Measured/Coil	3.2 ohms
Resistance (124°C)/Coil	4.5 ohms
$\Delta T$ at 40°C Ambient	84°C
Continuous Current	20 amps
Maximum Voltage	300 volts
Peak Current	50 amps
Peak Force	10.3 kN
Mutual Inductance $L_M$	.15H
Leakage Inductance $L_L$	.10H
Weight	)150 kg Copper Coils
	)112 kg Al Coils

Force measurements made on the prototype system showed reasonable agreement between the predicted force and current. However flux measurements Fig. 4.6 showed a marked discrepancy between the theoretical and measured flux densities along the centre line between two pairs of magnets. This is because the model of the magnets was too simple in assuming that flux flowed between the two outer poles. In practice there were alternative flux paths through the test frame and between the backs of the magnets which have lower reluctance than the path between the outer poles.

## DIMENSIONS

HEIGHT 350 mm

DIAMETER 300 mm

WEIGHT 150 kg

FORCE  $\pm 12$  kN

RESISTANCE 1.6 ohms (COLD)

RESISTANCE 2.25 ohms (HOT)

MUTUAL INDUCTANCE 15H

LEAKAGE INDUCTANCE 10H

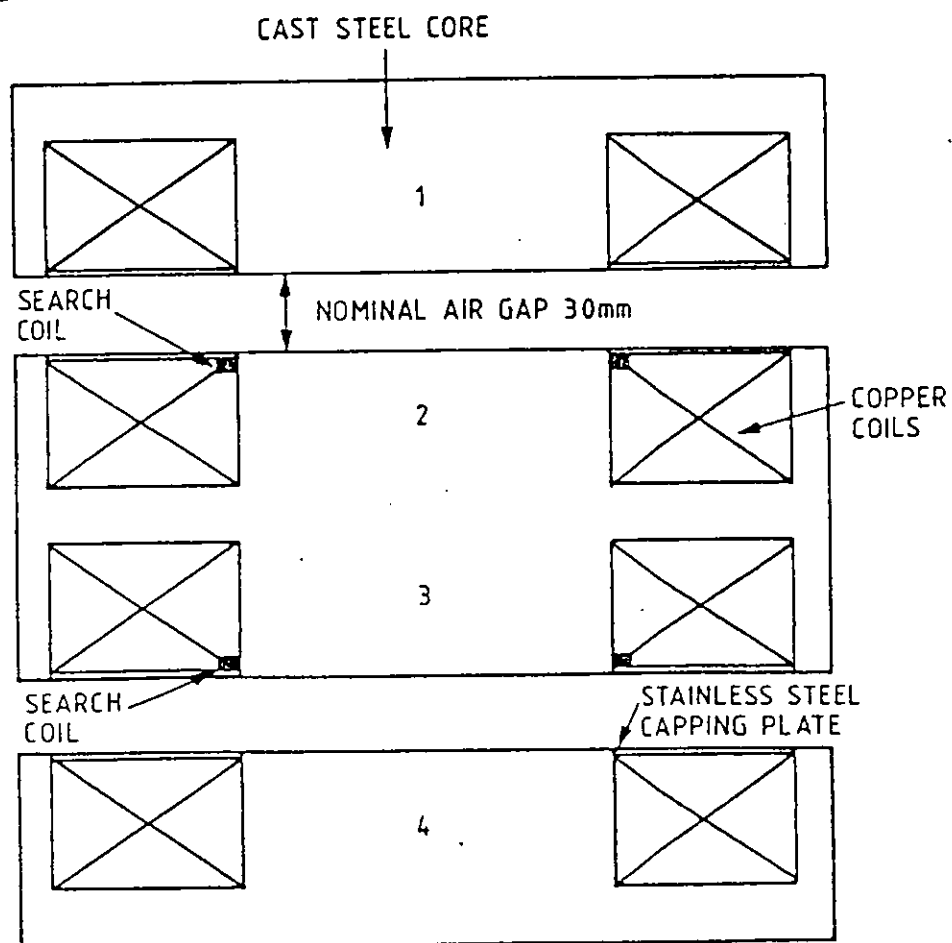


FIG. 4.5 ACTUATOR CROSS SECTION

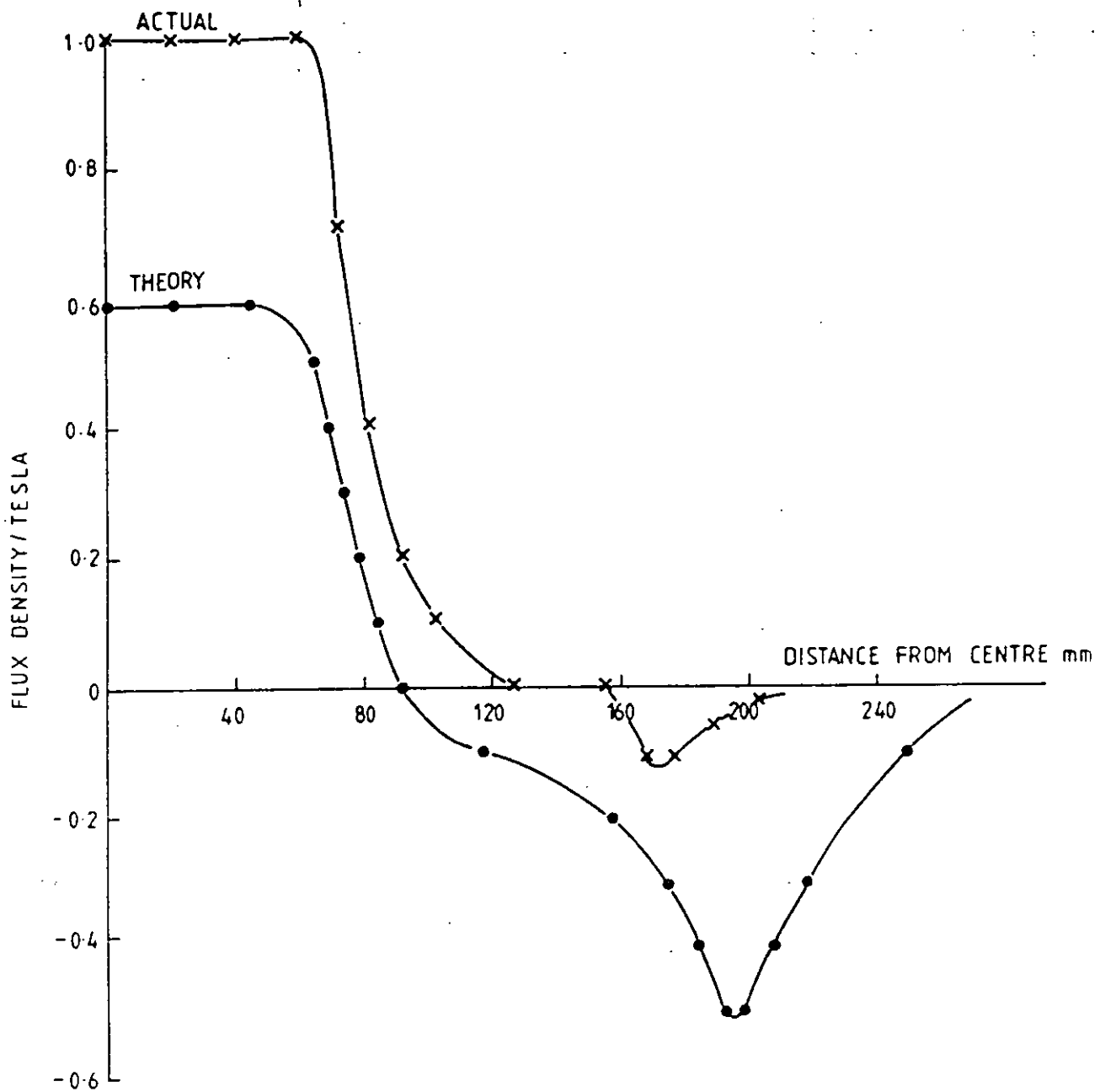


FIG. 4.6 FLUX DISTRIBUTION IN MAGNET AIRGAP

In the limit this is equivalent to shorting the outer poles and halving the path length which, from (4.2) will increase the force per unit area by a factor of 4 for a given current. If the outer poles are shorted they will generate no force, hence the effective area will be reduced. The flux density in the centre pole will also be increased causing saturation to occur at a lower current.

The idealised actuator will generate a force of 10.3 kN from a m.m.f of 35000 AT. Shorting the outer poles of the actuator causes saturation at 32000 AT, however as the actuator will produce 12 kN in this condition, it would be more efficient. This is not particularly easy to achieve owing to the congested nature of the bogie and the need to allow free lateral and longitudinal movement between the sections of the actuator. Restricted access has prevented flux measurements being made on the vehicle. Consequently the more conservative actuator performance has been assumed on the grounds of prudence.

## 4.6

Eddy Currents

The actuator cores are cast in magnetic steel and given their size, there could be quite significant eddy currents in the centre pole which need to be accounted for in the theoretical model.

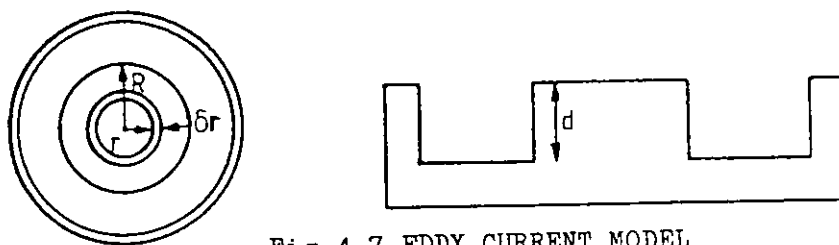


Fig 4.7 EDDY CURRENT MODEL

Consider an annulus in the centre pole  $\delta r$  wide and radius  $r$ . The resistance of the annulus will be:-

$$r_e = \frac{2 \pi r \rho_s}{d \delta r} \quad (4.27)$$

$\rho_s$  is the resistivity of steel.

It will be shown later that most of the flux generated by the magnets varies with a frequency of around 1 Hz. Thus, as a first approximation, the flux distribution can be assumed to be uniform over the pole and the flux linked by the element is:-

$$\Phi = B \pi r^2 \quad (4.28)$$

B is the flux density.

As the voltage induced by the flux is  $\frac{d\Phi}{dt}$

the power loss in the element due to the eddy current will be:-

$$\frac{(d\Phi)^2}{(dt)^2} = \frac{(dB)^2}{(dt)^2} \frac{\pi^2 r^4 d\delta r}{2\pi \rho_s r} \quad (4.29)$$

$r_e$

Integrating over the centre pole the power loss is:-

$$P_e = \frac{(dB)^2}{(dt)^2} \int_0^R \frac{\pi dr^3}{\rho_s^2} \delta r \quad (4.30)$$

$$= \frac{(dB)^2}{(dt)^2} \frac{\pi d R^4}{8\rho_s} \quad (4.31)$$

The mean r.m.s flux density along the height of the pole is .5T. Thus if the flux change is approximated to a 1 Hz sine wave.

$$B = B_M \text{ Sin } (\omega t) \quad (4.32)$$

$$\text{Then } \left( \frac{dB}{dt} \right)^2 = (\omega B_M \cos(\omega t))^2$$

$$\text{Over 1 cycle } (\cos(\omega t))^2 = 0.5$$

From the actuator geometry in Table 4.1 the power dissipation due to eddy currents is 31 watts which is small compared with the 650 watts dissipated in the magnet windings.

## 4.7

Linearisation of Actuator Characteristics

Section 4.3 showed that the actuator force is non-linear and, as the method of analysis described in Chapter 2 is linear, some method must be found of linearising the actuator characteristics.

Equation (4.2) shows that the actuator force can be described by the equation:-

$$F = K \frac{I^2}{G^2} \quad (4.33)$$

where K is constant

The change of force

$$\delta F = \frac{2 KI \delta I}{G^2} - 2 \frac{KI^2 \delta G}{G^3} \quad (4.34)$$

If the nominal operating force is  $F_0$  at a current  $I_0$  and air gap  $G_0$  (4.34) can be replaced by the linearised equation.

$$F = K_I I + K_g g \quad (4.35)$$

Where the current constant

$$K_I = \frac{2F_0}{I_0} \quad (4.36)$$

and the negative stiffness of the actuator

$$K_g = \frac{-2F_0}{G_0} \quad (4.37)$$

$$\text{The change in gap } g = z - z_b \quad (4.38)$$

The nominal force  $F_0$  is taken as the r.m.s actuator force.

An alternative method of linearisation follows the lines proposed in (61). In this method it is assumed that the actuator applies a sinusoidal force to the vehicle with an r.m.s equivalent to the random r.m.s force.

The force generated by the actuator

$$F = (\text{sign } I) K_{I2} I^2 \quad (4.39)$$

Where  $K_{I2}$  is a current constant.

For a sine wave with amplitude  $F_p$

$$(\text{sign } I) K_{I2} I^2 = F_p \sin \theta \quad (4.40)$$

so that

$$I = (\text{sign } I) \sqrt{\frac{F_p |\sin \theta|}{K_{I2}}} \quad (4.41)$$

The mean square current over 1 cycle

$$I^2 = \frac{1}{2} \left[ \int_0^\pi \frac{F_p}{K_{I2}} \sin \theta d\theta + \int_\pi^{2\pi} \frac{F_p}{K_{I2}} \sin \theta d\theta \right] \quad (4.42)$$



$$= \frac{1}{2} \left( \left[ \frac{-F_p \cos \theta}{K_{I2}} \right]_0^\pi + \left[ \frac{-F_p \cos \theta}{K_{I2}} \right]_\pi^{2\pi} \right)$$

$$= \frac{F_p}{K_{I2}} \quad (4.43)$$

Then

$$I_{rms} = \sqrt{\frac{F_p}{\pi K_{I2}}} = \sqrt{\frac{\sqrt{2} F_{rms}}{\pi K_{I2}}} \quad (4.44)$$

Taking the force constant

$$K_I = \frac{F_{rms}}{I_{rms}} \quad (4.45)$$

$$K_I = \sqrt{\frac{F_{rms} K_{I2}}{\sqrt{2}}} = 1.49 \sqrt{F_{rms} K_{I2}} \quad (4.46)$$

for comparison (4.36) gives

$$K_I = 2 \sqrt{F_{rms} K_{I2}} \quad (4.47)$$

The second method estimates the constant at 75% of the first.

Using the two methods produces a range of  $K_I$  between 112 N/A and 200 N/A depending on whether the outer poles are shorted or not and on the median current. Thus a compromise value of 150 N/A has been used.

A linearised block diagram for the actuators is given in Fig. 4.8.

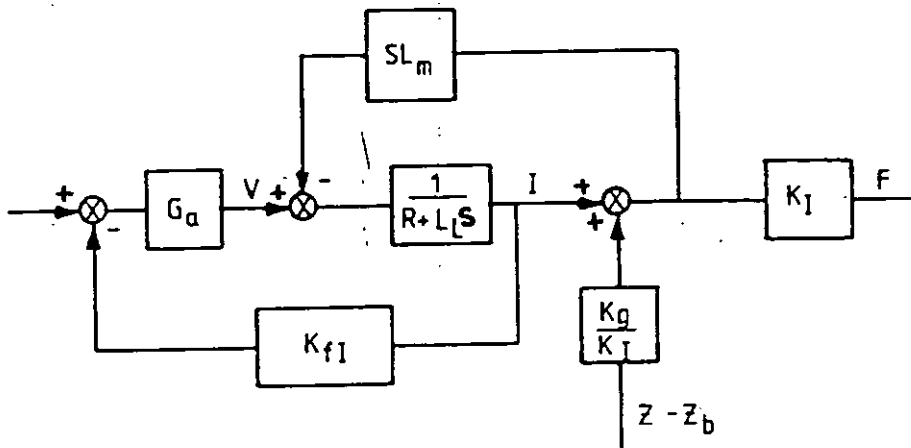


Fig. 4.8 MAGNETIC ACTUATOR

The representation includes the amplifiers, which have built in current feed back ( $K_{fI}$ ), and a forward gain  $G_a$ .

## CHAPTER 5

CLASSICAL CONTROL SYSTEM DESIGN

All the active suspensions were designed for a laden vehicle as this was anticipated to have the highest power consumption.

The classical control systems are modular so that the total system can be designed as a number of simple units. These are essentially split into two parts: a set of inner flux control loops around the actuators to control the actuator force, and a set of outer control loops to control the dynamic response of the vehicle.

### 5.1 Force Control Loop

In chapter 4 actuator force was shown to be a non-linear function of the airgap between magnets and the current. In order to provide smooth control of the actuator a force control loop is placed around the actuator and power amplifier. Past experience has shown that flux provides a very effective (if non-linear) measure of force. This is measured indirectly by means of search coils wound around the centre poles of the bogie-mounted magnets (2 and 3) in Fig 4.5. The reason for using search coils is that they are cheap, simple, robust and have a very good signal to noise ratio. The only sensible alternative would be a Hall effect devices. However they would intrude on the air space reducing the dynamic movement available, added to which they are not as robust as search coils and are prone to drift. Figure 5.1 shows the flux control loop block diagram.

Pulse width modulated power amplifiers, represented by a gain  $G_a$ , drive the actuators. The effective output voltage of the amplifiers is proportional to the mark period ratio which is itself proportional to the demand voltage. Current control is provided via the current feedback loop, gain  $K_{FI}$ .

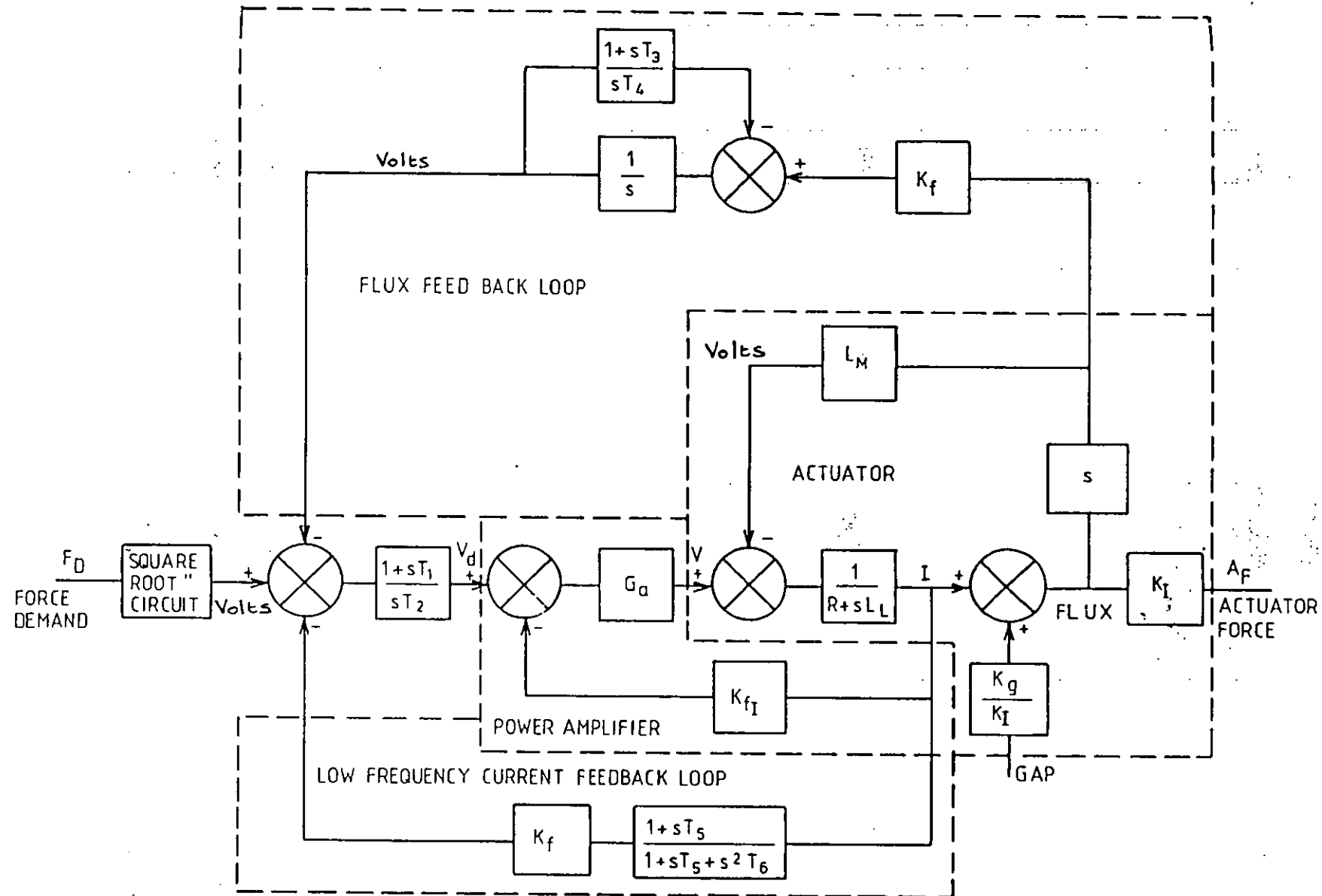


FIG.5-1.ACTUATOR CONTROL.

Flux is controlled by the feedback loop, gain  $K_f$ . As the search coils measure rate of change of flux the output from the coils has to be integrated ( $1/s$ ) to measure the flux. In order to prevent the integrator from drifting a second integrator  $((1 + sT_3)/sT_4)$  is placed in feedback around the flux integrator. Because this leaves the control loop with no feedback at low frequencies, an additional low frequency current feedback is included with filter transfer function:-  $(1 + sT_5)/(1 + sT_5 + s^2T_6)$ .

The gains are selected so that transfer function of the flux integrator and low frequency current filters complement each other:

$$\frac{1 + sT_5}{1 + sT_5 + s^2T_6} + \frac{s^2T_4}{1 + sT_3 + s^2T_4} = 1 \quad (5.1)$$

Cross-over between the flux and current loops occurs at  $0.5 H_z$ . Actuator force will change with air gap at low frequencies but because the change does not occur very quickly the resulting non-linearity is controlled by the outer control loops.

Proportional plus integral action is provided by the term  $((1 + sT_1)/sT_2)$ . A "square root" circuit is provided on the input demand signal  $F_D$  so that the force developed  $A_F$  is proportional to  $F_D$ .

A first estimate of the dynamic performance of the actuators was made using equation (5.2).

$$F/F_D = K_I(1 + T_1s)/K_f(1 + T_1s + (L_L + L_M)T_2s^2/K_F G_a) \quad (5.2)$$

$T_1$  and  $T_2$  were selected to produce poles at 11 Hz with 70% damping. The open loop response of the actuators, installed in the vehicle, was then computed to give a better estimate of the performance Fig. 5.2. This shows that the response approximates to a single pole with a natural frequency of 16 Hz and should produce a flat force response in the 0-10 Hz frequency regime which predominantly determines the ride of the vehicle.

## 5.2 Main Control Loops

Given the wide bandwidth of the actuators the dynamic performance of the vehicle can be determined by the main outer control loops. Two forms of control loop have been considered.

- 1) Absolute (Sky hook) damping
- 2) Position Control

### 5.2.1 Absolute (Sky Hook) Damping

Absolute damping, sometimes referred to as "sky hook" damper, offers the simplest form of active suspension. The damping force is generated relative to an absolute datum rather than a relative datum, as it is with a conventional passive suspension Fig 5.3. The transmissibility of the passive suspension is given by:-

$$\frac{z}{z_t} = \frac{1 + \frac{C}{K} s}{1 + \frac{C}{K} s + \frac{Ms^2}{K}} \quad (5.3)$$

High frequency transmissibility is

$$\frac{z}{z_t} \doteq \frac{C}{Ms} \quad (5.4)$$

and increases with the damping rate. For the sky hook damper the transmissibility is given by:-

$$\frac{z}{z_t} = \frac{1}{1 + \frac{C}{K} s + \frac{Ms^2}{K}} \quad (5.5)$$

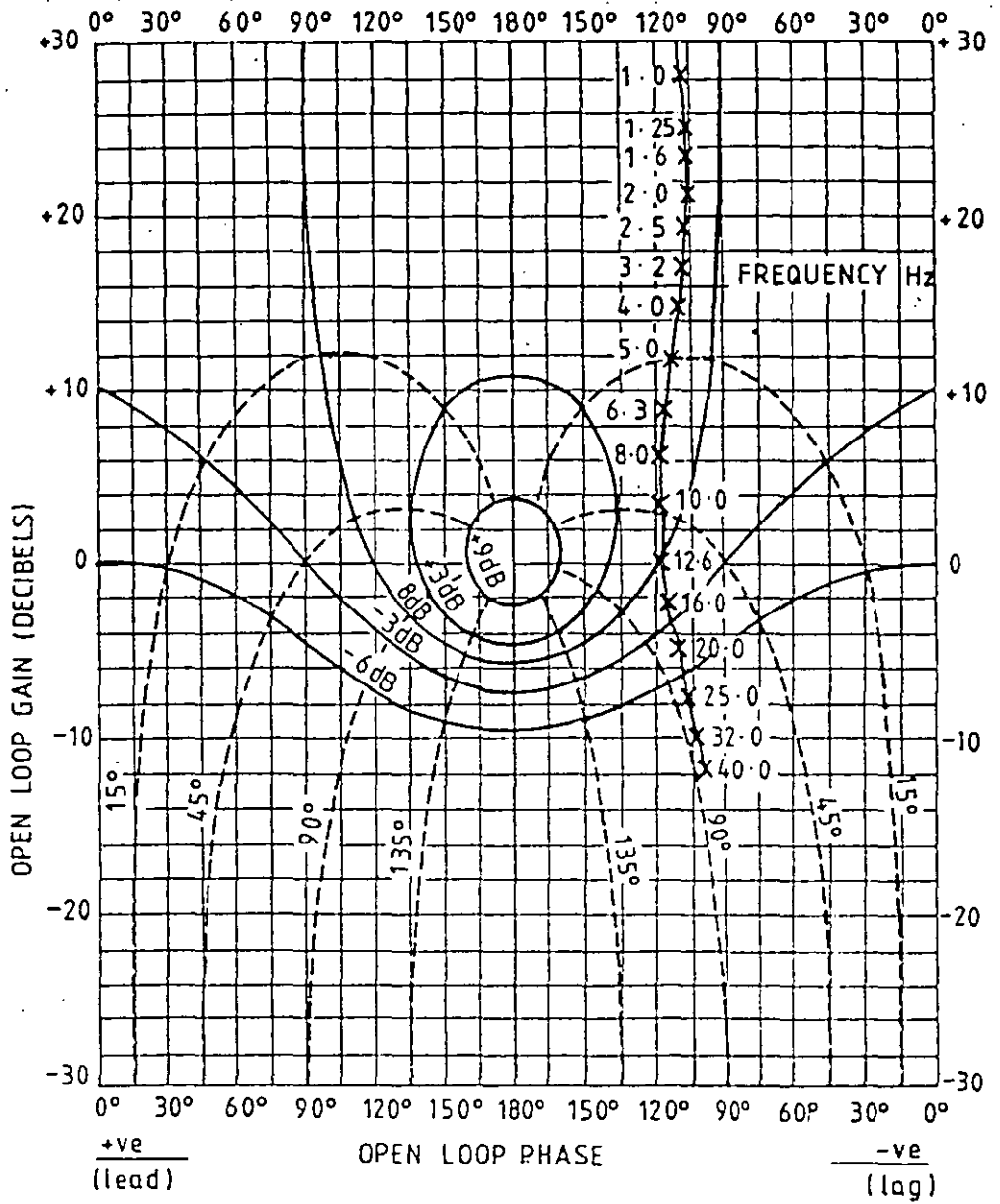


FIG.5.2 FORCE CONTROL OPEN LOOP RESPONSE

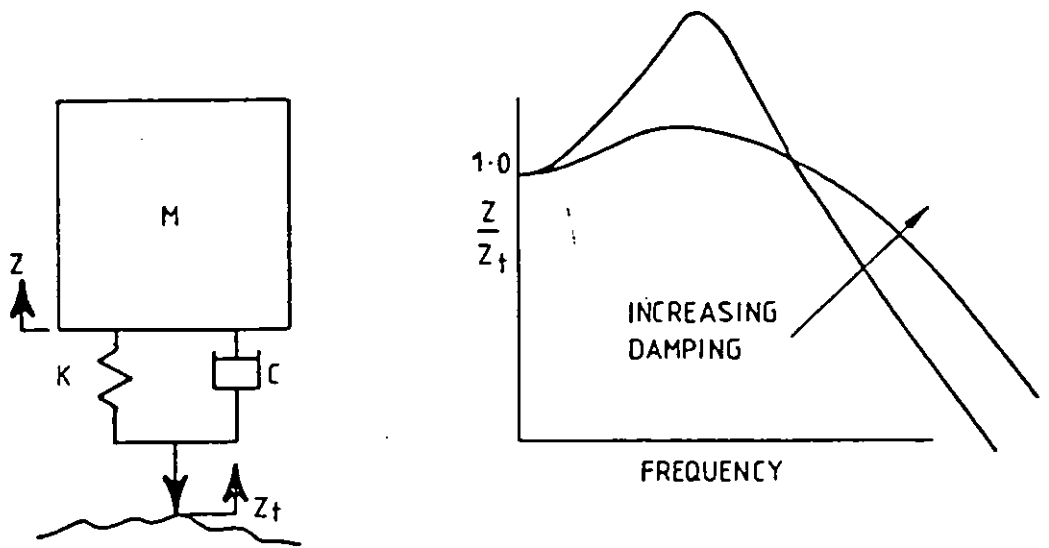


FIG. 5-3a. RELATIVE DAMPING

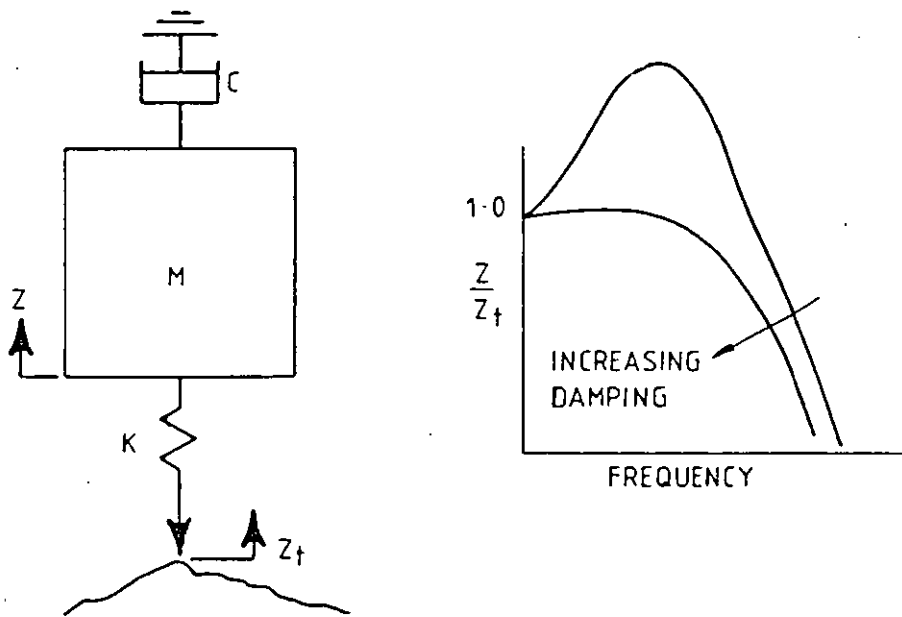


FIG. 5-3b. SKY HOOK DAMPING



and the high frequency transmissibility

$$\frac{z}{z_t} \doteq \frac{K}{Ms^2} \quad (5.6)$$

Not only is this independent of the damping rate, but it attenuates at 12dB/octave, compared with the 6dB/octave of equation (5.4). Thus with the sky hook damper the damping rate does not have to be a compromise between reducing the resonance peaks and the high frequency transmission, as it does with the relative damper.

In order to provide absolute damping it is necessary to provide a force demand signal ( $F_D$  in Fig 5.1) to the actuator which is proportional to the absolute vertical velocity of the vehicle. This can be provided by integrating the output of a vertical accelerometer. The resulting velocity signal has to be rolled off at low frequencies to avoid problems with drift. The cut-off frequency was chosen to be 0.2 Hz since there is no significant action required of the active system below this frequency.

Rather than fitting an accelerometer to each corner of the vehicle and allowing it to drive the associated actuator, the acceleration signals were summed to resolve the orthogonal modes of vibration (bounce, pitch and roll). The resulting signals were then integrated to form bounce, pitch and roll velocity demand signals. These were summed as demands for each actuator so that the forces were applied in a modal sense. Fig 5.4 shows the control system block diagram for the pitch and bounce modes. This method of operation prevents interaction between actuators. It also allows the flexible body modes, which the active suspension tends to excite, to be treated more easily as they can usually be associated with one of the rigid modes of vibration and thus have to be only dealt with once rather than four times.

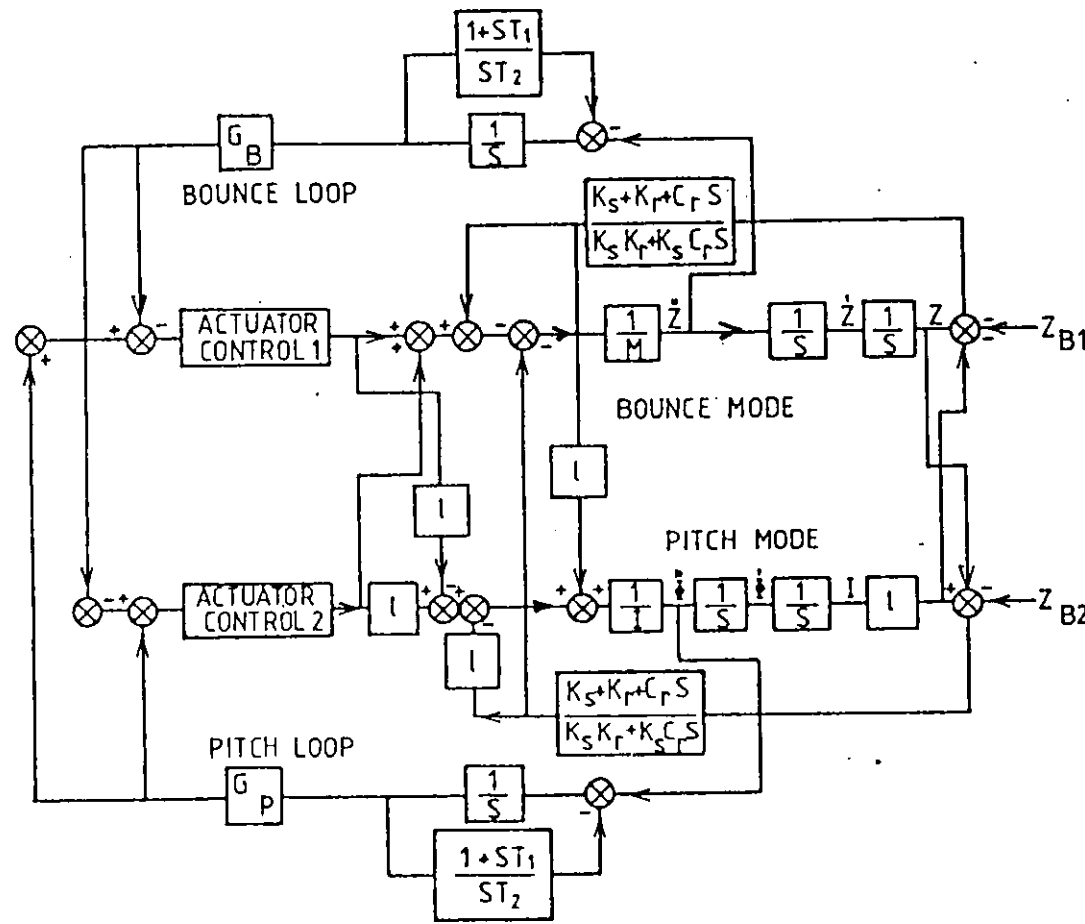


FIG. 5.4 ABSOLUTE DAMPING CONTROL BLOCK DIAGRAM

Because the modes of vibration were resolved independently the damping rate could be selected, to optimise damping in each mode, by the loop gains  $G_B$  and  $G_P$ . If the inner force control loops of the actuators are assumed to be perfect then it can be shown that:-

$$z/z_b = 1/(1 + (4 G_B/K_F K)s + (M/K)s^2) \quad (5.7)$$

Where

$$K = 4 (K_a + K_S K_R (K_S + K_R))$$

And the approximate pitch transfer function:-

$$\phi/\phi_b = 1/(1 + 4G_P/K_F K l^2)s + (4I/K l^2)s^2) \quad (5.8)$$

$G_B$  and  $G_P$  were selected to give around 70% damping. The controlled eigen values are given in table 5.1.

Table 5.1 Absolute Damping Eigen-Values

	Passive		Absolute Damping	
	Damping	Frequency	Damping	Frequency
Body Bounce	16%	1.0 Hz	85%	1.3 Hz
	100%	1.7 Hz	100%	1.0 Hz
Body Pitch	19%	1.4 Hz	60%	1.5 Hz
	100%	1.6 Hz	100%	1.3 Hz
Bogie Bounce	39%	5.8 Hz	40%	5.7 Hz
Bogie Pitch	55%	8.7 Hz	55%	8.7 Hz
Control Loop			59%	10.7 Hz

It will be noted that the absolute damping control system produces the desired increase in rigid body damping. There are also fairly significant shifts in frequency because of the change in emphasis between the real and complex poles. These eigen-values suggest that the gain in the pitch mode ought to be increased by a small amount and that in the bounce mode reduced.

Figs (5.5 and 5.6) show the open loop responses of the pitch and bounce modes. These show that the control loops are extremely well conditioned and that large increases could be made in the gain without destabilising the control systems. Examination of the closed loop phase lags show that they should not produce a degradation in performance below 5-6 Hz. While the theoretical responses are probably on the conservative side past experience has shown that it is better to err on the safe side.

## 5.2.2

Position Control

The position control system is the direct descendant of the BR Maglev Suspension (7, 8, 9, 10) and aims at resolving the compromise which is inherent in any suspension design, that of achieving the minimum acceleration without excessive suspension displacements. On a railway vehicle the body is required to follow the bogie at low frequencies, in order to get over hills in the vertical plane or through curves in the lateral plane, which requires the suspension displacement to be kept constant. At high frequencies it is required to decouple the body from the bogie, so that it is isolated from the high frequency track inputs which give rise to high accelerations.

Fig 5.7 shows how this can be achieved in practice with a unicycle model. Suspension displacement is kept constant at low frequencies by measuring the displacement and feeding the low frequency component to the actuators as a force demand, so that they oppose changes in suspension displacement. The high frequency component of the displacement is removed by means of a low pass filter. To isolate the vehicle from track inputs the absolute position in space must be kept constant. This is achieved by feeding the absolute position of the vehicle to the actuators as a force demand, so that it opposes changes in absolute position. In order to prevent interaction between the absolute and relative position signals, the absolute position signal is filtered by a high pass filter which complements the low pass filter on the relative position signal i.e.  $HP = 1 - LP$ . Dynamic

OPEN LOOP GAIN  
(DECIBELS)

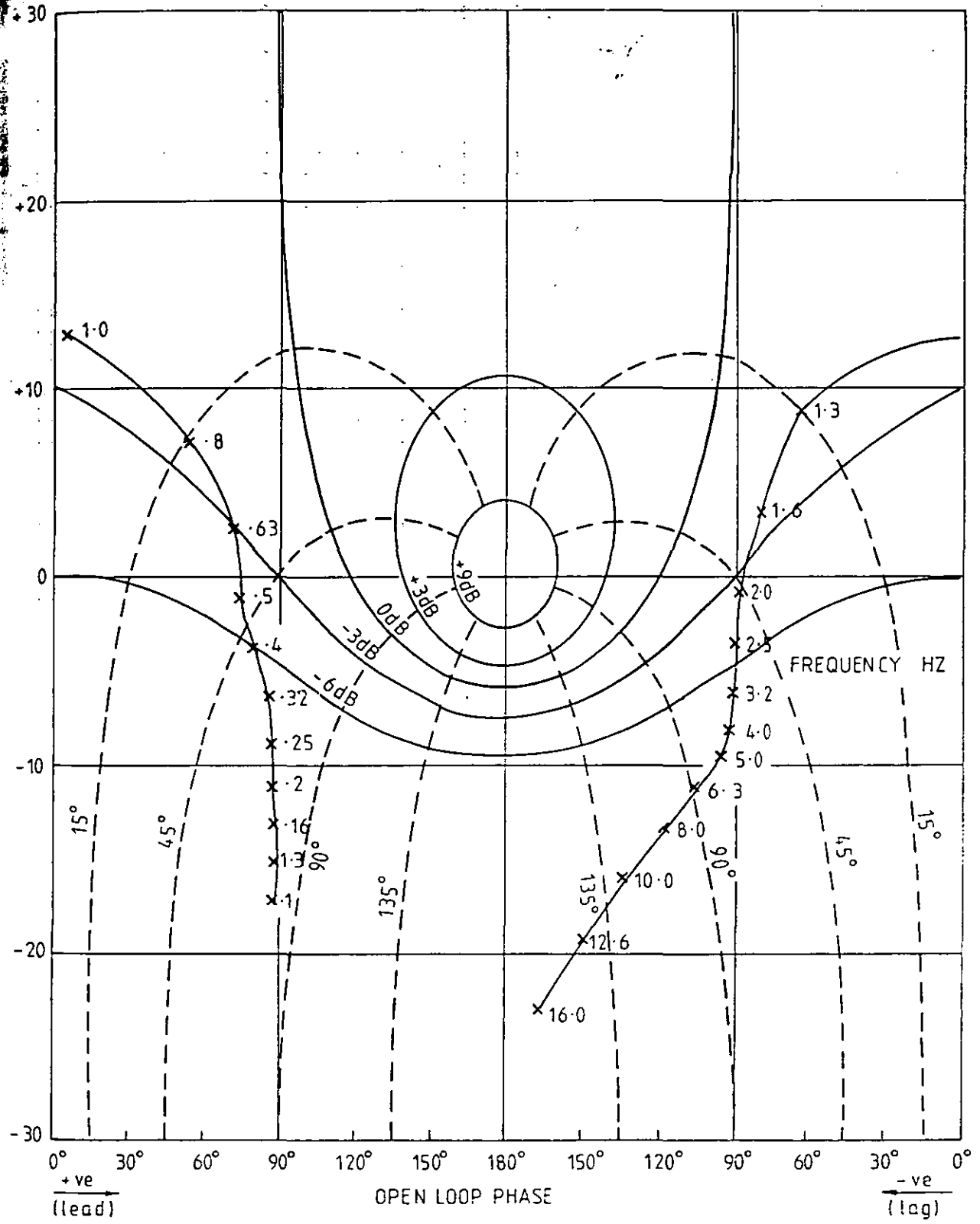


FIG. 5.5 MK III COACH BOUNCE CONTROL LOOP ABSOLUTE  
DAMPING OPEN LOOP RESPONSE

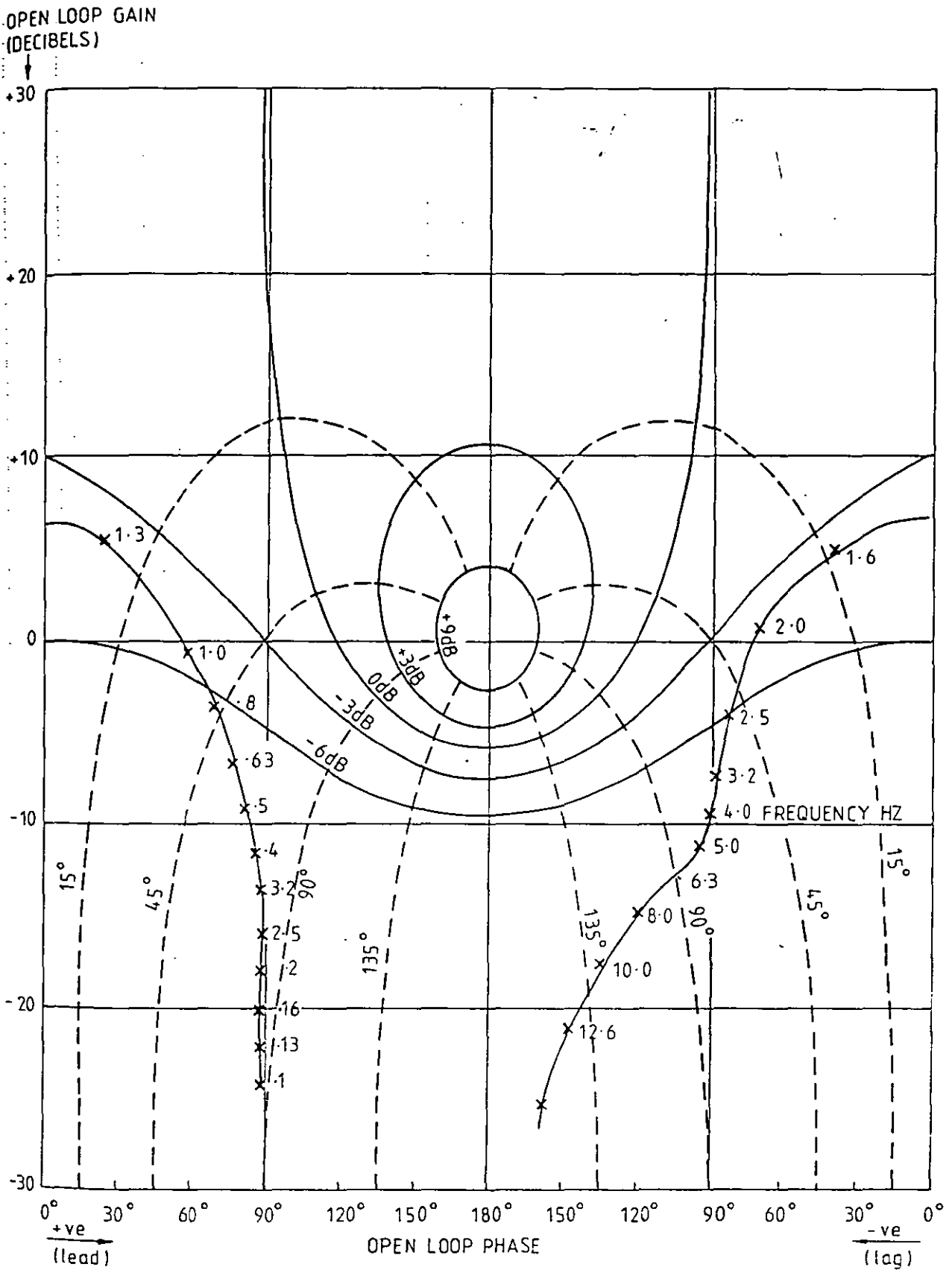


FIG. 5-6 MK III COACH PITCH CONTROL LOOP ABSOLUTE  
DAMPING OPEN LOOP RESPONSE

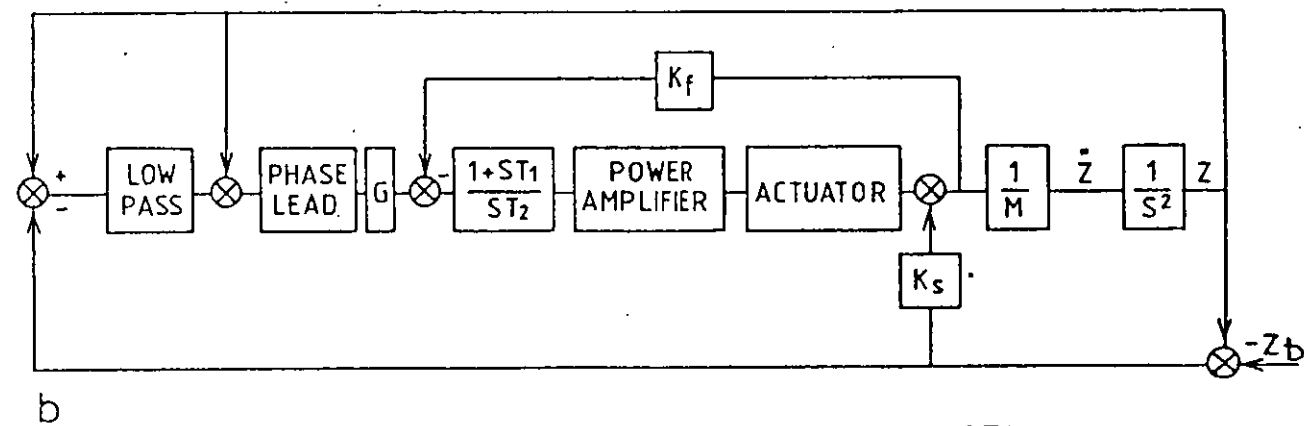
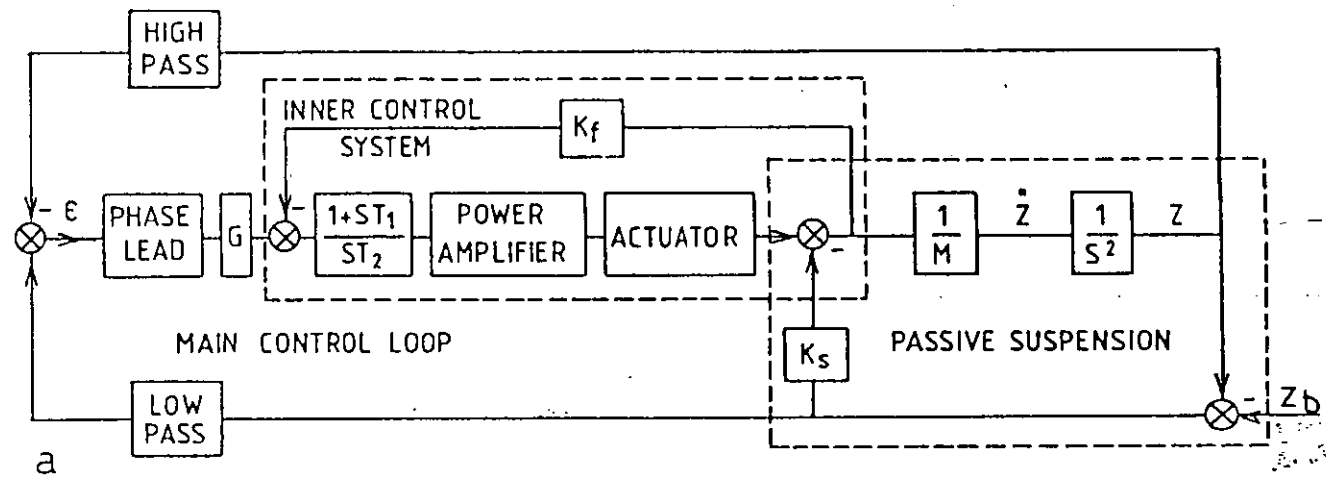


FIG. 5.7 POSITION CONTROL SYSTEM

performance is now determined by the pair of filters. Absolute position is measured by the double integration of an acceleration signal. Low frequency drift in the integrators is prevented by an integrator in feedback. Although this rolls off the absolute position signal below 0.2 Hz the effects are of little significance because the signal also pass through the high pass filter which rolls off at a higher frequency.

An alternative configuration of the control system is given in Fig 5.7b in which the absolute position signal is subtracted from the relative position signal, giving in effect the absolute position of the bogie. This is then filtered by a low pass filter. The absolute position signal is subtracted from the filtered bogie signal and the error signal used as a force demand. Thus the actuator applies a force to the vehicle which causes it to follow the bogie at low frequencies, with the response determined by the filter characteristics.

Control is applied to the vehicle modes of vibration, rather than each actuator having its own independent control system (Fig 5.8). With a position control system in which the vertical plane is controlled by four actuators some form of modal control is essential as in most cases only three of the relative displacement transducers can be zero at any one time causing independent actuators to fight each other. This form of modal control allows the suspension performance to be tailored to produce the greatest benefit for the smallest expenditure in power. Ride at the vehicle ends is inevitably worse than it is at the centre of the vehicle so that more effort should be put into reducing the pitch acceleration. This is quite easy to achieve with modal control. With independent controllers any improvements in ride will affect both modes equally.

Relative and absolute positions are measured by transducers at each corner of the vehicle. The transducer outputs are summed to form the bounce mode and subtracted to form the pitch mode.



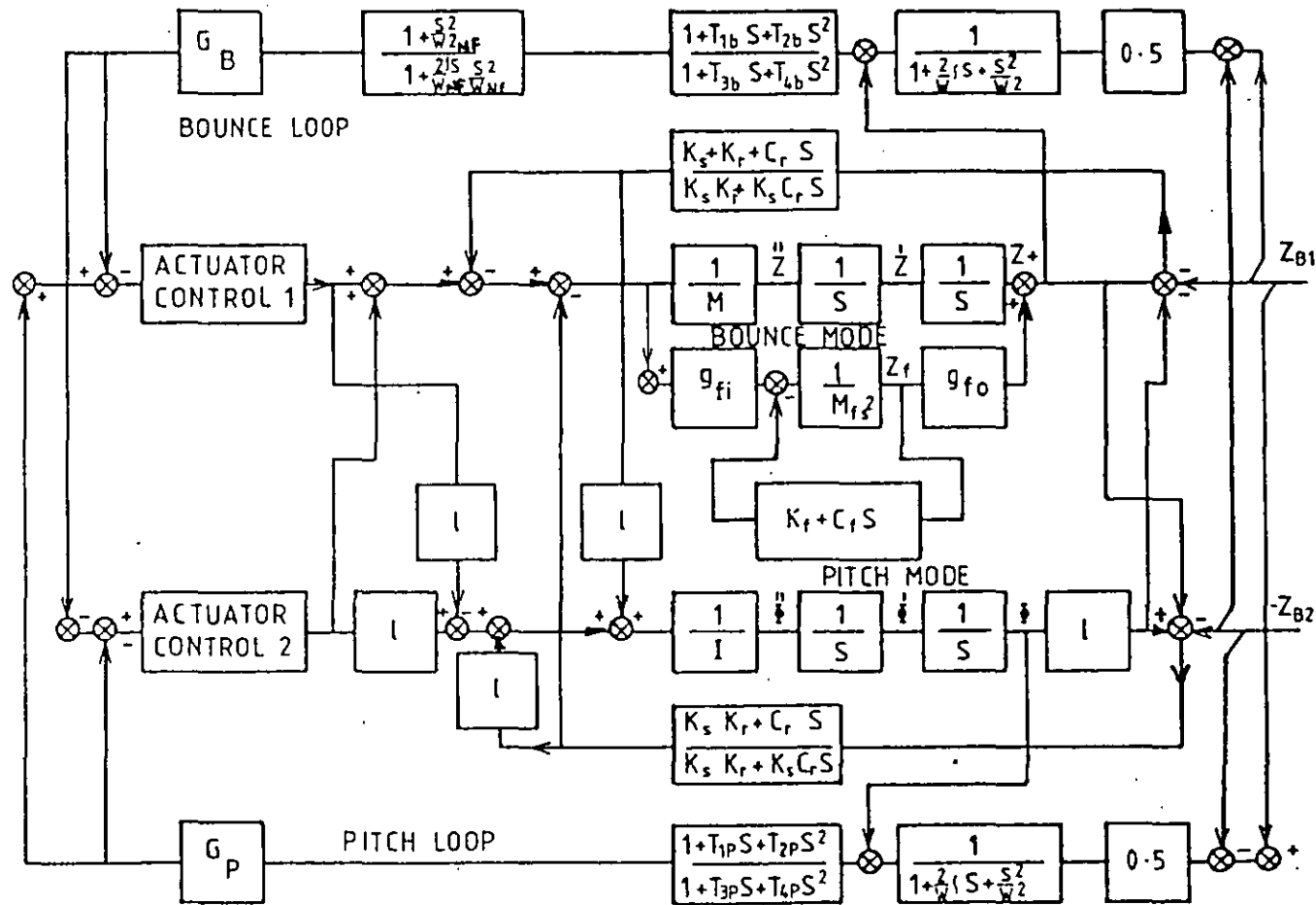


FIG.5.8 POSITION CONTROL BLOCK DIAGRAM

Both the pitch and bounce filters were selected from experience to be 1 Hz Butterworth filters ( $1/(1 + .22s + .025s^2)$ ). These have the same transfer function as the "sky hook" damper shown in Fig. 5.3. However the frequency of the pitch filter has been reduced compared with the rigid body frequency (1.4 Hz in table 3.1).

Main loop bandwidths should be at least twice the filter frequency. These are determined by the main loop gains  $G_B$  and  $G_P$  and can be calculated approximately from the expressions:-

$$\omega_B = \sqrt{\frac{4K_I G_B}{K_f M}} \quad (5.9)$$

$$\omega_P = \sqrt{\frac{4I K_I G_P}{K_f I}} \quad (5.10)$$

Phase compensation is provided by a complex lead/lag network of the form

$$(1 + 2\zeta s / \omega_1 + s^2 / \omega_1^2)(1 + 2\zeta s / \omega_2 + s^2 / \omega_2^2)$$

as this gives more phase lead, for a given high frequency gain, than a simple lead/lag network such as  $(1 + s/\omega_1)/(1 + s/\omega_2)$ . For a 20 dB high frequency gain the maximum lead is  $80^\circ$  for the complex network and  $55^\circ$  for the simple network.

Initial values of  $G_B$  and  $G_P$  were selected to give  $\omega_B$  and  $\omega_P$  of around 25 rad/s (4 Hz) and a maximum phase lead at 5 Hz. Maximum phase lead is given by:-

$$\omega_{\max} = \sqrt{\omega_1^2 \omega_2^2} \quad (5.11)$$

The open loop pitch response (Fig 5.9) shows that the gain is about 10 dB higher than desirable. For stability the control system should have a 10 dB gain margin i.e. the gain where the open loop response has 180° phase lag should be at least - 10 dB and 45° phase margin (i.e. when the open loop response has 0 dB gain it must not have more than 135° of phase lag). Reducing the gain by 12 dB gives more than adequate margins and a closed loop -3dB gain at 3 Hz. It is also worth noting that the open loop response crosses the line showing 90° closed loop phase lag at 6.5 Hz. The significance of this is that when the controller has more than 90° lag the actuators begin to produce a force with a component in phase with the input, which degrades the ride. Therefore with this control configuration the ride is not degraded until frequencies in excess of the bogie bounce frequency.

### 5.2.3 Flexible Body Mode

Fig 5.8 includes the primary bending mode. As it is symmetrical it is only affected by the bounce control loop. Two gain factors are shown,  $g_{fi}$  relating to the position of the actuators along the flexible body mode, and  $g_{fo}$  relating to the position of the accelerometers (used to measure absolute position) along the flexible mode. The gain factors are calculated as  $g_{fx} = z_{fx}/z_f$ .

The flexible body mode is at a much higher frequency than the rigid body mode (10 Hz compare with 1 Hz) and the high frequency transmissibility measured by the accelerometers can be approximated by:-

$$\frac{z_m}{F_a} = \frac{(K_f + C_f s + (M + g_{fi} f_{fo} M_f) s^2) s^2}{(M K_f s^2 + M C_f s^3 + M M_f s^4)} \quad (5.10)$$

$$z_m = z + z_f g_{fo}$$

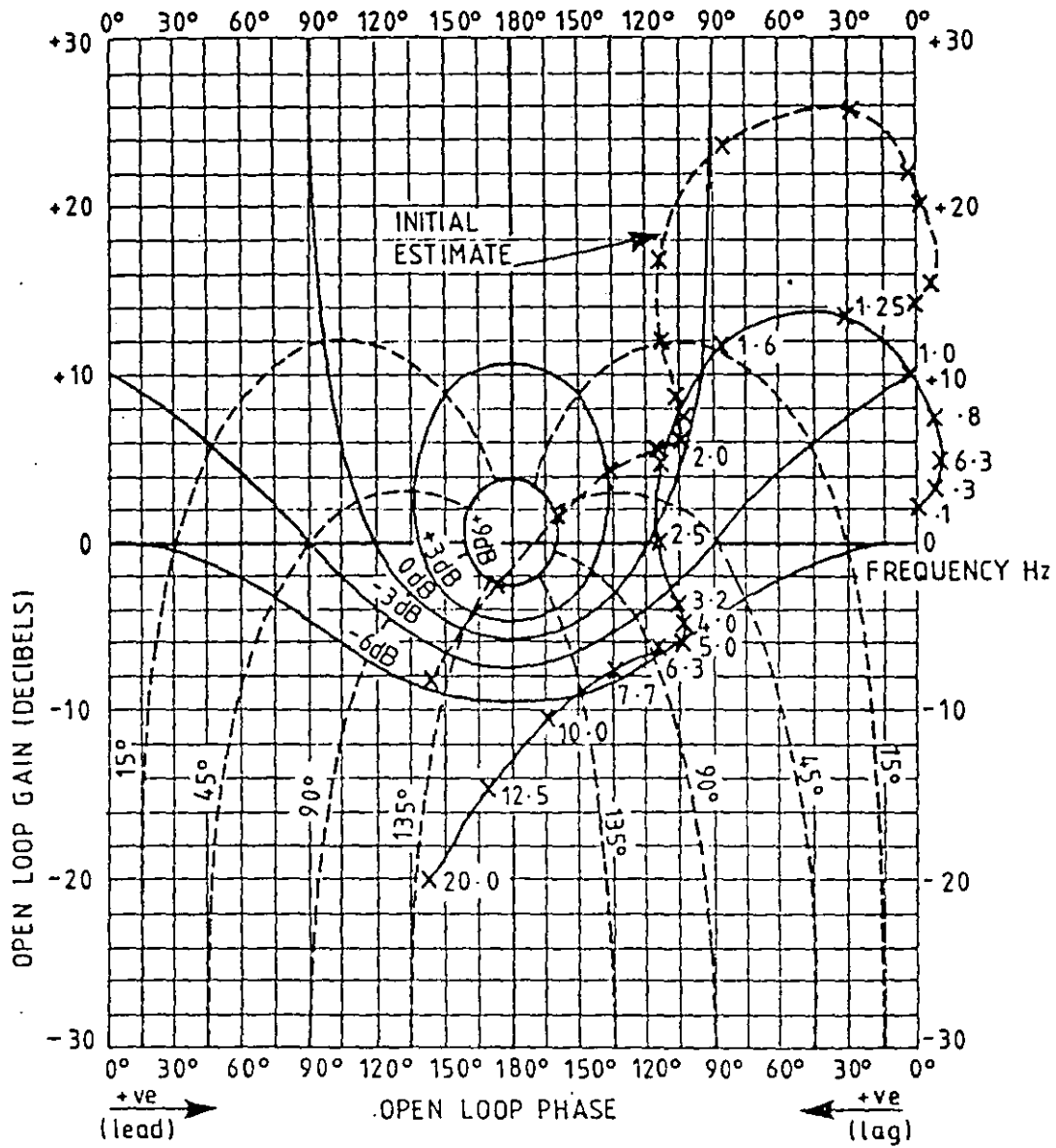


FIG. 5.9 PITCH POSITION CONTROL  
OPEN LOOP RESPONSE

and  $F_a$  is the sum of the four actuator forces. Above the flexible body frequency this is

$$\frac{z_m''}{F_a} = \frac{(g_{fi} g_{fo} M + M)}{M_f M} \quad (5.13)$$

a reasonable approximation as the mode only has 2% damping. Without the flexible mode the high frequency transmissibility:

$$\frac{z_m''}{F_a} = \frac{1}{M} \quad (5.11)$$

If  $g_{fi}$  and  $g_{fo}$  have the same sign (i.e. the accelerometers and actuators situated on the same side of the nodes) the transmittance with the flexible mode will be greater than without. This can create stability problems at high frequencies by reducing the gain margin.

Siting the accelerometers at the nodes will remove the effects of the flexible mode from the control circuit. Frequently this is not possible to achieve for physical reasons, added to which the nodes will tend to move as the vehicle is loaded, particularly if the loading is unsymmetrical. Placing the accelerometers at the opposite side of the node to the actuators causes a reduction in the high frequency transmissibility and the effect can be used to control the flexible mode. The problem with this solution is that separate accelerometers are required for the pitch and bounce modes as it becomes more difficult to resolve the pitch mode when the accelerometers are inside the bending nodes because they are closer together.

The second effect of the flexible mode can be seen in the bounce open loop response (Fig 5.10) which has been computed for a vehicle with the accelerometers over the actuators. Because of the low damping in the mode it goes through a large change in gain and phase around the resonant frequency. With the response shown in Fig 5.10 the stability margins are adequate. However a small reduction in damping would increase the size of the loop induced by the flexible mode, pushing it towards instability. The effect of the flexible mode can be eliminated by a narrow bandwidth band stop filter of the form

$$\left( \frac{1 + s^2/\omega_{nf}^2}{1 + 2\zeta s/\omega_{nf} + s^2/\omega_{nf}^2} \right)$$

This form of filter is often referred to as a notch filter. The effect of the notch filter on the open loop response is shown in Fig 5.10. A massive reduction in gain occurs around the centre frequency of the notch filter which removes the effect of the resonance. It will be noted however that there is a penalty as the system suffers from additional phase lag at low frequencies which will tend to degrade the performance. The amount of lag can be reduced by reducing the damping in the notch filter. This however may not be an acceptable solution as a fairly wide notch has to be used to accommodate the shift in the flexible body frequency from 10 Hz to 9 Hz between the tare and laden conditions, although in the laden condition the flexible mode is less of a problem as the passengers add damping to the system.

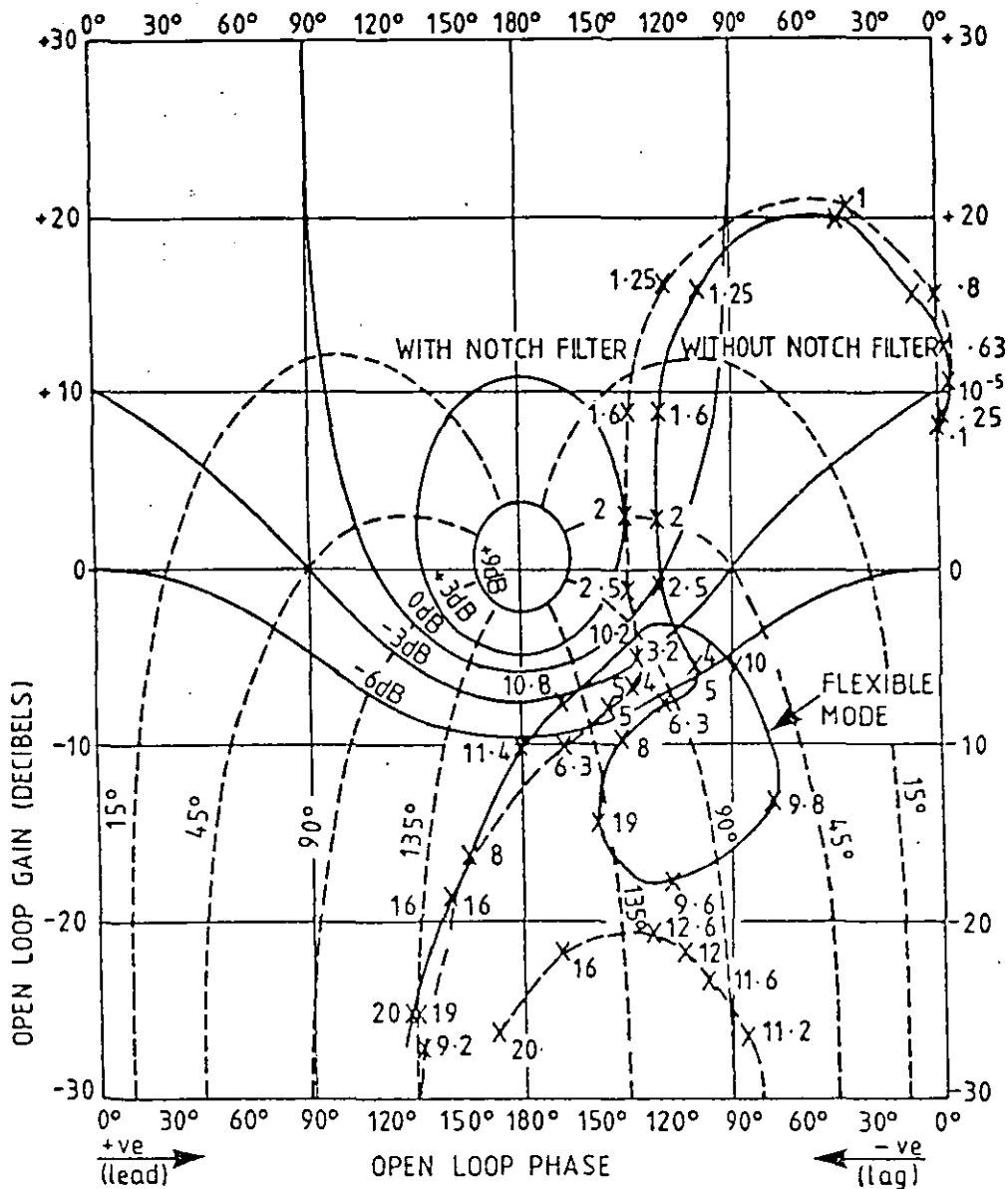


FIG 5.10 MK.III COACH BOUNCE CONTROL LOOP  
POSITION CONTROL OPEN LOOP RESPONSE

## 5.2.4

Position Control Eigen-Values

The position control closed loop eigen-values are given in table 5.2.

Table 5.2 Position Control Closed Loop Eigen-Values

Mode	Laden		Tare	
	Damping	Frequency	Damping	Frequency
Bounce Filter	74%	.81 Hz	73%	.84 Hz
Pitch Filter	74%	.84 Hz	73%	.87 Hz
Bounce Loop	35%	2.1 Hz	35%	2.1 Hz
	100%	1.8 Hz	100%	1.8 Hz
Pitch Loop	35%	2.2 Hz	35%	2.2 Hz
	100%	1.7 Hz	100%	1.7 Hz
Bounce Phase Advance	37%	9.4 Hz	37%	9.4 Hz
Pitch Phase Advance	37%	9.4 Hz	37%	9.4 Hz
Force Control Loops	82%	11.7 Hz	82%	11.7 Hz
Bogie Bounce	42%	5.8 Hz	43%	5.5 Hz
Bogie Pitch	55%	8.7 Hz	55%	8.7 Hz

These eigen-values shows a marked degree of interaction between different parts of the system. The eigen values of the filters were set at 1 Hz with 70% damping but the interaction reduces the frequency. The interaction is more pronounced in the laden case as the controller is working harder. Similiar interaction occurs between the poles of the phase advance network and the flux control loops as their frequencies are quite close.



Response to a Random Track Input

Vehicle responses to a rough main line track spectrum are shown in Table 5.3. These show that the biggest improvement in ride occurs at the trailing end of the vehicle with a 41% reduction in r.m.s. acceleration for absolute damping and a 54% reduction with the position control system. It will be noted that the power consumption of the position control system is significantly higher than the absolute damping system. This is because the position control system imposes a new characteristic on the suspension, rather than modifying the existing suspension. The effect of the position control system forcing the suspension is shown in the trailing end acceleration p.s.d. Fig 5.11. The majority of the improvement for both control configurations occurs at the rigid body frequency. Absolute damping shows a peak in transmission at the rigid body frequency while the position control system shows a peak at the main control loop bandwidth frequency.

While the power consumption of the position control system is high it is only 2 kW compared with an installed continuous power of 3.6 kW. The voltage and current are also considerably less than the power amplifiers are capable of handling (20 amps continuous, 50 amps peak and 300 volts).

It is also noted that the improvement in the weighted (RED) acceleration is less than the unweighted. This is because most of the improvement occurs at the rigid body frequency and Fig 2.4 shows that the weighting factor at this frequency is smaller than at other frequencies.

A p.s.d. of the trailing end currents (Fig 5.12) shows that most of the energy is in the region  $1 H_z$ , which justifies the eddy current analysis performed in section 4.6.

TABLE 5.3 Theoretical Performance of Active Suspension at 55 m/S

	Suspension								Actuator					
	Leading		Centre		Trailing		Displacement		Leading End			Trailing End		
	rms Accn		rms Accn		rms Accn		mm							
	m/s <sup>2</sup>		m/s <sup>2</sup>		m/s <sup>2</sup>		Leading Trailing							
	Red		Red	Red					Amps	Volts	Watts	Amps	Volts	Watts
Passive Laden	.61	.46	.30	.24	.79	.57	4.8	6.9						
Passive Tare	.62	.47	.32	.24	.80	.59	5.7	7.8						
Sky hook Laden	.43	.34	.20	.17	.47	.37	5.2	5.6	9.3	28.4	187	9.9	30.3	216
Position Laden	.37	.30	.16	.14	.37	.30	5.4	5.7	13.8	44.0	425	15.4	47.2	528
Position Tare	.38	.31	.17	.15	.38	.31	5.6	5.9	14.7	45.0	463	16.2	48.1	545

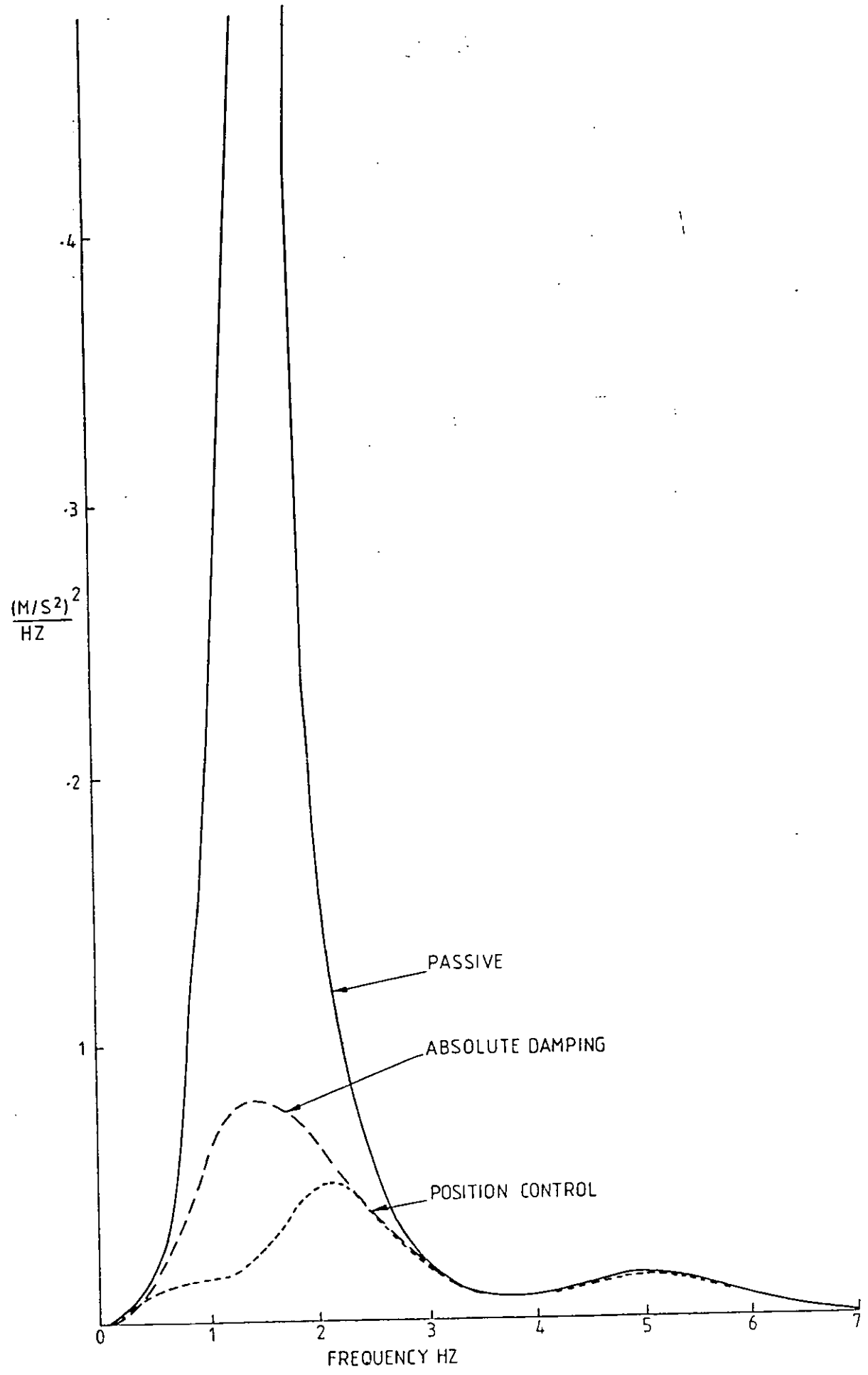


FIG. 5-11 TRAILING END ACCELERATION P.S.D. 55 m/s

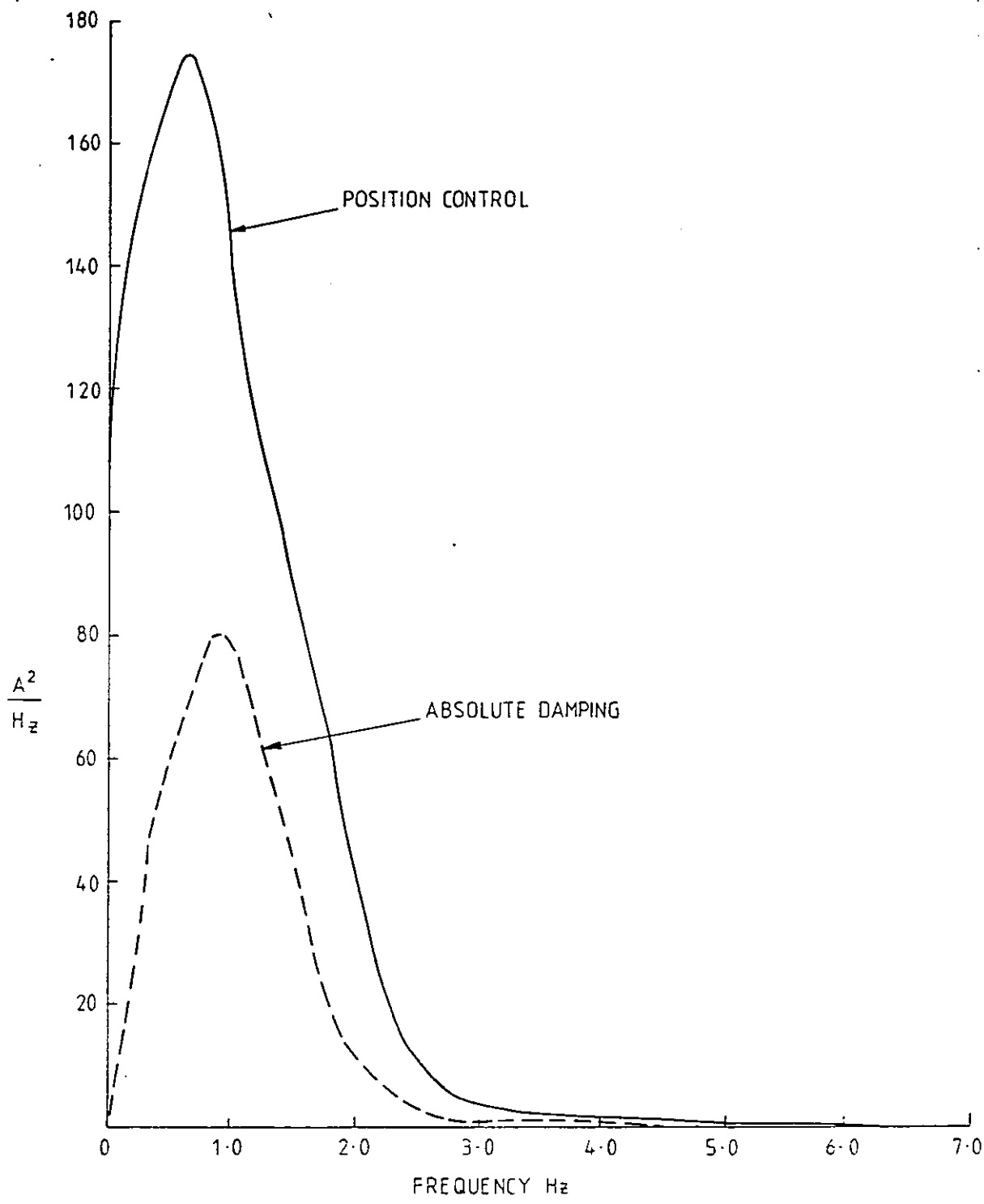


FIG. 5-12. TRAILING END CURRENT P.S.D.

There is very little change in vehicle ride and power consumption between the tare and laden states. Contrary to expectations the power consumption is slightly lower in the laden state than it is at tare. This is due to the slight reduction in passive suspension frequency when it is loaded.

Control system parameters and state equations for the classical control systems are given in appendix C.

## CHAPTER 6

OPTIMAL CONTROL SYSTEMS

Chapter 2 showed that optimal control systems require all the states of the system controlled to be available for feedback (Fig 6.1). They also require states relating to the system inputs (in this case the track) to be available as feed forwards.

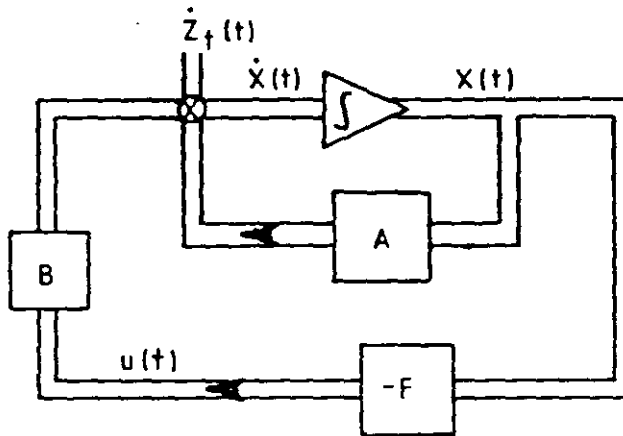


FIG 6.1 OPTIMAL REGULATOR

As it is not usually possible to measure all the states of the system to be controlled those which cannot be measured are recreated by an observer. The feedback gains are then provided from the observed values of the system (Fig 6.2).

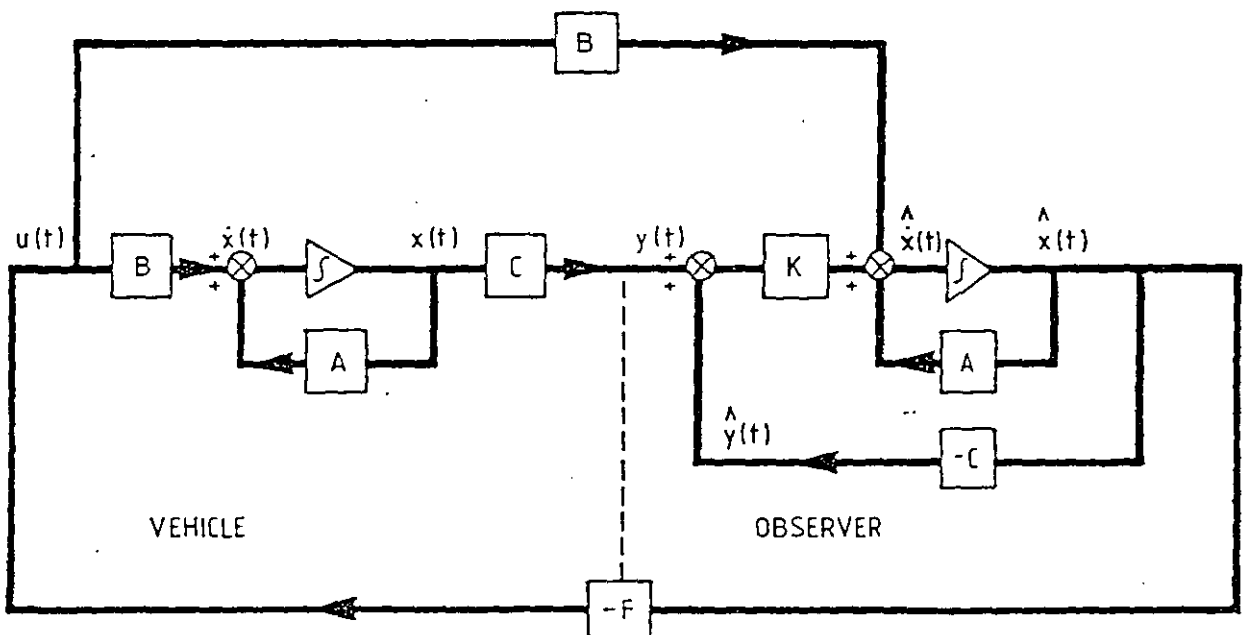


FIG 6.2 OPTIMAL REGULATOR WITH FEEDBACK PROVIDED FROM AN OBSERVER

Thus the optimal control system is designed in two stages, firstly the regulator then the observer.

### 6.1 Optimal Regulator Design

The regulator for the active suspension was designed to control the pitch and bounce modes only. This is because the actuators are only 500 mm from the centre line of the vehicle and cannot exert a very large influence in roll. Because the roll mode is not controlled only two actuators need be included in the model. The force generated by the actuators is then doubled to find the effect on the vehicle as both actuators at one end of the vehicle are driven together.

Fig 6.3 shows the actuator model.

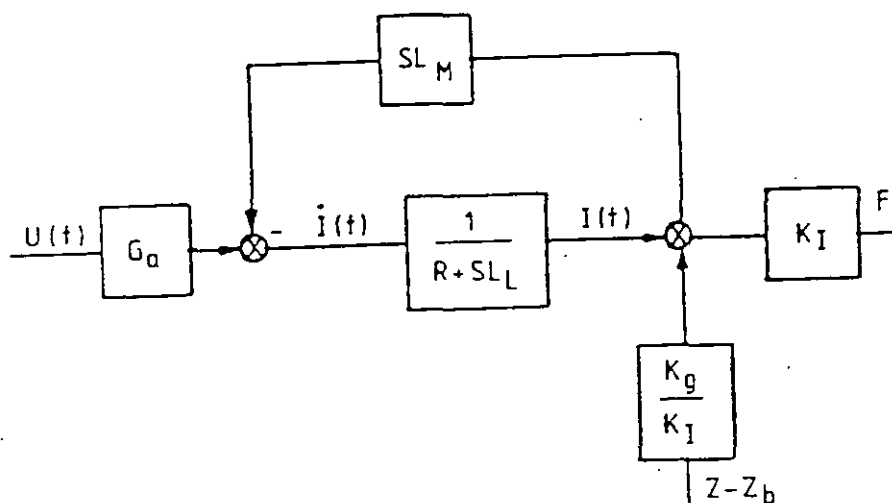


FIG 6.3 ACTUATOR MODEL USED IN OPTIMAL REGULATOR DESIGN

It will be noted that all feedbacks, including the current feedback inherent in the amplifier, have been omitted as the regulator design program calculates all the feedback gains. The control inputs are the power amplifier input demand voltages.

### 6.1.1 Track Inputs

An optimal regulator requires the system input dynamics to be available for feeding forward. Chapter 2 showed that railway track can be described by a white noise process  $w(t)$  intensity  $V$  where the vertical velocity profile is.

$$\dot{z}_t(t) = \sqrt{V} \quad (6.1)$$

or

$$z_t(s) = \sqrt{\frac{V}{s}} \quad (6.2)$$

In practice the modified form:

$$z_t(s) = \frac{\sqrt{V}}{(s + 1)} \quad (6.3)$$

is preferred as it does not have a zero eigen value which can create problems with the regulator design program, particularly if there is more than one zero eigen value in system. The effect of this modification is quite small as the pole is at a much lower frequency than the suspension frequencies.

A four axle vehicle, such as the Mk III coach, experiences a single track input with a time delay between each. This effect is difficult to include in the state model as the time delay cannot be adequately modelled in the time domain equations. In the  $s$  plane a time delay is described by the Laplace transform  $e^{-s\delta}$ , where  $\delta$  is the time delay. In the time domain they can be approximated by Padé approximations such as

$$\frac{1 - s\delta/2 + (s\delta)^2/12}{1 + s\delta/2 + (s\delta)^2/12} \text{ etc} \quad (6.4)$$



In reference (28) a first order approximation  $(1-s\delta/2)/(1+s\delta/2)$  was used in the design of an observer for a bogie. At 55 m/s the time delay between wheelsets on the bogie is 0.05 s and the first order Padé approximation produces an acceptable phase error ( $15^\circ$ ) up to a frequency of 5 Hz. With a secondary suspension the time delay between bogie centres is 0.3s and at 5 Hz a first order Padé approximation would produce a  $336^\circ$  phase error. In order to keep the phase error to  $15^\circ$  a fifth order approximation is required. Unfortunately this would generate extra states in the model causing it to become rather large (particularly as the states would have to be included in the observer). Thus initially the track modelled as four uncorrelated inputs. This has two advantages. The first is that the optimisation is independent of the direction of travel and the second is that it is independent of speed. Speed dependency comes from the phase relationship between the inputs. A vehicle with a pair of inputs separated by a distance  $l$  and travelling at velocity  $v$  will experience an inphase input:-

$$z_B/z_t = (1 + e^{-s\delta})/2 \quad (6.5)$$

and an anti-phase input:-

$$z_P/z_t = (1 - e^{-s\delta})/2 \quad (6.6)$$

where the time delay  $\delta = l/v$

$z_B$  and  $z_P$  have speed dependent reductions in transmissibility which, if matched to the bounce and pitch modes of vibration can make significant changes to the active suspension performance. However the optimisation will only hold for one speed.

### 6.1.2 Weighting Functions

It was shown in Chapter 2 that the optimal regulator is one which minimises a quadratic performance index of the form

$$J = \int_0^{\infty} (z^T R_3 z + u^T R_2 u) dt \quad (6.7)$$

Where

$$z = Nx$$

(6.8)

The critical factor in the design of the active suspension regulator is selection of the weighting matrices  $R_2$  and  $R_3$ .

The variables which are used in the weighting matrices are in fact fairly self evident:-

- 1) Active suspensions aim to minimise the accelerations experienced by the passengers, and hence must be included in the weighting matrix. Because the accelerations at the ends of the vehicle are higher than they are at the centre, the accelerations above the airsprings are used in the weighting matrix.
- 2) Secondary suspension displacement is limited with any form of suspension, but particularly so with an electromagnetic active suspension as air gaps must be kept to a minimum to reduce power consumption. Therefore secondary suspension displacement was also included in the weighting function.
- 3) Actuator currents were included as they are a major limiting factor in the design of the power amplifiers. They also directly affect the power consumed by the active suspension.
- 4) The input weighting factor is determined by the constraint on the actuator voltage to which it is directly related by the amplifier gain  $G_a$ .

Putting these variables into the performance index gives an equation of the form:-

$$J = \int_0^{\infty} \left[ \ddot{z}_1^2 a + (\ddot{z}_c)^2 a + (z_1 - z_{b1})^2 b + (z_2 - z_{b2})^2 b + (I_1)^2 c \right. \\ \left. + (I_2)^2 c + (v_1/G_a)^2 \lambda + (v_2/G_a)^2 \lambda \right] dt \quad (6.9)$$

Thus the  $z$  vector is  $(\ddot{z}_1, \ddot{z}_b, z_1 - z_{b1}, z_b - z_{b2}, I_1, I_2)^T$   
 and the  $u$  vector  $(V_1, V_2)^T$

$$\begin{aligned}
 z_1 &= Z - l\phi & z_b &= Z + l\phi \\
 R_3 &= \begin{pmatrix} a & 0 & 0 & 0 & 0 & 0 \\ 0 & a & 0 & 0 & 0 & 0 \\ 0 & 0 & b & 0 & 0 & 0 \\ 0 & 0 & 0 & b & 0 & 0 \\ 0 & 0 & 0 & 0 & c & 0 \\ 0 & 0 & 0 & 0 & 0 & c \end{pmatrix} \quad (6.10)
 \end{aligned}$$

and

$$R_2 = \begin{pmatrix} \lambda & 0 \\ 0 & \lambda \end{pmatrix} \quad (6.11)$$

Equal weighting functions were applied to each end of the vehicle to ensure symmetrical performance. Ideally the accelerations would be constant along the length of the vehicle. Since this is impossible, equalising them at the ends is the next best thing.

The weighting factors were selected on the basis of the required r.m.s performance of the variables in the weighting function. This is because the active suspension is attempting to minimise the response of the system to a random input and section 2.3.2 showed that ride can be described in terms of the r.m.s response. The values chosen were:-

1. Vertical acceleration ( $\ddot{z}_1$  and  $\ddot{z}_b$ ),  $2.2\%g$
2. Suspension displacement ( $z_1 - z_{b1}$ ) and ( $z_b - z_{b2}$ ), 8 mm
3. Current ( $I_1$  and  $I_2$ ), 12.5 Amps
4. Voltage ( $V_1$  and  $V_2$ ), 50 Volts

Target accelerations were selected on the basis of the recommendations made by ORE Committee C116 for the vertical r.m.s. accelerations of Inter-City vehicles.

8 mm r.m.s suspension displacement is dictated by the need to avoid bump stop contact. This represents just over 25% of the maximum displacement which should ensure very little bump stop contact.

Amplifier currents of 12.5 Amps represent 25% of the peak amplifier current of 50 Amps.

A very conservative voltage was selected from experience of problems encountered with the experimental system (60). The non-linear nature of the actuators requires a large instantaneous forcing voltage when the actuator force is reversed. If this is not available the demand signal will be clipped, producing unacceptable phase lags in the system. Thus the r.m.s. voltage was taken as 50 volts.

Equal weighting was given to each of the variables by setting the weighting factors (a, b, c and  $\lambda$ ) to the inverse of the required mean square performance

ie:-

$$a = 20 \text{ (m/s}^2\text{)}^{-2}$$

$$b = 15 \times 10^3 \text{ m}^{-2}$$

$$c = 6.4 \times 10^{-3} \text{ amps}^{-2}$$

$$\lambda = 0.36 \text{ volts}^{-2}$$

### 6.1.3 Regulators

A by product of the technique used to compute the optimal feedback matrix is the generation of the closed loop eigen values of the system. These are given in Table 6.1, compared with the passive suspension eigen values. It will be noted that the main effect of the regulator is to increase damping in the body modes with a small reduction in their frequencies. Analysis of the feedback gains shows that a significant amount of the extra damping is in effect "skyhook" damping, not surprisingly as all the states are fed back and the absolute pitch and bounce velocities of the vehicle body provide two of the states. The reduction in frequency is generated by the regulator introducing negative stiffness in parallel with the positive spring stiffness. Changes to the pitch mode are more significant than to the bounce mode. Actuator eigen values, at 3.1 Hz and 3.7 Hz are very much lower than the 11.7 Hz associated with classical controllers, making them more immune to noise.

Table 6.2 shows the vehicle performance computed at 55 m/s on poor quality mainline track. It is notable that the accelerations at the ends of the vehicle are equalised, as they are with the position control system. The optimisation makes a bigger improvement at the ends of the vehicle than it does at the centre, with a 68% reduction in rms acceleration at the trailing end compared with a 47% reduction in the centre.

Despite the impressive improvements the model does not meet the required target acceleration of 2.2g. In order to see if the target could be met the acceleration weightings (a in equation 6.9) were reduced by the ratio of the required and achieved mean square responses ie  $(2.2/2.5)^2$ , so that  $a = 15.5$ . Table 6.2 shows this to have been effective.

The suspension displacement was far less than the target value and it was felt that further improvement could be obtained by increasing it. Thus the relative displacement weighting function was increased by the actual and achieved performances. However this had little effect on the performance (see table 6.2) which means that the displacement is not a limiting value on the performance.

## 6.2 Optimal Observers

The regulators designed in section 6.1 require all 24 states in the vehicle model (Appendix D) to be available as feedbacks. This is clearly an impossible situation as some of the states cannot be measured and, even if all could be measured, the instrumentation required would be excessive. In order to overcome the problem an observer is used to recreate those states which cannot be measured. An observer is a model of the plant which is being observed (Fig 6.2). In order to cause the model to follow the plant the reconstructed states are compared with the plant variables which can be measured and the resulting error signals used to drive the model

ie:-

$$\dot{\hat{x}}(t) = A\hat{x}(t) + B u(t) + K [y(t) - Cx(t)] \quad (6.12)$$

Where  $\hat{x}(t)$  is the recreated, or observed variable vector. The observed output equation  $\hat{y}(t) = C\hat{x}(t)$ .

The accuracy with which the model follows the plant is determined by the observer feedback gain matrix K.

While increasing the gain of the feedback matrix will cause the observer to follow the plant more closely, it also makes it more susceptible to noise so that observer design is a compromise between state reconstruction and noise rejection.

The method of observer design used is that due to Kalman and Bucy (54). It assumes that the plant is driven by white noise and that there is white noise present on the measured signals. The method of determining the feedback matrix, by solution of the Riccati equation, is almost the same as the method used to determine the regulator feedback matrix, by solution of the observer Riccati equation.

$$0 = EV_3E^T - QC^T V_2^{-1}CQ + AQ + QA^T \quad (6.13)$$

$$\text{and the feedback matrix } K = QC V_2^{-1} \quad (6.14)$$

$V_3$  is the intensity of the noise source driving the plant, in this case the track velocity profile. and  $V_2$  the intensity of the noise on the measured signals. Section 2 shows the relationship between  $V_3$  and the track spectrum roughness factor.

### 6.2.1 Full Size Observer

The measurements made of a system for which an observer is to be constructed must be influenced by all the states of the system. For example an observer driven by an accelerometer at the centre of a vehicle will be capable of resolving the bounce mode of vibration but not the pitch mode and is therefore unacceptable on its own.

The minimum instrumentation required to observe the 24 degree of freedom model given in Appendix D is 4 accelerometers on the bogies over the axles. In practice, as the secondary suspension accelerations are much less than the primary suspension accelerations, and in a different frequency regime, an accelerometer above the secondary suspension at each end of the vehicle is required as well, or a noisy reconstruction would be made of the rigid body modes. Magnet currents at each end of the vehicle are also included as they are readily available giving eight measured variables in total.

As all the measured variables can, in theory, influence all the observed variables the observer feedback matrix will have 192 elements. To this must be added the 116 elements in the model itself, which makes the observer look rather big and unwieldy to design, build and commission.

Even analysis of the system is not particularly easy as a model of the system must contain the vehicle and the observer. In the model, used to analyse the controller, the observed variables are included in the state matrix as

$$\begin{bmatrix} \dot{\mathbf{x}}(t) \\ \dot{\hat{\mathbf{x}}}(t) \end{bmatrix} = \begin{bmatrix} \mathbf{A} & \mathbf{BF} & & \\ & \mathbf{KC} & \mathbf{A} - \mathbf{KC} + \mathbf{BF} & \end{bmatrix} \begin{bmatrix} \mathbf{x}(t) \\ \hat{\mathbf{x}}(t) \end{bmatrix} + \mathbf{E} z_t(t) \quad (6.15)$$

While the state matrix  $\mathbf{A}$  and the  $\mathbf{BF}$  matrix are relatively sparse for the system described, the observer computed for the system had some 480 of a possible 576 significant elements in the  $\mathbf{KC}$  matrix. The thought of entering such a matrix into the computer was rather daunting and, though it is possible to mechanise the process, the physical reality of such an observer must be questioned. Therefore the possibility of a simpler observer was investigated.

### 6.2.2 Small Model Regulator

Vertical ride is mainly determined by the secondary suspension, as the primary suspension natural frequencies are much higher than the secondary suspension frequencies.

Therefore the bogies were eliminated from the model used in the regulator program leaving a secondary suspension connected directly to two, uncorrelated, track inputs Fig 6.4. Appendix D gives the state equations of the small model.

A regulator was designed for the small model, using the weighting factors given in Section 6.1.2. The closed loop eigen values of the system are shown in Table 6.1. It will be noted that the body modes have a slightly higher frequency and more damping than they have on the full model.

The feedback gains from the small model were put into the full vehicle mode using only those states which are common to each model.

Table 6.2 shows that the responses for this model are almost identical with the full vehicle model, vindicating the use of the small model.

### 6.2.3 Small Model Observer

Observers were designed using the small model of the vehicle, Fig 6.4. The parameters selected to measure the system performance were the accelerations at the ends of the vehicle, secondary suspension displacements and magnet currents, as these are the variables required for the position control system, Chapter 5.

Noise input to the system is well defined and section 2.5 shows that the input variance for rough main line track at 55 m/s is  $4.34 \times 10^{-4}$  (m/s). However, measurement noise is less well defined and, in the absence of measured data, an educated guess was required.



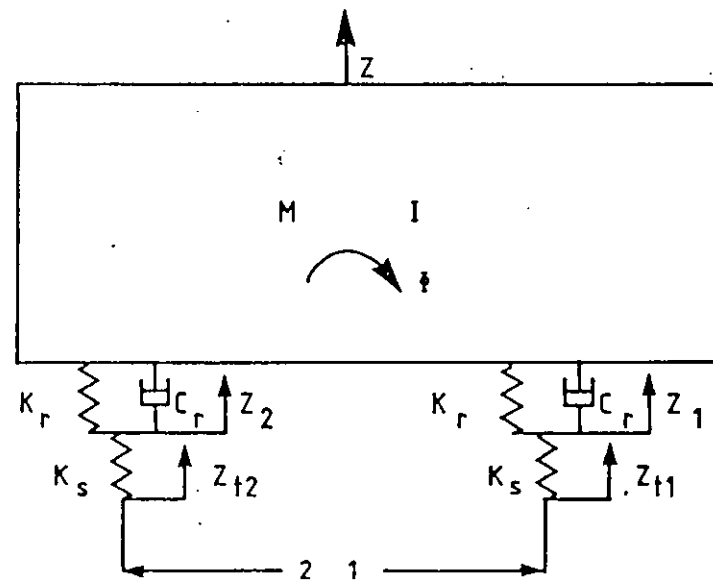


FIG.6.4 REDUCED MODEL OF VEHICLE USED TO CALCULATE THE OPTIMAL OBSERVER

In order that the measured variables contribute equally to the observer they should have similar signal to noise ratios. Thus the first guess at signal to noise ratio was 30dB on all variables. The variance of the measurement noise was calculated from the predicted responses with the simple regulator given in Table 6.1 (the variance is the mean square noise).

Table 6.3 shows the eigen values for this observer. The high frequency eigen-value, (-513.7 real or 81.7 Hz) are easy to understand and indicate that the observer will track the vehicle closely up to 80 Hz. However the low frequency eigen values (0.16 Hz) were at first much more difficult to understand and it took some time to realise that they came from the observer not measuring the absolute positions of the vehicle or track in space. Consider the simple single state observer in Fig 6.5 in which the measured variable is in fact the observed variable.

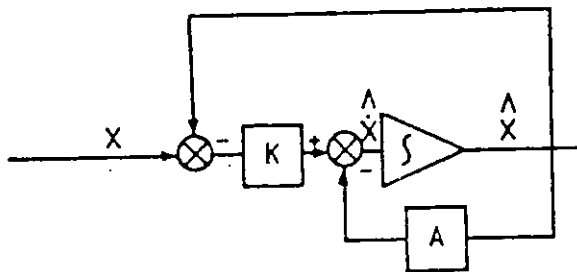


FIG 6.5 SINGLE STATE OBSERVER

The transfer function of the observer is:-

$$\frac{\hat{x}}{x} = \frac{K}{s + (A + K)} \quad (6.16)$$

Which is of course a low pass filter. The filter frequency increases with  $K$  while the dc tracking error

$$\frac{x - \hat{x}}{x} = \frac{s + A}{s + A + K} \quad (6.17)$$

decreases. Note that unless  $K \gg A$  there will be a significant dc tracking error.

Now consider a single observer in which the measured variable is the derivative of the variable to be observed Fig 6.6.

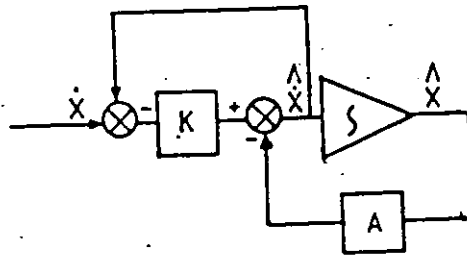


FIG 6.6 SINGLE STATE OBSERVER WITH DERIVATIVE INPUT

The transfer function of this observer is:-

$$\frac{\hat{x}}{x} = \frac{sK}{s(1+K) + A} \quad (6.18)$$

This is a high pass filter in which the filter frequency reduces as  $K$  increases. Note that once again there is a following error even at high frequencies :-

$$\frac{x - \hat{x}}{x} = \frac{s + A}{s(1+K) + A} \quad (6.19)$$

and  $K \gg 1$  to minimise the error.

The optimal observer program will tend to increase  $K$  as the signal to noise ratio decreases. For the low pass observer (6.16) the rationale behind this is fairly obvious as the noisier the signal the more heavily it will have to be filtered. The high pass observer (6.18) recreates the variable by integrating the derivative of the variable. Noise on the signal will cause the integrator to drift, therefore the higher the signal to noise ratio the less it will drift and the closer the pole can be to the origin of the  $s$  plane.

Table 6.2 shows that the response of the vehicle with the 30 dB signal to noise ratio is virtually the same as the regulator alone. However it was felt that the high frequency eigen value of this observer (-514 real or 82 Hz) was too high and would lead to problems. This was because only the rigid body modes had been included in the vehicle model and at 82 Hz the vehicle structure is extremely flexible. Added to which the instrumentation used to measure the vehicle will not perform very well at these frequencies. In particular the accelerometers chosen have a bandwidth of 34 Hz and are thus ineffective. In addition eddy currents in the magnets make the relationship between current and force or even measured flux and force very tenuous at these frequencies. Thus the effects of reducing the signal to noise ratio were investigated. In this case, included with the noise is uncertainty about the validity of the system model.

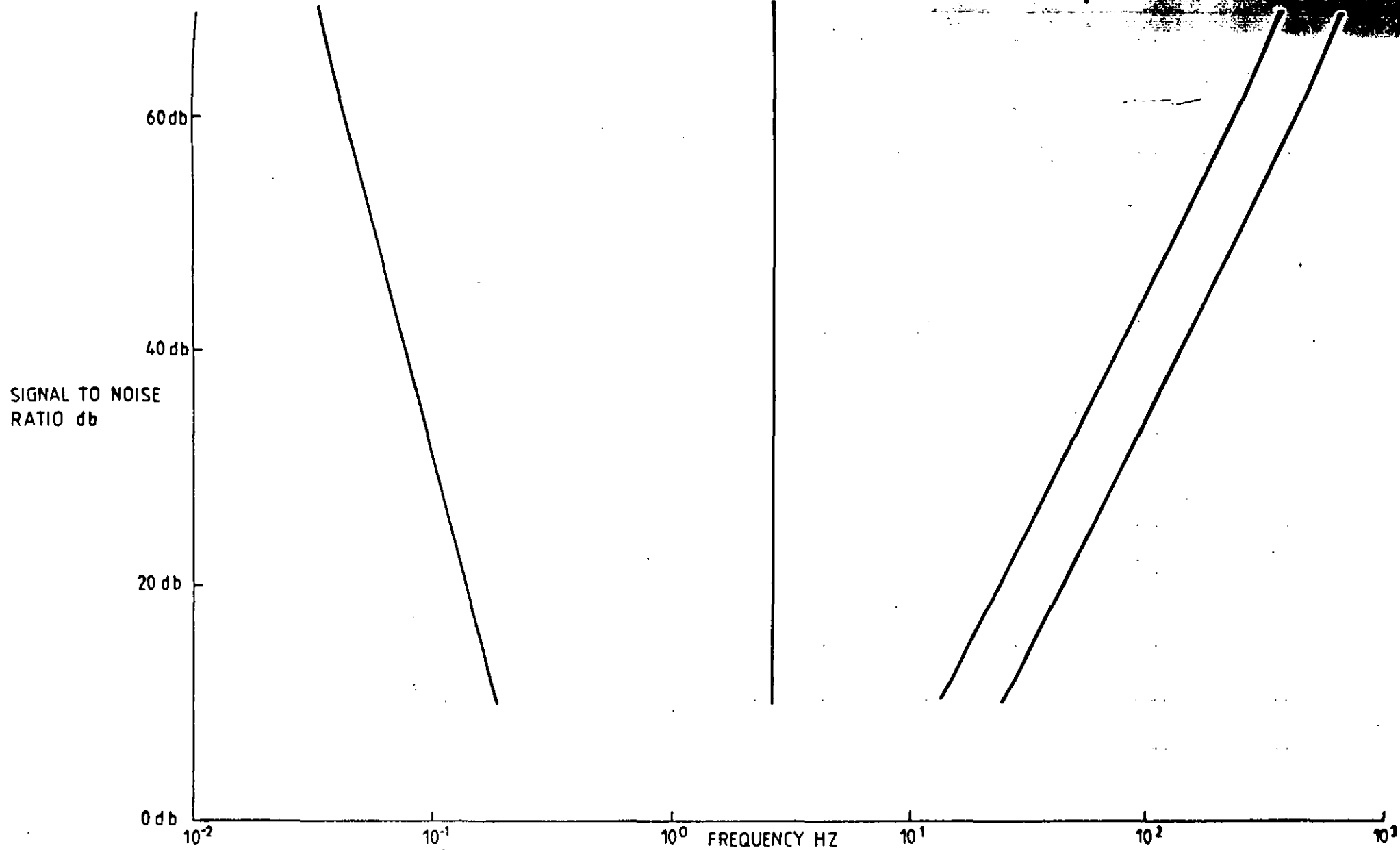
It was felt that a maximum observer frequency of around 26 Hz was required. As the feedback gain  $K$  is a function of the signal to noise ratio, reducing this by a factor of 10 should reduce the frequency by a factor of 3. The factor of 10 on signal to noise ratio means increasing the noise variance by a factor of 10. Table 6.3 shows that this was indeed effective and that the high frequency eigen value was reduced to 26 Hz when the observer was recomputed with 10 db signal to noise ratio. Note though that there is no similar movement in the low frequency eigen value.

The observer with 10 dB signal to noise ratio shows a degradation in performance over the 30 dB observer, Table 6.2, but the reduced bandwidth should produce a better conditioned control system which is less prone to exciting structural modes.

The observers so far have been chosen because they use the same instrumentation as the position control system. They require 6 transducers and with 10 states in the model the K matrix has 60 gains, most of which are significant. In theory the system could be observed by just the two accelerometers, which would reduce the K matrix to 20 elements. Therefore an observer was designed for a 10 db signal to noise ratio using only two accelerometers. Table 6.3 shows this to have produced very similar observer eigen values to the observer with the more complete set of instrumentation. Table 6.4 shows that the predicted performance is also the same.

Table 6.2 shows the decoupling effect of the low frequency poles on the observed variables. While it was easy to manipulate the high frequency poles with the full instrumentation, the low frequency poles proved more intractable and could not be manufactured. Fortunately they occur at about the same frequency as the low frequency roll off of the double integrator used to derive absolute position in the position control system.

The observer with accelerations as the only measurements however does show a linear relationship between signal to noise ratio and both high frequency and low frequency poles, Fig 6.7, over quite a large range of signal to noise ratio. The relationship breaks down when the high and low frequency poles approach the vehicle model poles. It will be noted that the low frequency eigen values change at half the rate of the high frequency values. This is because they are complex, where the high frequency poles are real, and a pair of complex poles attenuates a signal at twice the rate of a real pole.



**FIG. 6.7 MOVEMENT OF KALMAN FILTER POLES WITH SIGNAL TO NOISE RATIO WHEN ACCELERATION IS THE MEASURED VARIABLE.**

TABLE 6.1

Eigen-Values of a Mk III Coach with an Optimal Regulator

<u>Mode</u>	Passive Suspension		First Regulator Design		Increased Acceleration Weighting		Increased Suspension Displacement Weighting		Small Regulator	
	damping	Freq Hz	damping	Freq Hz	damping	Freq Hz	damping	Freq Hz	damping	Freq Hz
Body Bounce	.16	1.0	.36	.96	.41	.93	.41	.91	.53	1.10
	1.00	1.60	1.00	1.90	1.00	2.0	1.00	2.00	1.00	2.50
Body Pitch	.19	1.4	.51	1.18	.56	1.10	.57	1.00	.67	1.20
	1.00	1.60	1.00	2.10	1.00	2.30	1.00	2.30	1.0	2.5
Bogie Bounce In Phase	.39	5.80	.46	5.60	.49	5.50	.49	5.50		
Out of phase	.37	5.90	.56	5.30	.61	5.00	.61	5.00		
Bogie Pitch	.55	8.70	.55	8.70	.55	8.70	.55	8.70		
Controllers In phase			1.00	3.06	1.00	3.17	1.00	3.17	1.00	3.90
Out of phase			1.00	3.67	1.00	4.50	1.00	4.50	1.00	5.80



TABLE 6.2  
Active Suspension Performance 55 m/s

	Leading rms accn		Centre rms accn		Trailing Dis P accn		Sec		Leading		Trailing		z.	$\hat{z}$	$\phi$	$\hat{\phi}$	
	m/s <sup>2</sup>	Red	m/s <sup>2</sup>	Red	m/s <sup>2</sup>	Red	LE mm	TE mm	V	Amps	V	Amps					
Passive	.61	.46	.30	.24	.79	.57	4.8	6.9									
Classical Position	.35	.29	.16	.14	.34	.78	4.7	4.8	31	11	32	12					
Optimal Regulator	.24	.20	.16	.14	.25	.21	4.7	4.4	32	8.8	34	9.9	10.0			.47	
Regulator $\hat{z}$ Weighting increased	.21	.17	.14	.12	.21	.17	4.9	4.5	37	10	38	11	9.8			.42	
Regulator Z-Zt Weighting increased	.20	.17	.14	.12	.21	.17	5.0	4.6	38	10	39	11	9.9			.41	
Simple Regulator	.24	.20	.15	.13	.26	.21	4.6	4.5	31	9.2	33	10	10.1			4.7	
Observer 30 dB S/N	.27	.24	.16	.14	.28	.23	4.7	4.7	32	8.8	34	10	10.8	9.72		.52	.42
Observer 10 dB S/N	.30	.25	.18	.16	.32	.26	5.5	5.3	30	8.3	33	10	12.6	5.6		.61	.38
Reduced Observer 10dB S/N	.30	.25	.18	.16	.32	.26	5.5	5.3	29	8.2	33	9.7	12.7	4.7		.62	.32

TABLE 6.3

Small Model Optimal Observer Eigen-Values

30 dB Signal/Noise Ratio $\ddot{Z}$ , ZR and I Measured		10 dB Signal/Noise Ratio $\ddot{Z}$ , ZR and I Measured		10 dB Signal/Noise Ratio $\ddot{Z}$ and I Measured	
	Hz		Hz		Hz
-1.0	.16	-1.0	.16	-1.0	.16
-1.1	.17	-1.1	.17	-1.0	.16
-3.1	.49	-3.3	.52	-3.9	.62
-3.7	.59	-3.8	.60	-4.1	.65
-9.4	1.50	-9.3	1.48	-7.8	1.18
-10.0	1.59	-9.8	1.56	-7.7	1.22
-21.1	3.36	-21.0	3.34	-20.6	3.28
-22.4	3.56	-22.2	3.53	-21.7	3.45
-296.9	47.25	-95.0	15.12	-90.7	14.43
-513.7	81.75	-165.1	26.27	-162.6	25.88

## 6.3

Experimental Observers

The optimal controllers described so far have omitted the current feedback which was inherent in the design of the power amplifiers. As it was not possible to remove this feedback a regulator and two different forms of observer were designed with the current feedback included in the plant matrix.

## 6.3.1

Experimental Regulator

The small vehicle model Fig 6.4 was used for the experimental regulator. The additional elements required in the feedback are shown in Appendix D. A modification is required to the weighting matrix as the control input is no longer the only input to the power amplifier. The dynamic range of the control input is  $\pm 10$  V, therefore the weighting matrix was taken as 25% of the peak value (2.5 Volts) giving  $\lambda = .16$  as the inverse of the square, in line with the other weighting factors in section 6.1.2.

TABLE 6.4 Eigen-Values of Theoretical and Experimental Regulators

	Theoretical $\zeta$	Model Freq Hz	Experimental $\zeta$	Model Freq Hz
Body Bounce	( .53	1.1	.44	1.2
	( 1.0	2.5	1.0	2.2
Body Pitch	( .67	1.2	.59	1.4
	( 1.0	2.5	1.0	2.1
Actuators in Phase	1.0	3.9	1.0	8.0
Actuators in Anti Phase	1.0	5.8	1.0	10.7

Table 6.4 shows the regulator eigen-values for the experimental and theoretical regulators. The experimental regulator does not provide quite as much damping or frequency shift as the theoretical regulator. However the major change is the increase in the actuator eigen values, putting them at a similar frequency to those of the classical control systems.

### 6.3.2 Small Model Observer

Observers, similar to those described in Section 6.2.3, were designed around the experimental regulator. The observers had signal to noise ratios on the measured variables of 10 dB. Two observers were designed, one using acceleration, current and suspension displacement as the measured variables, and the other using just acceleration and current. The eigen-values of these two observers are compared with the equivalent theoretical observers in table 6.5. All the eigen-values are real and only the frequencies have been quoted.

TABLE 6.5 Small Vehicle Observer Eigen-Values

Theoretical Observers		Experimental Observers	
Accn, Rel Disp Current Hz	Accn, Current Hz	Accn, Rel Disp Current Hz	Accn, Current Hz
.16	.16	.16	.16
.17	.16	.17	.16
.52	.62	.45	.56
.60	.65	.67	.65
1.48	1.18	1.49	1.21
1.56	1.22	1.55	1.31
3.34	3.28	6.04	5.85
3.53	3.45	6.14	5.91
15.12	14.43	15.79	15.20
26.27	25.88	27.27	26.92

The main difference between theoretical and experimental observers are the increased eigen-values due to the regulators (3.34 Hz and 3.53 Hz in the theoretical observer and 6.04 Hz and 6.14 Hz in the experimental observer).

Table 6.6 shows the predicted performance of the observer, using the vehicle model used to compute table 6.2.

TABLE 6.6 Comparative Performance of Theoretical and Experimental Observers

	Theoretical Controller		Experimental Controller	
		Weighted Accn		Weighted Accn
<u>Rel Disp</u>				
Leading	5.5 mm		5.3 mm	
Trailing	5.3 mm		4.9 mm	
<u>Accn</u>				
Leading	.30 m/s <sup>2</sup>	.25 m/s <sup>2</sup>	.29 m/s <sup>2</sup>	.24 m/s <sup>2</sup>
Centre	.18 m/s <sup>2</sup>	.16 m/s <sup>2</sup>	.18 m/s <sup>2</sup>	.16 m/s <sup>2</sup>
Trailing	.32 m/s <sup>2</sup>	.26 m/s <sup>2</sup>	.32 m/s <sup>2</sup>	.26 m/s <sup>2</sup>
<u>Electrical</u>				
<u>Leading</u>				
Current	8.3 Amps		7.8 Amps	
Voltage	29.7 Volts		29.0 Volts	
<u>Trailing</u>				
Current	9.8 Amps		9.2 Amps	
Voltage	32.6 Volts		31.7 Volts	

These results show that the two observers are closely comparable in performance.

Table 6.8 at the end of the chapter shows the results for these observers with the corrected vehicle model.

#### 6.4 Modal Observers

Though the small model observer shows a significant reduction in size over a full vehicle observer it is still fairly complex. Therefore an alternative implementation was sought using a simpler method of reconstructing the unobserved states of the control system.

##### 6.4.1 Modal State Equations

Equation 6.20 is the state matrix of the small vehicle model with the experimental regulator.

"													
z	0	-27.7	0	0	-44.6	-44.6	.012	.012	58.5	58.5		z	
·z												z	
z	1.0	0	0	0	0	0	0	0	0	0		z	
Φ	0	0	0	-49.7	10.0	-10.0	-.0026	-.0026	-13.1	13.1		Φ	(6.20)
·Φ												Φ	
Φ	0	0	1.0	0	0	0	0	0	0	0		Φ	
·z <sub>1</sub>	1.0	4.9	-8.0	-39.0	-16.5	0	0	0	11.6	0		z <sub>1</sub>	
·z <sub>2</sub>												z <sub>2</sub>	
z <sub>2</sub>	1.0	4.9	8.0	39.0	0	0	0	0	0	11.6		z <sub>2</sub>	
·I <sub>1</sub>												I <sub>1</sub>	
I <sub>1</sub>	-.73E4	.28E4	.73E5	-.18E6	.12E6	-.45E5	-64.0	10.0	-.14E6	.56E5		I <sub>1</sub>	
·I <sub>2</sub>												I <sub>2</sub>	
I <sub>2</sub>	-.73E4	.28E4	-.73E5	.18E6	-.45E5	.12E6	10.0	-64.0	.56E5	-.14E6		I <sub>2</sub>	
·z <sub>t1</sub>												z <sub>t1</sub>	
z <sub>t1</sub>	0	0	0	0	0	0	0	0	-1	0		z <sub>t1</sub>	
·z <sub>t2</sub>												z <sub>t2</sub>	
z <sub>t2</sub>	0	0	0	0	0	0	0	0	0	-1		z <sub>t2</sub>	

Cross coupling between the actuators is relatively small (with a cross feedback gain of about 1/3 that of the gain about the actuator). By ignoring the cross coupling it is possible to rewrite the equations in  $I_1$  and  $I_2$  as equations

(6.21) and (6.22).

$$\begin{aligned}
 I_1 = & - \frac{113 \dot{z}}{(1 + .015 s)} + \frac{44 z}{(1 + .015 s)} + \frac{1137 \dot{\phi}}{(1 + 0.15 s)} \\
 & - \frac{2822 \phi}{(1 + .015 s)} + \frac{1861 z_1}{(1 + .015 s)} - \frac{701 z_2}{(1 + .015 s)} \\
 & - \frac{2171 z_{t1}}{(1 + 0.15 s)} + \frac{930 z_{t2}}{(1 + 0.15 s)} \qquad (6.21)
 \end{aligned}$$

$$\begin{aligned}
 I_2 = & - \frac{113 \dot{z}}{(1 + 0.15 s)} + \frac{44 z}{(1 + .015 s)} - \frac{1137 \dot{\phi}}{(1 + .015 s)} \\
 & + \frac{2822 \phi}{(1 + .015 s)} - \frac{701 z_2}{(1 + .015 s)} + \frac{1861 z_1}{(1 + 0.15 s)} \\
 & + \frac{930 z_{t1}}{(1 + .015 s)} - \frac{2171 z_{t2}}{(1 + 0.15 s)} \qquad (6.22)
 \end{aligned}$$

The pole  $(1 + .015 s)$  occurs at a relatively high frequency compared to the rigid body eigen-values so that the numerators of (6.21) and (6.22) can be substituted into (6.20) to form the reduced state equation (6.23).

A further refinement of the equations can now be made to resolve the in-phase and anti-phase components of  $z_1$  and  $z_2$  and  $z_{t1}$  and  $z_{t2}$  giving a bounce and pitch mode model of the vehicle, Equations (6.24) and (6.25).

"										"	
z	-2.6	-26.7	0	0	-31.3	-31.3	43.5	4.5		z	
.										.	
z	1.0	0	0	0	0	0	0	0		z	
"										"	
Φ	0	0	-5.9	-35.1	3.3	-3.3	-5.2	5.2		Φ	(6.23)
.										.	
Φ	0	0	1.0	0	0	0	0	0		Φ	
.										.	
z <sub>1</sub>	1.0	4.9	-8.0	-39.5	-16.5	0	11.6	0		z <sub>1</sub>	
.										.	
z <sub>2</sub>	1.0	4.9	39.0	0	0	-16.5	0	-11.6		z <sub>2</sub>	
.										.	
z <sub>t1</sub>	0	0	0	0	0	0	-1.0	0		z <sub>t1</sub>	
.										.	
z <sub>t2</sub>	0	0	0	0	0	0	0	-1.0		z <sub>t2</sub>	



$$\begin{bmatrix} \ddot{y} \\ \dot{z} \\ \dot{z}_I \\ \dot{z}_t \end{bmatrix} = \begin{bmatrix} -2.6 & -26.7 & -62.6 & 87 \\ 1.0 & 0.0 & 0.0 & 0.0 \\ 1.0 & 4.9 & -16.5 & 11.6 \\ 0.0 & 0.0 & 0.0 & -1 \end{bmatrix} \begin{bmatrix} z \\ z_I \\ z_t \end{bmatrix} \quad (6.24)$$

$$z_I = z_1 + z_2 \quad z_t = z_{t1} + z_{t2}$$

$$\begin{bmatrix} \ddot{\phi} \\ \dot{\phi} \\ \dot{\phi}_I \\ \dot{\phi}_t \end{bmatrix} = \begin{bmatrix} -5.91 & -35.1 & -53.3 & 83 \\ 1.0 & 0.0 & 0.0 & 0.0 \\ 1.0 & 4.9 & -16.5 & 11.6 \\ 0.0 & 0.0 & 0.0 & -1 \end{bmatrix} \begin{bmatrix} \phi \\ \phi_I \\ \phi_t \end{bmatrix} \quad (6.25)$$

$$\phi_I = (-z_1 + z_2)/8 \quad \phi_t = (-z_{t1} + z_{t2})/8$$

Note: these are the controlled modal vibrations of the vehicle.

#### 6.4.2 Modal Observers

Observers were designed around the modal models. These were driven by acceleration signals at the ends of the vehicle alone. The accelerations were added to give the bounce acceleration and subtracted to give the pitch acceleration. The eigen-values are given in Table 6.7.

TABLE 6.7 Modal Observer Eigen-Values

	Damping	Frequency
Bounce Observer	.92	.19 Hz
	.92	.19 Hz
	1.00	1.25 Hz
	1.00	10.60 Hz
Pitch Observer	.93	.19 Hz
	.93	.19 Hz
	1.00	1.41 Hz
	1.00	10.14 Hz

STOR-A-FILE IMAGING LTD

---

**DOCUMENTS  
OF POOR  
ORIGINAL  
HARD  
COPY**

The low frequency eigen values are at similar frequencies to those of the full observer. However the high frequency eigen values, at 10.6 Hz and 10.2 Hz, are much lower than those of the larger observer (28 Hz) owing to the absence of the actuators with their associated high frequency poles. Each observer requires 14 gain elements, 4 in the feedback matrix (K) and 10 in the state matrix (A), making for a very much more compact model of the system.

Figure 6.8 shows how the controller was implemented, with the states which could not be measured (the vehicle modes) being supplied by the observers, and those which could (the actuator currents) from direct measurements of the system.

Table 6.8 gives the predicted performance of the experimental controllers with the corrected vehicle model. These show that there is little to choose between the two forms of observer in terms of performance, though the modal observers are considerably simpler in practice.

## 6.5 Comparison of Classical and Optimal Controllers

Comparing the performance of the optimal and classical controllers the optimal give slightly more improvement in ride than the position control system and a fairly significant improvement over the absolute damping controllers. It is in power consumption however that the optimal controllers score most strongly over the position control system since they consume less than half. Fig 6.9 shows the trailing end acceleration p.s.d.'s for the controllers. The optimal controllers and absolute damping show a fundamental reduction in the passive suspension characteristics. The position control system however shows a peak at 2.2 Hz due to the main control loops while the improvement at the rigid body frequency is much better than the other controllers. This is because the position control system imposes the filter transfer function on the suspension rather than modifying what exists, and the choice of filters is not necessarily the best.

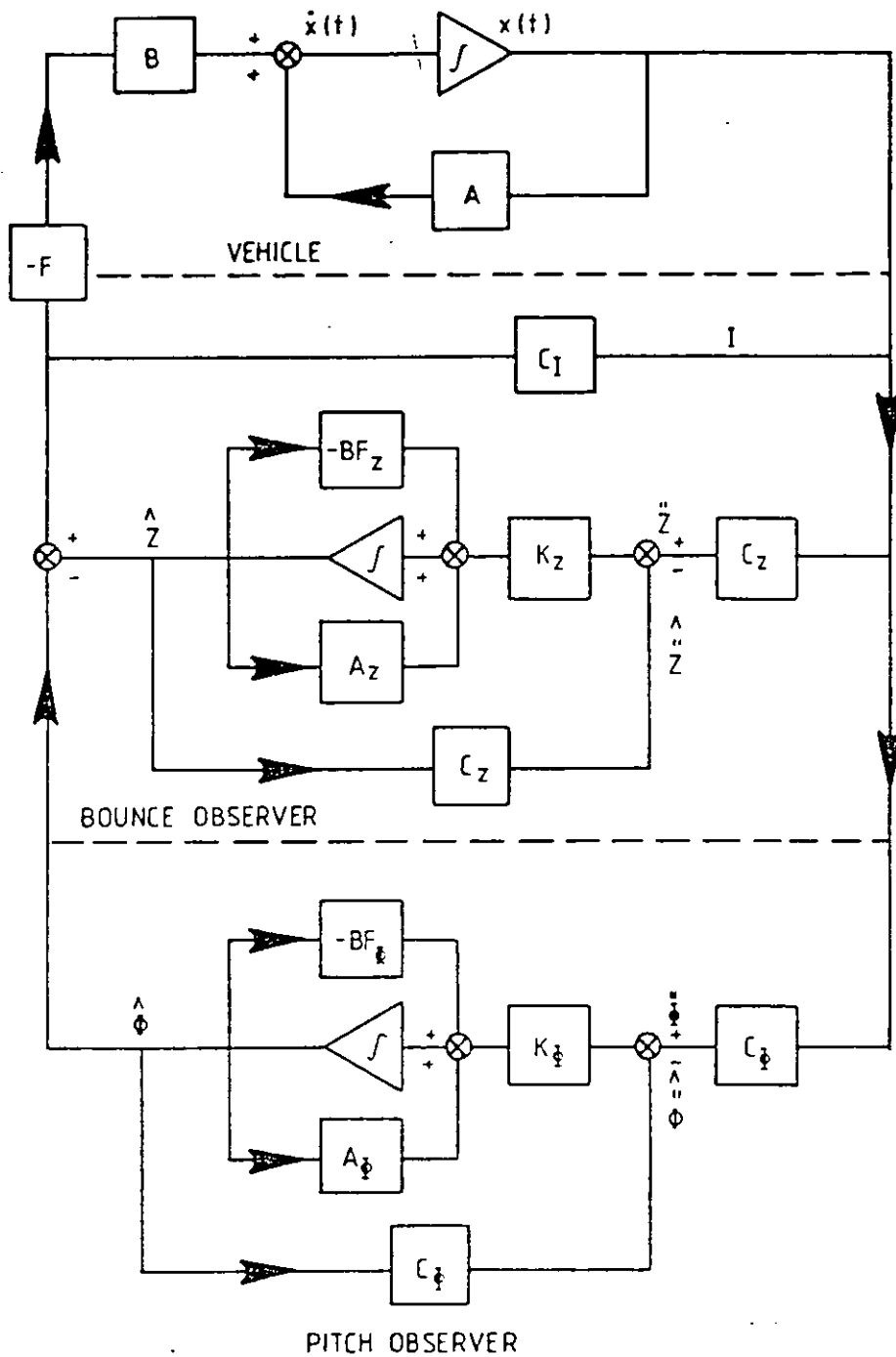


FIG. 6.8. MODAL OBSERVERS

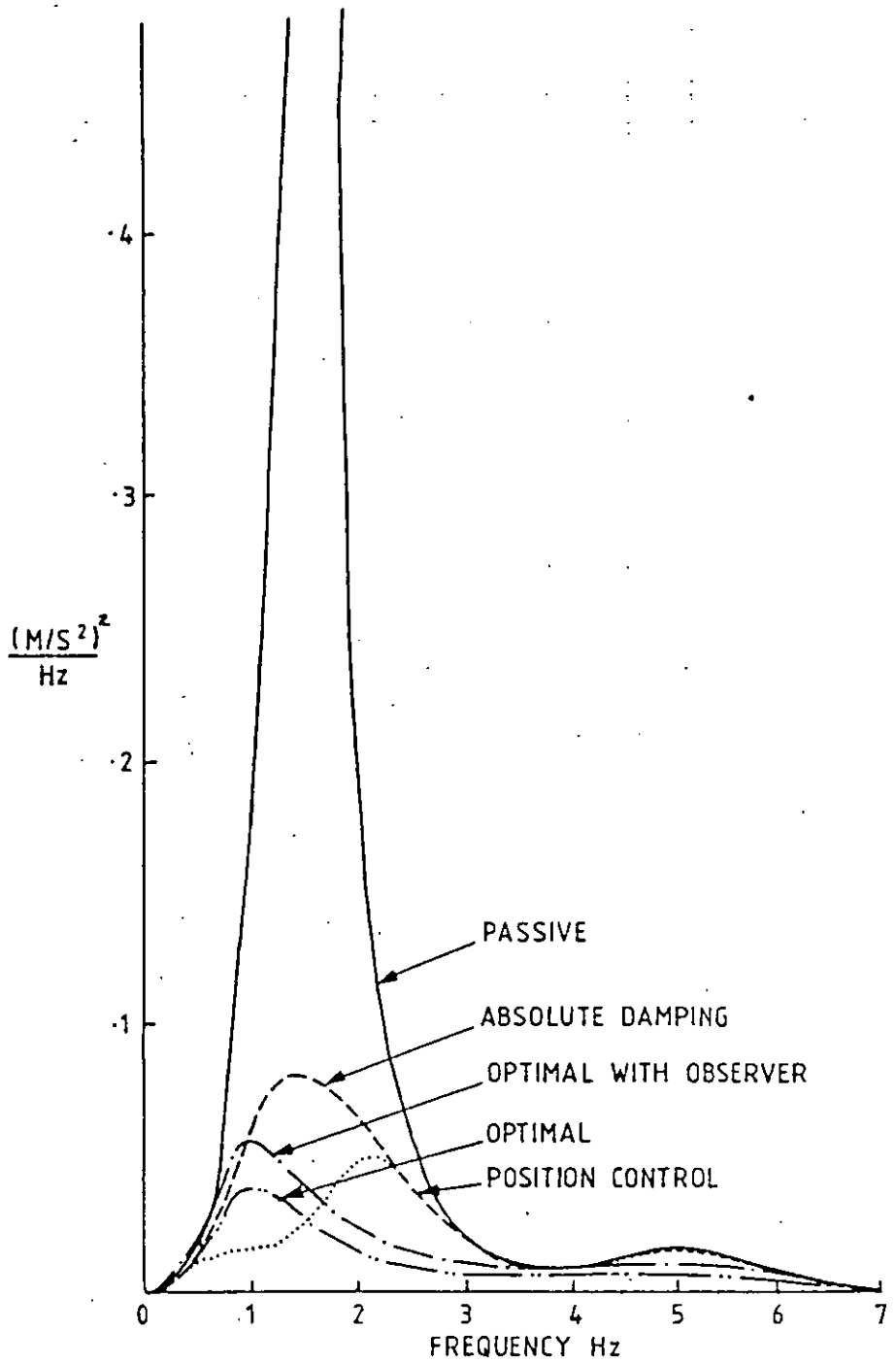


FIG.6.9 TRAILING END ACCELERATION P.S.D. 55m/s.

Butterworth filters were selected for their optimum dynamic characteristics, minimal overshoot and settling time; it is evident from the results that they do not minimise the power consumption. Better results could probably be obtained by modifying the filters. This would require quite a major iteration on filter frequency, damping and pole zero combinations for the controller. A method of doing this will be reviewed later in chapter 11 .

The performance at 44 m/s is given in Table 6.9 for comparison with experimental data.

TABLE 6.8 Theoretical Performance of Active Suspension at 55 m/s

	Suspension						Actuator						171 871		
	Leading rms Acc <sup>n</sup> m/s <sup>2</sup>		Centre rms Acc <sup>n</sup> m/s <sup>2</sup>		Trailing rms Acc <sup>n</sup> m/s <sup>2</sup>		Displacement mm		Leading End			Trailing end			
	RED		RED		RED		Leading	Trailing	Amps	Volts	Watts	Amps		Volts	Watts
Passive	.61	.46	.30	.24	.79	.57	4.8	6.9							
Sky Hook	.43	.34	.20	.17	.47	.37	5.2	5.2	4.2	28	187	10.0	30	216	
Position	.37	.30	.16	.14	.37	.30	5.4	5.7	13.8	44	425	15.4	47	528	
Small Observer	.34	.27	.20	.17	.39	.30	5.6	6.1	9.1	33	183	11.3	38	283	
Modal Observer	.34	.27	.20	.17	.39	.30	5.6	6.0	9.2	33	189	11.2	37	279	

TABLE 6.9 Theoretical Performance of Active Suspension at 44 m/s

	Suspension						Actuator							
	Leading rms Acc <sup>n</sup> m/s <sup>2</sup>		Centre rms Acc <sup>n</sup> m/s <sup>2</sup>		Trailing rms Acc <sup>n</sup> m/s <sup>2</sup>		Displacement mm		Leading End			Trailing end		
	RED	RED	RED	RED	RED	RED	Leading	Trailing	Amps	Volts	Watts	Amps	Volts	Watts
Passive	.55	.41	.23	.18	.64	.46	6.1	6.0						
Sky Hook	.36	.28	.16	.14	.36	.28	4.5	4.4	8.2	24	146	8.0	24	136
Position	.29	.23	.14	.12	.28	.23	4.7	4.8	12.1	38	327	12.8	38	366
Small Observer	.29	.23	.15	.13	.31	.24	4.9	4.9	8.2	28	153	9.3	30	194
Modal Observer	.28	.22	.17	.14	.30	.24	5.6	5.1	9.0	29	103	9.8	29	188



## 6.6

Time Delayed Inputs

In order to assess the effect of more representative time delayed track inputs on regulator design the experimental regulator (Section 6.3.1) was redesigned with the time delay between the inputs represented as a 5th order Padé approximation.

$$1 - \frac{s\delta}{2} + \frac{(s\delta)^2}{9} - \frac{(s\delta)^3}{72} + \frac{(s\delta)^4}{1008} - \frac{(s\delta)^5}{30240} \quad (6.26)$$

$$1 - \frac{s\delta}{2} + \frac{(s\delta)^2}{9} - \frac{(s\delta)^3}{72} + \frac{(s\delta)^4}{1008} - \frac{(s\delta)^5}{30240}$$

The revised state equations are given in Appendix D. The time delay  $\delta$  was taken as .29s representing the delay between bogie centre at 55 m/s.

Table 6.10 compares the performance of a vehicle fitted with a regulator designed with uncorrelated inputs and one with a regulator with time delayed inputs.

At the design speed of 55 m/s there is very little to choose between the performance of the two regulators. At 44 m/s, (the most likely operating speed for the vehicle when not operating at 55 m/s), the ride produced by the two regulators is very similar but the power consumption of the trailing actuators has been increased as the trailing input generated by the Pade approximation is out of phase with the real input.

It would seem from this exercise that the decision taken in Section 6.1.1 to model the track using uncorrelated inputs is validated, since including the correlation provides no improvements in performance. Added to this observers with correlated inputs would be more complicated and sensitive to changes in speed and direction.

TABLE 6.10 Comparison of Small Regulator and Time Delayed Regulator

55 m/s	Suspension						Actuator							
	Leading rms Acc <sup>n</sup> m/s <sup>2</sup>		Centre rms Acc <sup>n</sup> m/s <sup>2</sup>		Trailing rms Acc <sup>n</sup> m/s <sup>2</sup>		Displacement mm		Leading End			Trailing end		
	RED		RED		RED		Leading	Trailing	Amps	Volts	Watts	Amps	Volts	Watts
Small Regulator	.31	.25	.18	.15	.35	.27	5.5	5.6	10.1	33	211	11.7	37	286
Time Delayed	.31	.25	.20	.17	.37	.29	5.2	5.7	9.5	31	184	10.9	39	250
44 m/s														
Small Regulator	.26	.20	.14	.12	.27	.24	4.8	4.6	9.0	28	167	9.7	29	197
Time Delayed	.27	.21	.15	.13	.27	.24	4.9	4.6	8.7	27	154	11.6	36	286

152

CHAPTER 7

TRAIN MODES

During testing the experimental controllers demanded more power than anticipated. Measured open loop responses also indicated strong interaction between the experimental vehicle and the vehicles to which it was attached. As earlier work on British Rail Mk II and Mk III coaches (65, 66) had shown that there is a strong vertical interaction between adjacent vehicles in a train through the gangway connections, a theoretical investigation of the problem was carried out.

The interaction comes from friction between gangway connections. The gangways themselves behaving like stiff springs. Laboratory coaches were modeled as the connecting vehicles. This had three advantages. First, they are relatively simple to model, thus keeping the system model to a reasonable size. Secondly, they have a relatively stiff secondary suspension, so that the effect on the experimental vehicle was as bad as could be expected in service. Lastly it was representative of the experimental conditions. Fig 7.1 shows the experimental train. The state equations are given in Appendix E. It will be noted that the connection is modelled as a linear spring and damper using values given in (65, 66).

The results in Table 7.1 show that the effects of the train modes are more pronounced on the active suspensions than the passive. This is partly due to the friction in the gangway connections increasing damping in the passive vehicle, which is more lightly damped than is desirable.

In terms of performance the position control system maintains the improvement in ride better than the other control systems. However the power consumption rises to a point where it is only just acceptable. Of the optimal controllers the small vehicle model does not perform very well at all with the train model. This is because the observer, with its extensive instrumentation, no longer represents the system which it is trying to observe. The simpler modal observers however still perform quite effectively.

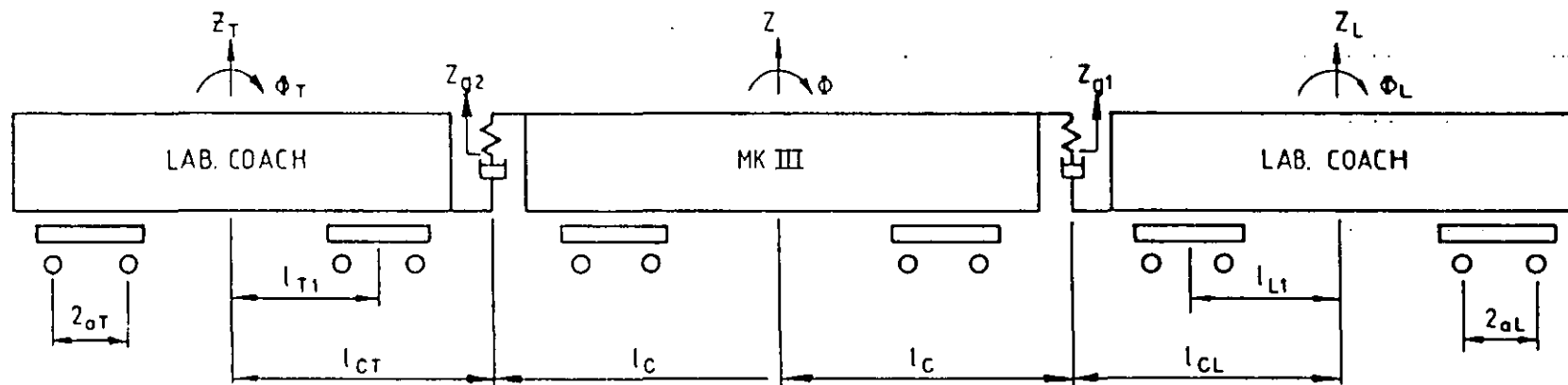


FIG. 7-1 EXPERIMENTAL VEHICLE IN TRAIN

Table 7.2 has also been included, showing the performance at 44 m/s, as this was the speed at which most of the vehicle testing took place. The biggest improvement in ride occurs at the leading end of the vehicle, unlike the uncoupled vehicle where it occurs at the trailing end. At 55 m/s the reduction in r.m.s acceleration is 41% at the leading end with position control. While this increases to a 51% reduction at 44 m/s the improvement at the trailing end of the vehicle is reduced from 25% to 17%.

Trailing end acceleration p.s.d's (Fig 7.2) show that there is a significant shift in the frequency distribution of the acceleration energy when the vehicle is in a train, compared to the free vehicle (Fig 7.3). Passively the rigid body peaks were reduced due to the increased damping from the end connection. This is offset to some extent by an increase in vibration around 4.8 Hz due to the stiffness of the gangway connections. Actively all the control systems showed an increase in energy at the rigid body modes as the control systems had to influence three vehicles rather than one. Note that the position control system also shows a peak at the rigid body frequencies. Some reduction is made in the high frequency vibration, particularly by the optimal control system. However this does not totally offset the degradation in performance at low frequencies as the control system gains are not very high at 4.8 Hz. It is perhaps worth considering that if the position control system did not have the generous phase margins that it does have, the ride at the high frequencies could easily be degraded.

The problem of gangway end connections is in some ways peripheral to the active suspension study. Reference (65) showed that the effect was not evident in prototype Mk III coaches which had a much softer corridor end connections. In a production vehicle with an active suspension it would make more sense to modify the gangway end connections rather than the control system as the power consumption of the control system would be reduced as well as the ride being improved.

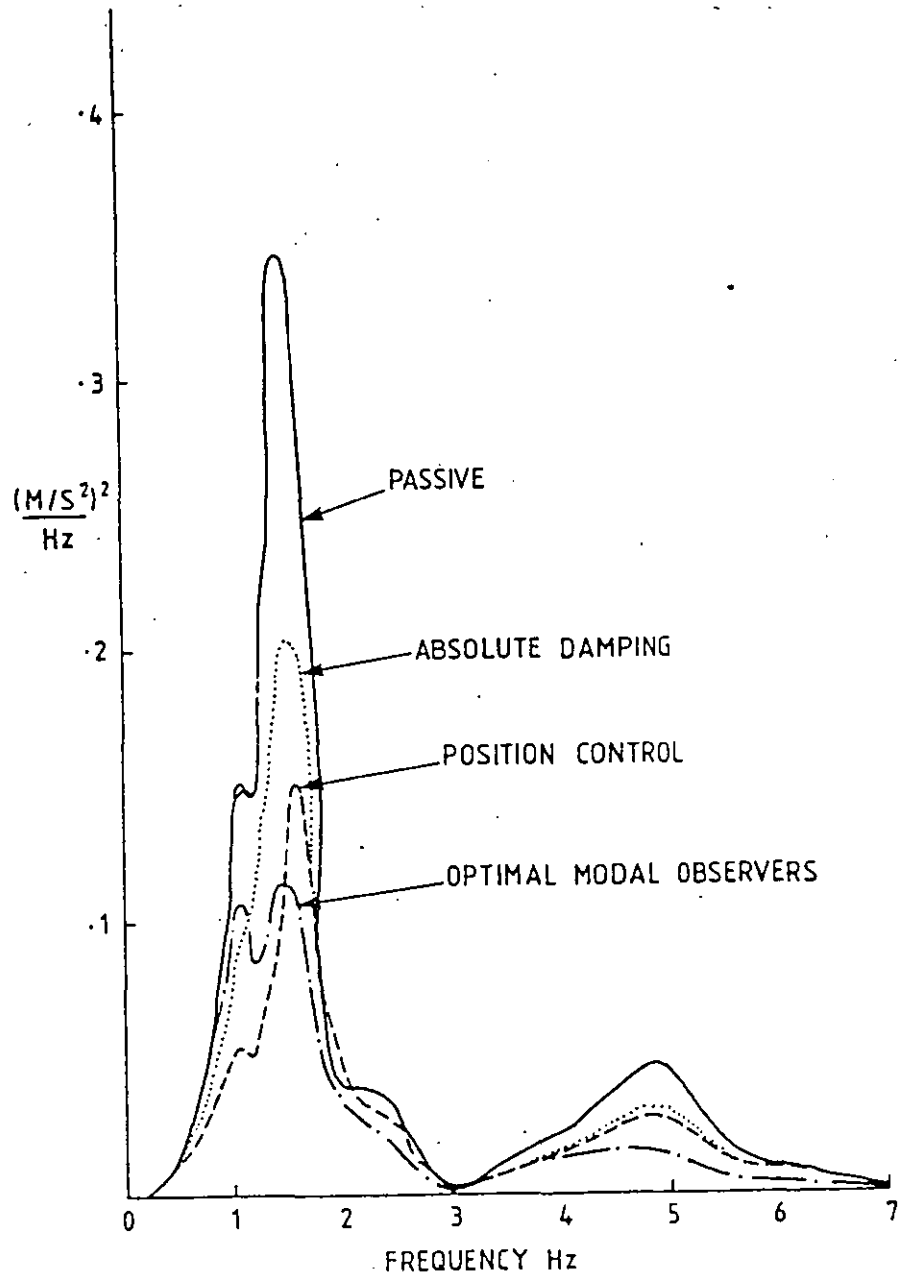


FIG. 7.2 TRAILING END ACCELERATION P.S.D. 55m/s  
WITH VEHICLE IN TEST TRAIN

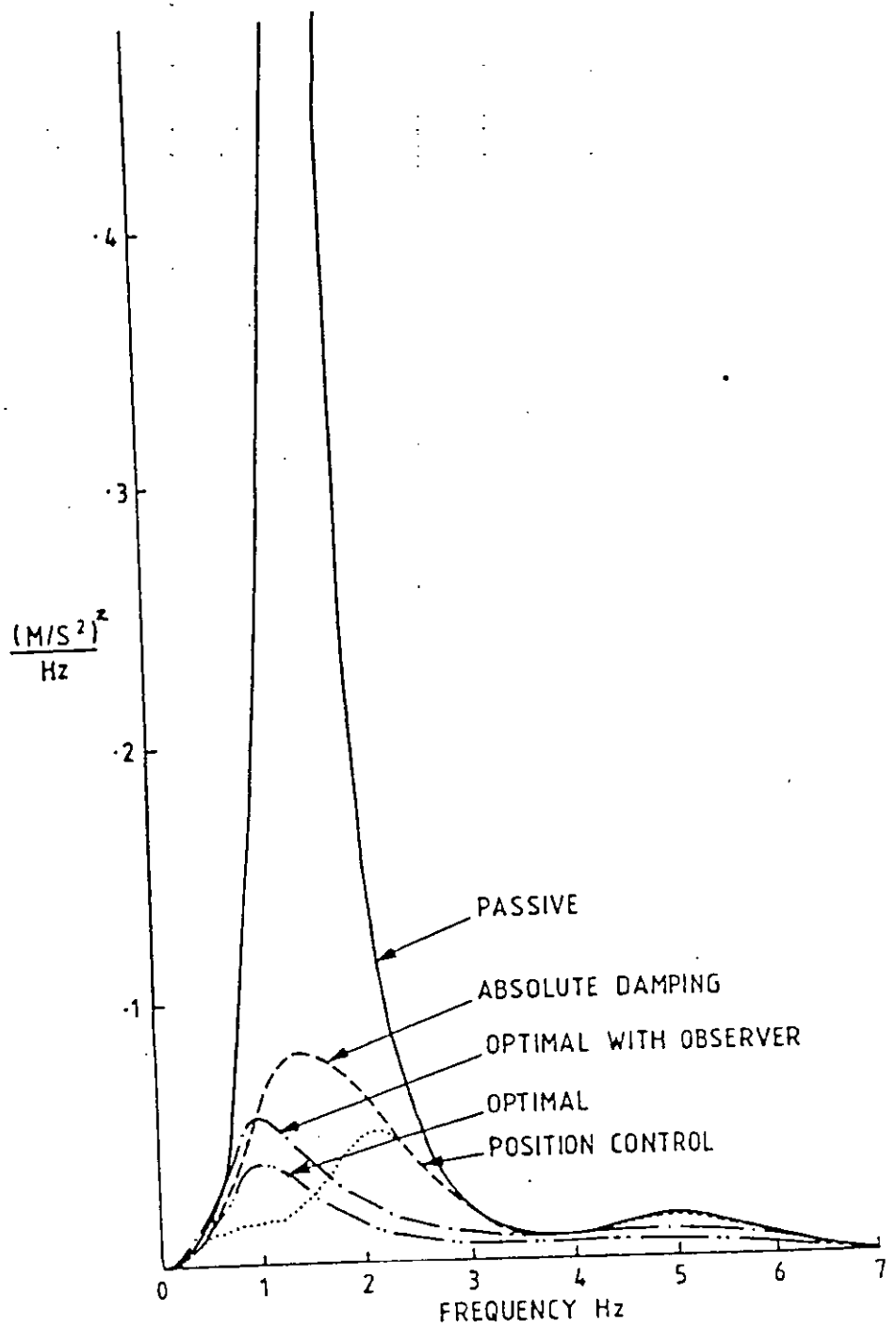


FIG.7.3 TRAILING END ACCELERATION P.S.D. 55m/s.

TABLE 7.1

MK III Coach Active Suspension Theoretical Performance 55 m/s Vehicle in Test Train

	SUSPENSION						ACTUATOR							
	LEADING rms Accn <sup>n</sup> m/s <sup>2</sup>		CENTRE rms Accn <sup>n</sup> m/s <sup>2</sup>		TRAILING rms Accn <sup>n</sup> m/s <sup>2</sup>		DISPLACEMENT mm		LEADING END			TRAILING END		
	RED		RED		RED		LEADING TRAILING	AMPS	VOLTS	WATTS	AMPS	VOLTS	WATTS	
Passive	7.6	5.7	3.1	2.4	5.7	4.6	4.1	4.3						
Sky Hook	5.6	4.2	2.4	1.9	4.7	3.7	4.1	5.0	13.9	45	429	12.2	38	329
Position	4.5	3.5	2.4	2.0	4.3	3.5	5.3	5.3	26	85	1498	22	71	1055
Small Observer	6.5	4.9	2.8	2.2	4.8	3.9	4.5	5.3	8.7	31	167	9.4	33	199
Modal Observers	5.4	3.9	3.6	2.0	4.0	3.2	4.9	5.7	15.1	49	352	13.4	53	304



TABLE 7.2

MK. III Coach Active Suspension Theoretical Performance 44 m/s Vehicle in Test Train

	SUSPENSION						ACTUATOR							
	LEADING rms Accn <sup>n</sup> m/s <sup>2</sup>		CENTRE rms Accn <sup>n</sup> m/s <sup>2</sup>		TRAILING rms Accn <sup>n</sup> m/s <sup>2</sup>		DISPLACEMENT mm		LEADING END			TRAILING END		
	RED		RED		RED		LEADING TRAILING	AMPS	VOLTS	WATTS	AMPS	VOLTS	WATTS	
Passive	5.3	3.9	3.0	2.2	3.6	2.9	3.1	3.5						
Sky Hook	3.6	2.7	2.0	1.5	3.1	2.5	3.0	4.0	11.0	34	275	10	31	224
Position	2.6	2.0	1.7	1.4	3.0	2.5	4.4	4.6	20	64	919	17.4	55	678
Optimal Modal Observers	3.7	2.7	2.4	1.8	3.1	2.4	3.2	4.8	10.6	35	181	9.3	34	150

CHAPTER 8  
CONTROL SYSTEM ELECTRONICS

The electromagnetic active suspension fitted to British Rail Mk III Coach M.12094 was primarily intended to provide service experience of active suspensions. Therefore all the equipment had to be manufactured to a standard which would accept the use and abuse of the railway environment (62). As the two classical control systems were more fully developed than the optimal control systems the experimental equipment was designed around them. This led to some compromises having to be made when the optimal control systems were implemented.

8.1 Power Electronics

The power supply schematic is shown in Fig. 8.1. Current is supplied to the actuators via 4 quadrant pulse width modulated (P.W.M.) transistor power amplifiers. There is a current feedback built into the amplifiers so that the amplifiers provide an output current which is proportional to the demand signal. With a P.W.M amplifier the effective voltage applied by the amplifier is proportional to the mark period ratio of the amplifier. Subsequently the amplifiers have been designed to provide an analogue output voltage and current.

Power for the amplifiers is supplied from a 300 V d.c. bus, which appears to be quite conservative, compared to the 40-60 Volts r.m.s predicted in earlier chapters. This was chosen because of the non-linear nature of the amplifiers. Chapter 4 showed that the actuator force is proportional to the square of the actuator current and if a sinusoidal force at frequency  $\omega$  is applied to the vehicle the current will be

$$I = \frac{F_p \sin(\omega t)}{\sqrt{K_{I2}}} \quad (8.1)$$

in which  $F_p$  is the peak force and  $K_{I2}$  a force constant. The voltage required to produce this sinusoidal force

$$V = L \frac{dI}{dt} = \frac{\omega L}{2} \sqrt{\frac{F_p}{K_{I2}}} \frac{\cos(\omega t)}{\sqrt{\sin(\omega t)}} \quad (8.2)$$

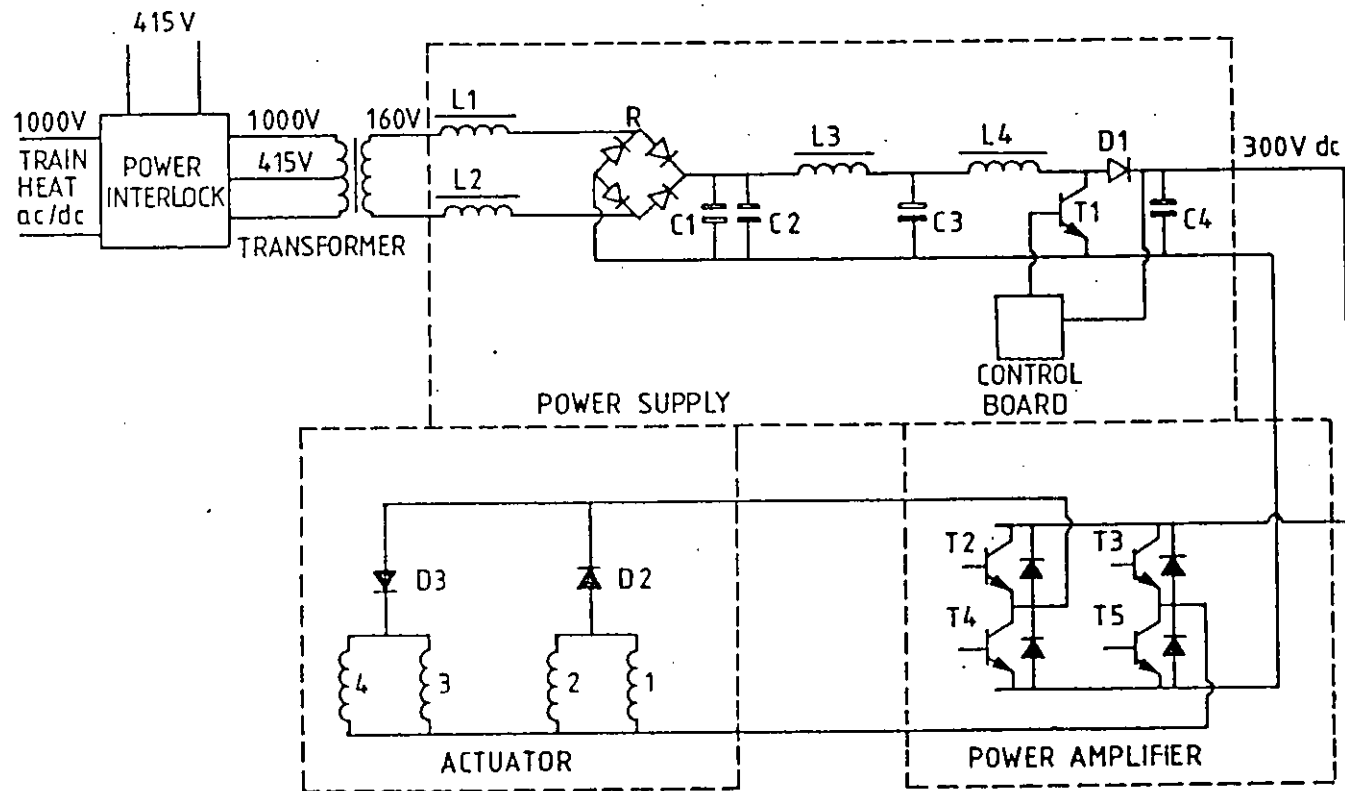


FIG.8.1 POWER ELECTRONICS

which is infinite when  $\omega t = 0$ . Thus to produce a credible response excess forcing voltage is required when the direction of the force is reversed.

### 8.1.1 Power Supply Unit

The 300 V d.c. bus was generated by a flyback converter supplied from a 160 V transformer secondary winding (Fig. 8.1). The input chokes  $L_1$  and  $L_2$  reduce the input surge to the capacitor bank,  $L_3$  reduces the ripple to capacitor  $C_3$ . Voltage step up is provided by switching transistor  $T_1$  on and off. When  $T_1$  is in the on state a current flows in choke  $L_4$  to ground. When it is switched off the decaying flux in  $L_4$  causes the voltage to rise to the point where the energy stored in the choke can be transferred to the capacitor bank  $C_4$ . By controlling the mark-period ratio of transistor  $T_1$  the voltage on the bus can be kept constant.

Two primary tapings were provided on the transformer. A 415 V tapping to enable the active suspension to be powered from a standard 415 V supply (either a shore supply or a laboratory coach) and a 900 V tapping to allow the system to be powered from the train heat supply (E.T.H). It is the variation in the train heat supply voltage (590 V to 1060 V) which led to the requirement for a sophisticated power supply. The power supply unit had to be tolerant to interruptions in the E.T.H supply, lasting up to 15 s, when the train passed through neutral sections between feeder stations.

Though the coach was normally hauled by an a.c. electric locomotive, which provides an a.c. train heat supply, it was possible for it to be hauled by a diesel electric locomotive which provides a d.c. train heat supply. This required the power supply to be interlocked so that power was only connected to the transformer when an a.c. supply was present. (Fig 8.2.)

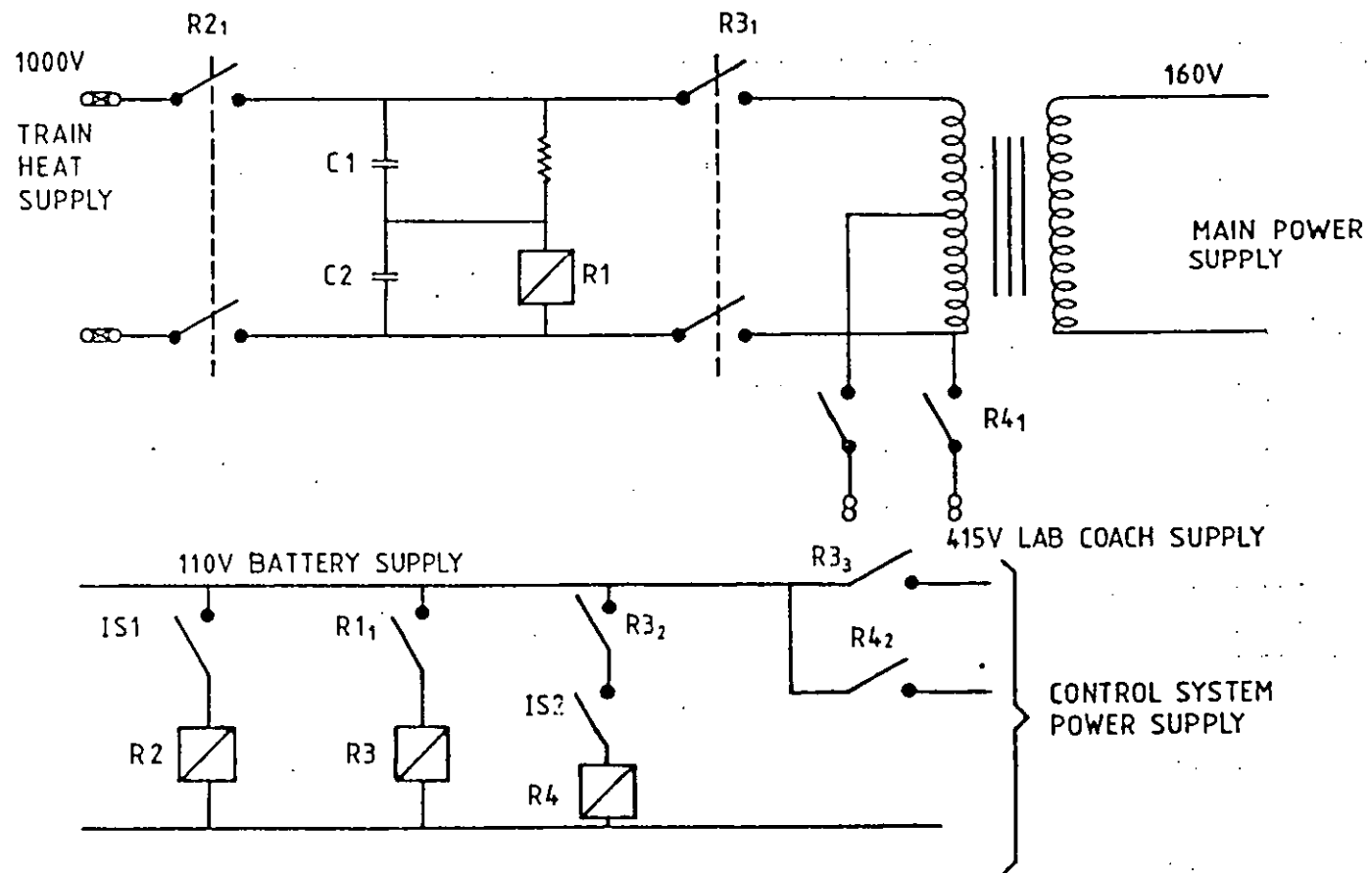


FIG. 8. 2 POWER INTERLOCK

FRS/AS/AS/AS

1.62

Table 8.1 Power Supply Specification

<u>Power Supply Unit</u>	
Supply Voltage	590 V - 1060 V nominal 900 V d.c.
or	415 V a.c.
Secondary Voltage	160 V a.c.
D.C. Bus	300 V d.c.
Continuous Power	3.6 kW
Peak Power	13 kW
<u>Power Amplifier</u>	
Continuous Current	20 Amps
Peak Current	50 Amps

## 8.2

Instrumentation

Active suspensions require instrumentation which is rugged and reliable. Accuracy and linearity are of secondary importance as the system controls the dynamic performance of the vehicle which does not require precise control.

Unfortunately most commercial instrumentation is designed to give accurate readings under laboratory conditions and is not very suitable for fitting to a railway vehicle operating under service conditions. The instrumentation fitted to M.12094 was selected from experience.

Actuator current was measured internally in the power amplifiers by d.c. current transformers. Analogue current signals were provided by the amplifiers for use within the control system. Analogue voltage signals were also provided internally in the amplifier by potential dividers. These were only used to monitor system performance and not for control purposes.

Flux was measured by integrating the output of search coils around the centre poles of magnets 1 and 2 in Fig 4.5. These are both cheap and rugged and have a very good signal to noise ratio. The alternative would be Hall effect devices which are more susceptible to noise, intrude into the airgap (and thus risk damage) and make a very localised measurement of flux which may not be representative. They do however measure the absolute value of flux.

Acceleration was measured by Schaevitz A411  $\pm 3$  g inductive accelerometers. These are not normally considered suitable for instrumentation purposes as they have a relatively limited bandwidth (32 Hz) compared with most instrumentation accelerometers ( $> 200$  Hz). However they are ideal for control systems with bandwidths of less than 20 Hz. Their biggest advantage is that they are almost indestructible tolerating  $\pm 1000\%$  over range without permanent damage. Other accelerometers may be destroyed by little more than 100% over range. The accelerometers are conditioned by the circuit in Fig. 8.3. Amplifier A2 is a Wein bridge oscillator output voltage established by A1 and TR1.

The 5 kHz oscillation is fed to the accelerometer which forms a bridge with resistors  $R_{14}$  and  $R_{15}$  and  $RV_1$  provides zero offset. The bridge output is fed to the multiplier X1 which acts as a phase sensitive detector. The resistors and capacitors around A5 remove the 10 kHz ripple from the output signal so that the output is a d.c. signal proportional to  $\ddot{z}$ . Signal conditioning is kept close to the accelerometers and the unit has very good noise immunity. The accelerometers were mounted inside the vehicle skirt, to protect them from the environment. The mounting position was close to the primary bending node to reduce the effect of coupling with the control system.

Displacement was measured by capacitive displacement transducers, which had been developed by British Rail for use on the Maglev Vehicle (63)(64). They have no moving parts and should be free from the wear problems which beset potentiometers, and to a lesser extent LVDTs.

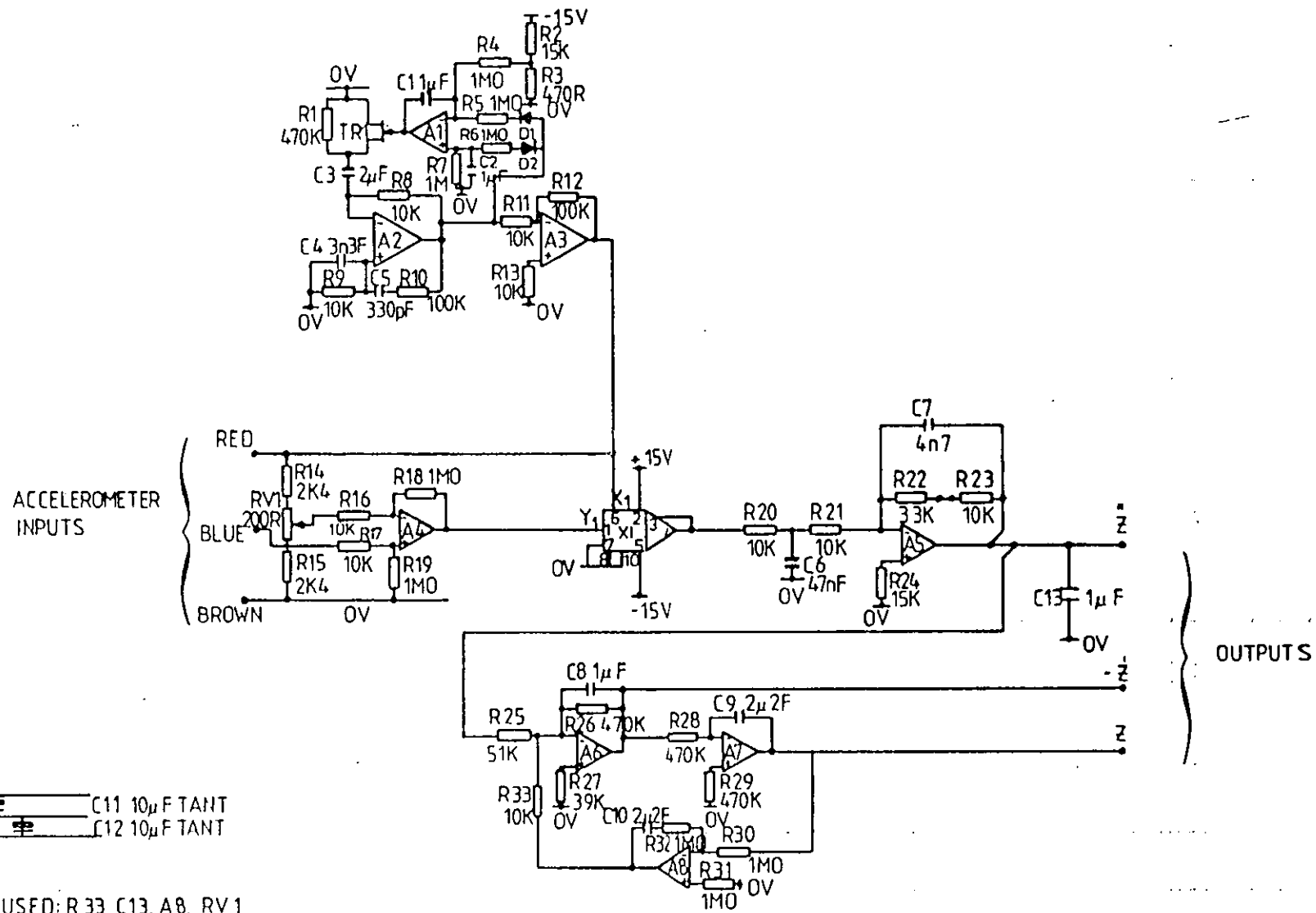


FIG 8.3 ACCELEROMETER UNIT



Table 8.2 Transducer Scalings

Analogue Current	.1 V/A
Analogue Voltage	60 V/A
Current Demand	.2 V/A
Flux	.2 V/A of armature current at 33 mm airgap
Acceleration	2 V/m/s <sup>2</sup>
Displacement	80 V/m

### 8.3 Classical Control System Layouts

Chapter 5 described how the classical control systems control the modes of vibration independently, allowing them to be broken down into 13 modules. These modules require 4 different control cards.

#### 8.3.1 Position Control System

Fig. 8.4 shows the position control system schematic. There are accelerometers, displacement transducers and actuators at each corner of the vehicle numbered 1 to 4 as shown.

The acceleration and displacement signals from the corners of the vehicle are summed to form modal acceleration and displacement signals.

$$\begin{pmatrix} z \\ \Phi \\ \theta \end{pmatrix} = \begin{pmatrix} .1 & 1 & 1 & 1 \\ -1 & -1 & 1 & 1 \\ -1 & 1 & 1 & -1 \end{pmatrix} \begin{pmatrix} z_1 \\ z_2 \\ z_3 \\ z_4 \end{pmatrix} \quad (8.3)$$

These signals are fed to the modal filter boards which integrate the acceleration signal twice to form the absolute modal position. The absolute and relative position signals are then filtered by a pair of complementary high and low pass filters.

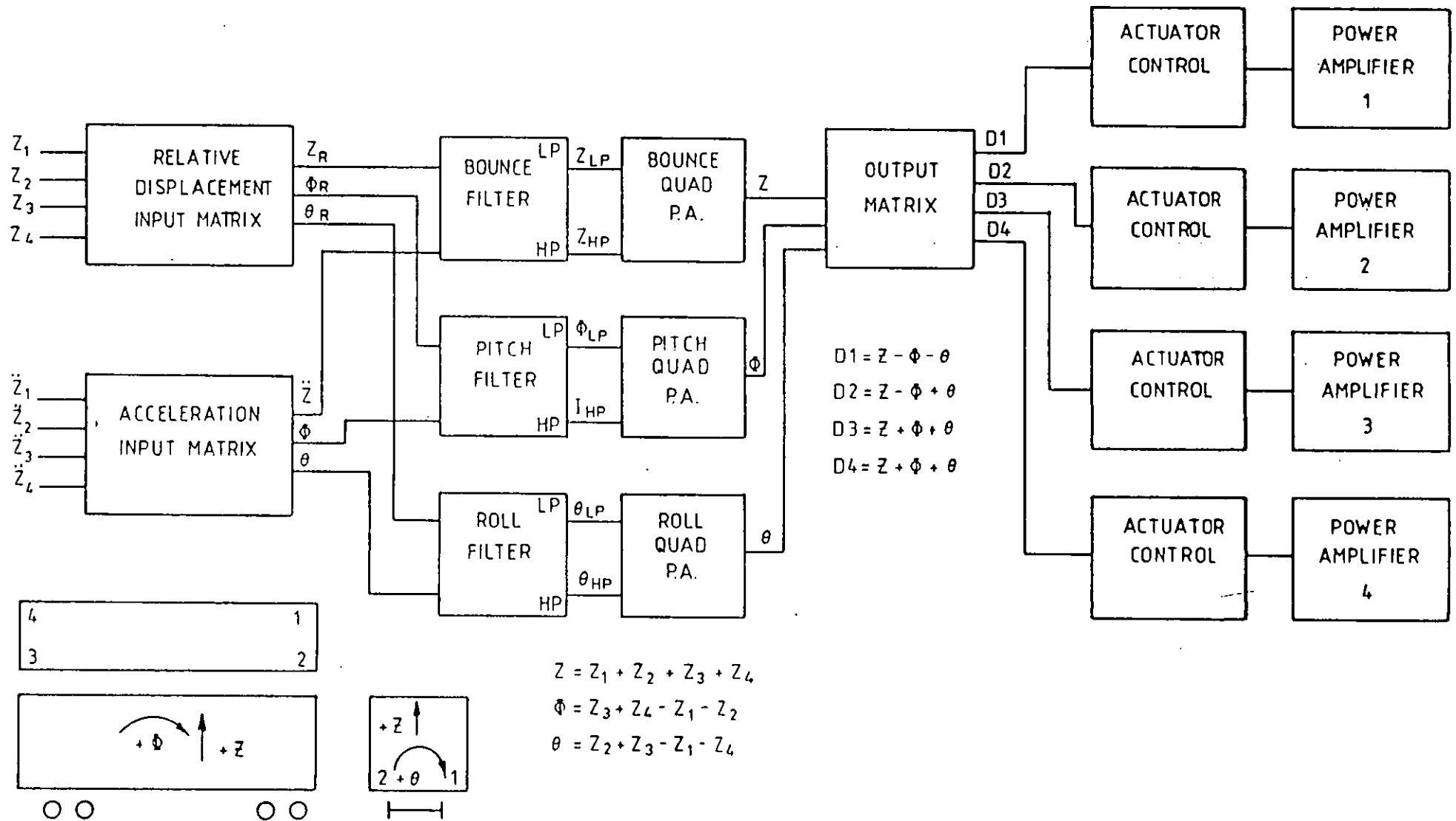


FIG. 8-4 LAYOUT SCHEMATIC POSITION CONTROL

The filter boards feed onto a phase advance board which provides phase compensation for the modal control loops. These boards also contain narrow bandwidth band stop filters (notch filters) to remove the effects of flexible body modes on the control system. Notch filters were included within the modal control loops as each flexible body mode can usually be associated with one of the rigid body modes.

The modal signals are recombined on the output matrix board to form demands for each of the actuators.

$$\begin{matrix} D1 \\ D2 \\ D3 \\ D4 \end{matrix} = \begin{matrix} 1 & -1 & -1 \\ 1 & -1 & 1 \\ 1 & 1 & 1 \\ 1 & 1 & -1 \end{matrix} \begin{matrix} z \\ \phi \\ \theta \end{matrix} \quad (8.4)$$

The output demands D1, D2, D3 and D4 are then fed to the actuator control boards which turn the demands into an actuator force demand.

### 8.3.2 Absolute Damping

Fig. 8.5 shows the absolute damping schematic. In this configuration the relative displacement matrix is redundant.

The modal acceleration signals are fed to an absolute damping board which integrates the acceleration once to form an absolute velocity signal. This is then fed to a board containing a notch filter. The modal outputs from the notch filter boards are then fed into the output matrix board.

The control circuits for this option could have been provided on fewer boards. However the system was designed so that boards could be interchanged with the position control boards in the card frame making the system more flexible. To change from the position control system to the absolute damping control system the Filter Modules are replaced by the Absolute Damping Modules and the Phase Advance Modules by the Absolute Damping Notch Filter Modules

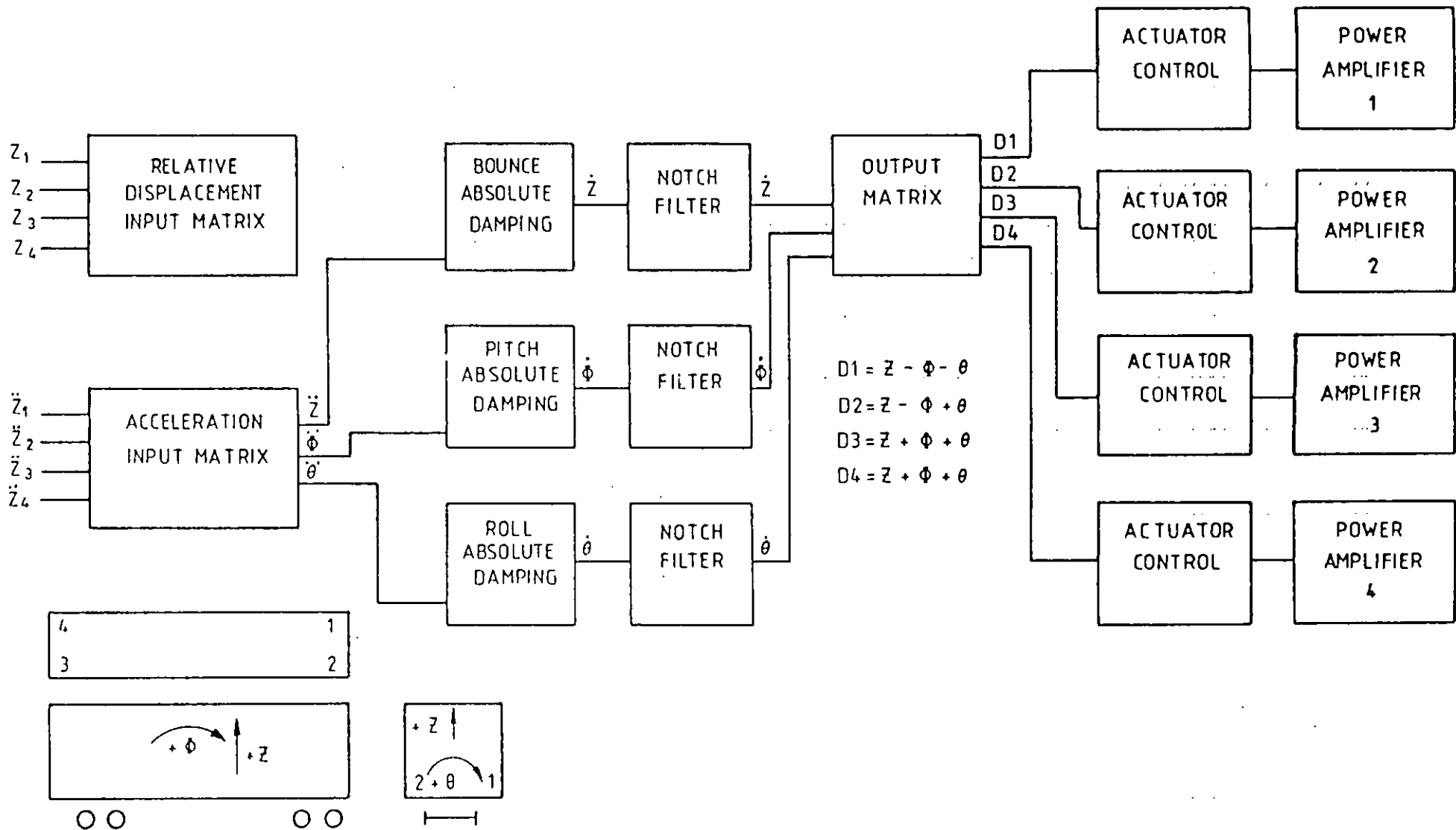


FIG. 8-5 LAYOUT SCHEMATIC ABSOLUTE DAMPING

## 8.4 Control Circuits

### 8.4.1 Matrix Boards

A common p.c.b. was used for the three matrices, acceleration input matrix, relative displacement input matrix and output matrix (Fig. 8.6).

Input signals are buffered by the differential amplifiers (A1, A2, A3, A4). Select on test resistors are provided to the +15 V rails to trim any offsets.

The signals are summed on amplifiers A5, A6, A7 and A8. Provision is made to allow any combination of input signals to be summed on any of the amplifiers.

### 8.4.2 Actuator Control Unit

The actuator control unit is shown in Fig. 8.7. There is one per amplifier and the unit is common to the position control and absolute damping control systems. The unit controls the current in the power amplifier so that the force produced by the actuator is proportional to the force demand signal  $D_n$ , where  $n$  is the actuator number.

Force is controlled by controlling the actuator flux, which is measured by search coils in the centre magnets (2 and 3) in Fig. 4.5. The output from the search coils ( $p\phi_1$  and  $p\phi_2$ ) is measured by the differential amplifiers A1 and A2 and then summed by amplifier A3. The output of A3 is integrated by A4 to derive a flux signal, as the flux coils measure rate of change of flux. A5 provides integral feedback around A4, to prevent it from drifting, giving the transfer function between A3 and A4:-

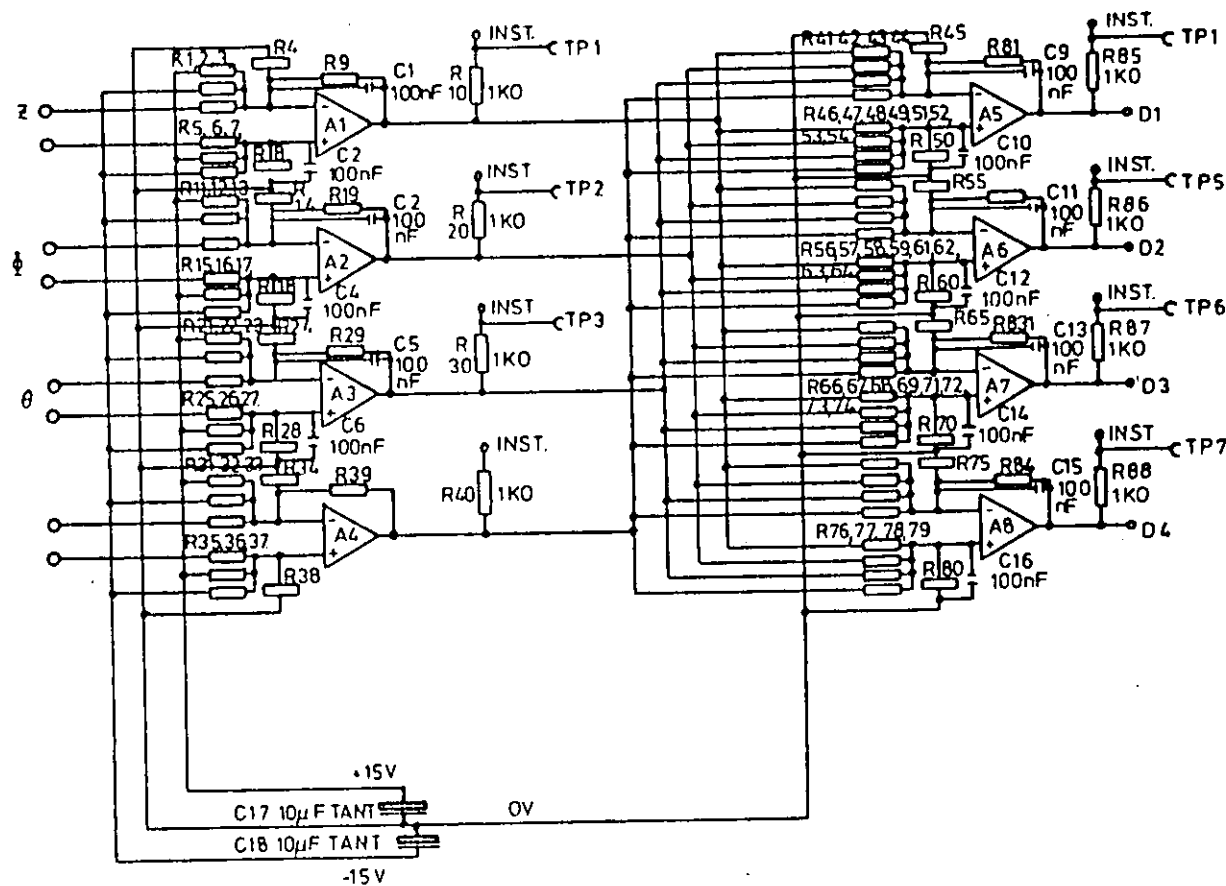


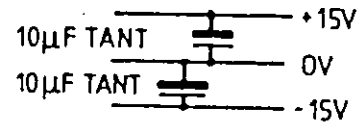
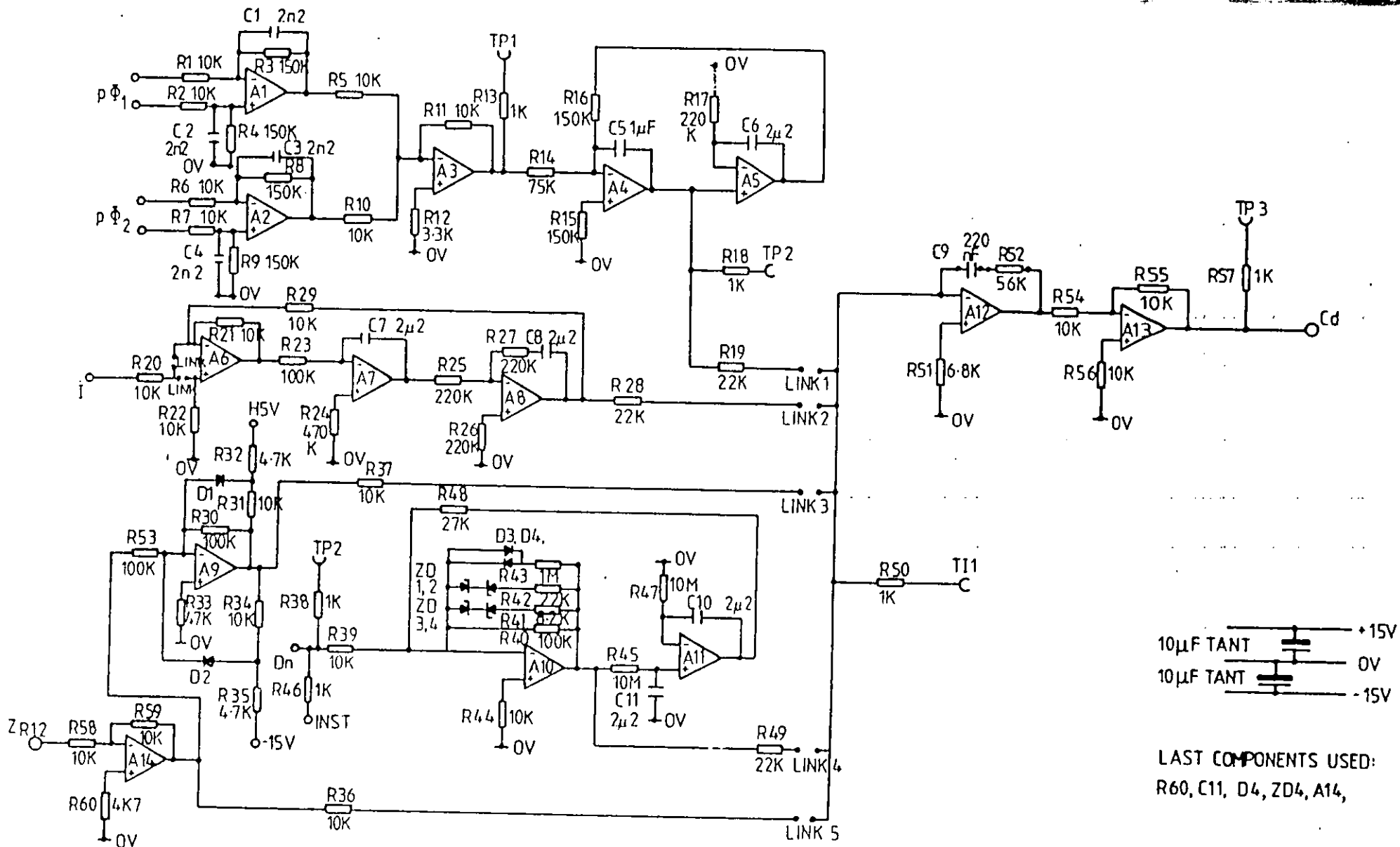
FIG 8-6 OUTPUT MATRIX

LAST COMPONENTS USED:

A8, R88, C18

C1-C16 100nF

ALL IC.s 558 TYPE



LAST COMPONENTS USED:  
 R60, C11, D4, ZD4, A14,

FIG. 8-7 ACTUATOR CONTROL UNIT

$$\frac{V_4}{V_3} = \frac{-R_{16} R_{17} C_6 s}{R_{14} (1 + R_{17} C_6 s + R_{16} R_{17} C_5 C_6 s^2)} \quad (8.5)$$

As the integrator is decoupled below 0.5 Hz a low frequency current signal is added to the control loop as compensation. Though this makes the low frequency loop gain dependent upon the air gap the changes in gain take place slowly enough for the outer control loops to accommodate them. The transfer function of the low pass filter, which is made up of amplifiers A6, A7 and A8 is:-

$$\frac{V_8}{I} = \frac{-(1 + R_{27} C_8 s)}{1 + R_{27} C_8 s + R_{23} R_{25} C_7 C_8 s^2} \quad (8.6)$$

Because force is proportional to the square of flux a non-linear circuit is provided on amplifier A10 which takes the "square root" of the demand signal  $D_n$ , so that the force generated is proportional to the demand.

$$V_{10} = \frac{-D_n \sqrt{|D_n|}}{|D_n|} \quad (8.7)$$

The "square root" is in fact a piece wise smooth linearisation of the function generated by the diodes and zener diodes. This provides better control than a true square root circuit, using multipliers, as the small signal gain around zero of a true square root circuit would be infinite, leading to a noisy circuit.

Amplifier A9 provides an electronic bump stop. The output of A9 is limited  $\pm 10$  V by the potential dividers and diodes. If the relative displacement output at the corner  $ZR_n$  is between  $\pm 10$  V the signal inputs to the flux loop on  $R_{36}$  and  $R_{37}$  will cancel each other out. If  $ZR_n$  goes outside the range A9 will limit and a signal will be fed into the control loop opposing any further change in  $ZR_n$ .



Proportional plus integral drive action is provided by amplifier A12, which has the transfer function:-

$$\frac{V_{12}}{V_{10}} = - \frac{(1 + R_{52} C_9 s)}{R_{49} C_9 s} \quad (8.8)$$

Output from the board  $C_d$  is fed to the power amplifiers which supply a current proportional to  $C_d$ .

### 8.4.3 Position Control Filter Module

A filter module (Fig. 8.8), is provided for each of the three modes of vibration bounce, pitch and roll ( $z, \Phi, \theta$ ).

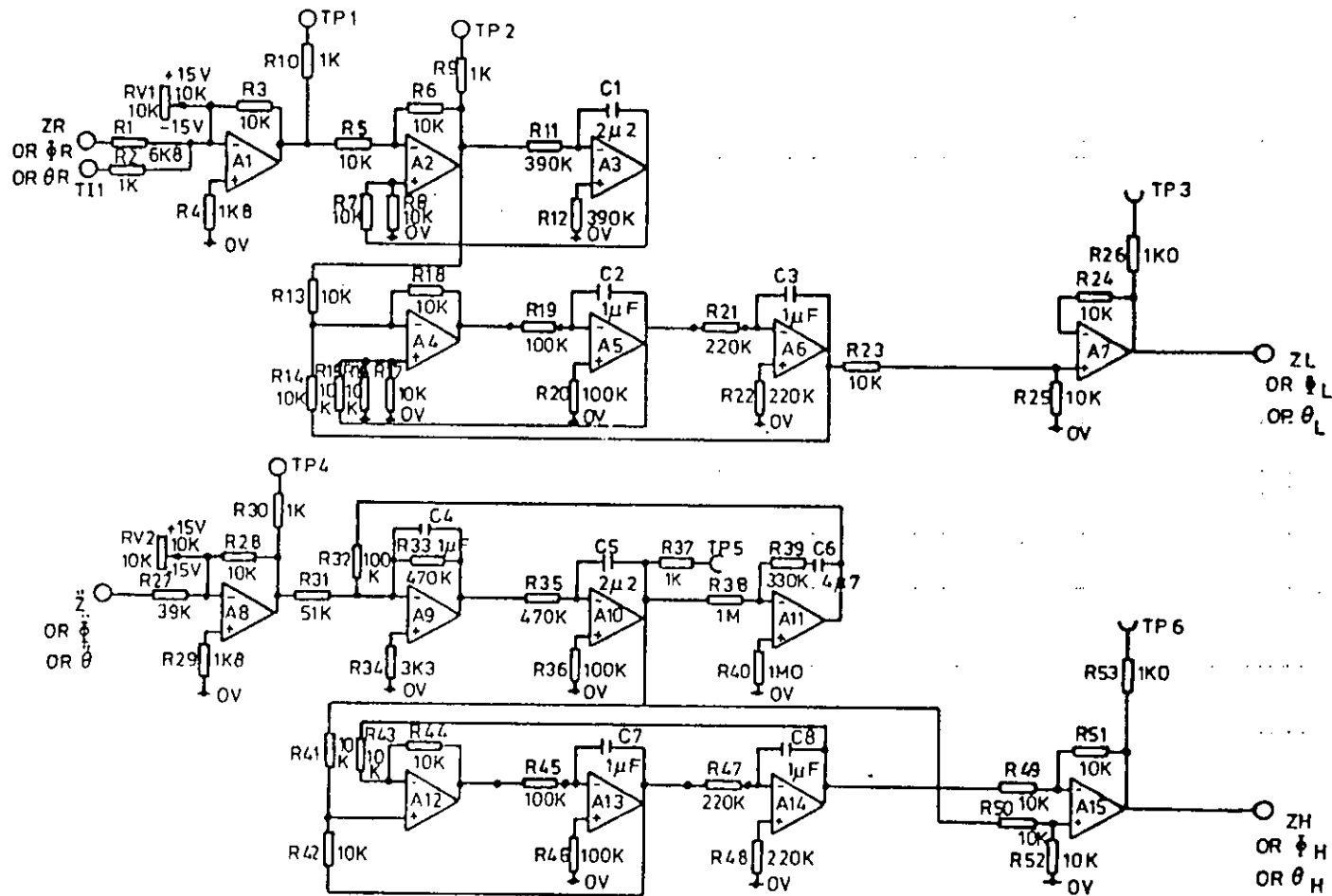
Relative displacement, resolved into mode of vibration, is input to the board, from the relative displacement input matrix board, on amplifier A1. A test input, T11, is provided to enable test signals to be injected into the control system. Amplifiers A2 and A3 provide a high pass filter (frequency 0.2 Hz) to decouple the control system from the suspension at d.c. This is required to prevent the control system coming into conflict with the airsprung levelling valves. The transfer function of the filter is:-


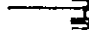

$$\frac{V_2}{V_1} = \frac{-R_{11} C_1 s}{1 + R_{11} C_1 s} \quad (8.9)$$

Amplifiers A4, A5 and A6 provide the low frequency part of the pair of complementary filters. It is a 1 Hz 2 pole Butterworth filter with the transfer function.

$$\frac{V_6}{V_2} = \frac{-1}{1 + R_{21} C_3 s + R_{19} R_{21} C_2 C_3 s^2} \quad (8.10)$$

Modal acceleration is input from the acceleration matrix board on Amplifier A8. The gain of A8 is higher on the pitch acceleration board than the other two boards as the accelerometers are closer to the centre line of the vehicle than the displacement transducers, and it is desirable to maintain constant scaling between boards.



$10\mu\text{F TANT}$   +15V  
 $10\mu\text{F TANT}$   0V  
 -15V

ALL RESISTORS TR5 2%  
 ALL I.C.s 588 TYPE  
 LAST COMPONENTS USED: R53, C8, A15.

FIG. 8-8 FILTER MODULE

Amplifiers A9 and A10 integrate the acceleration twice to provide absolute position, and integrator A11 prevents them from drifting, providing roll off below 0.2 Hz. The transfer function of the double integrator is

$$\frac{V_{10}}{V_8} = \frac{R_{32} R_{33} R_{38} C_6 s}{R_{31} R_{33} + R_{31} R_{33} R_{39} C_6 s + R_{31} R_{32} R_{35} R_{38} C_5 C_6 s^2 + R_{31} R_{32} R_{33} R_{35} R_{38} C_4 C_5 C_6 s^3} \quad (8.11)$$

The high pass half of the pair of complementary filters is provided by A12, A13, A14, A15.

$$\frac{V_{15}}{V_{10}} = \frac{R_{47} C_8 s + R_{45} R_{47} C_7 C_8^2 s^2}{1 + R_{47} C_8 s + R_{45} R_{47} C_7 C_8^2 s^2} \quad (8.12)$$

The scalings on this board are

Relative displacement	900 V/m
Acceleration	2 V/m/s <sup>2</sup>
Velocity	40 V/m/s
Absolute displacement	40 V/m

#### 8.4.4 Position Control Phase Advance Module

Each of the modal control loops has a phase advance module, fed from the filter module, which provides phase compensation for the control loop (Fig. 8.9). Amplifier A1 sums the outputs from the high pass and low pass filters. Resistor  $R_5$  is used to control the gain of amplifier A1 and the control loop gain.

Loop gain can also be controlled by  $R_{33}$ ,  $R_{40}$  and  $C_5$  around A6. This combination was provided to enable the loop gain to be increased more at low frequencies than it is at high frequencies.

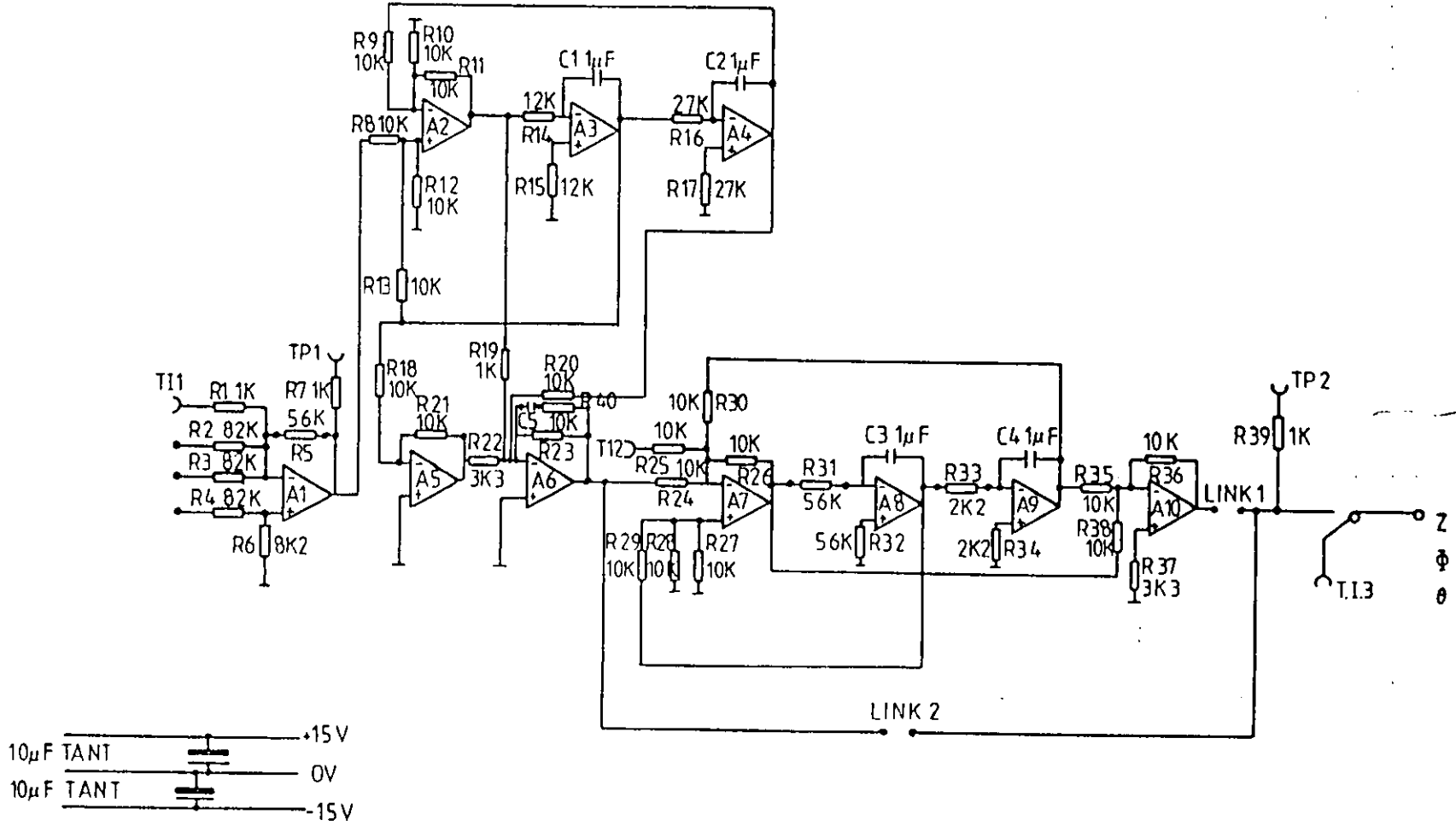


FIG 8.9 PHASE ADVANCE MODULE

Frequency compensation is provided by the phase advance network A2, A3, A4, A5 and A6. The transfer function is

$$\frac{V_6}{V_1} = \frac{R_{23} + R_{23} R_{16} C_2 s + R_{23} R_{14} R_{16} C_1 C_2 s^2}{1 + R_{16} C_2 s + R_{14} R_{16} C_1 C_2 s^2} \quad (8.13)$$

A notch filter is provided by A7, A8 and A9 to reduce interaction with the structural modes.

The transfer function is:-

$$\frac{V_6}{V_{10}} = \frac{1 + R_{31} R_{32} C_3 C_4 s^2}{1 + R_{33} C_4 s + R_{31} R_{33} C_3 C_4 s^2} \quad (8.14)$$

Note that the notch filter can be by-passed if it is not required.

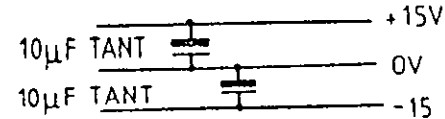
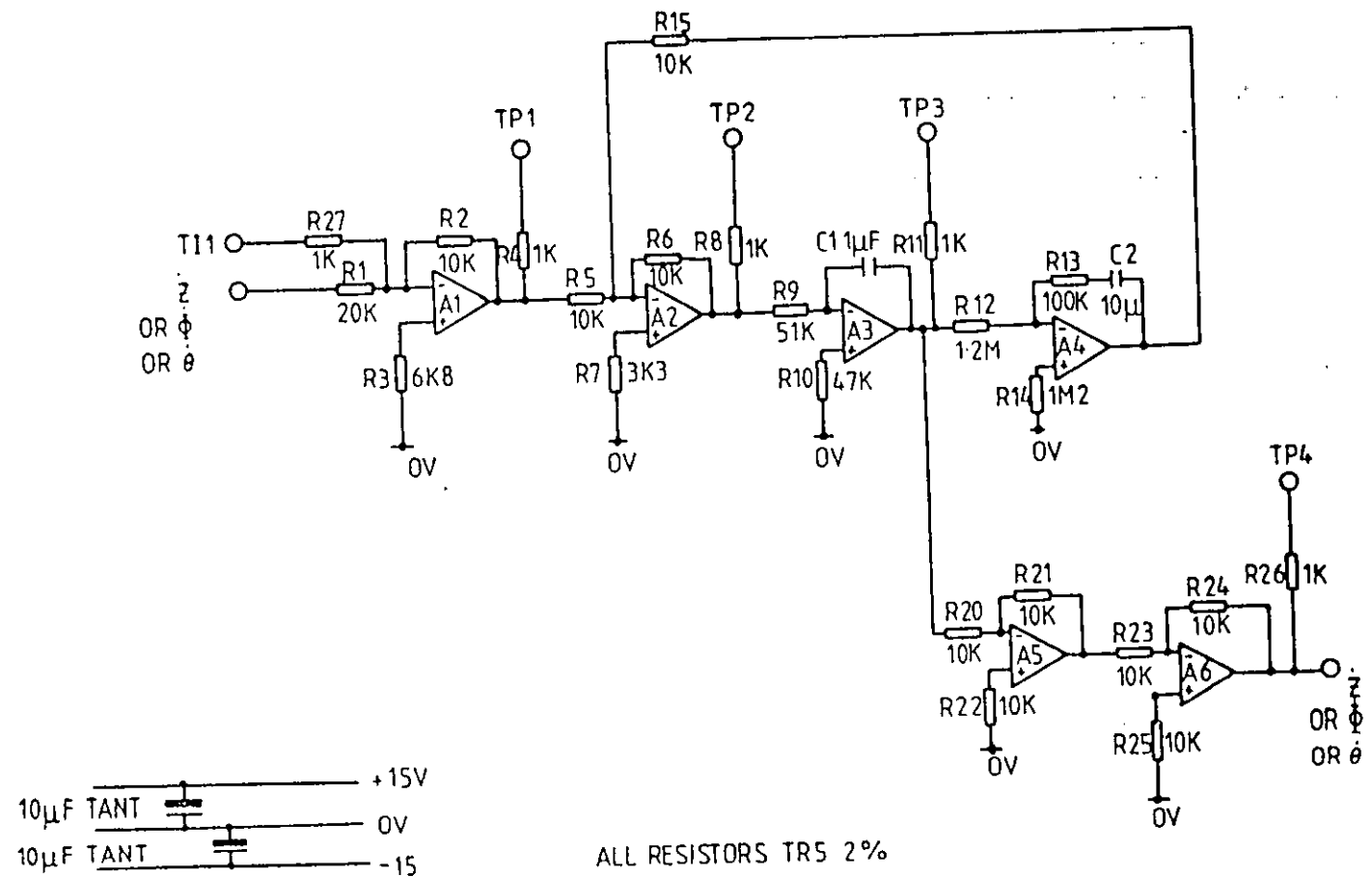
The control loop can be broken to allow a test signal to be input at TI3, to measure the open loop response (TP2/TI3) during commissioning.

#### 8.4.5 Absolute Damping Circuit

The absolute damping circuit Fig. (8.10) is an alternative to the position control filter board described in Section 8.4.3, and replaces it in the card frame. There is one board for each of the bounce, pitch and roll modes.

Modal acceleration, from the acceleration matrix, is integrated by A3 to provide modal velocity. Amplifier A4 provides integral feedback to prevent the integrator drifting. This gives a roll up at 0.2 Hz. The transfer function is

$$\frac{V_3}{V_1} = \frac{R_{12} C_2 s}{1 + R_{13} C_2 s + R_9 R_{12} C_1 C_2 s^2} \quad (8.15)$$



ALL RESISTORS TR5 2%  
 ALL I.C.s. 558  
 LAST COMPONENTS USED: R26, C2, A6

FIG. 8-10 ABSOLUTE DAMPING CIRCUIT

#### 8.4.6 Absolute Damping Notch Filter Circuit

The absolute damping notch filter board Fig. (8.11) is an alternative to the position control phase advance module described in Section 8.4.4, and replaces it in the cardframe. This board is used in conjunction with the absolute damping circuit in Section 8.4.5.

The notch filter is made up from amplifiers A3, A4, A5 and A6 and has the transfer function:-

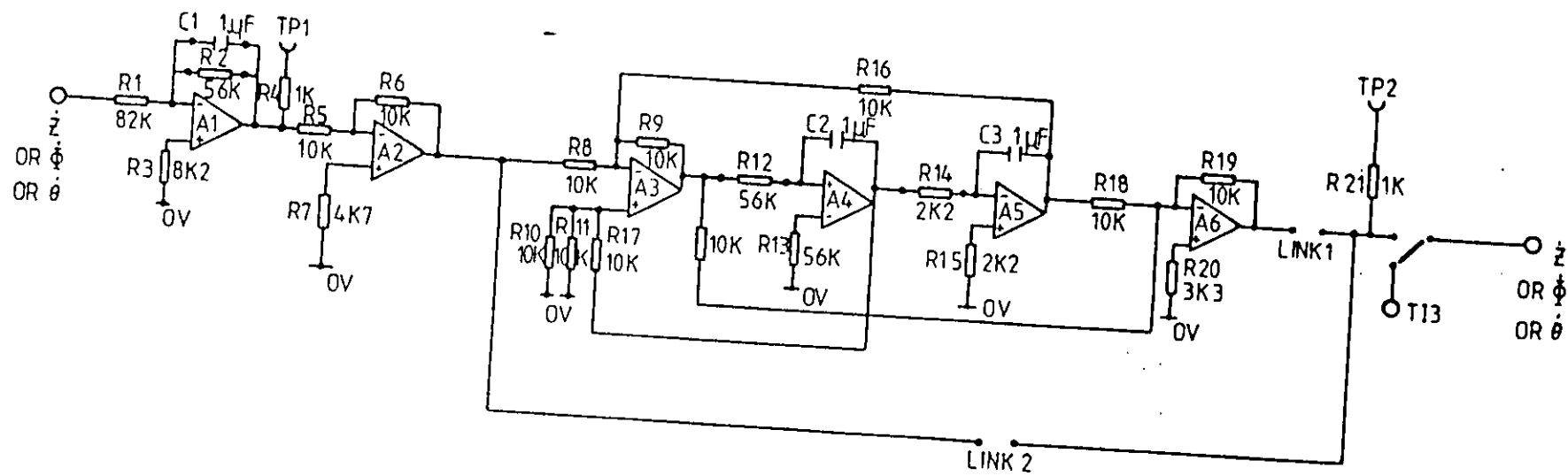
$$\frac{V_6}{V_2} = \frac{1 + R_{12} R_{14} R_2 C_3 C s^2}{1 + R_{14} C_3 s + R_{12} R_{14} C_2 C_3 s^2} \quad (8.16)$$




It can be by-passed if it is not required. The control loop can be broken to allow a test signal to be input at  $TI_3$  to measure the open loop frequency response (TP2/TI3).

#### 8.5 Small Model Observer

An optimal controller was built based on the small model observer described in Section 6. Some concessions had to be made in order to fit the observer into a card frame designed for the classical control system. The main problem of adaptation was the shortage of back plane connections on the 24 pin Hypertac connectors used in the controller. This was overcome by including a ribbon cable connector on the front of the control cards to bus the relevant connections across. Ribbon cable numbers and signal scalings are given in Table 8.3.

The first ten lines of the ribbon cable carry the observed variables. The next six lines the measurement errors (i.e. the measured variable minus the observed variable). The final eight lines carry the flux and current signals as these are not available on the back plane.



$10\mu\text{F TANT}$   +15V  
 $10\mu\text{F TANT}$   0V  
 $10\mu\text{F TANT}$   -15V

ALL RESISTORS TR5 2%  
 ALL ICs 558 TYPE  
 LAST COMPONENTS USED: R21, C3, A6

**FIG. 8-11 ABSOLUTE DAMPING NOTCH FILTER CIRCUIT**



TABLE 8.3 Optimal Observer Variables and Scalings

Optimal Control Cable No.	Variable	Scaling
	$\ddot{z}$	2 V/m/s <sup>2</sup>
1	$\dot{z}$	10 V/m/s
2	$z$	40 V/m
	$\ddot{\Phi}$	16 V/Rad/s <sup>2</sup>
3	$\dot{\Phi}$	8 V/Rad/s
4	$\Phi$	320 V/Rad
	$\dot{z}_1$	10 V/m/s
5	$z_1$	40 V/m
	$\dot{z}_2$	10 V/m/s
6	$z_2$	40 V/m
	$\dot{I}_1$	.02 V/Amp/s
7	$I_1$	.2 V/Amp
	$\dot{I}_2$	.02 V/Amp/s
8	$I_2$	.2 V/Amp
	$\dot{z}_{t1}$	10 V/m/s
9	$z_{t1}$	40 V/m
	$\dot{z}_{t2}$	10 V/m/s
10	$z_{t2}$	40 V/m
11	$\ddot{z}_{1E}$	2 V/m/s <sup>2</sup>
12	$\ddot{z}_{2E}$	2 V/m/s <sup>2</sup>
13	$z_{R1E}$	40 V/m
14	$z_{R2E}$	40 V/m
15	$I_{1E}$	.2 V/Amp
16	$I_{2E}$	.2 V/Amp
17	$I_1$	.2 V/Amp
18	1	.2 V/Amp
19	$I_2$	.2 V/Amp
20	2	.2 V/Amp
21	$I_3$	.2 V/Amp
22	3	.2 V/Amp
23	$I_4$	.2 V/Amp

The observer is built up on seven boards, the first three generate measurement errors:-

- 1) Acceleration Error
- 2) Relative Displacement Error
- 3) Current Error

There are three optimal control matrix boards which use the same p.c.b with different resistors. These generate the observed variables, in effect performing the integration:

$$\hat{x} = \int (A \hat{x} + KC(y-\hat{y}))dt \quad (8.17)$$

Control demands are summed on the output matrix.

Note that though the vehicle is capable of controlling bounce pitch and roll, the roll mode was not included in the controller. There are two reasons for this; the first is the small influence which the actuators can exert in roll, due to their closeness to the vehicle centre line, and the second is that the increase in the size of the observer would have made it almost impossible to accommodate within the control card frame.

#### 8.5.1 Actuator Control

The interface with the amplifiers was via the same actuator control boards Fig. 8.7. Flux and current feedback were disconnected by removing links 1 and 2, current feedback being provided from the observer. Integral action was removed from the board by shorting capacitor  $C_9$ . Resistor  $R_{52}$  was also reduced to 22 K to give correct scaling.

### 8.5.2 Acceleration Error Board

Acceleration errors ( $\ddot{z}_{1E}$  and  $\ddot{z}_{2E}$ ) are generated on the acceleration error board Fig. 8.12. Amplifiers A1, A2, A3 and A4 provide differential input buffers for the accelerometer signals. Amplifiers A5 and A6 sum the observed variables to generate the observed acceleration at end 1 ( $\hat{\ddot{z}}_1$ ). The measured values at end 1 are added to A6 to generate the acceleration error  $\ddot{z}_{1E}$ . Amplifiers A7 and A8 perform a similar function for the observed acceleration and acceleration error at end 2 ( $\ddot{z}_2$  and  $\ddot{z}_{2E}$ ).

Two amplifiers are used when generating the acceleration signals to accommodate positive and negative signals, rather than summing them on a single differential amplifier, as scaling presents fewer problems.

The acceleration error board replaces the acceleration input matrix board, Section 8.3.1, in the classical control system.

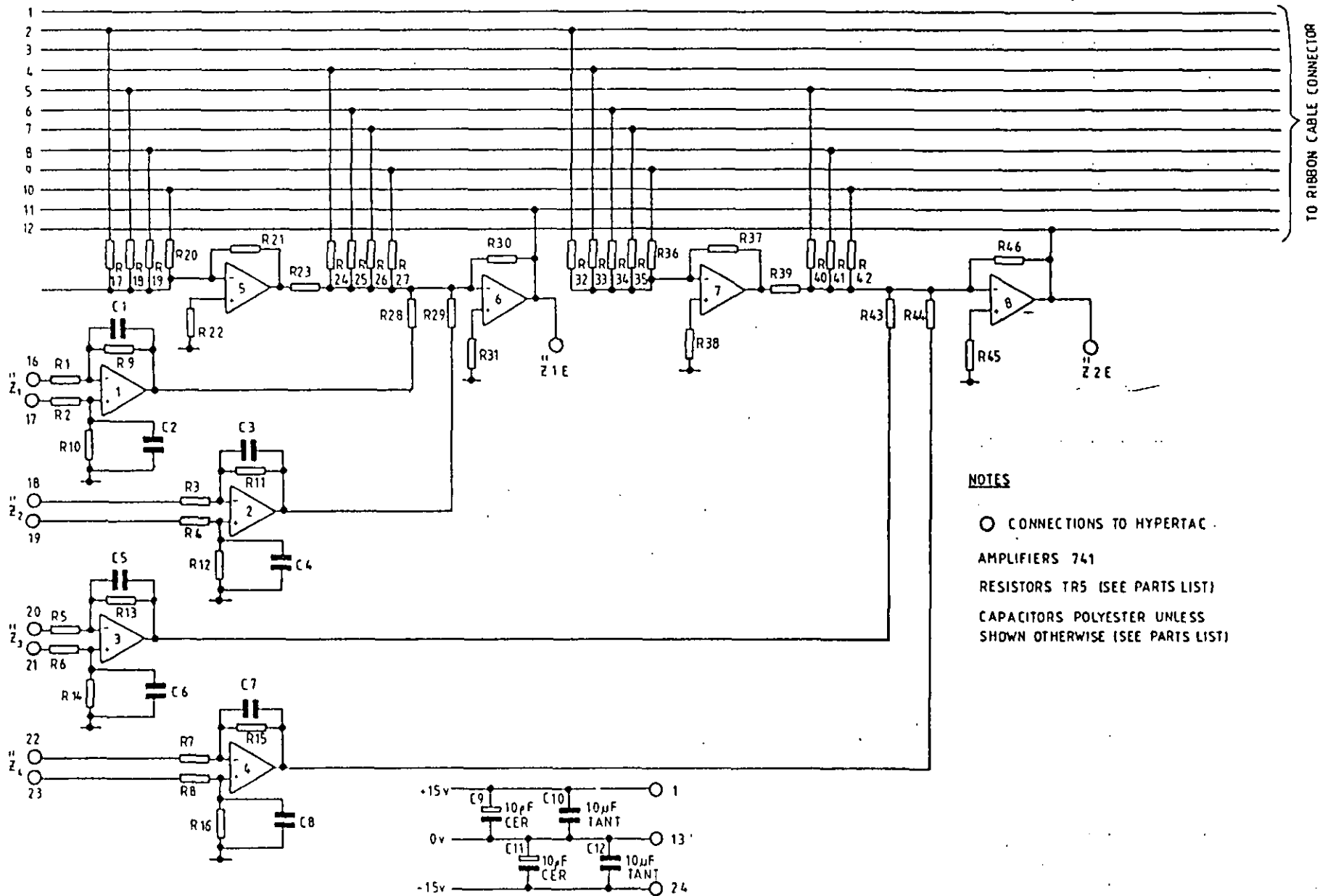
### 8.5.3 Relative Displacement Error Board

Relative displacement signals from each corner of the vehicle are buffered on amplifiers A1, A2, A3 and A4 (Fig. 8.13). These are then summed on A6 and A7 to derive the mean relative displacements at the ends of the vehicle. The signals are a.c. coupled to prevent the control system from interacting with the mechanical air spring levelling valves at low frequencies.

Amplifiers A7, A8, A9 and A10 are used to generate the observed relative displacements and hence by subtracting the measured relative displacement, the relative displacement errors

$$(\ddot{z}_{R1E}, \ddot{z}_{R2E}).$$

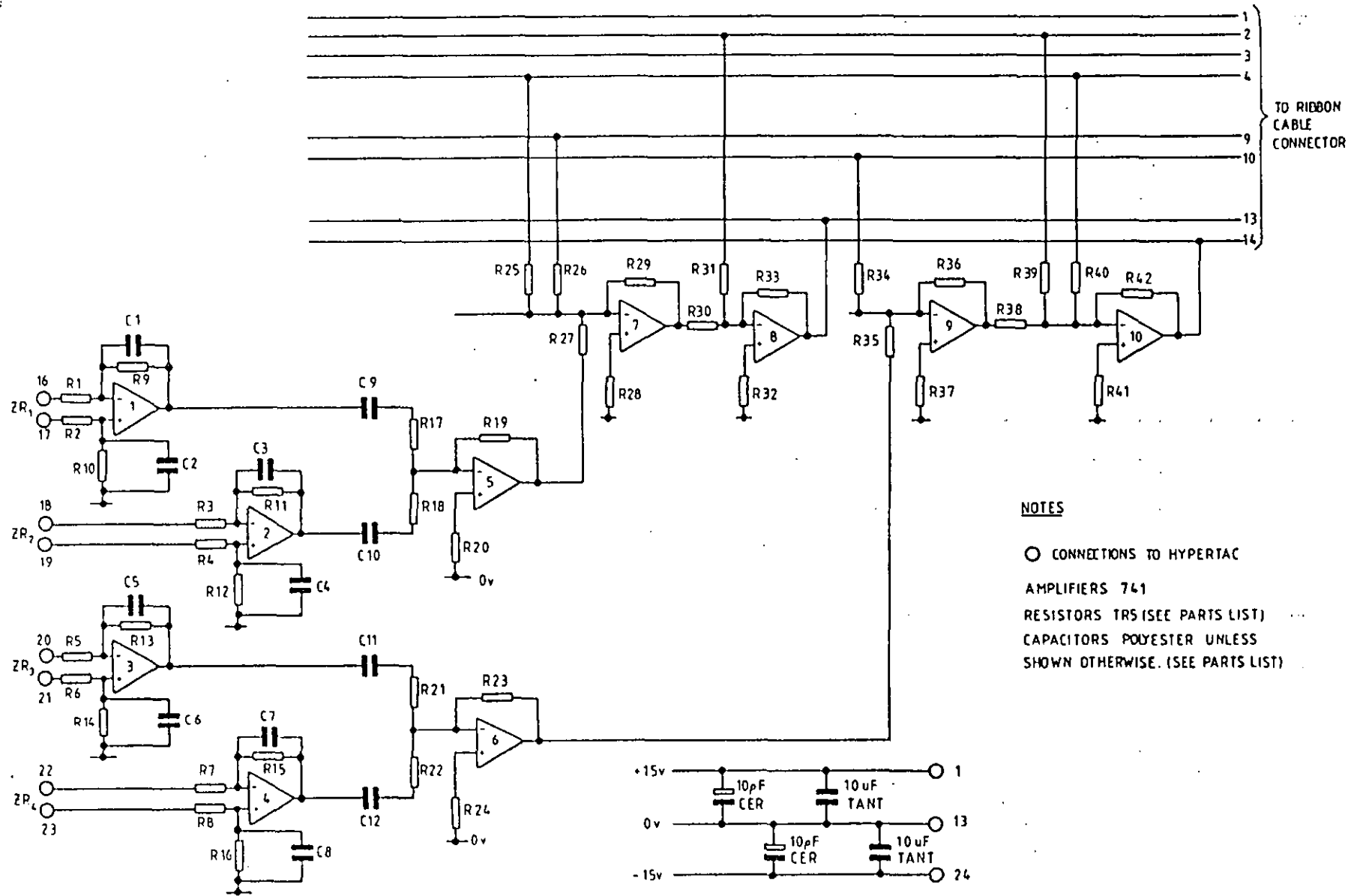
The relative displacement error board replaces the relative displacement input board in the position control system, Section 8.3.1.



**NOTES**

- CONNECTIONS TO HYPERTAC
- AMPLIFIERS 741
- RESISTORS TR5 (SEE PARTS LIST)
- CAPACITORS POLYESTER UNLESS SHOWN OTHERWISE (SEE PARTS LIST)

FIG. 8-12 ACCELERATION ERROR



- NOTES**
- CONNECTIONS TO HYPERTAC
  - AMPLIFIERS 741
  - RESISTORS TR5 (SEE PARTS LIST)
  - CAPACITORS POLYESTER UNLESS SHOWN OTHERWISE. (SEE PARTS LIST)

FIG. 8-13. RELATIVE DISPLACEMENT ERROR.

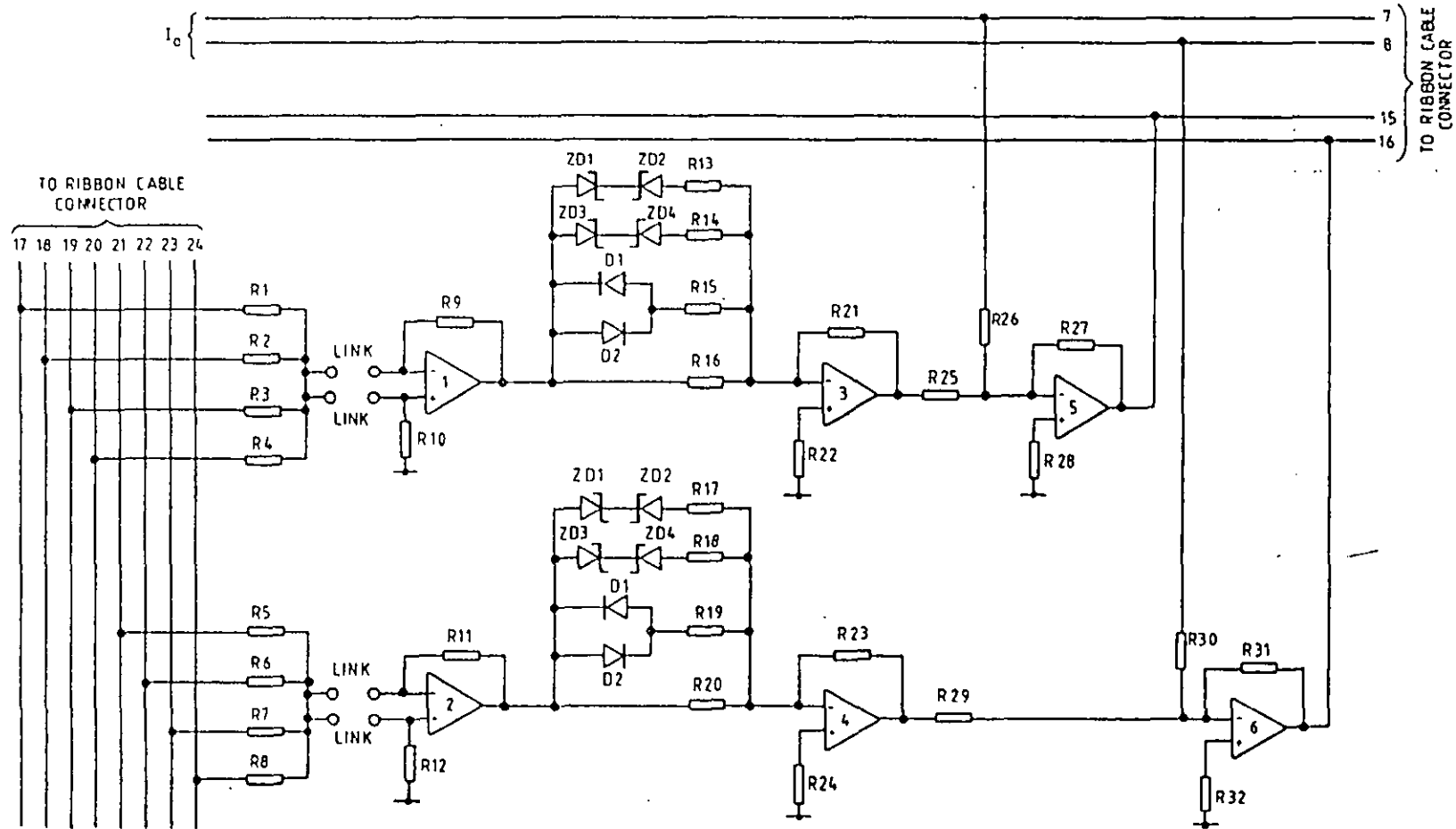
#### 8.5.4 Current Error Board

Linear models of the vehicle were used to design the regulator and observer and the physical model of the observer is also linear. Section 8.4.2 showed that the actuator characteristics were linearised. With such a model there is very little difference between controlling the magnet current and the magnet flux as the r.m.s variation in air gap is less than 25% of the total airgap, and flux is approximately proportional to current. In practice large transients occur and, particularly when the air gaps become small, the relationship does not hold. Then it becomes preferable to control flux rather than current as this is more closely related to the actuator force.

In the observer model the actuator force is represented by the actuator current. However, as flux provides a better measure of force, the measured variables used to drive the observer modal currents are a mixture of flux and current. A mixture is used as the flux signal is generated by integrating the output of a search coil, which has to be decoupled at d.c. to prevent the integrator drifting Section 8.4.2. Current is used at low frequencies to compensate for the shortfall in the flux signal.

Flux signals and the complementary low frequency current signals are available on the actuator control boards (Fig. 8.7) at TP2 and TP4 respectively. These are summed on amplifiers A1 and A2 (Fig. 8.14) to provide mean flux signals at each end of the vehicle.

As the electromagnets do not operate very close to magnetic saturation the force generated is proportional to the square of the flux. In order to produce a force proportional to the demand signal the actuator control board contains a "square root" circuit on an amplifier  $A_{10}$ . Similarly, because the observer is a linear model of the system, the amplifiers  $A_3$  and  $A_4$  have circuits which produce the "square" of the flux so that the model currents in the observer are a linearisation of those in the actuator.



TO RIBBON CABLE CONNECTOR

17 18 19 20 21 22 23 24

-1 measured

TO RIBBON CABLE CONNECTOR

NOTES

- CONNECTION TO HYPERTAC
- AMPLIFIERS 741
- RESISTORS 1R5 (SEE PARTS LIST)
- CAPACITORS POLYESTER UNLESS SHOWN OTHERWISE (SEE PARTS LIST)
- ZENER DIODES BZY 88

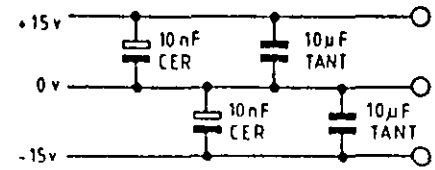


FIG. 8-14. CURRENT ERROR.

The "squaring" circuit is the reverse of the "square rooting" circuit as it contains the non-linear elements on the input rather than the feedback. The signal is squared by a piece wise linear diode function generator, the output of A3.

$$V_3 = \frac{-V_1}{|V_1|} V_1^2 \quad (8.18)$$

The difference between the measured and observed fluxes/currents is taken on amplifiers A5 and A6 to generate the current error signals ( $I_{1E}$ ,  $I_{2E}$ ).

The current error board replaces one of the filter modules in the position control system.

#### 8.5.5 Optimal Control Matrix Board

The observed variables are generated by four optimal control matrix boards, Fig. 8.15. Each board consists of three pairs of amplifiers. The first amplifier of the pair is a straight summing amplifier and the second an integrator. This allows all the observed state variables and error signals to be summed on the integrator in either polarity. The gain of each signal is determined by the resistor connecting the ribbon cable to the amplifier pair.

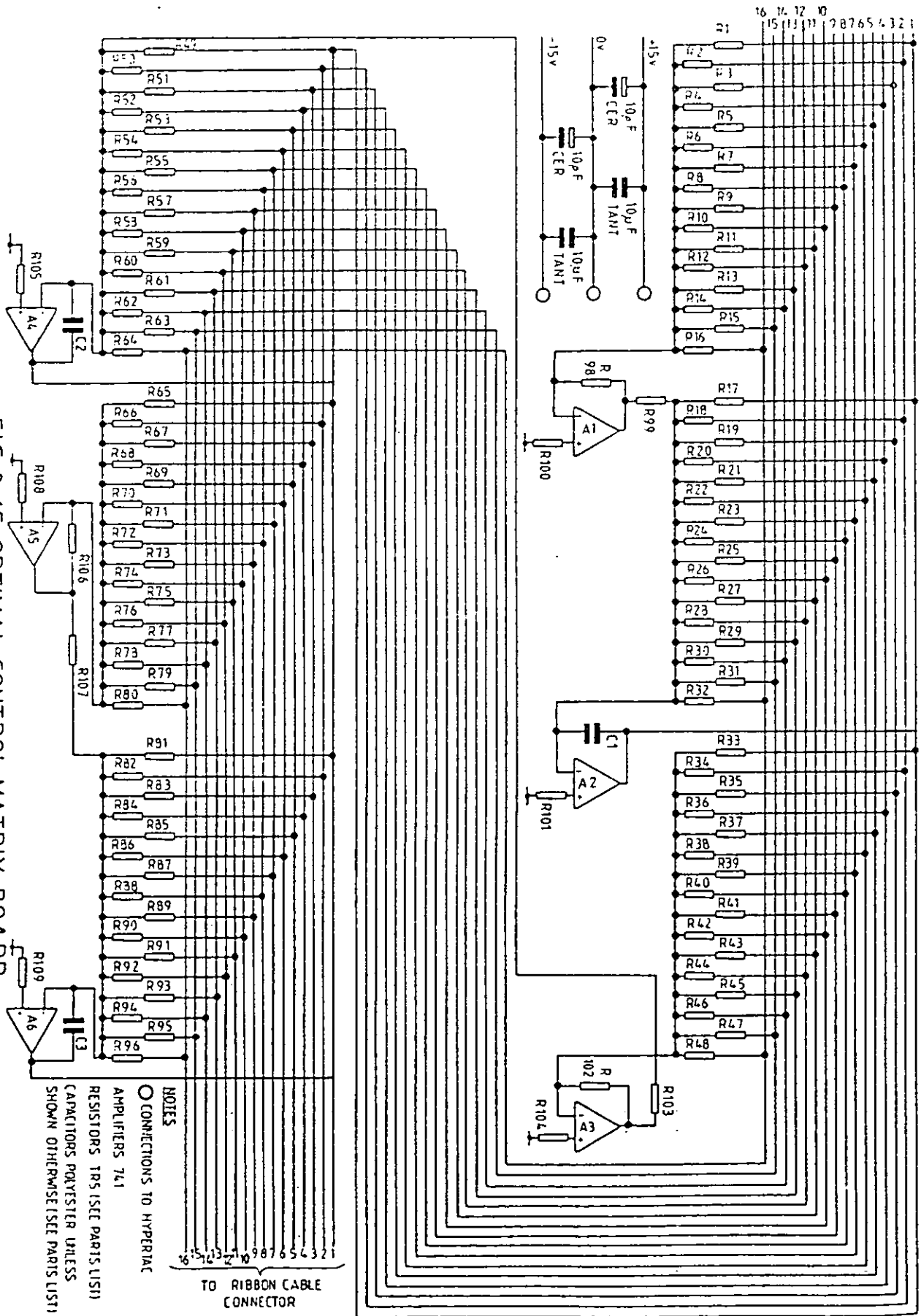
The input to the integrators sum to the derivatives of the state variables i.e. ( $\dot{x}$  in Fig. 6.2), hence the outputs of the integrators are the state variables ( $x$  in Fig. 6.2). The gain from the observed variables to the integrator is derived from the state equations of the regulator model ( $A$  in Fig. 6.2) and the gain from the error signals from the error feedback matrix ( $K$  matrix in Fig. 6.2).

The four matrix boards generate the following variables:-

- 1)  $\dot{z}$  and  $z$
- 2)  $\dot{\phi}$  and  $\phi$
- 3)  $z_1$ ,  $I_1$ ,  $z_{t1}$
- 4)  $z_2$ ,  $I_2$ ,  $z_{t2}$



FIG 8-15 OPTIMAL CONTROL MATRIX BOARD



- NOTES
- CONNECTIONS TO HYPERLAT
  - AMPLIFIERS 741
  - RESISTORS 1%5 (SEE PARTS LIST)
  - CAPACITORS POLYESTER UNLESS SHOWN OTHERWISE (SEE PARTS LIST)

TO RIBBON CABLE CONNECTOR

If two summing amplifiers and an integrator were used to generate each state variable, it would be possible to have the derivatives of the state variables available. While this would be useful in deriving the acceleration errors (Section 8.5.2) it would require a further 10 lines on the ribbon cable, making the observer more cumbersome.

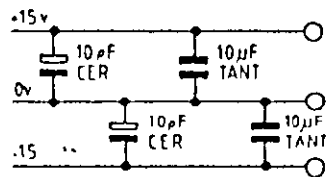
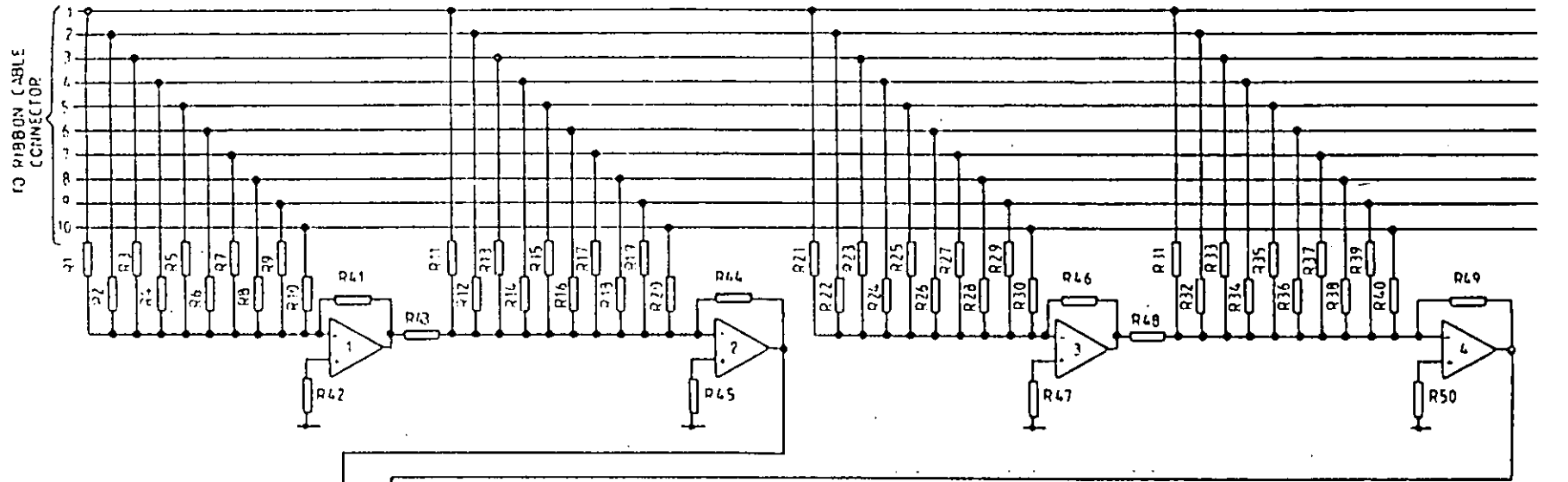
Note that the vehicle model used in the observer includes the regulator feedbacks.

These boards are placed in the filter module and phase advance module slots of the card frame.

#### 8.5.6 Output Matrix and Notch Filters

The actuator demands are resolved on the output matrix and notch filter board, Fig. 8.16.

In theory the flexible body modes can be included in the optimal control system design. However this requires a fairly good knowledge of the shape of the flexible modes, particularly the position of the accelerometers relative to the nodes. This knowledge is not available for the primary bending mode, as the accelerometers are too close to the nodes to resolve it satisfactorily. The vehicle could be loaded in a manner which would cause the nodes to shift, placing the accelerometers on the opposite side of the node to that in which it was modelled, with disastrous consequences. Therefore the flexible modes are eliminated by notch filters. Without the notch filters the flexible body states would have to be included in the observer plant matrix with the associated problems that increased observer size bring.



NOTES  
 ○ CONNECTION TO HYPERTAC  
 AMPLIFIERS 741  
 RESISTORS 1% (SEE PARTS LIST)  
 CAPACITORS POLYESTER UNLESS SHOWN  
 OTHERWISE (SEE PARTS LIST)

FIG. 8-16. OUTPUT MATRIX AND NOTCH FILTERS

Flexible body modes occur as either in-phase or anti-phase modes. Therefore the actuator demands have been resolved as in-phase and anti-phase demands to facilitate the implementation of the notch filters. Amplifiers A1 and A2 sum the anti-phase actuator demands and A3 and A4 sum the in-phase actuator demands. Amplifiers A5, A6, A7 and A8 provide an in-phase notch filter while amplifiers A9, A10, A11 and A12 provide an anti-phase notch filter.

The board replaces one of the phase advance modules in the position control system. The in-phase and anti-phase demands from the board are resolved on the output matrix board, Fig. 8.6, to form actuator demands.

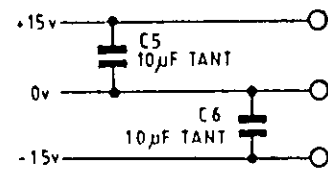
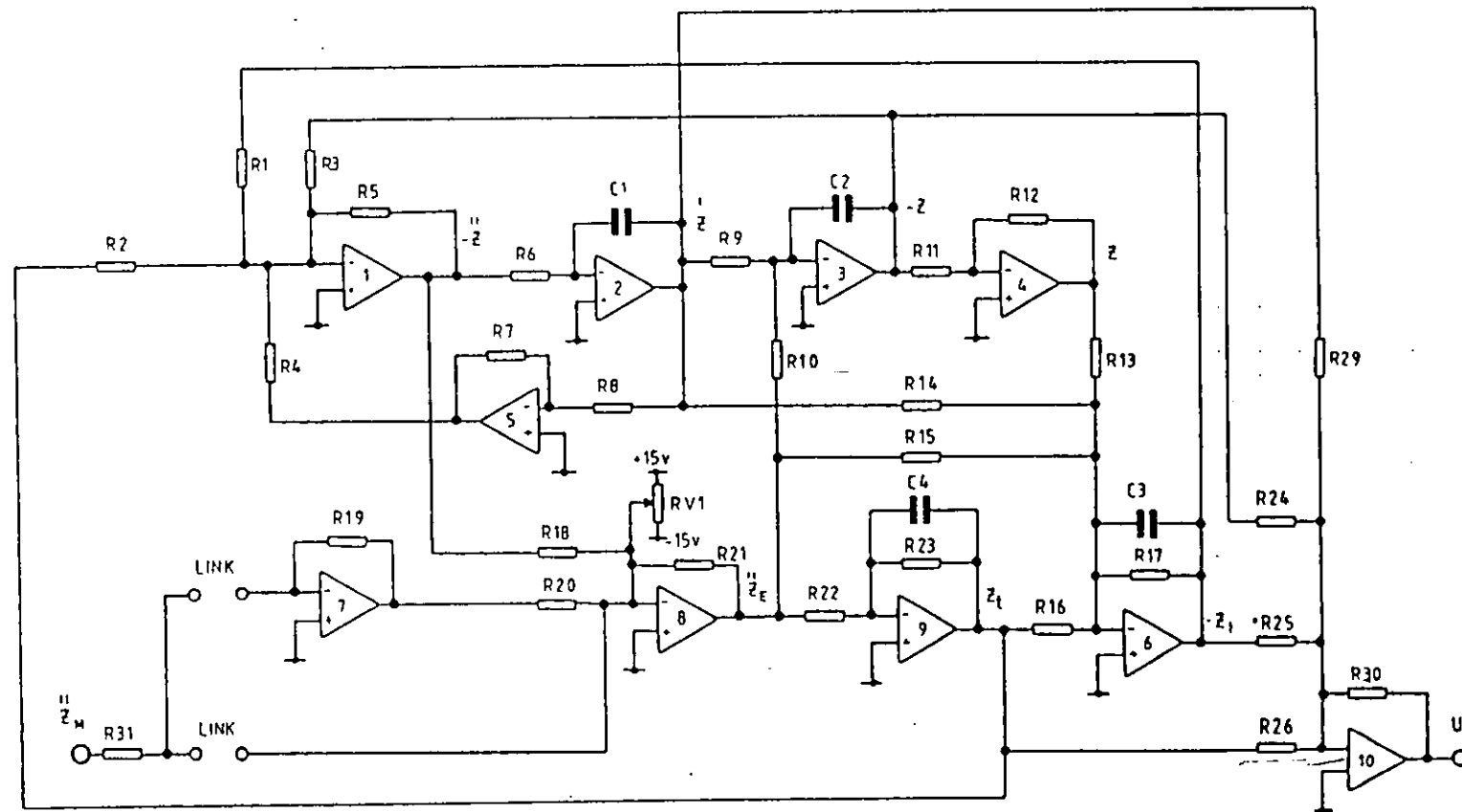
### 8.6 Modal Observer

The modal observers are much easier to implement in the card frame than the small model observer. Current feedback is provided from measurements of flux and current rather than the observer. Thus the only modification required to the actuator control (Fig. 8.7) is the shorting of capacitor  $C_9$  and replacing  $R_{52}$  with a 22 K resistor. The feedback links 1 and 2 are left in place.

Modal observer boards, Fig. 8.17, replace the filter boards in the card frame. There is one for each of the bounce and pitch modes. Modal accelerations are fed to each board from the acceleration matrix board. Provision is made for reversing the signal with A7. The variable scalings are the same as those given in Table 8.3.

The observers re-create the modes as a direct analogue equivalent. The acceleration error is formed on amplifier A8 and the control demand  $u$  on Amplifier A10.

Output from the modal observers is fed to the absolute damping notch filter boards and then to the output matrix.



NOTES

- CONNECTIONS TO HYPERTAC
- AMPLIFIERS 741
- RESISTORS TR5 (SEE COMPONENT LIST)
- CAPACITORS POLYESTER UNLESS SHOWN OTHERWISE (SEE COMPONENT LIST)

FIG. 8-17 MODAL OBSERVER

## 8.7

Card Frame

Fig. 8.18 shows the control electronics installed in the vehicle set up for the absolute damping mode. The top row of cards from left to right are:-

- 1) + 15 V switch mode power supply.
- 2) Relative displacement input matrix.
- 3) Acceleration input matrix.
- 4) Bounce absolute damping board.
- 5) Pitch absolute damping board.
- 6) Roll absolute damping board.
- 7) Bounce notch filter board.
- 8) Pitch notch filter board.
- 9) Roll notch filter board.

The second row contains the four actuator controls together with a test facility and the control system interlocking.

The third row is a second card frame holding the capacitive displacement transducer electronics.

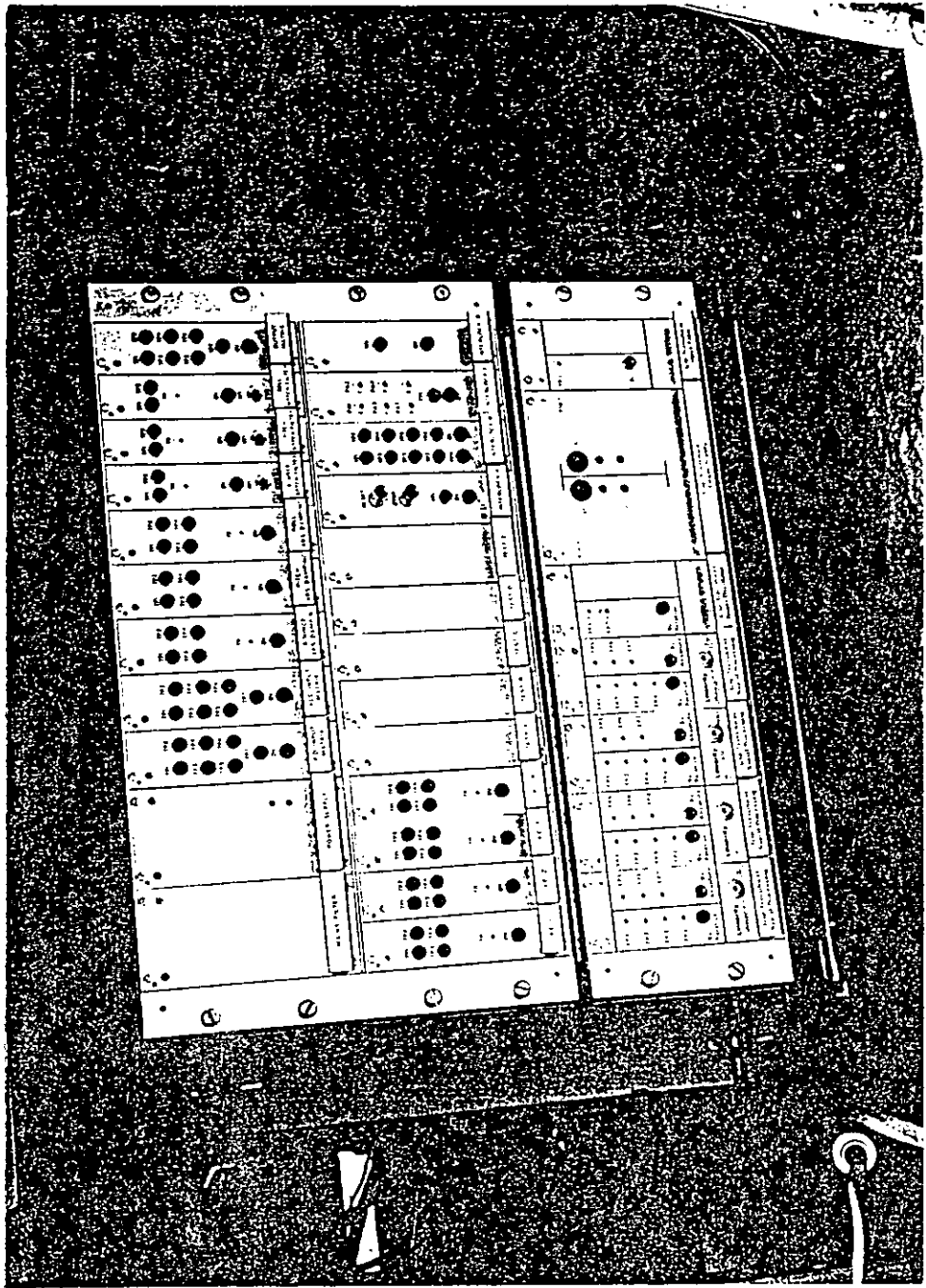


FIG. 8-18 CONTROL RACK

CHAPTER 9  
COMMISSIONING AND TESTING

Initial commissioning of the active suspension took place in February 1984. This was followed by a period of testing on the West Coast Main Line between Crewe and Carnforth in March 1984 and a second period of testing in April-May 1984 between Crewe and Carstairs. During the March tests the two classical control systems were tested and shortcomings identified. It was at this stage that problems were encountered with the Small Model Optimal Observer giving rise to a rethink of the optimal control system which led to the Modal Observers. In the second series of tests the modal observers were tested, along with improvements to the classical control systems.

After the first two series of tests the vehicle was returned to service, operating in the Sky Hook damping mode, while the data was analysed and methods of improving performance assessed. The vehicle was returned from service in February 1985 for modifications and a third series of tests was conducted in March 1985 between Crewe and Carforth.

Experimental Instrumentation for the final series of tests was

- 1)  $\pm 2$  g vertical accelerometers above the air springs and at the vehicle centre.
- 2)  $\pm 2$  g lateral accelerometers at one end of the vehicle and vehicle centre.
- 3)  $\pm 5$  g vertical accelerometers above the centre of the bogies.
- 4) 100 mm potentiometers across the secondary suspension.
- 5) ac current transformers on the input to and output from the transformer.
- 6) dc current transformer on the power supply output.
- 7) Potential dividers on the power supply voltages.
- 8) Voltage, current and flux from each amplifier were measured from the control system instrumentation.



Data was recorded digitally on a DEC Redcor computer sampled at .50 samples/s, except for the ac signals which were sampled at 200 samples/s as required. Note that analogue rms values of the ac signals were also provided.

The data was analysed using British Rail's extensive suite of data analysis programs.

### 9.1 System Commissioning

The system is protected by a system of power and logic interlocks to protect the vehicle and control system in the event of a system fault. These are described in Ref 57. Though these are fairly comprehensive no serious faults were encountered during commissioning, on occasions however some of the logic had to be overridden to enable the system to operate.

Once a functional power interlock had been established power was supplied to the transformer and the output voltage checked. Power was then supplied to the PSU and eventually the power amplifiers. Having established power output from the amplifiers the actuators were connected. The amplifiers were driven from the actuator control boards (Fig 8.7). There were no feedbacks connected on the actuator control boards and capacitor C9 was shorted to provide a proportional drive signal. A drive signal was then applied to the actuators to establish correct polarity of the magnet coils and flux coils. If one magnet coil has incorrect polarity the actuator draws current without producing a noticeable force or output from the flux coils. Reversing one pair of connections corrects the problem. Flux coil connections may also have to be reversed to obtain correct polarity of the flux signals. Having achieved correct polarity of the actuator coils and flux loops the actuator control loops can be closed. The closed loop frequency response of the actuators was measured using a Hewlett Packard HP 8742 spectrum analyser and shown to have a flat response up to 15 Hz.

### 9.1.1 Skyhook damping-static performance

When the actuator control loops have been commissioned it is possible to drive them together in the bounce, pitch and roll modes. In this manner it is possible to check the polarity of the accelerometers and measure the open loop responses of the control loops using a spectrum analyser. These are shown in Figs 9.1 and 9.2 for the Pitch and Bounce modes respectively. The measured open loop responses for the skyhook damping system is much as expected from theory. Note that the vehicle was not connected to any other vehicles when the responses were measured.

### 9.1.2 Position control-static performance

There are two problems when commissioning the position control system; not only have the displacement transducers and accelerometer to be of the same polarity but they must also have the same scaling. This is a particular problem with this controller as the system is stable with the inputs reversed because it is decoupled at dc. In order to check polarity and scaling the actuators are used to drive the vehicle. Because there is no track input to the vehicle the absolute and relative displacements should be the same (neglecting deflections of the primary suspension). The transfer function is then taken between either displacement and the sum of the complementary filter outputs. If the scaling is correct there will be no change in gain or phase at the filter crossover frequency.

The open loop responses of the control loops was measured Figs 9.3 and 9.4. While these show very good gain and phase margins the low frequency gain and phase do not agree very well with the theoretical predictions. At one stage it was thought that this was due to the relative displacement inputs being reversed, as this would produce similar phase characteristics. However this was not the case as reversing the inputs produced an even greater advance in phase. An explanation for the phenomenon

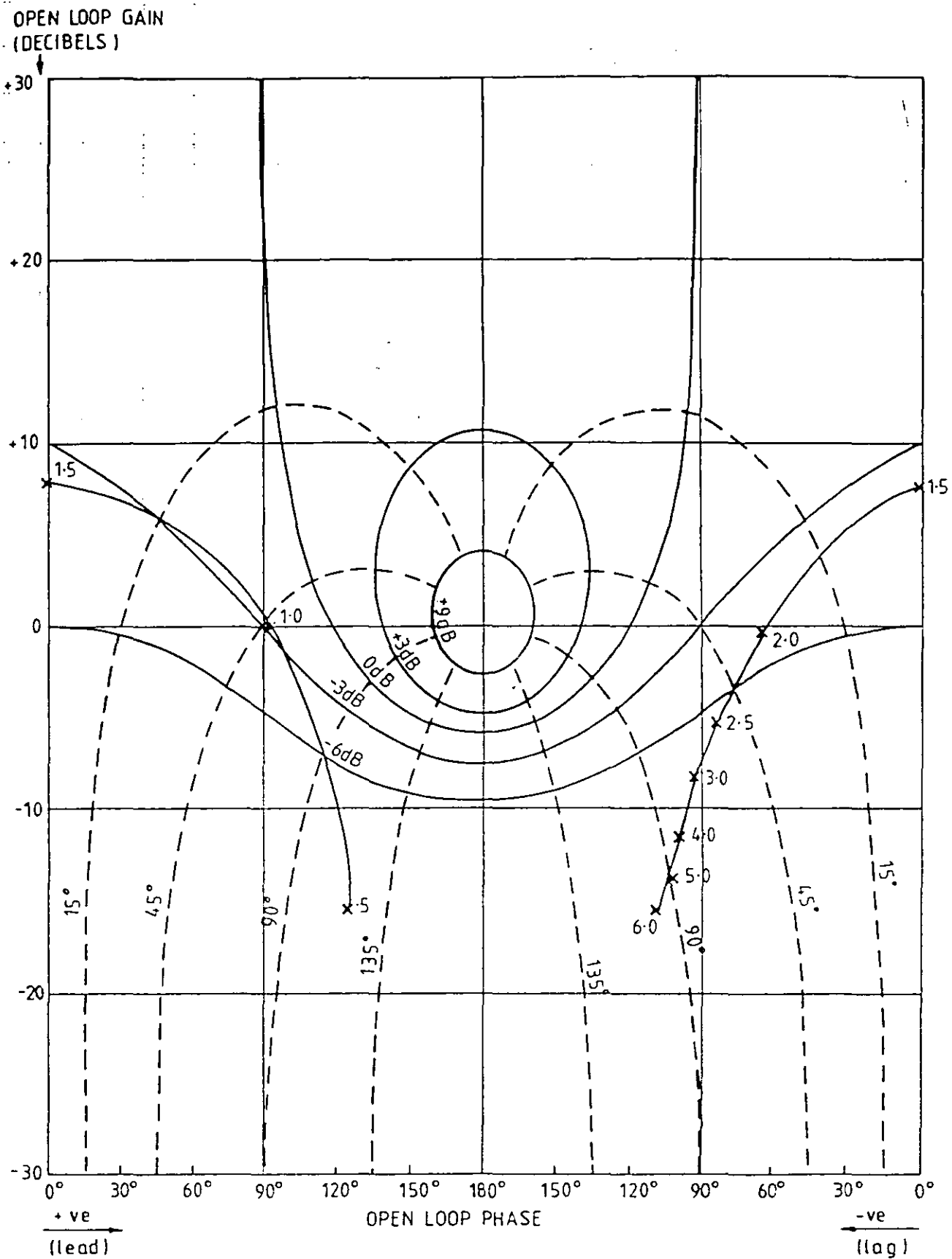


FIG. 9.1 BOUNCE ABSOLUTE DAMPING OPEN LOOP RESPONSE

OPEN LOOP GAIN  
(DECIBELS)

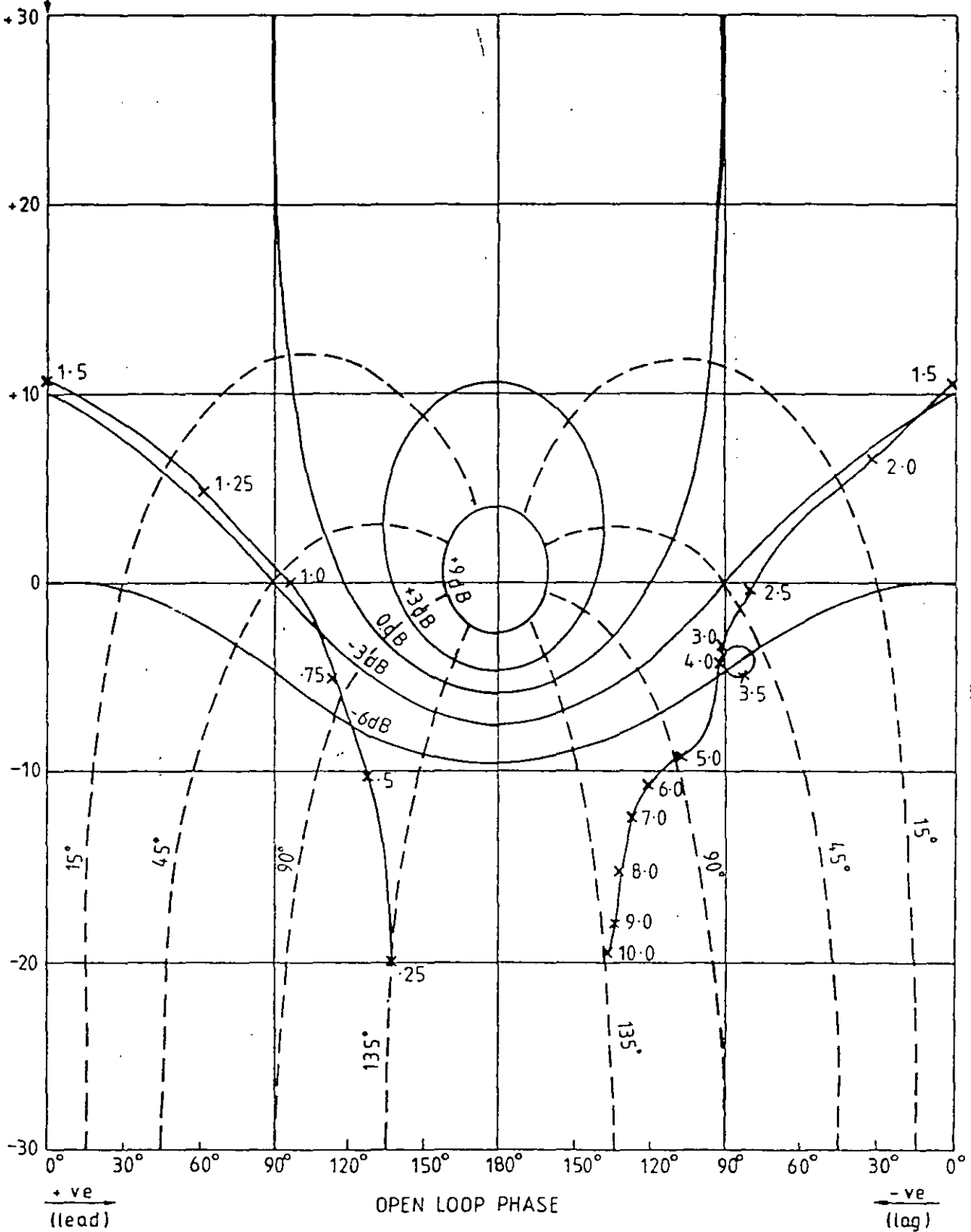


FIG.9.2 PITCH ABSOLUTE DAMPING OPEN LOOP RESPONSE

OPEN LOOP GAIN  
(DECIBELS)

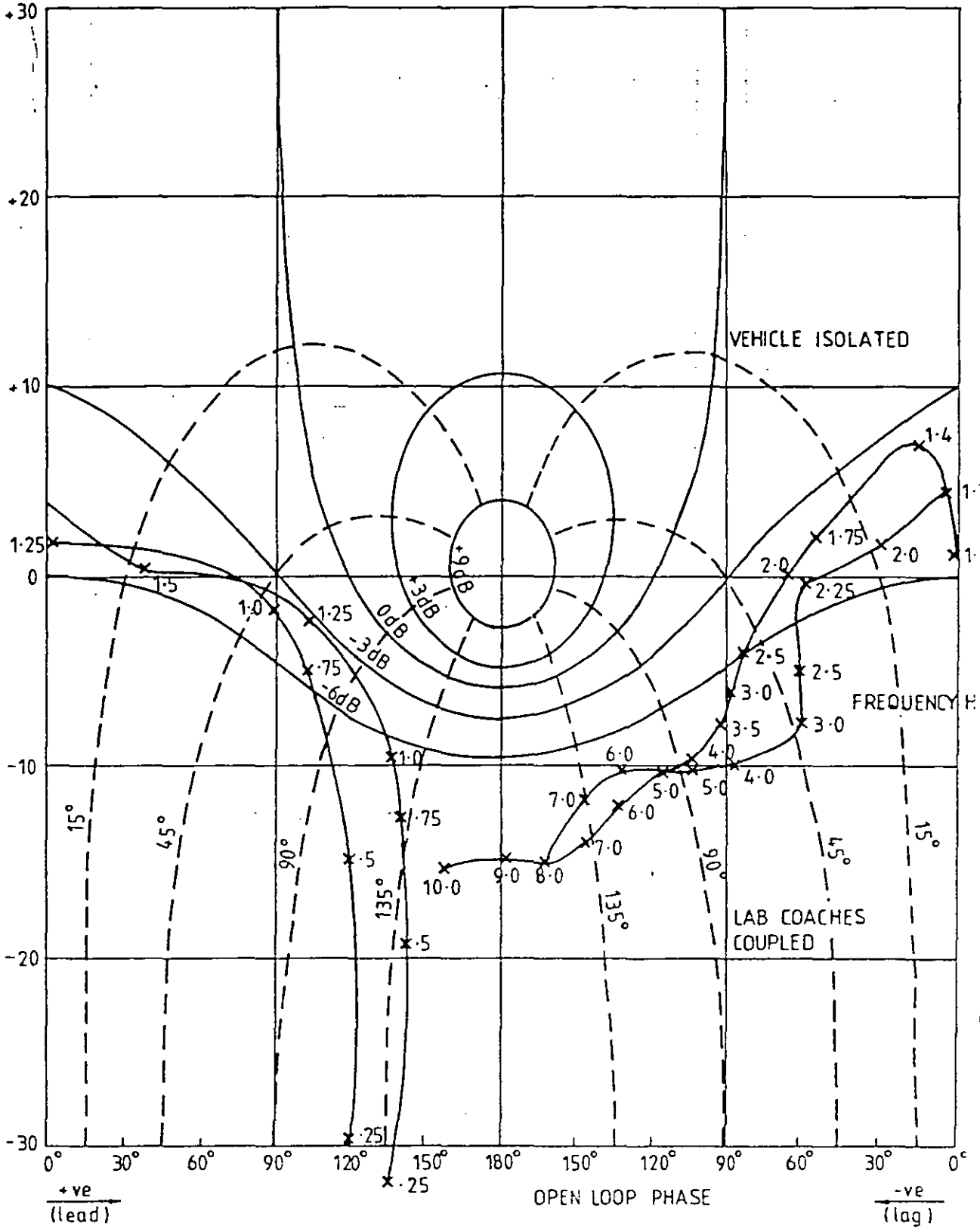


FIG. 9.3 BOUNCE POSITION CONTROL OPEN LOOP RESPONSE

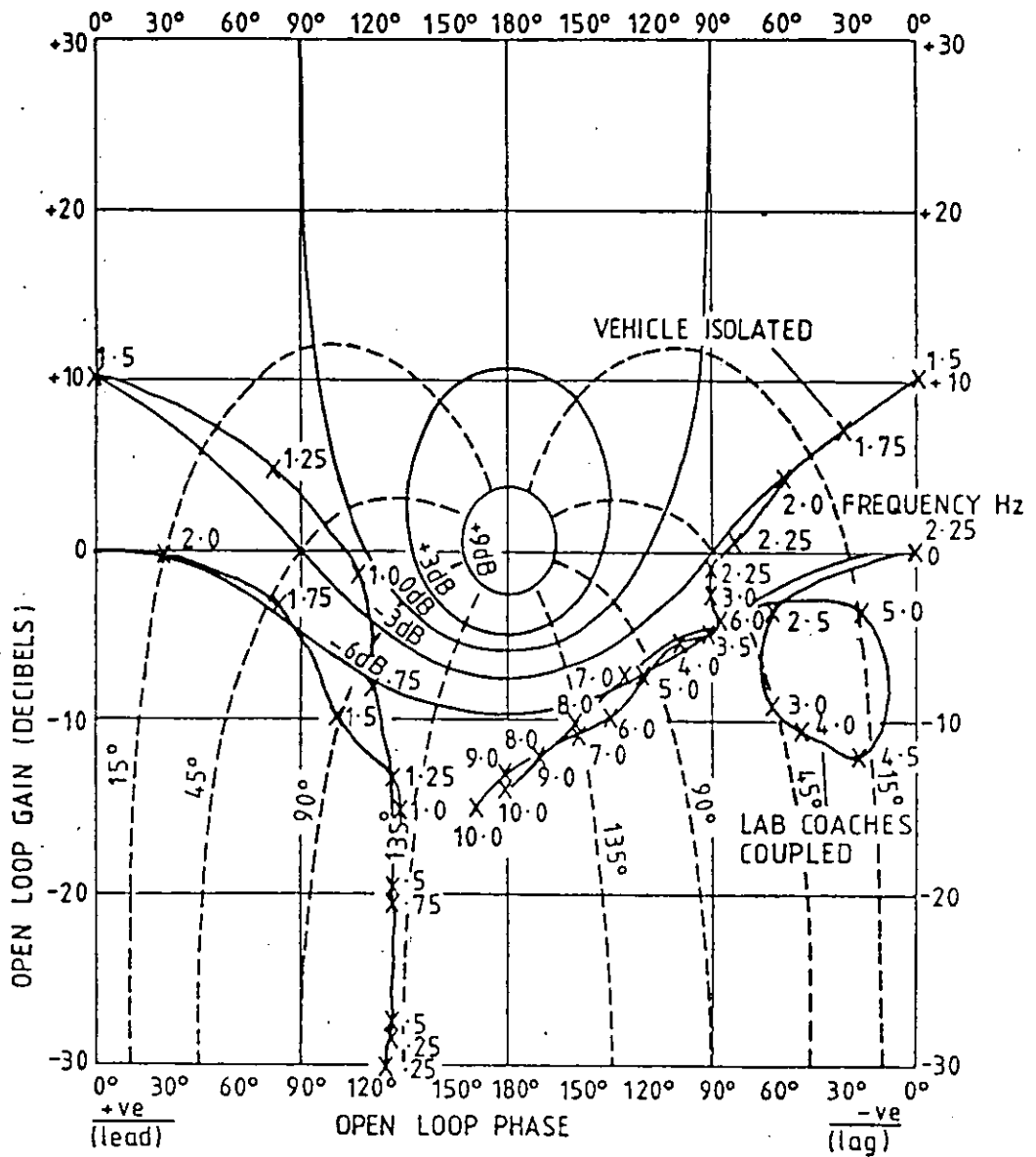


FIG. 9.4 PITCH POSITION CONTROL  
OPEN LOOP RESPONSE

found after the vehicle had to be returned to service and is given in Section 9.5.

The effects of the corridor connections is shown very clearly in the pitch loop response (Fig 9.4) with the vehicle coupled in the train. Low frequency gain is greatly reduced while the resonant effect of the corridor connections is shown by the loop between 2.5 Hz and 5.0 Hz. The loop suggests lower damping than is present while running as the actuators do not "break out" the friction between the connections. Note that the high frequency responses are much the same.

Structural vibrations were not excited by either of the classical control systems, thus the notch filters were not required.

### 9.1.3 Small model observer commissioning

Commissioning the small model observer had a flying start as the polarity and scaling of the actuators and instrumentation were already known to be correct once the classical control systems had been commissioned.

The observer matrix boards (Section 8.5.5) were commissioned first with the instrumentation disconnected. Each set of instrumentation was then coupled to the observer in turn, and finally the output connected to the actuators. Fault finding was difficult throughout, due to the large degree of interaction between various parts of the circuit.

When the observer was stabilised and the loops closed, stability was marginal as the observer drifted quite badly. The drift was induced by the instrumentation and exaggerated by the coarse scaling required on the observed position control signals. Absolute positions are generated by integrating a first order system of the form  $x_0 = \dot{x}_1/(s+1)$ . The system is a straight gain at dc, so that any dc offset in the derivative ( $\dot{x}_1$ ) will be transmitted to the output. The classical control systems have

integral feedback to cater for this problem. Drift on the accelerometers comes from the vehicle rolling so that they gain a lateral component. The relative position signals drift because of the airsprung levelling valves. However it was felt that the most serious component came from the actuator currents. The high small signal gain of the actuator control non-linear "square root" circuit (section 8.4.2) causes the actuator currents to hunt slightly around the zero point; an effect which is apparent with the classical control systems but is of no consequence as the forces generated are infinitesimal. The hunting however upsets the observer as control currents are generated from small differences in the coarsely scaled position signals. The drift problem prevented this control system from being tested on the track.

A flexible body mode was excited by the controller at 27 Hz. The mode occurred in both the pitch and bounce loops and had to be eliminated with notch filters.

In Section 6.2.3 it was stated that the effective signal to noise ratio used to design the observers was reduced because of uncertainty in the model. Fig 9.5 shows the measured transfer function between acceleration and flux; ideally this would have a flat gain and phase response at high frequencies, which is clearly not the case. The increasing gain characteristic is due to eddy currents making the actuator characteristics non-linear at high frequencies. Coupling of flexible modes also increases the transmissibility.

#### 9.1.4 Modal observers static performance

Commissioning the modal observers was much simpler than the small model observer as the boards are a direct replacement for the absolute damping boards. To check performance of the boards the observer transfer functions were measured (Fig 9.6 and 9.7). Open loop responses were then measured to assess stability,



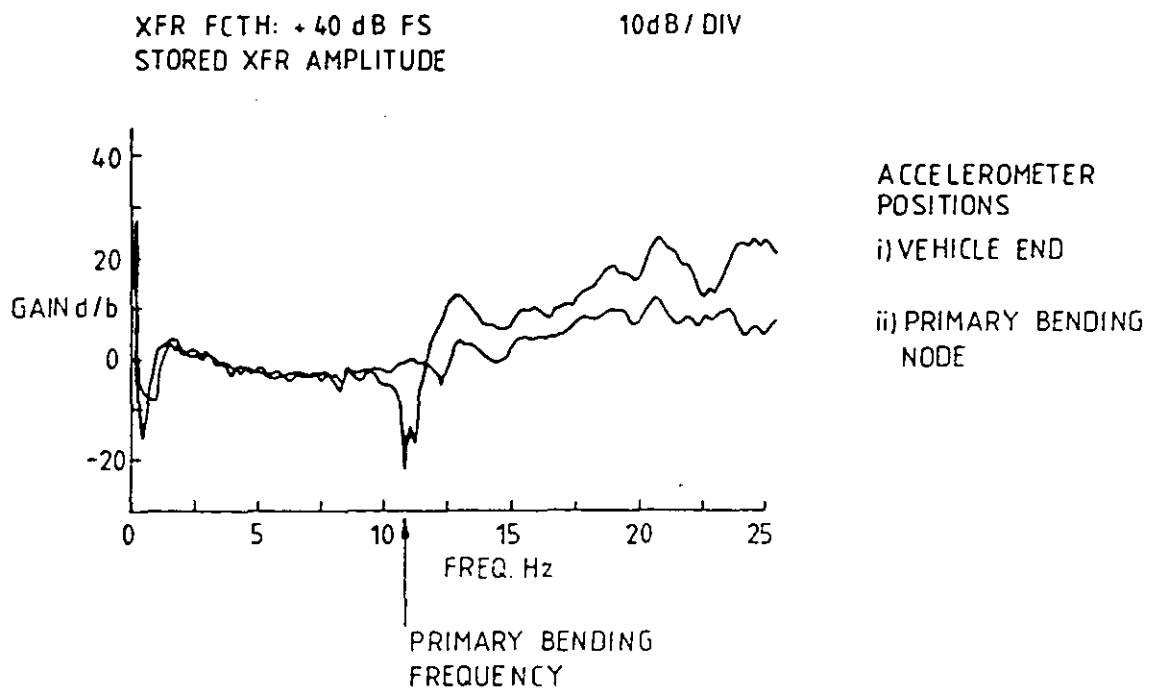


FIG. 9.5 ACCELERATION/FLUX FREQUENCY RESPONSE ACTUATORS OPERATING IN PHASE, WITH THE ACCELEROMETERS POSITIONED.

- i) AT THE END OF THE VEHICLE
- ii) AT THE PRIMARY BENDING NODES

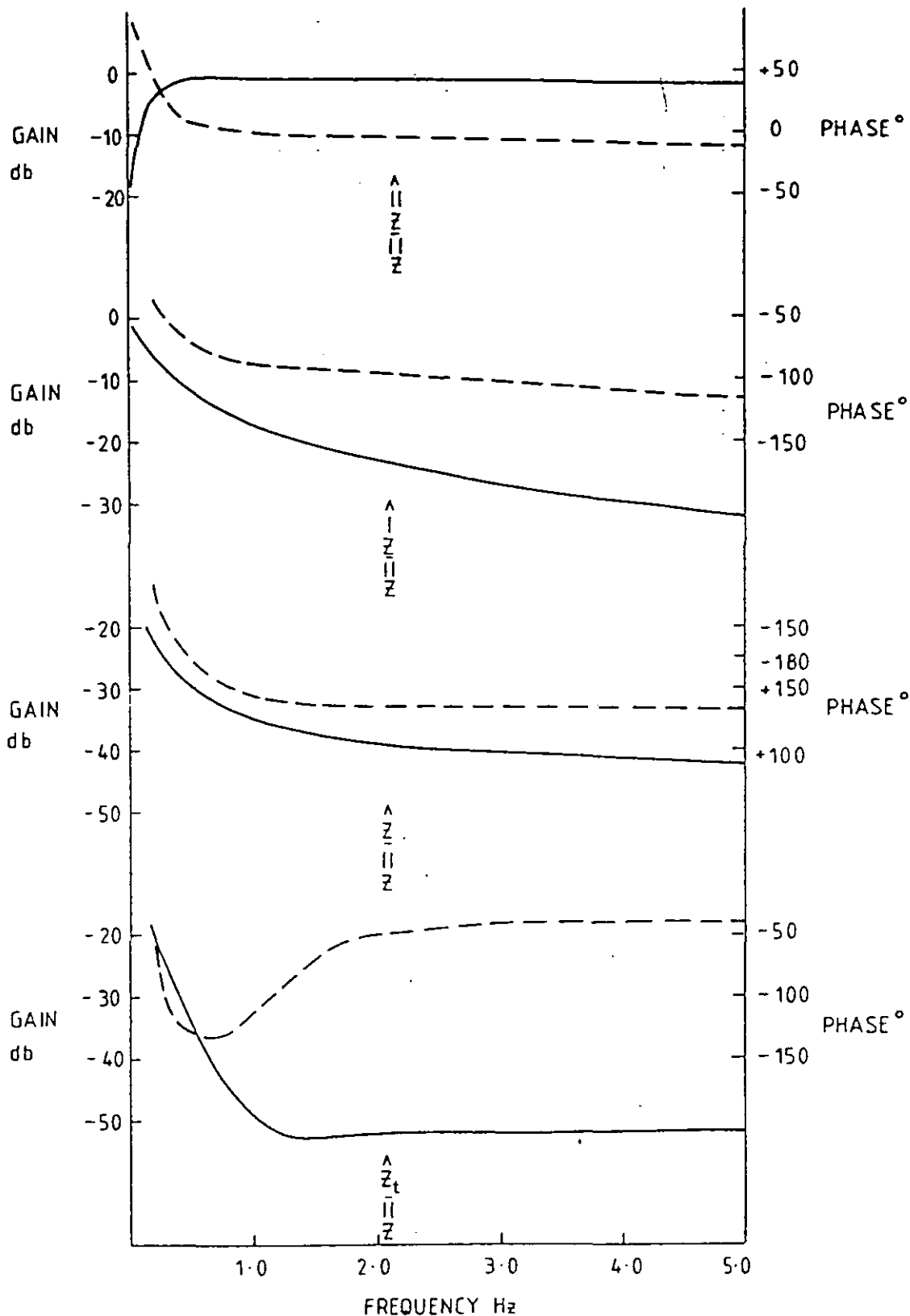


FIG. 9.6 BOUNCE MODAL OBSERVER TRANSFER FUNCTIONS

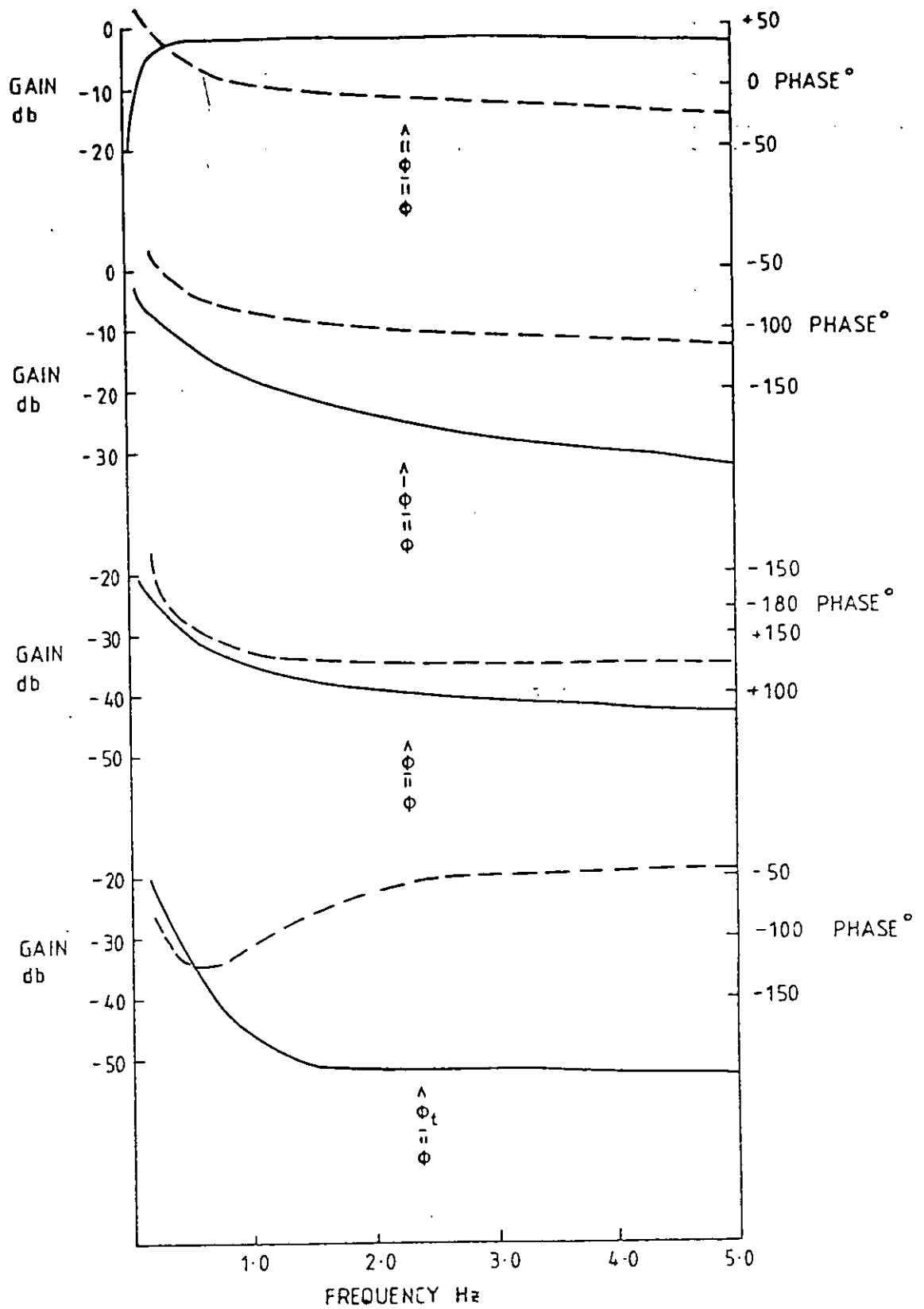


FIG.9.7 PITCH MODAL OBSERVER TRANSFER FUNCTIONS

Fig 9.8 and 9.9, these loops were measured with the lab coaches connected so that the low frequency gain is under estimated. It will be seen however that the phase margins of this controller are very good. Once again notch filters had to be used to eliminate the 27 Hz flexible body modes.

Drifting only proved to be a problem with this controller while the vehicle was in motion. Because the observer has been reduced to a single input single output device the drift was cured in the same manner in which it was with the classical control system, by an integrator in feedback around the observer. Further reference will be made to this in Section 9.3.3.

## 9.2 Power Supply

During the first two periods of testing it proved difficult to achieve the predicted performance. This was largely due to the gangway interaction described in Chapter 7. There was also a shortfall in power delivered by the power supply unit, this was overcome in the last series of tests by increasing the power supply voltage (an additional winding on the transformer having been provided for this contingency). Mean and peak powers for the control configurations tested are given in Table 9.1

TABLE 9.1

Power Consumption measured at 44 m/s West Coast Main Line

	Mean Power	Peak Power
	kW	kW
Sky Hook Damper	3.8	20
Position Control	4.5	28
Improved Position Control	3.9	27
Modal Optimal Control	4.5	24

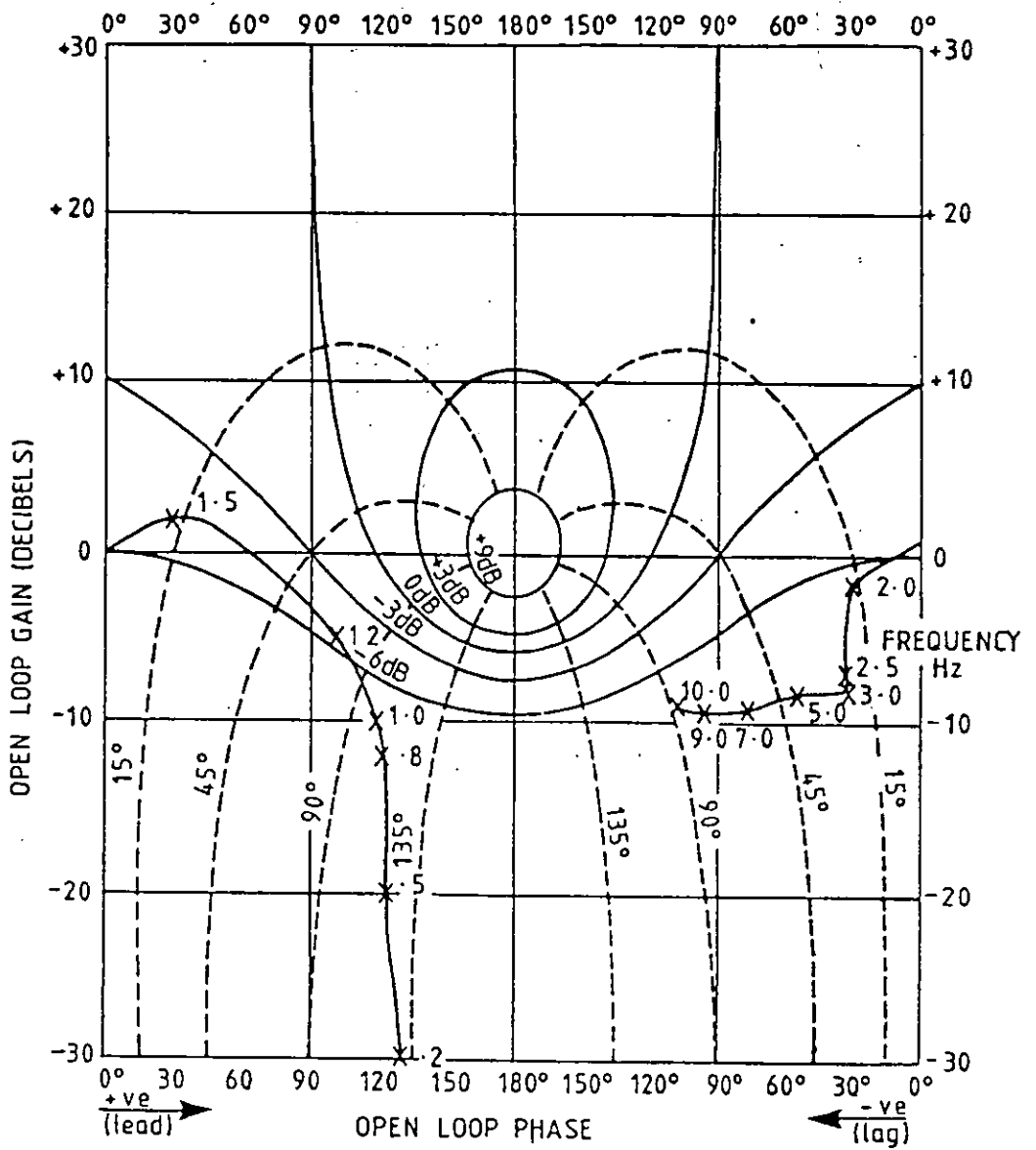


FIG. 9.8 MODAL OPTIMAL CONTROL MEASURED BOUNCE OPEN LOOP RESPONSE

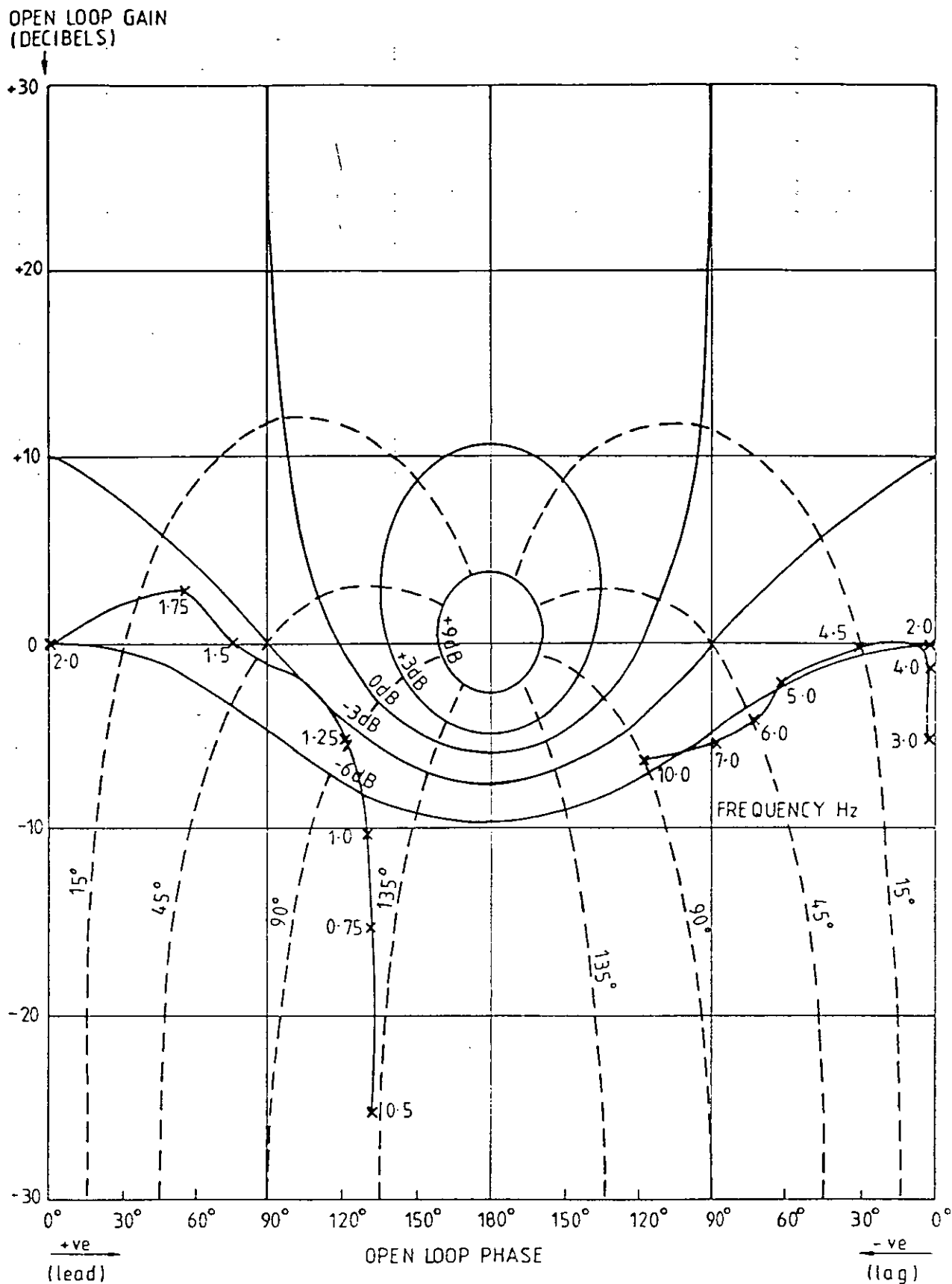


FIG. 9.9 MODAL OPTIMAL CONTROL MEASURED  
PITCH OPEN LOOP RESPONSE

Power was derived by multiplying measured current and voltage. The current was measured with a dc current transformer and voltage by a potential divider across the supply.

Two things stand out from Table 9.1; the first is that the controllers draw the rated power of 4 kW, and the second is that the peaks are in the region of five times the mean. For actuators having a square law characteristic responding to a stochastic input it would be expected that the mean peak ratio would be only two to one, however there are quite large deterministic features in railway tracks which account for the peaks. Fig 9.10 shows the power supply voltage, current and power for the "Sky Hook" damper control system. Large transients caused the supply voltage to fold back. In extreme cases the under voltage protection on the amplifiers cause them to switch off. This limited performance in the first two series of tests. This large peak to mean power ratio represents something of a problem in the design of a power supply for an active suspension as the peaks cannot be supplied from the ETH line. It is notable that despite 54,000  $\mu\text{F}$  capacitance in the power supply (representing  $5 \times 10^3$  J at 300 V) the transients still appear on the transformer input. The capacitor bank is also required to accept the energy returned to the supply from the actuators.

### 9.3 Track Tests

The experimental results quoted in this section refer to the last series of tests and represent the best performance achieved from each of the control systems. Unfortunately operating difficulties prevented each controller being tested over the same section of track at the same speed but there is sufficient passive data for comparative purposes. Though they are not strictly accurate a normalised set of results is presented at the end of the section to ease the problem of comparison between controllers.

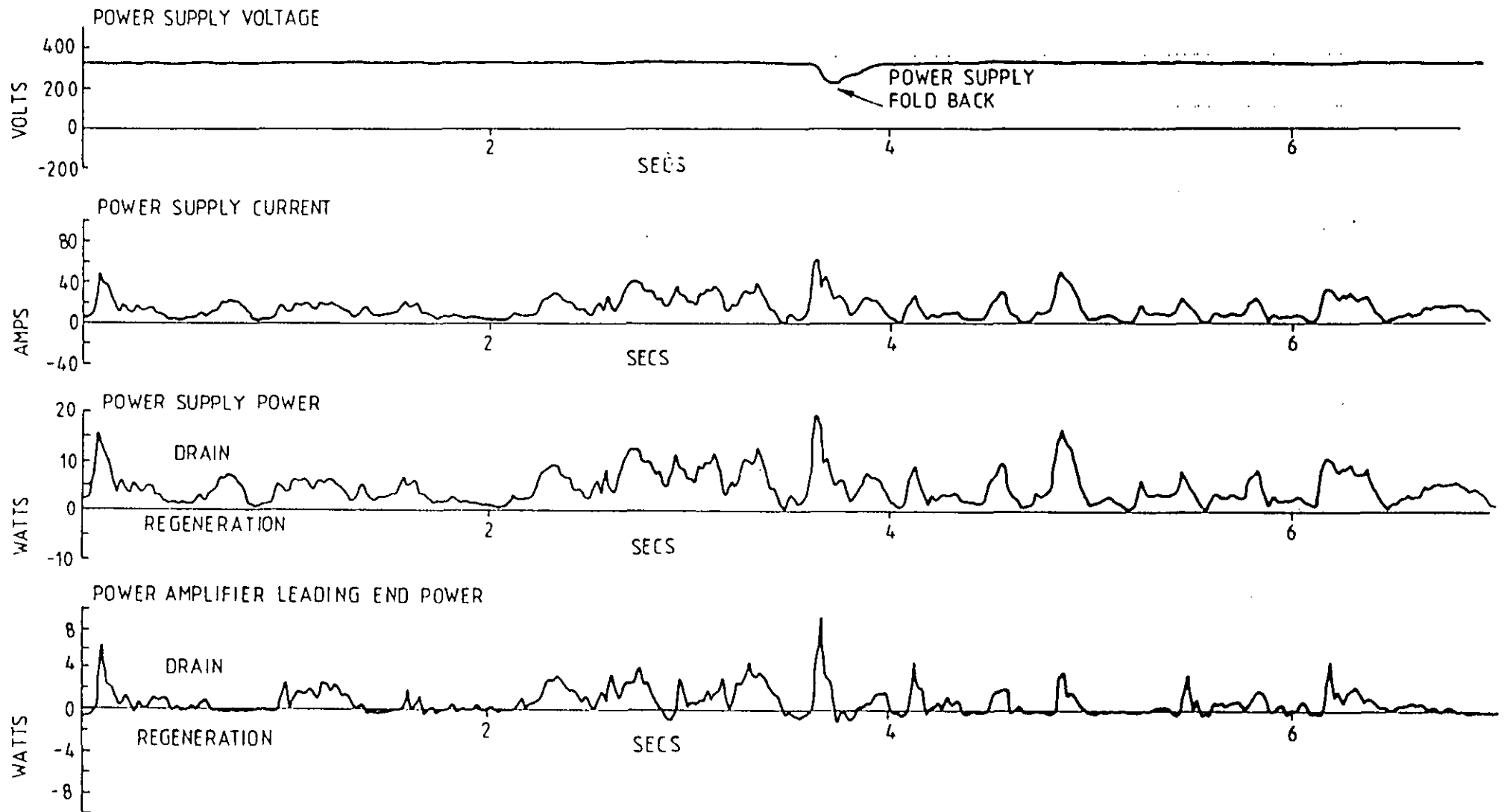


FIG. 9.10 POWER SUPPLY VOLTAGE CURRENT AND POWER WITH LEADING END  
AMPLIFIER POWER, SKYHOOK DAMPING



### 9.3.1 "Sky Hook" damper experimental results

The "Sky Hook" dampers performed well and proved very amenable to modification. Increasing the control loop gains increased damping and reduced the rigid body peaks. Initially the controller produced excessive suspension displacements which lead to bumpstop contact. Examination of the displacement psd's showed that the large displacements occurred at very low frequencies. This was cured by increasing the integral feedback gain so that the low frequency roll up of the absolute damping integrator occurred at 0.5 Hz rather than the 0.2 Hz the system was designed for Fig 9.11 shows that most of the improvement occurs through reducing the rigid body peak, though there is some improvement at the higher frequency generated by the corridor connections. Fig 9.12, the trailing end current psd shows that most of the control action occurs at the rigid body frequency.

Results are summarised in Table 9.2 in comparison with passive results measured on the same section of track. A maximum reduction in rms acceleration of 40% is shown.

TABLE 9.2 "Sky Hook" Dampers Measured Performance  
44 m/s WCML Travelling South

	rms Accn %			Displacement mm	
	Leading	Centre	Trailing	Leading	Trailing
Passive	3.7	2.1	3.3	4.3	3.9
Sky Hook	2.1	1.7	2.1	5.1	5.5

	Leading End			Trailing End			Power Supply	
	Volts	Amps	Watts	Volts	Amps	Watts	Amps	Watts
	rms	rms		rms	rms		rms	$\times 10^3$
Sky Hook	64	16	585	42	16	425	14	3.8

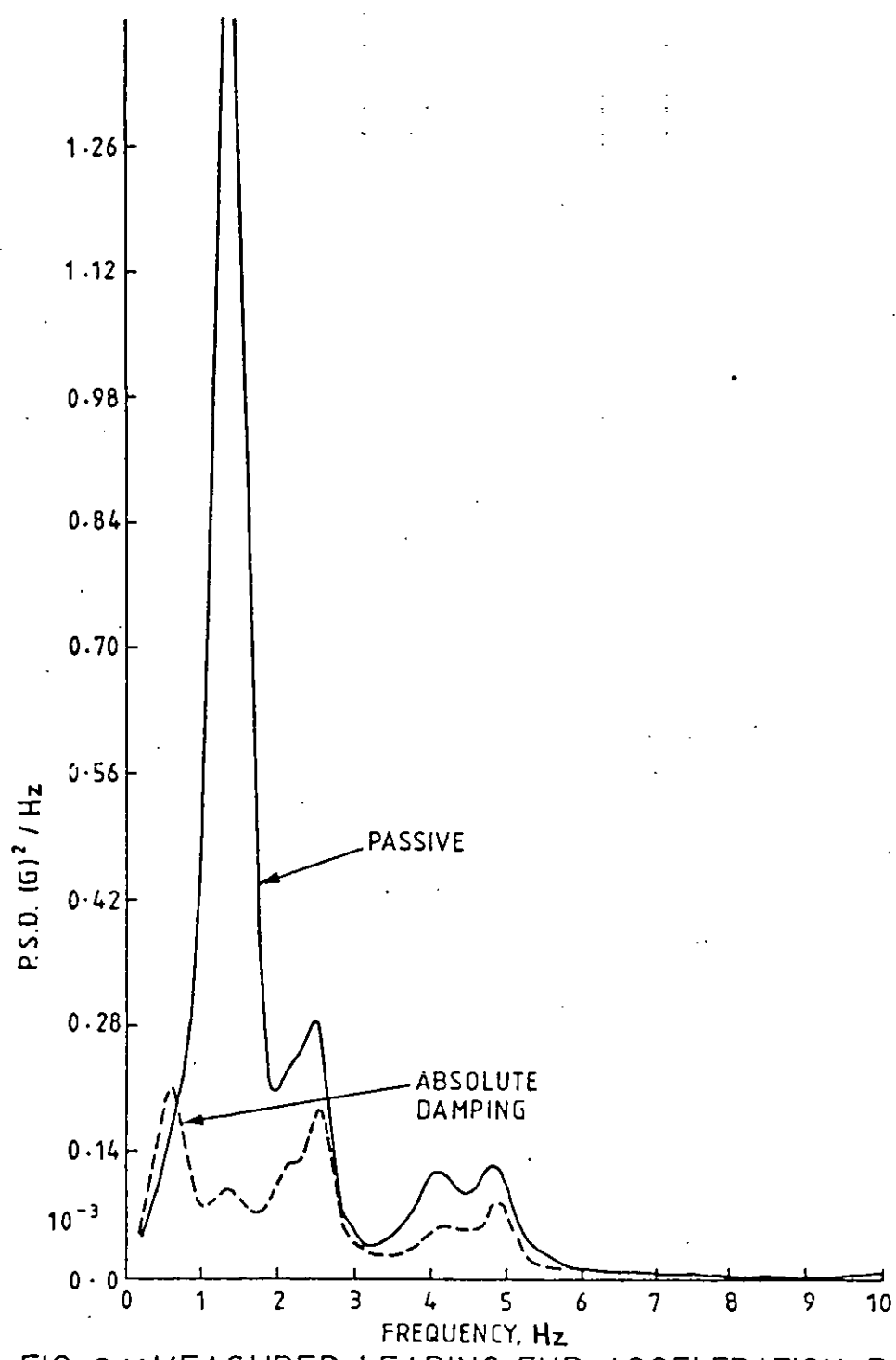


FIG. 9.11 MEASURED LEADING END ACCELERATION P.S.D.

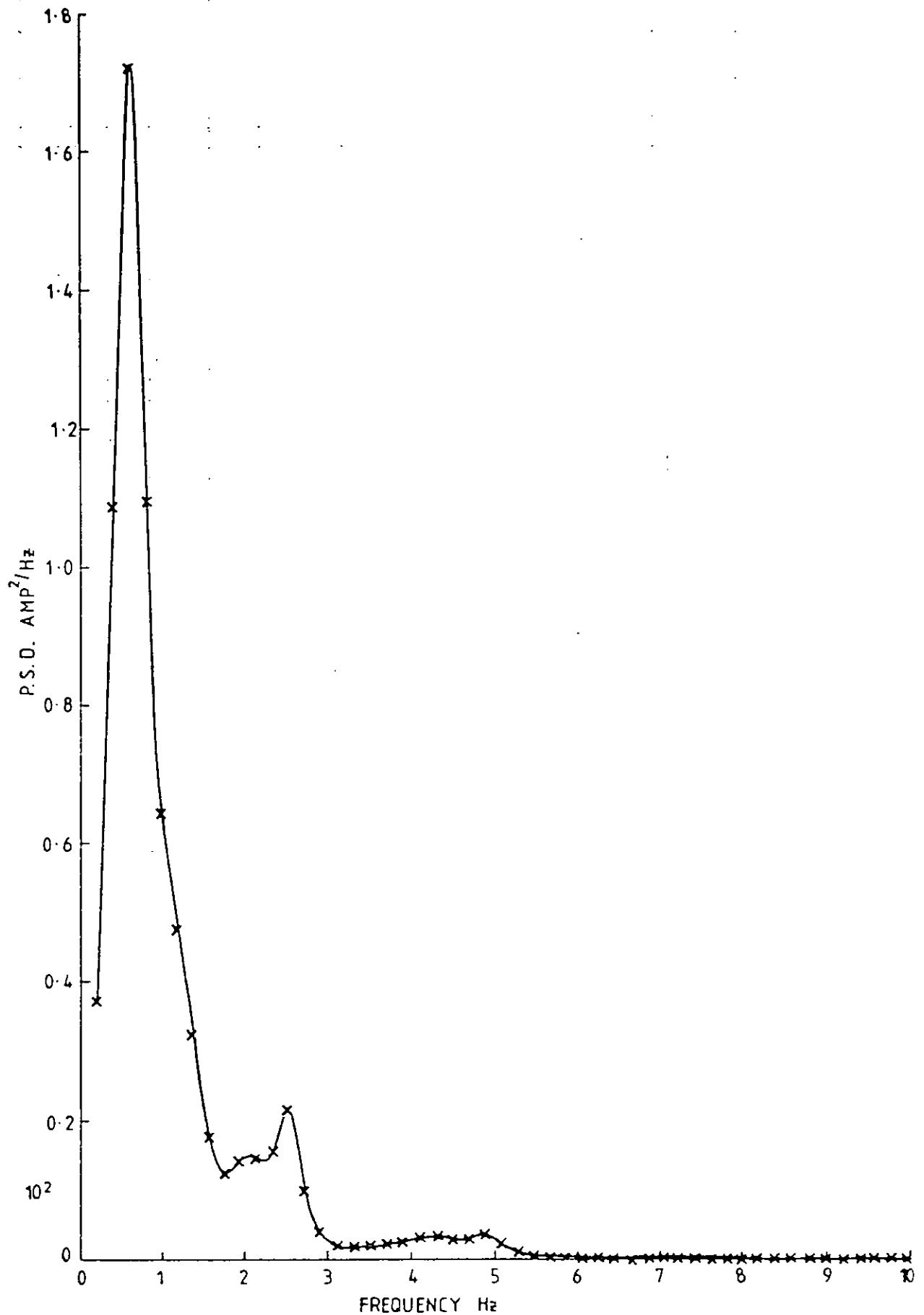


FIG. 9.12 SKY HOOK DAMPING LEADING END CURRENT P.S.D.

### 9.3.2 Position control measured performance

In the first two series of tests the power supply limited the performance improvements achieved. Even when these limitations were removed the pitch rigid body mode proved very difficult to reduce to the levels predicted theoretically. With the design control loop gains a reduction of around 30% was achieved in leading end rms acceleration (Table 9.3). Fig 9.13 shows that as well as the short fall in performance at the rigid body frequency the controller produces a degradation in ride above 6Hz. Fig 9.14, the acceleration psd at the centre of the vehicle, shows this problem even more clearly as the high frequency content from the actuators degrades the ride. The control system couples through the flexible body mode and a longitudinal shuttle motion of the bogies. The degradation at 0.5 Hz is caused by the imperfect nature of the absolute position signal. Increasing the gains in attempt to reduce the pitch rigid body mode has the desired effect on the rigid mode, but increases the high frequency degradation.

Further improvements were made in performance by changing the main loop gain from a simple gain to a lag lead network  $[1 + sT_1]/(1 + sT_2)$  with break points at 0.5 Hz and 1.5 Hz. This enhances the low frequency gain and not the high frequency. Fig 9.15 shows the modification to have been partially effective. Further increases in low frequency gain however once again led to problems with the power supply.

The pitch mode presents the biggest problem as it is more strongly coupled with the connecting vehicles than the bounce mode. It is also notable that at 44 m/s there is a "cut out" frequency (i.e. a frequency where the track inputs are in anti-phase) at 1.375 Hz in the bounce mode, which coincides with the rigid body bounce frequency.

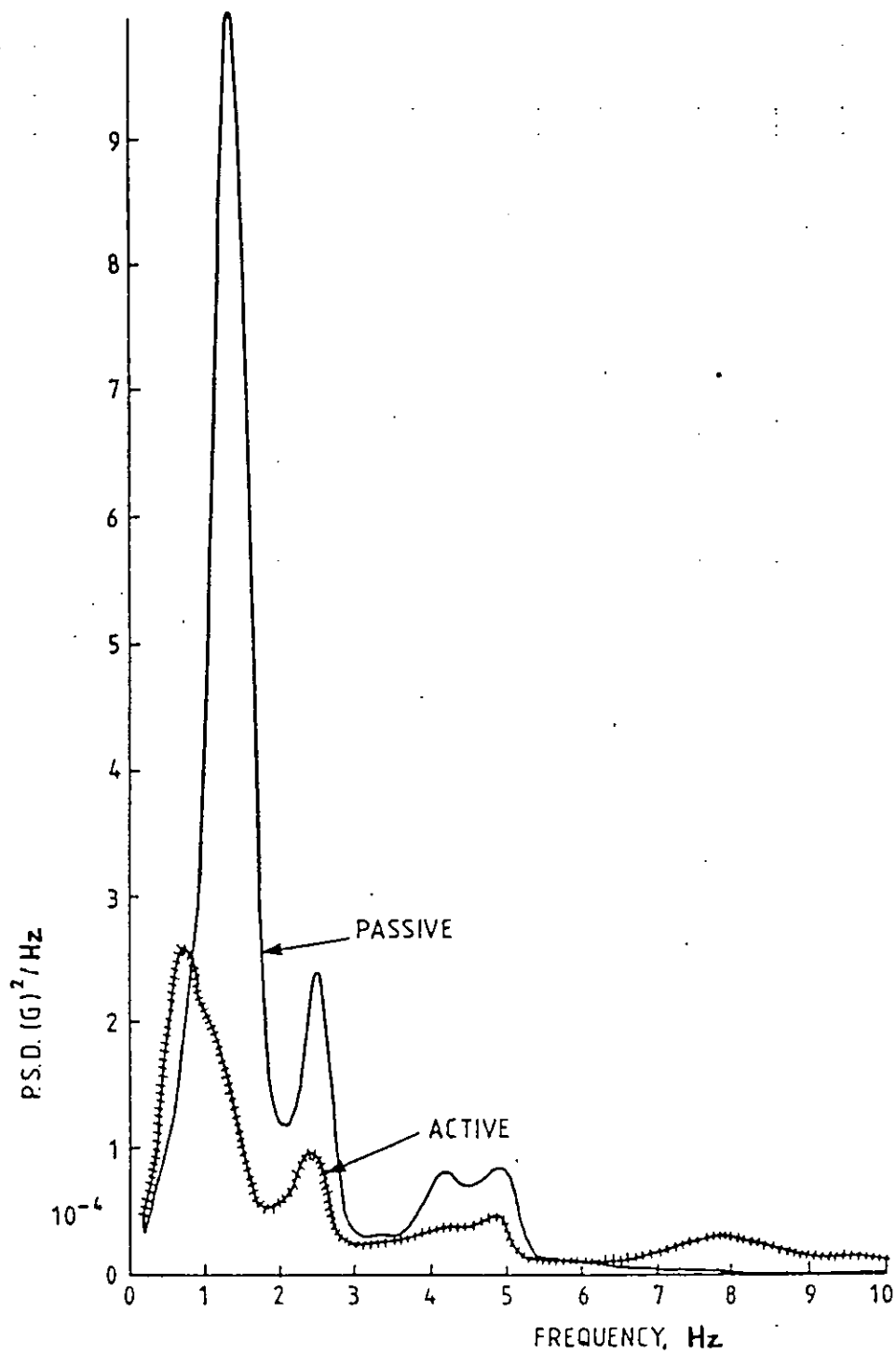


FIG. 9.13 POSITION CONTROL LEADING END P.S.D. 44 m/s.

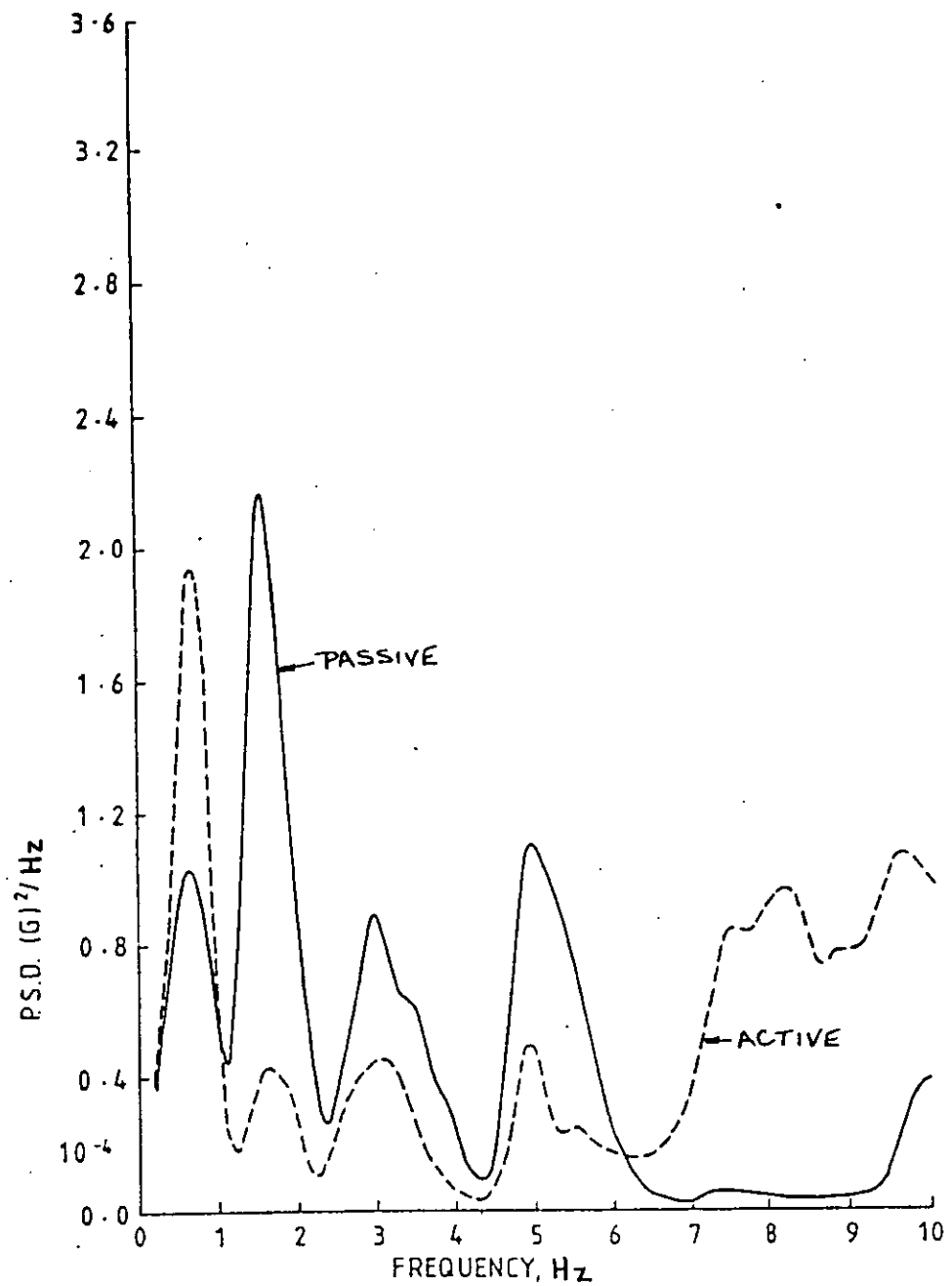


FIG.9.14 MEASURED ACCELERATION P.S.D. VEHICLE CENTRE POSITION CONTROL

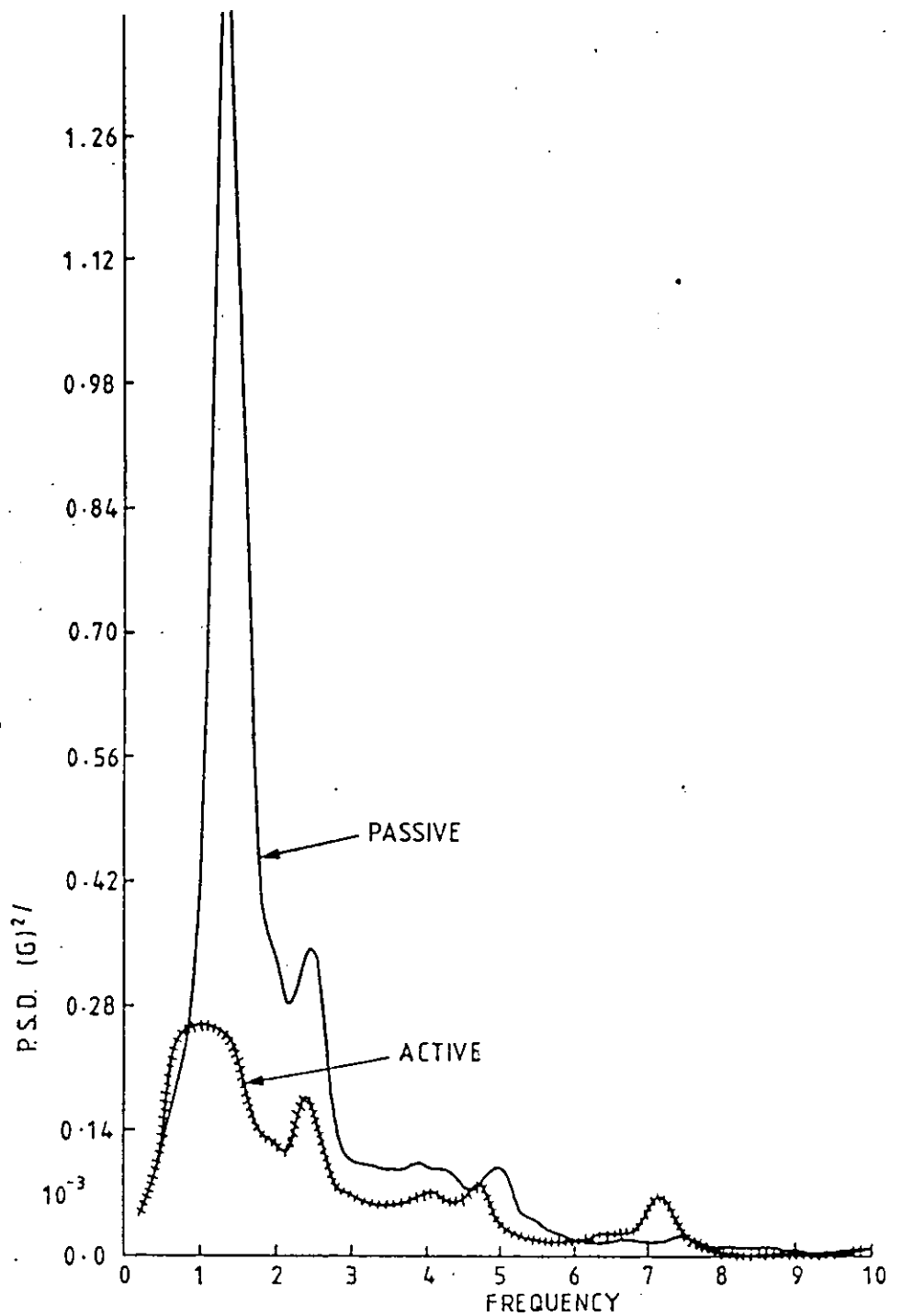


FIG. 9.15 MODIFIED POSITION CONTROL LEADING END  
P.S.D. 44m/s.

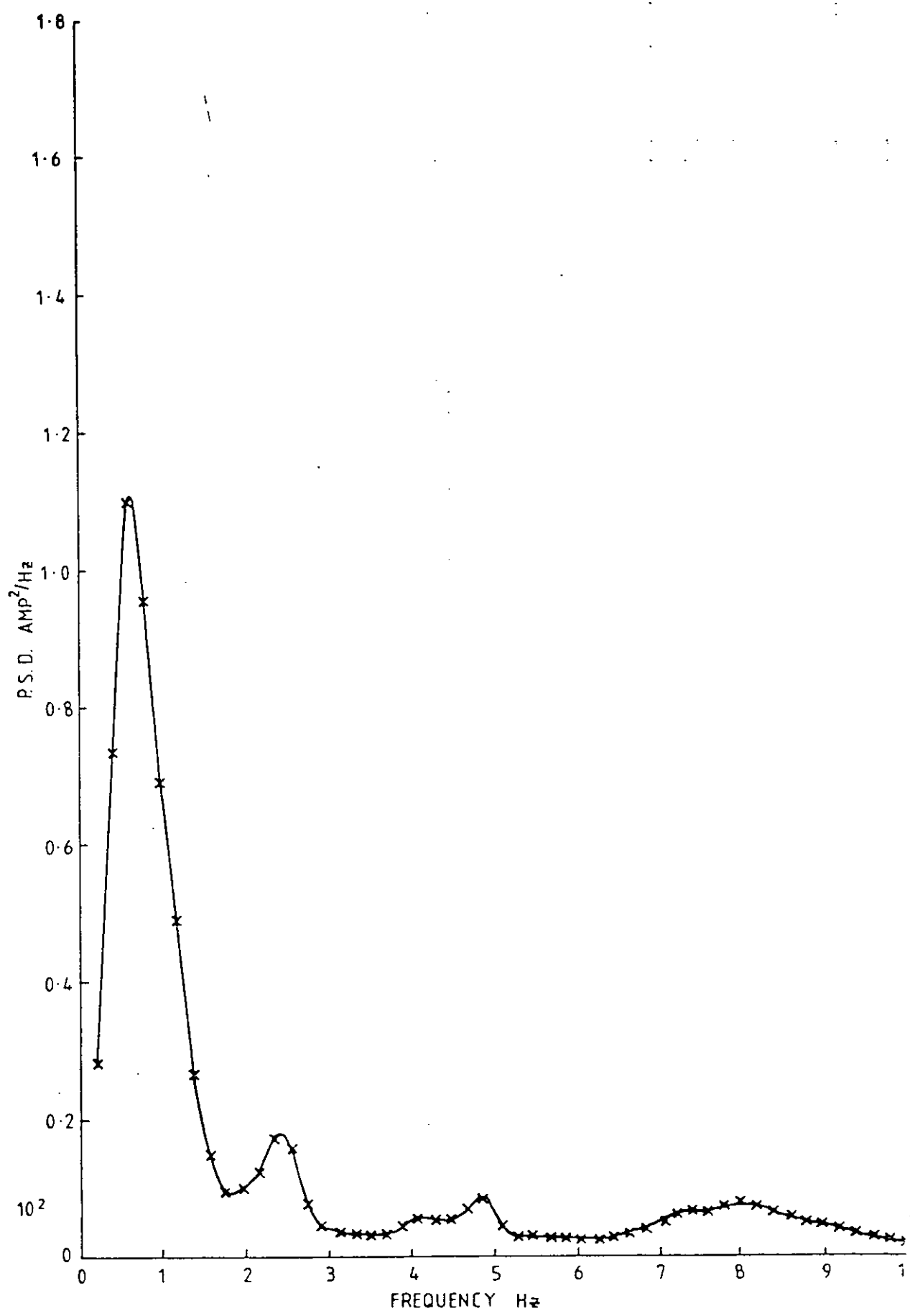


FIG. 9.16 POSITION CONTROL LEADING END CURRENT P.S.D.



Fig 9.14 shows that most of the control effort occurs at the rigid body frequencies. Table 9.3 summarises the test results.

Table 9.3 Position Control System Measured Performance

44 m/s West Coast Main Line

9.3a Position Control Travelling South

	rms Accn %g			Sec Displacement mm	
	Leading	Centre	Trailing	Leading	Trailing
Passive	3.1	1.8	2.9	3.6	3.1
Position	2.2	2.2	2.5	5.3	5.5

	Leading End			Trailing End			Power Supply	
	Volts	Amps	Watts	Volts	Amps	Watts	Amps	Watts
	rms	rms		rms	rms		rms	$\times 10^3$
Position	93	15.3	858	61	16	624	19	4.5

9.3b Improved Travelling North

	rms Accn %g			Sec Displacement mm	
	Leading	Centre	Trailing	Leading	Trailing
Passive	3.9	2.1	2.8	4.2	3.7
Improved					
Position	2.5	1.8	2.0	4.5	5.2

	Leading End			Trailing End			Power Supply	
	Volts	Amps	Watts	Volts	Amps	Watts	Amps	Watts
	rms	rms		rms	rms		rms	$\times 10^3$
Improved								
Position	47	16	503	74	13	512	15	3.9

It is worth noting that the revised control system reduces the power consumption, as well as improving the ride; thus showing that the power of the active suspension can be used negatively.

9.3.3 Modal optimal control measured performance

Initially there was a drift problem with the modal observers induced by the accelerometers. This only showed up during

running and was cured by integral feedback around the observers. Table 9.4 shows the suspension displacement to be somewhat higher than is desirable and this is associated with the drift problem. An adjustment of the integrator feedback gain and damping should cure the problem but there were insufficient test runs available to prove this point.

Fig 9.17 shows that the pitch rigid body mode is not attenuated as much as desired for the same reasons as those outlined in Section 9.3.2 for the position control system. Namely that this mode is very strongly coupled through the gangway connections to the adjoining vehicles. Here one of the biggest limitations of the optimal control design process is revealed. Because the controller is designed from a sophisticated model of the system using complex computer programs, when the system does not match up to the model it is very difficult to make intuitive changes to the control system gains in the field to achieve the required improvements in performance, making development of the optimal control system more difficult. However it is felt that given time it should be possible to improve the performance of this controller to match that of the "Sky Hook" Damper and surpass it.

Fig 9.18 shows once again that the majority of the control action takes place around the rigid body frequency.

Table 9.4 Optimal Control with Modal Observers Measured Performance 44 m/s West Coast Main Line Travelling North

	rms Accn %g			Sec Displacement mm	
	Leading	Centre	Trailing	Leading	Trailing
Passive	3.5	1.8	2.5	3.5	3.2
Modal					
Optimal	2.2	1.5	1.9	5.0	7.0

	Leading End			Trailing End			Power Supply	
	Volts	Amps	Watts	Volts	Amps	Watts	Amps	Watts
	rms	rms		rms	rms		rms	$\times 10^3$
Modal								
Optimal	46	16	560	73	17	780	18	4.5

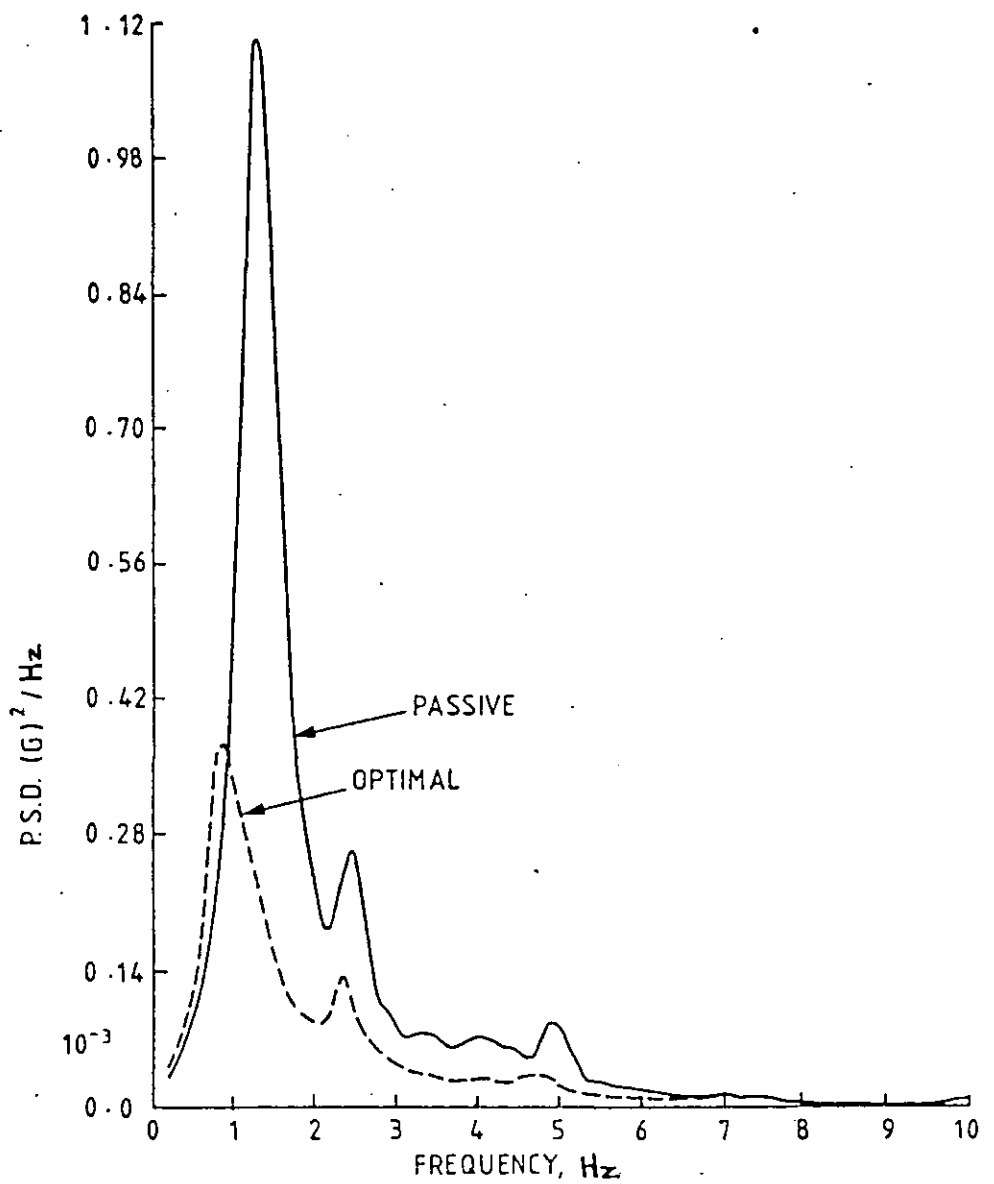


FIG. 9.17 MEASURED LEADING END ACCELERATION P.S.D.'s

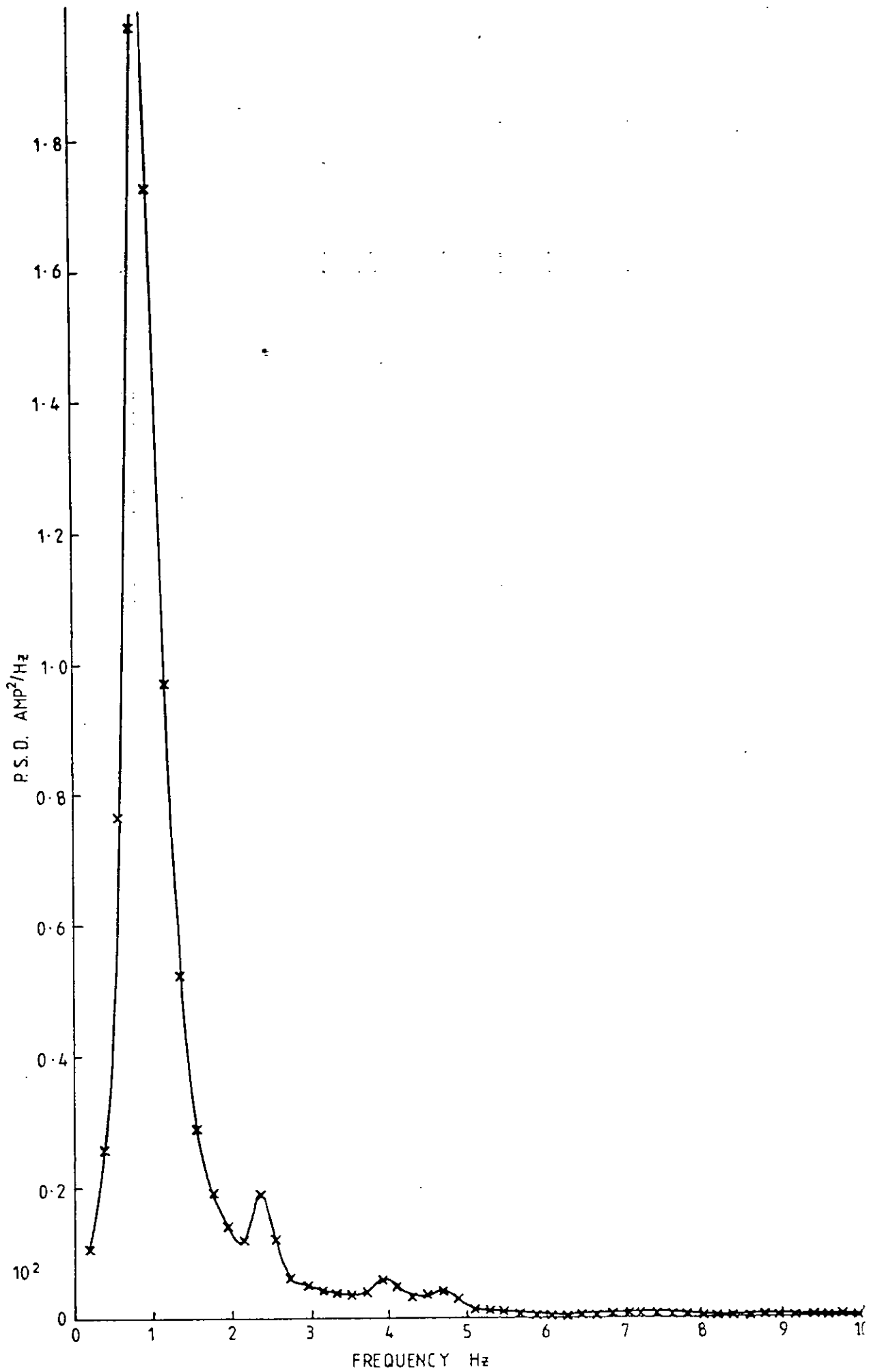


FIG. 9.18 MODAL OPTIMAL CONTROL LEADING END CURRENT P.S.D.

#### 9.4 Comparative Performance

It will be noted that the voltage and power measured at one end of the vehicle is consistently higher than at the other. This is because one of the laboratory coaches connected to the test vehicle had a stiffer suspension than the other (this was not the case for the first two series of tests when a different pair of Laboratory Coaches was used). As the experimental results presented for the "Sky Hook" damper and Position Control were measured when travelling north, while those for the Revised Position Control and Modal Optimal Control measured in a southbound direction, the normalised results presented in Table 9.5 must be treated with some caution. However they do give a measure of the relative performance between control systems.

Table 9.5 Normalised Ride Data 44 m/s

	rms Accn %g			Sec Displacement mm	
	Leading	Centre	Trailing	Leading	Trailing
Passive	3.9	2.1	2.8	4.2	3.7
Sky Hook	2.2	1.8	1.8	5.7	5.3
Position	2.6	2.2	2.5	5.8	5.4
Improved					
Position	2.5	1.8	2.0	4.5	5.2
Modal					
Observer	2.4	1.6	2.1	5.4	7.5

The results show that the best performance was obtained from the Sky Hook Damper. This is due to the fact that it is more immune to imperfections in the model used to describe the vehicle, and the train, than the more sophisticated control

systems. It is also much simpler to make intuitive modifications to the control system in the field to overcome short comings. Given further development time it is felt that the performance of the modal observers can be improved to equal or better the Sky Hook damper. However obtaining further performance improvements from the position control system will be very difficult as it was not possible to induce sufficient gain into the main control loop to enable it to function in the manner in which it was conceived. The normalised results in Table 9.5 show that the "Sky Hook" dampers perform better than predicted, the modal observers about as well as predicted and the position control system poorer than predicted. The simplicity of the "Sky Hook" dampers enabled the controller to be manipulated very easily to achieve the best possible results.

A problem which beset all the systems at one stage was bumpstop contact. This was due to the type of levelling valves fitted to the vehicle, which are now being replaced. These tend to come loose making height control rather erratic. When bumpstop contact occurs all the controllers detect this as an input to the system which must be relieved. This causes the actuators to drive the vehicle into even firmer bumpstop contact, usually resulting in repeated bumpstop contacts. The problem is relieved by the electronic bumpstops on the actuator control boards (Section 8.4.2).

Deterministic track inputs were assumed to be responsible for the large power demands in Section 9.2. The influence of one form of deterministic input is shown in all the acceleration psd's, that being the peaks occurring at 2.5 Hz and 5 Hz. These are due to 18 m rail lengths. Though the results were all measured on welded rail the rail is rolled in 18 m lengths which are then welded together. The theoretical track spectrum shown in Fig 2.2 should contain a contribution from the 18 m rail lengths, a problem which is being dealt with in British Rail at the time of writing.

### 9.5 Position Control Revisited

Since completing the experimental work the active suspension which is the basis of this thesis some of the pcbs have been used for an active lateral suspension. During this project a fault was found on the Phase Advance Module pcb Fig 8.12. R20 was connected to the output of A6 rather than the input. The effect of this fault is to produce the low frequency open loop characteristics shown in Figs 9.3 and 9.4 as the faulty phase advance network is ac coupled and has  $90^\circ$  phase advance at dc. However the increase in low frequency gain, and associated phase lag, of the revised position control system are indicative of what would have been achieved without the fault as the controller had reached the limits of the available power supply. The fact that this compromise was reached is an indication of the robustness of classical design techniques.

## CHAPTER 10

### DIGITAL CONTROLLERS

Digital controllers have been designed for the active suspension but have not yet been implemented. In this chapter the methods used to design and analyse the digital control systems will be described and an assessment made of their performance.

In order to be comparable in cost to the analogue control system it will replace, the digital controller has to be designed around a commercial microprocessor, rather than a mini-computer. Consequently the digital control system has been based on designs aimed at the Motorola MC 68000 16 bit microprocessor, as 8 bit processors are not capable of performing the required number of calculations in the time available.

#### 10.1 Classical Control System Design and Analysis

Having reviewed various techniques of designing digital control systems<sup>(67,68)</sup>, it was decided that the most straightforward method would be a direct transformation of the analogue controllers using bi-linear z transforms. The reason for adopting this technique is that the transformation is made by the following direct substitution for the Laplace operators in the continuous transfer function.

$$s = \frac{2}{T} \frac{(1 - z^{-1})}{(1 + z^{-1})} \quad (10.1)$$

$z^{-1}$  is the unit time delay  $e^{-sT}$  and T the sample period. Other techniques, such as the z transform, require the transformation of the complete transfer function and it was felt that they would be less amenable to modification during the development phase. The bi-linear transform also has the additional benefit that the frequency response of the continuous transfer function is warped to fit in half the sample period so that high frequency aliases do not occur at control frequencies. Substituting  $j\omega$  for s equation 10.1 it can be rewritten as:



$$\omega = \frac{2}{T} \tan \omega_1 \frac{T}{2} \quad (10.2)$$

where  $\omega$  is the frequency of the continuous system and  $\omega_1$  the frequency of the sampled system. Note that, provided  $\omega_1$  is less than 10% of the sample frequency  $\omega_s$ , there is virtually no difference between the analogue and digital transfer functions.

Having found a design technique some method of analysis was required. The main objection to the techniques proposed in references (68) and (69) is that they avoid the issue of a sampled data controller being used to control a continuous plant. The techniques either require a discrete model of the continuous plant to be formed, for instance by z transformation of the plant, or a continuous model of the sampled data controller to be formed by the W or W' transform. Note that the W transform is in effect the inverse of the bi-linear z transform. Even though a frequency response can be computed from these techniques it will not be one which can be compared to measurements taken of the control system during development. Therefore a technique was evolved which is an extension of one evolved by Goodall<sup>(70)</sup> for analysing continuous systems from their block diagrams.

#### 10.1.1 Complex frequency response program

Reference 70 describes how the frequency response of a complex vector  $x(s)$  can be computed by solution of the equation:-

$$x(s) = P(s)x(s) + R(s)u(s) \quad (10.3)$$

by substituting  $j\omega$  for  $s$

$u(s)$  is an input vector

$P(s)$  the system matrix

$R(s)$  the system input matrix

The technique evolved for the present investigation extends this to combine the continuous plant and the digital controller by the equations

$$\begin{aligned}x_c(s) &= P_c(s)x_c(s) + Q_c(s)x_s(z) + R_c(s)u(s) \\x_s(z) &= Q_s(z)x_c(s) + P_s(z)x_s(z) + R_s(z)u(s)\end{aligned}\quad (10.4)$$

$x_c(s)$  is a complex vector of the continuous variables

$x_s(z)$  is a complex vector of the sampled variables

$u(s)$  is a complex input vector

$P_c(s)$  is the continuous system matrix

$P_s(z)$  the sampled data system matrix

$Q_c(s)$  the sampled to continuous coupling matrix

$Q_s(z)$  the continuous to sampled coupling matrix

$R_c(s)$  continuous input matrix

$R_s(z)$  sampled input matrix

The elements of  $P_c(s)$ ,  $Q_c(s)$  and  $R_c(s)$  are entered into the program as second order polynomials of the form:-

$$H_{mn}(s) = \frac{a_0 + a_1s + a_2s^2}{b_0 + b_1s + b_2s^2}\quad (10.6)$$

When the system frequency response is being computed the frequency response of each element of  $P_c$ ,  $Q_c$  and  $R_c$  is computed from the expression

$$\begin{aligned}H_{mn}(\omega) &= \left[ \frac{a_0 - a_2\omega^2}{(b_0 - b_2\omega^2)^2 + b_1^2\omega^2} (b_0 - b_2\omega^2) + \frac{a_1b_1\omega^2}{(b_0 - b_2\omega^2)^2 + b_1^2\omega^2} \right] \\ &+ j \left[ \frac{a_1\omega(b_0 - b_2\omega^2) - b_1\omega(a_0 - a_2\omega^2)}{(b_0 - b_2\omega^2)^2 + b_1^2\omega^2} \right]\end{aligned}\quad (10.7)$$

Similarly the elements of  $P_s(z)$ ,  $Q_s(z)$  and  $R_s(z)$  are entered into the program as second order polynomials of the form:-

$$H_{mn}(z) = \frac{\alpha_0 + \alpha_1z + \alpha_2z^2}{\beta_0 + \beta_1z + \beta_2z^2}\quad (10.8)$$

When the system frequency response is being computed the frequency response of each element of  $P_s$ ,  $Q_s$  and  $R_s$  is computed from the expression

$$H_{mn}(\omega) = \frac{(Ar.Br + Ai.Bi) + j(Ai.Br - Ar.Bi)}{Br^2 + Bi^2}\quad (10.9)$$

where

$$A_r = \alpha_0 + \alpha_1 \cos(\omega T) + \alpha_2 (\cos^2(\omega T) - \sin^2(\omega T)) \quad (10.10)$$

$$A_i = j(\alpha_1 \sin(\omega T) + 2\alpha_2 \cos(\omega T) \sin(\omega T)) \quad (10.11)$$

$$B_r = \beta_0 + \beta_1 (\omega T) + \beta_2 (\cos^2(\omega T) - \sin^2(\omega T)) \quad (10.12)$$

$$B_i = j(\beta_1 \sin(\omega T) + 2\beta_2 \cos(\omega T) \sin(\omega T)) \quad (10.13)$$

T is the sample delay and the z operator is mapped into the s plane by the term

$$z = e^{sT}$$

The computer program computes the matrices  $P_c(\omega)$ ,  $Q_c(\omega)$ ,  $R_c(\omega)$ ,  $Q_s(\omega)$ ,  $P_s(\omega)$  and  $R_s(\omega)$  for each frequency  $\omega$ . The response vectors  $x_c(\omega)$  and  $x_s(\omega)$  are then computed by solution of the equation

$$\begin{bmatrix} x_c \\ x_s \end{bmatrix} = \begin{bmatrix} P_c & Q_c \\ Q_s & P_s \end{bmatrix} \begin{bmatrix} x_c \\ x_s \end{bmatrix} + \begin{bmatrix} R_c \\ R_s \end{bmatrix} u \quad (10.15)$$

Setting

$$P = \begin{bmatrix} P_c & Q_c \\ Q_s & P_s \end{bmatrix} \text{ and } R = \begin{bmatrix} R_c \\ R_s \end{bmatrix} \quad x = \begin{bmatrix} x_c \\ x_s \end{bmatrix}$$

Equation 10.15 is solved using a real linear equation solving subroutine (F04 AGF)<sup>(46)</sup> rearranging the matrices as

$$\begin{bmatrix} I - P_R & -P_I \\ -P_I & I - P_R \end{bmatrix} \begin{bmatrix} x_R \\ x_I \end{bmatrix} = \begin{bmatrix} R_R & -R_I \\ R_I & R_R \end{bmatrix} \begin{bmatrix} u_R \\ u_I \end{bmatrix} \quad (10.16)$$

$P_R$  is the real part of P

$P_I$  is the imaginary part of P

$R_R$  is the real part of R

$R_I$  is the imaginary part of R

$x_R$  is the real part of the x vector

$x_I$  is the imaginary part of the x vector

$u_R$  is the real part of the u vector

$u_I$  is the imaginary part of the u vector

Note that the complex nature of the  $u$  vector comes from the fact that it is programmed to accommodate the time delays between inputs. As the program was written to solve railway problems the time delay on the input is specified as a distance (the distance between the first and  $n^{\text{th}}$  wheelset is  $l_n$ ) so that the time delay on the input  $\delta_n = l_n/V$  which is accounted for as

$$u_n(s) = e^{-s\delta_n} \quad (10.17)$$

The program computes the response vector  $x$  for each frequency in rectangular and polar form, with gain expressed as both a ratio and in dBs. Responses to a track spectrum can also be computed giving the psd's of the  $x$  vector. Weighted rms accelerations and power consumption can be computed in line with the frequency response program described in Chapter 2.

#### 10.1.2 Classical controller performance

In order to validate the program the position control system described in Chapter 5 was modelled (Fig 10.1 and Appendix F). Agreement between the two programs was excellent.

The transfer functions of the analogue controller were then transformed using bi-linear transforms. A sample rate of 100/s was taken as it is 8 times the maximum control system eigenvalue. Fig 10.2 shows the control system block diagram. It will be noted that in addition to the control blocks, anti-aliasing filters have been included on the analogue/digital converters and a zero order hold for the digital to analogue converters. The anti-aliasing filters are single pole with a 3 dB point at 50 Hz. The transfer function of the zero order hold is  $(1 - z^{-1})/sT$ . Appendix F contains the equations for the analogue and digital control systems used in this section.

Open loop responses were computed for the digital and analogue models and these are shown in Fig 10.3 and 10.4. Frequency warping of the transfer functions causes significant shifts in gain even as low as 5 Hz, reducing the gain margin. Rematching the frequency compensation would restore the margin, but the

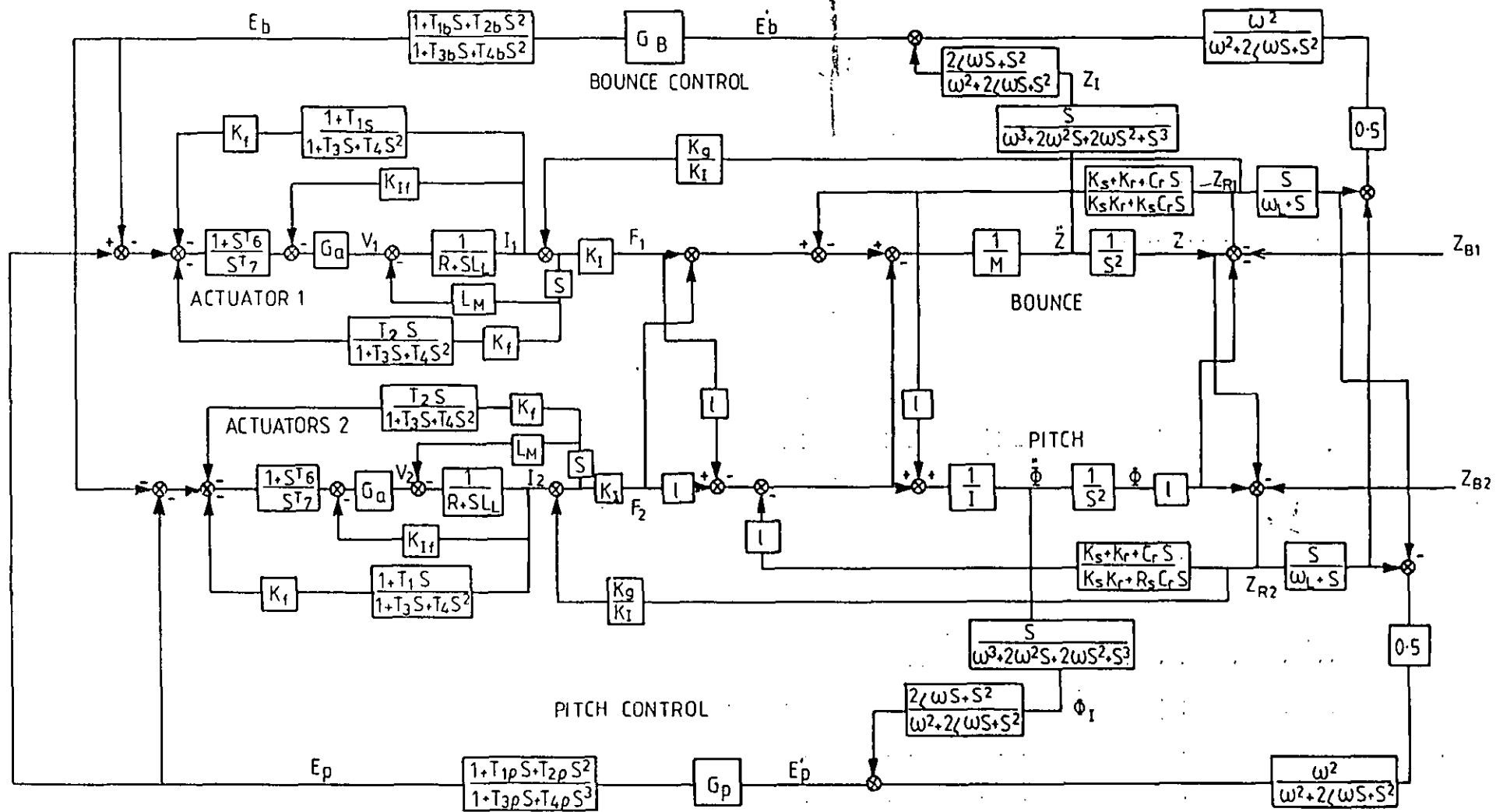


FIG. 10.1 ANALOGUE POSITION CONTROL BLOCK DIAGRAM

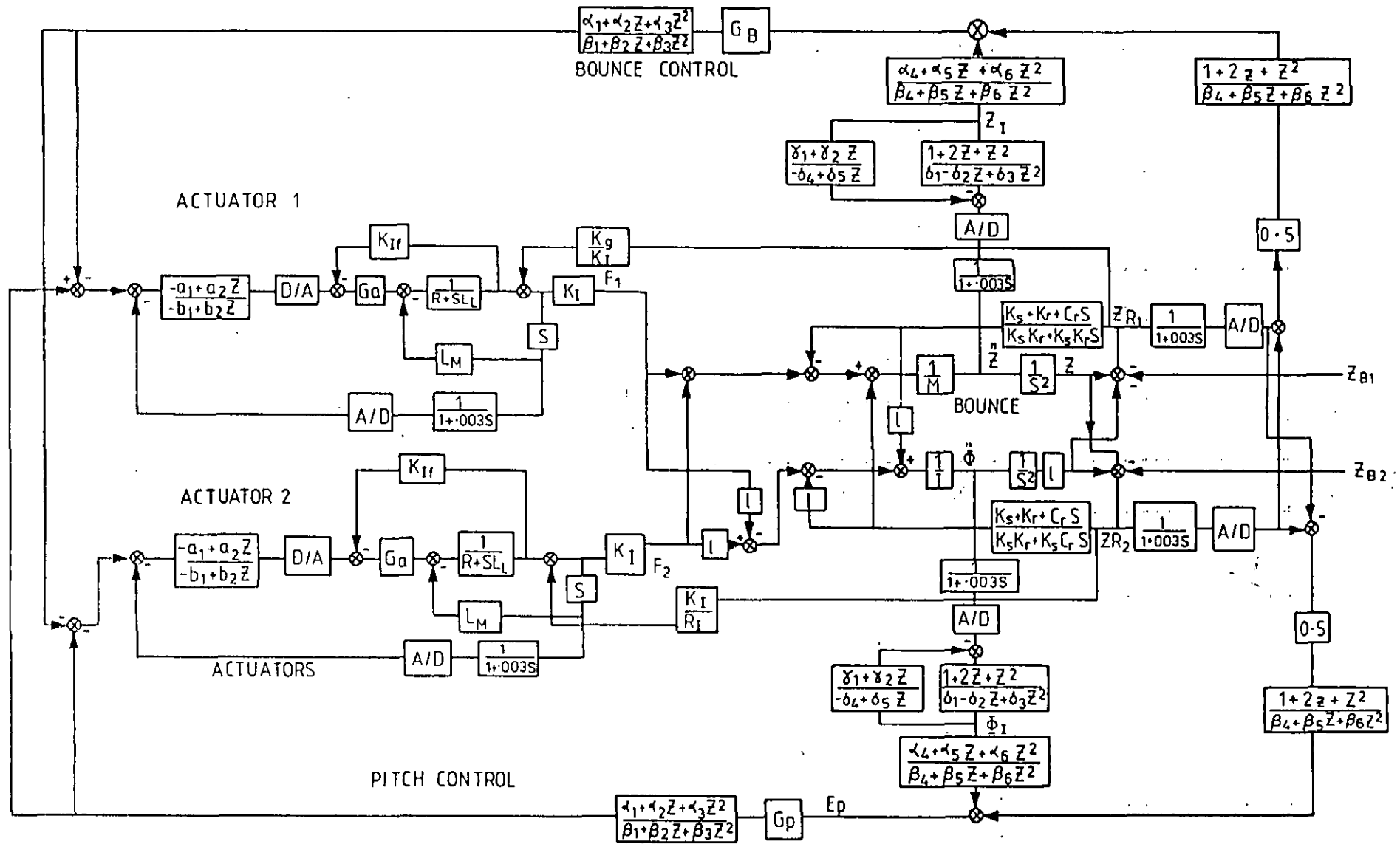


FIG. 10·2 DIGITAL POSITION CONTROL BLOCK DIAGRAM

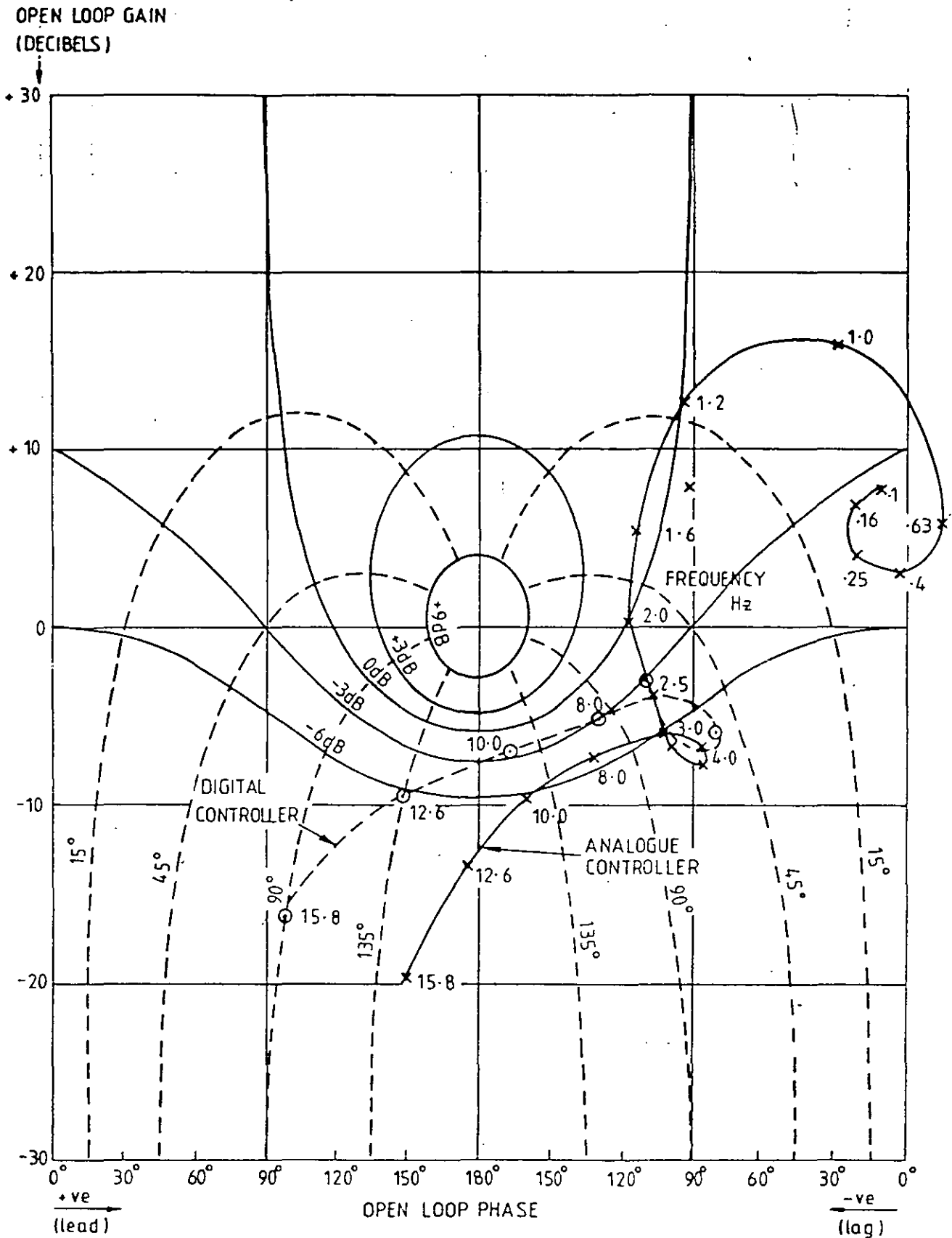


FIG. 10.3 BOUNCE OPEN LOOP RESPONSE POSITION CONTROL WITH DIGITAL AND ANALOGUE CONTROL SYSTEMS

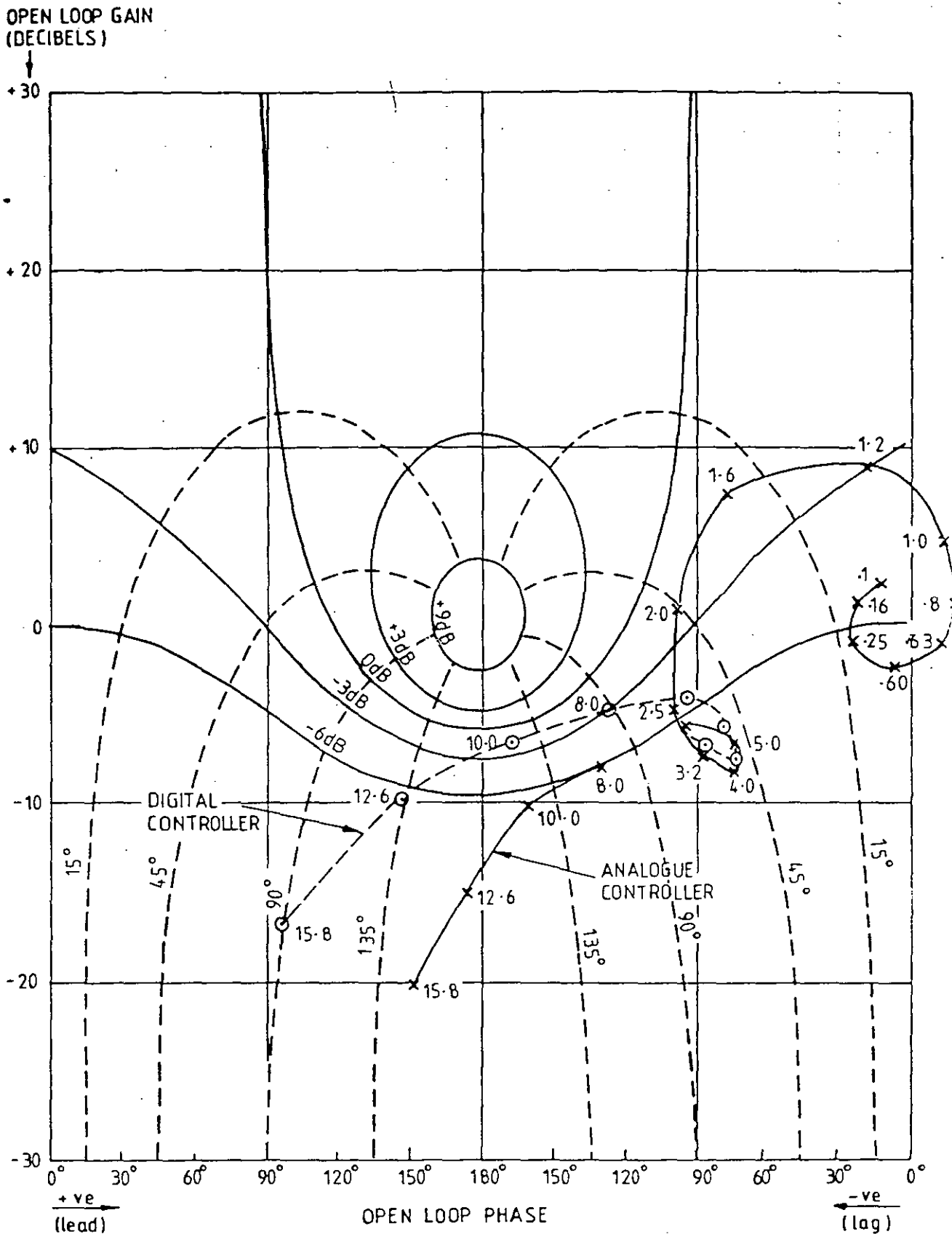


FIG.10.4 PITCH OPEN LOOP RESPONSE POSITION CONTROL

DIGITAL AND ANALOGUE CONTROL SYSTEMS



sampled controller would still be more limited in performance. Extra lag can be seen in the transfer function arising from the anti-aliasing filters and zero order holds. Frequency warping also produces a gain error in the absolute position signals at high frequencies, as the sampled data integrators attenuate the acceleration signal at a much faster rate than analogue integrators. An additional source of performance reduction which has not been included in the model is computation delay which will add extra phase lag at high frequencies.

Despite the reduction in gain margin the rms performance measurements for the sampled data controller are identical to those for the analogue control system. A sampled data version of the Sky Hook damper also produces the same results as the analogue controller. These results are not really very surprising as there is very little energy in the vehicle responses above 5 Hz where the digital controllers are almost identical to the analogue controllers.

## 10.2 Optimal Control System Design and Analysis

There are three options available when designing an optimal digital controller. These are:-

- 1) Making a discrete version of an analogue observer designed for an analogue regulator.
- 2) Direct digital design of an observer designed for an analogue regulator.
- 3) Direct digital design of an observer designed for a digital regulator.

The following section describes the computer programs written to design and analyse the optimal control systems.

### 10.2.1 Digital regulator design

When designing a digital regulator for a continuous system it is necessary to form a discrete model of the system. The first stage in digital regulator design was to write a subroutine to

do this. Note that the same subroutine is also capable of translating a continuous observer into a discretised version. Given the continuous system represented by the state equation:-

$$\dot{x}(t) = Ax(t) + Bu(t) \quad (10.17)$$

it can be represented in a discrete form by the equation

$$x_{i+1} = \Phi x_i + \Gamma u_i \quad (10.18)$$

$x_i$  and  $u_i$  are the state and input vectors at instant  $i$ .

$\Phi$  is the transition matrix

$\Gamma$  is the discrete input matrix

The relationship between the discrete and continuous matrices as

$$\Phi(T) = e^{AT} \quad (10.19)$$

$$\text{and } \Gamma(T) = \int_0^T \Phi(\tau) B \, d\tau \quad (10.20)$$

where  $T$  is the sample interval.

For a sample data controller the sample interval must be very much less than the minimum system time constant and the transition matrix can be computed successfully from a Taylor series, without the problems encountered with numerical accuracy described in Chapter 2.

$$\Phi(t) = I + At + \frac{A^2 T^2}{2!} + \frac{A^3 T^3}{3!} \text{ etc} \quad (10.21)$$

and

$$\int_0^T \Phi(\tau) d\tau = \left[ T + \frac{AT^2}{2!} + \frac{A^2 T^3}{3!} + \frac{A^3 T^4}{4!} \text{ etc} \right] \quad (10.22)$$

In the examples considered in the rest of this chapter the Taylor series in equations 10.21 and 10.22 converged in less than 12 elements. The test for convergence was that the last element to be computed adds less than 0.1% to the matrix.

The general approach taken to the digital regulator design was that given in Reference 68. (A word of warning : treat this reference with care as there are a lot of arithmetic errors in the first edition of the book.)

As well as discretising the system equations it is also necessary to form discrete forms of the continuous control system weighting function.

Given a continuous weighting function of the form

$$J = \int_0^t (x^T D x + u^T E u) d\tau \quad (10.23)$$

The equivalent discrete function is the series

$$J = \frac{1}{2} \sum_{i=0}^{N-1} [x_i^T \ u_i^T] \begin{bmatrix} D_{11} & D_{12} \\ D_{21} & D_{22} \end{bmatrix} \begin{bmatrix} x_i \\ u_i \end{bmatrix} \quad (10.24)$$

where

$$D_{11} = \int_0^T \phi^T(\tau) D \phi(\tau) d\tau \quad (10.25)$$

$$D_{22} = \int_0^T [f^T(\tau) D f(\tau) + E] d\tau \quad (10.26)$$

$$D_{12} = \int_0^T \phi^T(\tau) D f(\tau) d\tau \quad (10.27)$$

$$D_{21} = D_{12}^T \quad (10.28)$$

10.24 can in fact be re-written as

$$J = \frac{1}{2} \sum_{i=0}^{N-1} x_i^T D' x_i + u_i^T E' u_i \quad (10.29)$$

where

$$D' = D_{11} - D_{12} D_{22}^{-1} D_{21} \quad (10.30)$$

$$E' = D_{22} \quad (10.31)$$

$$u'_i = u_i + D_{22}^{-1} D_{21} x_i \quad (10.32)$$

In order to solve the discrete regulator equation, equation (10.18) has also to be reformulated as

$$x_{i+1} = (\phi - [D_{22}^{-1} D_{21}]) x_i + [u'_i] \quad (10.33)$$

making

$$\phi' = \phi - [D_{22}^{-1} D_{21}] \quad (10.34)$$

the regulator seeks to find a feedback matrix  $C$  to minimise equation 10.29 with

$$u'_i = Cx_i \quad (10.35)$$

For the remainder of the section

$$\phi = \phi', \quad D = D' \quad \text{and} \quad E = E'$$

The feedback matrix  $C$  was found in a similar method to that used for the continuous regulator by solution of the canonical form of the discrete Riccati equation:-

$$\begin{bmatrix} x \\ \theta \end{bmatrix}_{i+1} = \begin{bmatrix} \phi + E^{-1} [^T \phi^T D] & - E^{-1} [^T \phi^{-T}] \\ -\phi^{-T} D & \phi^{-T} \end{bmatrix} \begin{bmatrix} x \\ \theta \end{bmatrix}_i \quad (10.36)$$

$\theta$  is the adjoint variable

The  $z$  transform of equation 10.36 has symmetrical sets of eigenvalues  $\lambda$ ,  $\lambda^{-1}$  with  $\lambda$  lying inside the unit circle of the  $z$  plane and  $\lambda^{-1}$  (the inverse) lying outside the unit circle.

Forming a matrix of the eigenvectors

$$\begin{bmatrix} X_Z & X_E \\ \Lambda_Z & \Lambda_E \end{bmatrix}$$

where  $[X_Z \Lambda_Z]$  are the eigenvectors inside the unit circle and  $[X_E \Lambda_E]^T$  those on the outside then the feedback matrix

$$C = -E^{-1} [\Phi^{-T} (\Lambda_E X_E^{-1} - D)] \quad (10.37)$$

As in the continuous case complex arithmetic is avoided by only using one half of a complex conjugate pair of eigenvectors for the columns of  $[X_E \Lambda_E]^T$ . The real parts forming one column and the imaginary parts a second.

The program produces the closed loop eigenvalues of the system as a side effect. These are mapped to the equivalent position in the  $s$  plane, as it is more meaningful, using the expression

$$z = e^{sT} \quad (10.38)$$

$$\text{as } s = \sigma + j\omega \quad (10.39)$$

$$\sigma = \frac{\ln \sqrt{\frac{\text{Re}^2 + \text{Im}^2}{T}}}{T} \quad (10.40)$$

and

$$\omega = (\tan^{-1} (\text{Im}/\text{Re}))/T \quad (10.41)$$

Re and Im are the real and imaginary parts of the eigenvalue in the  $z$  plane.

### 10.2.2 Digital observer design

The digital observer program assumes that there is zero computation time between system measurements being made and the observed variable being computed. If the system is excited by a white noise process  $w_1$  variance  $Q_d$  and the observed variables are corrupted by white noise  $v$  variance  $R_d$  then:-

$$x_{i+1} = \phi x_i + \Gamma w_1 \quad (10.42)$$

$$y_i = Hx_i + v. \quad (10.43)$$

$y$  is the measured vector  
and  $H$  the measurement matrix.

The error is

$$\hat{x}_{i+1} = x_{i+1} + K (y_{i+1} - \hat{y}_{i+1}) \quad (10.44)$$

$$K = PH^T R_d^{-1} \quad (10.45)$$

$$P = \phi^{-1} (M - [Q_d]^T) \phi^{-T} \quad (10.46)$$

$M$  is found from the eigenvectors of the canonical matrix

$$\left[ \begin{array}{c|c} \phi^T + H^T R_d^{-1} H \phi^{-1} & -H^T R_d^{-1} H \phi^{-1} \\ \hline -\phi^{-1} [Q_d]^T & \phi^{-1} \end{array} \right] \quad (10.47)$$

$$M = X_E \Lambda_E^{-1}$$

$X_E \Lambda_E^{-1}$  come from the matrix of the eigenvectors

$$\begin{bmatrix} X_Z & X_E \\ \Lambda_Z & \Lambda_E \end{bmatrix}$$

with  $[X_Z \Lambda_Z]^T$  being the eigenvectors of the eigenvalues lying inside the unit circle of the  $z$  plane and  $[X_E \Lambda_E]^T$  being the eigenvectors of the eigenvalues outside unit circle in the  $z$  plane. Hence again the  $z$  plane eigenvalues are mapped into the  $s$  plane.

### 10.2.3 Analysis of the optimal controllers

A frequency response method was adopted for analysing the controllers which enabled a mixture of continuous and sampled elements to be used. This is described by equations 10.50 and 10.51

$$\dot{x} = Ax + Gx_i + Bu \quad (10.50)$$

$$x_{i+1} = \Phi x_i + \Gamma x + \beta u_i \quad (10.51)$$

$x$  and  $u$  are the continuous state and input vectors

$x_i$  and  $u_i$  are the discrete state and input vectors

$A$  is the continuous state matrix

$B$  the continuous input matrix

$\Phi$  transition matrix

$\beta$  discrete input matrix

$G$  digital to analogue matrix

$\Gamma$  analogue to digital matrix

The equations are solved for a frequency  $\omega$  by a real linear subroutine (F04AGF)<sup>(46)</sup> after configuring 10.50 and 10.51 as

$$\left[ \begin{array}{cc|cc} -j\omega I & -A & 0 & -G \\ -A & j\omega & -G & 0 \\ \hline 0 & -\Gamma & -j\sin\omega T & \cos\omega T - \Phi \\ -\Gamma & 0 & \cos\omega T - \Phi & j\sin\omega T \end{array} \right] \begin{bmatrix} xI(\omega) \\ xR(\omega) \\ \hline x_i I(\omega) \\ x_i R(\omega) \end{bmatrix} = \begin{bmatrix} 0 & B \\ B & 0 \\ \hline 0 & \beta \\ \beta & 0 \end{bmatrix} \begin{bmatrix} uI(\omega) \\ uR(\omega) \\ \hline u_i I(\omega) \\ u_i R(\omega) \end{bmatrix} \quad (10.52)$$

The suffixes I and R denote the imaginary and real parts of the vector respectively.

The computer program computes ride statistics and power consumption in line with the continuous programs (Chapter 2) and the complex frequency response program in 10.1.1.

#### 10.2.4 Optimal regulator

The small vehicle model described in Section 6.2.3 was used for the design of a digital regulator. The regulator was designed using the procedure given in Section 10.2.1 for a series of sample rates. These are given in Table 10.1. For the higher sample rates the eigenvalues in the continuous and sampled

regulators correspond very well. However, where the sample rate is less than twice the frequency of the maximum eigenvalue (i.e. 20 Hz) the design program still produces eigenvalues which are symmetrically placed on the inside and outside of the unit circle, but some of these end up on the negative real axis of the  $z$  plane (i.e. the eigenvalue  $\zeta = .67, 13.5$  Hz). As the negative real axis of the  $z$  plane is in fact equivalent to half the sample frequency, any closed loop eigenvalues lying on this axis represent states which are in practice uncontrollable.



TABLE 10.1  
DIGITAL REGULATOR EIGENVALUES

Continuous		SAMPLE RATE							
		200 Hz		100 Hz		50 Hz		20 Hz	
$\zeta$	Hz	$\zeta$	Hz	$\zeta$	Hz	$\zeta$	Hz	$\zeta$	Hz
.44	1.2	.43	1.2	.43	1.2	.43	1.2	.43	1.2
1.00	2.2	1.0	2.2	1.0	2.2	1.00	2.2	1.00	2.2
.59	1.4	.59	1.4	.59	1.4	.59	1.4	.59	1.4
1.00	2.1	1.00	2.1	1.0	2.1	1.00	2.2	1.00	2.2
1.00	8.0	1.0	8.0	1.0	8.0	1.00	8.2	.67	13.5
1.00	10.7	1.00	10.7	1.00	10.8	1.00	11.4	1.00	10.62

### 10.2.5 Optimal observers

Digital versions of the small model observer (Section 6.2.3) were designed for 100 Hz and 200 Hz sampling. The analogue version of this observer has an eigenvalue at 27 Hz which in theory calls for the higher sample rate. Table 10.2 shows that the observer design program reduces the frequency of the high frequency eigenvalues with 100 Hz sampling.

TABLE 10.2  
Digital Observers

Sample Rate	Continuous		100 Hz		200 Hz	
	$\zeta$	Hz	$\zeta$	Hz	$\zeta$	Hz
	1.00	.17	1.00	.17	1.00	.17
	1.00	.18	1.00	.18	1.00	.17
	1.00	.45	1.00	.45	1.00	.45
	1.00	.66	1.00	.66	1.00	.66
	1.00	1.49	1.00	1.49	1.00	1.49
	1.00	1.55	1.00	1.55	1.00	1.55
	1.00	6.05	1.00	6.02	1.00	6.02
	1.00	6.14	1.00	6.13	1.00	6.13
	1.00	15.79	1.00	15.33	1.00	15.70
	1.00	27.27	1.00	25.08	1.00	26.67

Despite the reduction in frequency of the high frequency eigenvalue the computed performance of this controller is identical to that of the analogue control system it replaces.

Digital versions of the modal observers (Section 6.4) were designed for 100 Hz sampling. Theoretical assessments of the performance showed it to be the same as the analogue system which it replaces. The digital observers have their eigenvalues located in the same part of the s plane as the analogue observers.

### 10.3 Resolution

An estimate has been made of the signal resolutions required to implement the digital control systems. The main requirement of a digital system is that the passengers should not be able to detect the incremental changes in force. As there is no data available some assumptions have been made to the levels which will be detectable. These are aimed to be on the conservative side so that when experimental controllers are available the effect of resolution can be investigated in detail.

The analogue to digital conversion is via an 8-channel multiplexed A/D converter with 12 bit resolution, while digital to analogue conversion is via 12 bit D/A's. 12 bits is becoming something of a standard as it provides quite good resolution with an attainable signal to noise ratio (70 dB).

The signal to the amplifier produces a current, as the force is proportional to the square of the current the force generated by the amplifiers will not be the same for each bit. The smallest change in output will produce a force of .003 N and the largest 12 N on any actuator. These should be undetectable as they produce an acceleration of only .02%g, or about 1% of the proposed vertical ride standard in Chapter 2.

The classical control systems generate a flux signal from a rate of change of flux. The time constant on the integrator circuit is 1.25 s so that the least significant bit of the flux change signal has to be held for 125 cycles, at 100 Hz sampling, to produce a least significant bit output on the flux signal. Thus if the flux signal has 12 bit resolution the internal variables in the integrator have to be stored to 19 bits. The double integrator which produces the absolute position signal has a similar time constant but requires two integrations giving a requirement for 25 bit internal variables.

The longest time constant in the optimal control systems is again 1.25 secs, suggesting 19 bit resolution on the internal variables.

This rather crude analysis led to the conclusion that variables in the controller could be stored as 16-bit variables, but that calculations within control blocks had to be performed to 32 bit accuracy, integer arithmetic being used for all calculations.

Using these assumptions control algorithms were written for each of the four control schemes which have been considered.

Estimated computation times for the algorithms on an 8 MHz, MC 68000 are given in Table 10.3.

TABLE 10.3 Digital Controller Computation Time

Controller	Implementation Time in ms
Sky Hook Damper	1.75
Position Control	2.50
Small Model Optimal	5.07
Modal Observers	2.50

All the controllers can be executed with the 10 ms available. However the time for the small model observer is significantly longer than the other controllers. This reveals a potential problem with sampled data optimal observers. The observer transition matrix has very few zero elements so that the number of calculations to be performed expands as the square of the number of variables. Thus by expanding the size of the observer by one or two states it quickly reaches a size where the control algorithm cannot be implemented within the available sample period.

#### 10.4 Why Digital?

So far this chapter has demonstrated that it is possible to design a digital controller which provides the same performance as the analogue control system which it replaces. It is doubtful that the digital control system will be able to offer any advantages in terms of performance for a vertical active suspension. A lateral active suspension is a different proposition as conditions at the wheel rail interface can vary over a wide range, changing the dynamics of the suspension, thus making some form of adaptive control system, where a digital control system is almost essential, look very attractive.

The analogue control system has a complex system of interlocks and fault detection, provided by relays and discrete logic components. In a digital control system these functions can be provided within the processor, along with self test and fault diagnostic subroutines, for little extra cost and increase in system complexity. In addition the control systems described in the thesis contain redundant information, as only three of the four accelerometers and displacement transducers provided are required to resolve the modal information required to control the bounce, pitch and roll modes. It would be much simpler to use this information to detect a failed transducer in a digital control system than it is in an analogue controller. Having detected a failure an alternative control configuration could be provided until the fault is rectified.

CHAPTER 11A COMPUTER AIDED DESIGN METHOD

Ever reducing computing power and cost is making design techniques available which could not be considered a few years ago. During the course of this project the author and his supervisor, R M Goodall, were given the chance to sample a program written by the Institute fur Dynamik der Flugsysteme at Deutsche Forschungs und Versuchsanstalt fur Luft und Raumfahrt (DFVLR) Munich. The program allows the designer to define the structure of the control system, but leaves certain parameters in the controller "free" for the computer to optimise a set of specified design criteria. It is intended that the program is run in an interactive manner so that the designer can trade off different aspects of the optimisation to obtain the best overall performance. As with linear optimal control, the optimal solution to the specified performance criteria may not in fact be the best overall solution.

11.1 Summary of the design technique

A full description of the technique is given in (71), but a summary is appropriate for completeness. The control system designer must:-

1. Supply a model of the system in a generalised state space form, as defined in Section 11.2.2.
2. Identify a set of free control parameters  $\underline{k}$  within the controller which the optimisation process may vary, and provide initial values.
3. Specify a set of performance indices  $\underline{G}$  by which the system performance may be rated quantitatively.

The performance indices which may be incorporated are various, but must all be positive definite (i.e. greater than 0 at all times), and also must all reduce for better performance.

Typical performance indices may be based upon the following

criteria:-

1. The trajectory of the control system following a step input.
2. The trajectory of the control system following a disturbance input.
3. The response of the system to a random input.
4. The position of the system eigenvalues and the damping ratio (i.e. the stability margins)
5. Bounds on the controller/eigenvalues (in the  $s$  plane)
6. Limiting of the feedback gains

Having provided the computer with data as above, the method proceeds as follows. Firstly the control system performance is calculated using the initial values for the control parameters  $\underline{k}$  to give  $\underline{G}(0)$ , an initial set of values for the performance vector. The designer then provides a vector  $\underline{C}$  for the desired values of the performance vector. The first value  $\underline{C}(0)$  for this vector must be limited such that all components of  $\underline{C}(0)$  are greater than or equal to  $\underline{G}(0)$ . The computer then carries out a first optimisation run, adjusting  $\underline{k}$  to minimise the vector  $\underline{G}$ , but always seeking to minimise the element with the largest ratio  $C_i/G_i$ . At the end of this optimisation run a resulting performance vector  $\underline{G}(1)$  is printed. The process continues with the designer steering the optimisation in the direction required using new values for  $\underline{C}$  - for example if after the fourth iteration  $G_i$  may be reduced at the expense of others then  $C_i(5)$  is set equal to  $G_i(4)$ . In this way it is possible to push the performance vector  $\underline{G}$  into the most acceptable set of values, but always with the multiple design objectives represented by  $\underline{G}$  being taken care of simultaneously and individually.

Another facility which enhances the designer's ability to guide the process is that of placing a restriction on which of the control parameters  $\underline{k}$  may be varied. This enables the designer to use his experience and overall understanding of the system in order to assist the optimisation process.

## 11.2 System description

One of the main problems encountered was devising a suitable model of the system for the DFVLR program. This arose because the program separates the plant and the control system into different state equations while the program developed by the author on the British Rail computer describes the system as a single state equation.

### 11.2.1 British Rail Equations

The British Rail state and output equations are:

State Equation:

$$\dot{x} = Ax + Bq \quad (11.1)$$

Output Equation:

$$y = Dx + G\dot{x} + Eq \quad (11.2)$$

x = State Vector

q = Input Vector

y = Output Vector

A = State Matrix

B = Input Matrix

D = State Output Matrix

G = State Derivative Output Matrix

E = Input Vector Output Matrix

### 11.2.2 DFVLR Equations

The DFVLR program describes the system by 5 equations.

State Equations:

$$\dot{x} = Ax + Bu + Eq \quad (11.3)$$



## Measured Variables

$$y_m = C_m x + F_m q \quad (11.4)$$

## Controller State Equations:

$$\dot{x}_r = A_r x + B_r y_m + E_r r \quad (11.5)$$

## Control Signals:

$$u = C_r x + D_r y_m + F_r q \quad (11.6)$$

## Output Equations:

$$y_a = Cx + Du + Fq \quad (11.7)$$

$x$  = State Vector

$u$  = Control Vector

$q$  = Input Vector

$r$  = Command Input Vector

$y_m$  = Measured Variable Vector

$x_r$  = Controller State Vector

$y_a$  = Output Vector

$A$  = Plant Matrix

$B$  = Control Input Matrix

$E$  = Plant Input Matrix

$C_m$  = Measurement Matrix

$F_m$  = Input Measurement Matrix

$A_r$  = Controller State Matrix

$B_r$  = Controller Input Matrix

$E_r$  = Command Input Matrix

$C_r$  = State Control Matrix

$D_r$  = Control Measured Matrix

$F_r$  = Control Input Matrix

$C$  = State Output Matrix

$D$  = Control Output Matrix

$F$  = Input Output Matrix

In practice the plant and controller states are separated within the BR state vector so that the BR equations can be described by the following matrix equation:

$$\begin{bmatrix} \dot{x} \\ \dot{x}_r \end{bmatrix} = \begin{bmatrix} A+BD_r & BC_r \\ B_r C_m & A_r \end{bmatrix} \begin{bmatrix} x \\ x_r \end{bmatrix} + \begin{bmatrix} E+BF_m \\ B_r F_m \end{bmatrix} q + \begin{bmatrix} BF_r \\ E_r \end{bmatrix} r \quad (11.8)$$

(8)

Note however that the BR equations do not allow an independent control input  $r$ .

### 11.2.3 Position Control Small Model

The control system used as a test example was the position control system described in Chapter 5. A simple pitch and bounce model of the suspension was devised to keep the size of the system matrix small. This is shown in Fig 11.1. It will be noted that the track input to the vehicle has been modelled as a flat spectrum for vertical track velocity, which is filtered by a low pass filter of the form  $(1/1+s)$ .

Fig 11.2 shows the actuator control which is devised to produce a flat force response up to about 10 Hz. There are two actuators at each end of the vehicle; as each pair of actuators operate in phase only one is modelled and the force produced doubled.

Fig 11.3 shows the main loops which control the dynamic response of the vehicle. It will be noted that the pitch and bounce modes are controlled independently. The inputs to the vehicle  $z_{t1}$  and  $z_{t2}$  are summed to form a bounce input and a pitch input. These inputs are then fed to a pair of low pass filters, which represent the required dynamic performance of the system. The low frequency inputs generated by the filters are compared to the modal displacements to form modal error signals. These error signals are then used as force demand signals for the actuators with suitable phase and gain compensation.

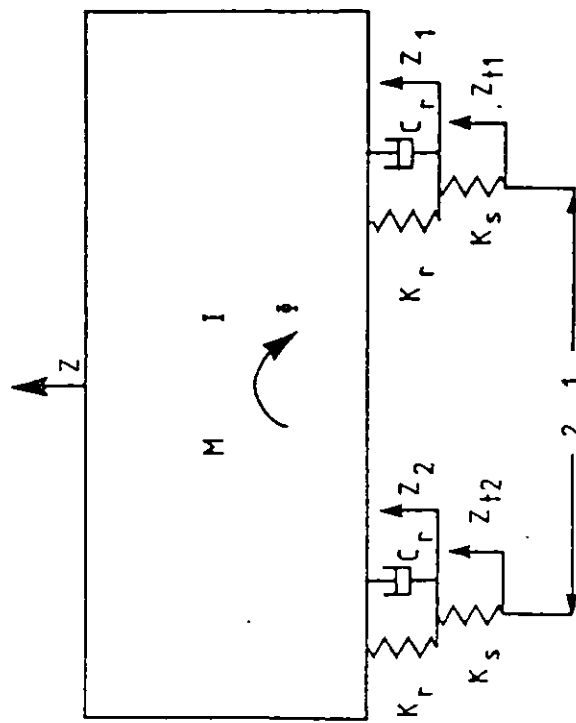


FIG.11.1 REDUCED MODEL OF VEHICLE

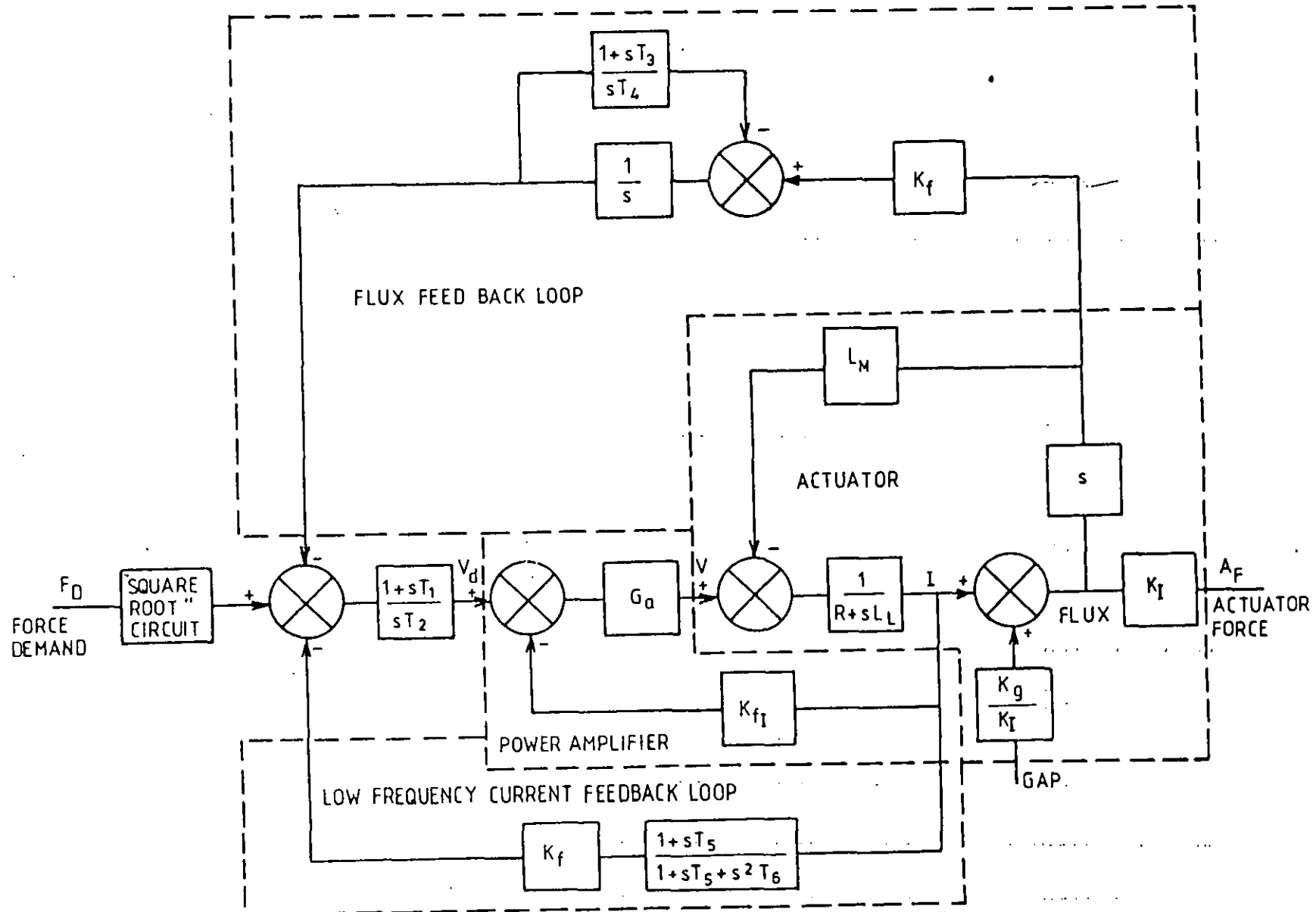


FIG.11.2ACTUATOR CONTROL.

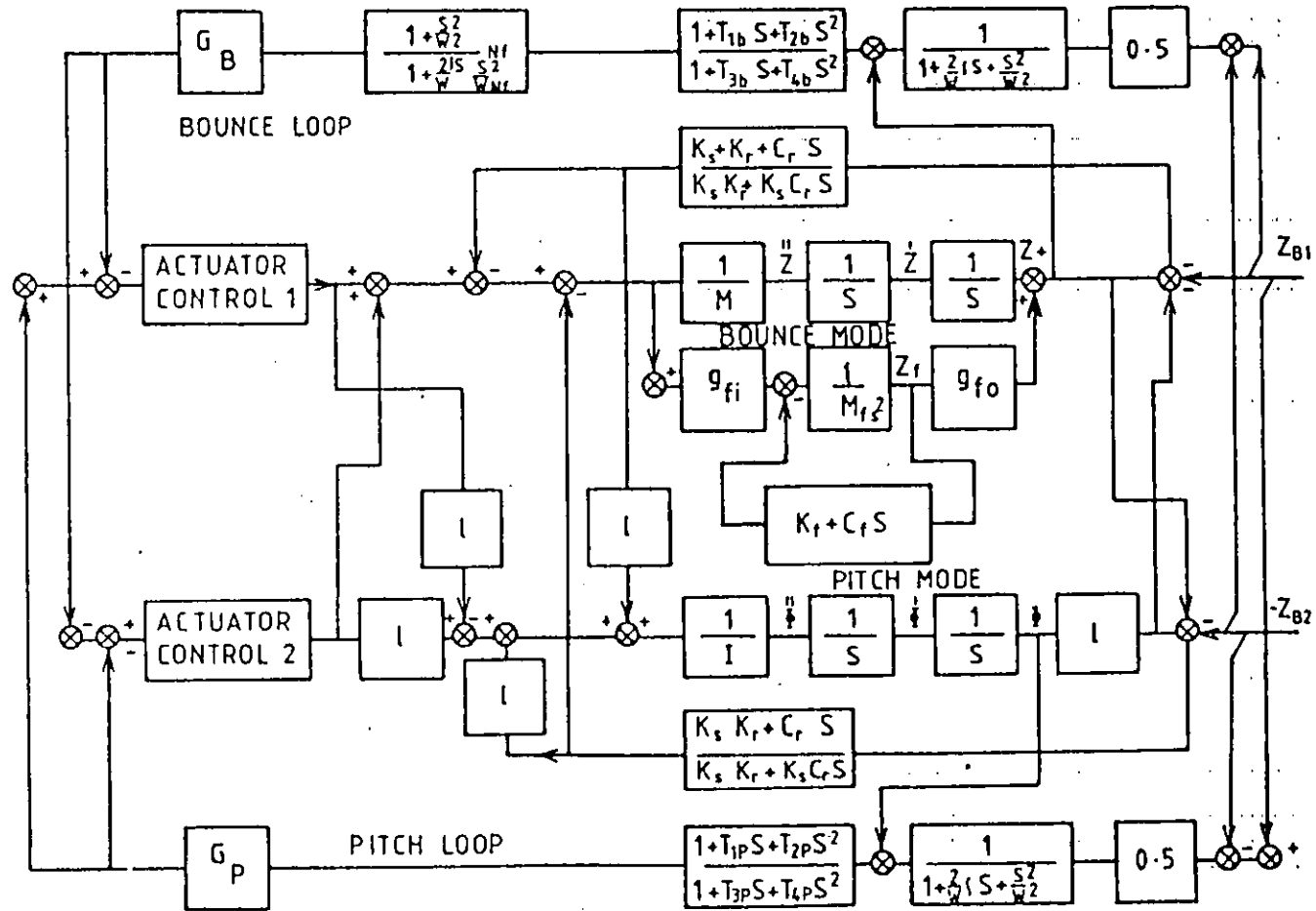


FIG.11.3 POSITION CONTROL BLOCK DIAGRAM

#### 11.2.4 Revised Equations

As the control system equations had to be extensively modified, at short notice, to suit the DFVLR program, they have been reformulated from first principles since returning. The revised equations are given in Appendix G. It should be noted that the loop gains are only 25% of those originally used in the DFVLR program.

Tables 11.1 and 11.2 give the eigenvalues and rms accelerations computed from this model. Passive accelerations were calculated by setting the force gain factor  $K_I=0$ .

It will be noted that the reduction in rms is less than that shown in Chapter 5. There are two reasons for this:

- 1) The absence of bogies, which provide significant filtering in the frequency range above 5 Hz.
- 2) The simplified track spectrum used has more high frequency content than that used in the main study.

#### 11.2.5 Specification of Performance Indices

It was anticipated initially that the design process would allow both for the stochastic track inputs which govern ride quality and for the deterministic track inputs corresponding to vertical gradients, etc, although the latter is normally of secondary importance for a vertical suspension.

A set of six criteria for the "mechanical" performance were generated - rms accelerations and suspension deflections at leading and trailing ends for stochastic inputs, and maximum suspension deflections for the deterministic input. The equations corresponding to these are listed below, although the deterministic input case was not in fact used.

$$G_1 = \sqrt{\int_0^{\infty} A_1^2(\omega) d\omega} ; a_1 = z + \phi$$

$$G_2 = \sqrt{\int_0^{\infty} A_2^2(\omega) d\omega} ; a_2 = z + \phi$$

$$G_3 = \sqrt{\int_0^{\infty} D_1^2(\omega) d\omega} ; d_1 = z + \phi - Z_{t1}$$

$$G_4 = \sqrt{\int_0^{\infty} D_2^2(\omega) d\omega} ; d_2 = z - \phi - Z_{t2}$$

$$G_5 = |d_1|_{\max}$$

$$G_6 = |d_2|_{\max}$$

Another four criteria were generated for rms variations in the major control inputs of magnet currents and voltages:-

$$G_7 = \sqrt{\int_0^{\infty} I_1^2(\omega) d\omega}$$

$$G_8 = \sqrt{\int_0^{\infty} I_2^2(\omega) d\omega}$$

$$G_9 = \sqrt{\int_0^{\infty} V_1^2(\omega) d\omega}$$

$$G_{10} = \sqrt{\int_0^{\infty} V_2^2(\omega) d\omega}$$

The remaining two criteria related to the system eigenvalues, the first to put a limit on their frequency, and the second to force a minimum level of damping:-

$$G_{11} = \text{Max} |I_m(\lambda)|$$

$$G_{12} = \text{Max} \left| \frac{\text{Re}(\lambda)}{I_m(\lambda)} \right|$$

### 11.3 Trials of the design technique

Three separate trials were carried out, starting with different set of initial control parameters. The first trial used initial values which corresponded to those from the classical control design as described in the previous section, but was terminated when it was realised that there was a programming error which was preventing the computer from altering one of the free control parameters. The loop gains used in this run were a factor of 4 higher than in the actual control system design. This in fact perpetuated a mistake which had been made in the initial design of the position control system.

The second trial started with a set of values in which the main loop gains were reduced by a factor of 4 in an attempt to bring the eigenvalues of these loops to more acceptable levels. It was during this trial that the way in which the technique works was really appreciated, but unfortunately the improvements given by the optimisation were very disappointing, especially since it was known that the set of initial values used for the first trial gave better performance for the acceleration levels (Criteria 1 and 2). Table 11.3 charts the results of the six optimisation runs carried out during this second trial. In the first run we tried to optimise the main loop stability by setting  $C(12) = G(12)$  in order to concentrate on the damping ratio. There was some improvement but the initial values were obviously good. In the second run the objective was to reduce acceleration levels (i.e. improve the ride quality), and so the ride parameters were concentrated upon. The effect was slight worsening in ride quality and an improvement in stability; hence a third run was carried out with  $C(12)$  increased so as to take the emphasis off stability. There were small improvements in ride, the computer apparently having traded this off against stability margins by increasing the main loop gains. A further attempt to continue this trade off in the fourth run was not particularly successful, and two subsequent optimisation runs had negligible effect. For some reason it did not seem possible



to force the computer to take advantage of permitted increases in the criteria governing the suspension deflection, voltage and current in order to obtain improved ride quality.

It was therefore decided to start again on a third trial, using initial values which were known to give a real improvement in ride quality compared with the passive case. The values of the performance criteria for this condition are given in Table 11.4. Contrasting these with  $G(4)$  in Table 11.3 shows that to achieve this improvement the voltage and current are approximately doubled, with some increase in the suspension deflection. The major difference is in the much reduced stability margins in the main loops as indicated by criterion 12. Another optimisation run was carried out to concentrate again on ride quality, to prevent further degradation of stability, and to permit further increases in suspension deflection, voltage and current. However, this produced no significant improvement.

#### 11.4 Conclusions

Lack of time prevented any further investigation of the problems. The "best" result produced was using values which had been derived by a classical control approach, but it seems most unlikely that this is truly the optimum, especially since the electromagnets were still operating below their maximum capability. It is more likely that something in the optimisation procedure, the formulation of the problem or the authors application of the technique was the inhibiting factor.

Despite the somewhat disappointing nature of the results, the overall concept of the design technique is impressive, and its potential warrants further consideration, in particular to identify why the optimisation was unable to move to a known condition giving better performance. A new model of the system with an improved structure has been prepared, and it is hoped

that this will enable further progress to be made towards resolving some of the unanswered questions arising from the first attempt to use the method.

The program has been refined since these tests and a new trial has been proposed, though not yet carried out. It would be very useful to try the train model with the program to see how it deals with the problem of interaction.

A similar technique is being developed by Lukel (Paderbon University)<sup>(72)</sup> based on optimal rather than classical control theory and a comparison of the two techniques is to be made in 1986. Developments in this area are eagerly awaited as they represent the way forward in control system design.

It is perhaps worth reflecting that, while it is possible to make a theoretical optimisation of a control system, the optimisation is only as good as the plant model and the problem of optimising a real control system is one in which much further effort is required.

TABLE 11.1MK III COACH ACTIVE SUSPENSION SMALL MODEL EIGENVALUES

<u>Damping</u>	<u>Frequency</u>	<u>Mode</u>
83%	11.8 Hz	Controllers in phase
39%	9.3 Hz	Bounce phase advance
100%	2.24 Hz	Bounce main loop
36%	2.26 Hz	Bounce main loop
83%	11.8 Hz	Controllers in anti-phase
39%	9.2 Hz	Pitch phase advance
100%	2.0 Hz	Pitch main loop
35%	2.6 Hz	Pitch main loop
70%	1.0 Hz	Bounce filter
70%	1.0 Hz	Pitch filter

TABLE 11.2RMS RESPONSES

<u>Active</u>	<u>Passive</u>	
6.1%g	10.0%g	Acceleration, leading end
3.0%g	3.5%g	Acceleration, centre
5.6%g	10.0%g	Acceleration, trailing end
5.7 mm	7.5 mm	Suspension displacement, 1 end
5.6 mm	7.7 mm	Suspension displacement, 2 end
14.0 amps		Current, leading end
60.0 volts		Volts, leading end
14.0 amps		Current, trailing end
58.0 volts		Volts, trailing end
431.0 watts		Power, leading end
436.0 watts		Power, trailing end

TABLE 11.3

## RESULTS OF SECOND TRIAL

	RUN 0	RUN 1		RUN 2		RUN 3		RUN 4		RUN 5		RUN 6		UNITS
	<u>G</u> (0)	<u>C</u> (0)	<u>G</u> (1)	<u>C</u> (1)	<u>G</u> (2)	<u>C</u> (2)	<u>G</u> (3)	<u>C</u> (3)	<u>G</u> (4)	<u>C</u> (4)	<u>G</u> (5)	<u>C</u> (5)	<u>G</u> (6)	
1	7.8	8	7.9	7.9	8.1	8.1	7.8	7.78	7.7	7.73				% 'g'
2	6.8	8	6.9	6.9	7.1	7.1	7.0	7.0	7.04	7.05				% 'g'
3	5.6	10	5.7	10	5.6	10 <sup>+</sup>	5.7	10 <sup>+</sup>	5.7	10 <sup>+</sup>				mm
4	4.3	10	4.3	10	4.1	10 <sup>+</sup>	4.4	10 <sup>+</sup>	4.5	10 <sup>+</sup>				mm
5	-	-	-	-	-	-	-	-	-	-				-
6	-	-	-	-	-	-	-	-	-	-				-
7	11	20	10.7	20 <sup>+</sup>	10.3	20 <sup>+</sup>	11.2	20 <sup>+</sup>	11.4	20 <sup>+</sup>				V
8	7.6	20	7.5	20 <sup>+</sup>	7.2	20 <sup>+</sup>	7.9	20 <sup>+</sup>	8.2	20 <sup>+</sup>				V
9	3.2	4	3.1	4	2.9	4 <sup>+</sup>	3.2	4 <sup>+</sup>	3.3	4 <sup>+</sup>				A
10	2.3	4	2.2	4	2.1	4 <sup>+</sup>	2.4	4 <sup>+</sup>	2.5	4 <sup>+</sup>				A
11	55.3	80	55.7	80	55.4	80 <sup>+</sup>	55.7	80 <sup>+</sup>	55.6	80 <sup>+</sup>				rad/s
12	3.5	3.52	3.4	3.52	3.3	4 <sup>+</sup>	3.8	4.5 <sup>+</sup>	3.9	4.5 <sup>+</sup>				-
$3\omega_D^2$	3169	*	3023		3023							*		*
$3\omega_P^2$	3169	*	3249		3249							*		*
$G^1$	$.5 \times 10^6$	*	$4.8 \times 10^5$	*	$4.4 \times 10^5$	*	$5.8 \times 10^5$	*	$6.4 \times 10^5$			*		*
$G^1_{P}$	$.5 \times 10^6$	*	$4.7 \times 10^5$	*	$4.3 \times 10^5$	*	$4.8 \times 10^5$	*	$4.7 \times 10^5$			*		*
$\omega^2$	40									*		*		*
$\omega^2$	40									*		*		*

\* Permitted to change

+ Slope X10

TABLE 11.4

RESULTS OF THIRD TRIAL

<u>Performance Criteria</u>	<u>Values</u>
1	5.7%'g'
2	5.7%'g'
3	6.4 mm
4	4.2 mm
5	-
6	-
7	19.7 V
8	16.2 V
9	7.9 A
10	7.3 A
11	64 rad/s
12	23

<u>Constants</u>	<u>Values</u>
$3 \omega_b^2$	3169
$3 \omega_p^2$	3169
$G_b^1$	$2 \times 10^6$
$G_p^1$	$2 \times 10^6$
$\omega_1^2$	40
$\omega_2^2$	40

CHAPTER 12CONCLUSIONS AND FUTURE WORK12.1 Conclusions

Throughout the thesis reference has been made to classical and optimal control systems. It is perhaps interesting to reflect that, in the limit, given a perfect actuator and infinite control action optimal control theory produces a suspension which is a simple spring with a sky hook damper (18). The system will have 70% critical damping and the transfer function of a two pole Butterworth filter. This is the ideal which has in fact been aimed for with both the Sky Hook dampers and the Position Control Systems.

The aim of the thesis however has been to find the best control system for a practical active suspension operating under realistic operating constraints. In this respect optimal control theory quickly provided a regulator which exceeded the performance of the two classical control systems. However the classical control systems were designed and analysed before the optimal regulator, making selection of the weighting function used to design the optimal control system considerably easier than it would have been if it had to be designed from scratch. It is also worth reflecting that the classical control systems themselves were the product of considerable prior experience.

It was in the realms of practical implementation that the strengths of the classical control systems really showed. This was because they were designed with implementation in mind, in particular which variables can be measured most easily and then how they can be manipulated to best effect. Optimal control theory on the other hand makes the assumption that all the states of the system are available for feedback. With any but the simplest system however this is clearly an impossibility and it is either necessary to compromise the design with the instrumentation that is available, or recreate unmeasured states with the aid of an observer.

While it is possible to achieve the theoretical regulator performance with an observer, the observer is only as good as the system model used to design it. Here it was found that to represent the full active suspension required an observer of an impractical size and considerable compromise had to be accepted to find a realisable observer. One of the compromises was a reduction in the notional signal to noise ratio used to design the observer as it was impossible to accommodate any of the structural modes which the active suspension is prone to excite. In the end a successful compromise was achieved with the modal observers, though once again it must be stressed that the design drew heavily on classical design experience. When digital controllers are considered not only does increasing complexity give rise to control algorithms which are difficult to debug but there is a definite limit to the size of algorithm which can be implemented within one sample period if multiple processors are to be avoided.

So far experimental data has run contrary to theoretical prediction, as the simplest control system (the sky hook damper) produced the biggest improvements in performance. This is because it is more immune to imperfections in the model used to describe the vehicle, and train, than the more sophisticated control systems. It was also much simpler to make intuitive modifications to the control system in the field to overcome short comings. Given further development time it is felt that the performance of the modal observers can be improved to equal, or better, that of the sky hook damper. However a considerable amount of experience will be required with the optimal control theory to obtain the best results. The technique described in Chapter 11 may also be capable of producing improvements, but whether these can be realised in practice remains to be seen. In control system design and analysis predictions are only as good as the theoretical model and it is often impossible to realise theoretical improvements in practice.

The success of any control system design technique must be measured by how well the theory translates to a practical control system. In the case considered in this thesis the classical control systems translate quite well because implementation is implicit from the start. On the other hand a liberal attitude had to be taken to optimal control theory to achieve a practical controller and the best controller ultimately is likely to contain a combination of both classical and optimal control theory.

## 12.2 Future Work

With the present system further development work is required to see if it is possible to achieve any more improvements in performance with the modal observers. Development of a digital control system is also an essential requirement as it should be possible to produce a more reliable controller which is capable of diagnosing its own faults. However the prime requirement of the experiment on the service railway vehicle is to gain operating experience; since access to the vehicle is strictly limited both these developments have been delayed.

Probably a more important development is to extend the present line of investigation to lateral suspensions, since the lateral ride of railway vehicles degenerates more quickly with speed than the vertical ride. Development of a digital controller is also very important in this context as lateral dynamic performance varies with speed, wheel rail geometry and surface conditions in the contact patch between the wheel and rail. With the range of variations possible some form of adaptive or self tuning control system should be capable of paying dividends.

## 12.3 Acknowledgements

I would like to thank British Rail for permission to publish this thesis and those colleagues who helped with the experimental work.



I would also like to thank my academic supervisor Roger Goodall for his help and guidance. Last but not least I would like to thank my wife and family for their moral support.

REFERENCES

- 1) Karnopp D.C., "Are Active Suspensions Really Necessary?" ASME Publication, 78-WA/DE-12, 1978.
- 2) Goodall R.M. Williams R.A., "Dynamic Criteria in Maglev Suspension Design" I Mech E Conference C393/84 1984.
- 3) Boocock D., Newman M., "The Advanced Passenger Train" paper presented to Railway Division I Mech E 1976.
- 4) Marshall J.J., Halfpenny D. "Tilt Technology" paper presented to Railway Division of I Mech E 1977.
- 5) Harborough P.R. "Passenger Comfort During High Speed Curving". AAR/BR Conference 1984.
- 6) Pennington K.W., Pollard M.G., "The Development of An Electro-Mechanical Tilt System for Advanced Passenger Train" 28Mech E Conference C299/83 1983.
- 7) Pollard M.G., Williams R.A., "The Dynamic Behaviour of a Low-Speed Electro-Magnet Suspension" the Dynamics of Vehicles on Roads and on Railway Tracks. Swets and Zeitlinger B.V. Amsterdam 1975.
- 8) Goodall R.M., "Suspension and Guidance Control System for DC Attraction Maglev Vehicle". IEE Conference Publication No. 142 1976.
- 9) Linder D., "Design and Testing of a Low Speed Magnetically Levitated Vehicle". IEE Conference Publication No. 142, 1976.
- 10) Goodall R.M., Williams R.A., Barwick R.W., "Ride Quality Specification and Suspension Controller Design for a Magnetically Suspended Vehicle" Institute of Measurement and Control Synop. 1978.

- 11) Williams R.A., Spooner E "Maglev Now and the Future" Conference Report, Railway Engineer 1984.
- 12) Goodall R.M., Williams R.A., Lawton A., "Practical Applications of Actively Controlled Suspension to Railway Vehicles. "ASME Winter Conference 1979.
- 13) Harborough P., "An Actively Controlled Lateral Suspension for Railway Vehicles." British Railways Board, R & D Division MR DOS1 1981.
- 14) Goodall R.M., Williams R.A., Lawton A., Harborough P., "Railway Vehicle Active Suspensions in Theory and Practice". The Dynamics of Vehicles on Roads and on Railway Tracks. Swets and Zeitlinger B.V. Lisse 1981.
- 15) Williams R.A. "Railway Vehicle Suspensions enter the Electronic Age" IEE Conference Publication 203 1981.
- 16) Hedrick J.R., Wormley D.N., "Active Suspensions for Ground Transport Vehicles - A State of the Art Review". Mechanics of Transport Suspension Systems, ed B. Paul et al ASME AMD - Vol 15 1975.
- 17) Hedrick J.R., "Railway Vehicle Active Suspensions" Vehicle Systems Dynamics Vol 10. No. 4-5 1981.
- 18) Goodall R.M., Kortum W., "Active Controls in Ground Transportation - A Review of the State of the Art and Future Potential". Vehicle System Dynamics Vol 12 No. 4-5 1983.
- 19) Nishio A., Nishimwa S., Kikuchi I., Shirane Y., Yamada J., "High Speed Tilting Vehicles Controlled by Airsprings". Sumitomo Metals Research. Vol 20 No. 1 1972.
- 20) Kayserling U., " Power Bogies of the DB 200 km/h ET405. Incorporating Body Tilt Through the Secondary Air Suspension". Rail Eng Int Vol 4 No. 9, 1974.

- 21) Toran A., "A Practical Application of the Principle of Natural Pendulation to the Talgo System". Paper given at Railway Dynamics Synopsium. Asociacion de Investigacion del Transporte 1977.
- 22) Gonzales J., "Passengers will Sample Tilting Train in Spring". Rail Gaz Int Vol 133 No. 2 1977.
- 23) Nilstam N., "Swedish Body Tilting Electric Set for Very High Speed on Severely - Curved Main Lines". Rail Engineering International Vol 11 No. 2 1982.
- 24) Jindai et al. "Fundamental Study on Semi-Actively Controlled Pneumatic Servo Suspension for Rail Cars". ASME Publication, 81-RT-6, 1981.
- 25) Sarma G.N., Kozin F., "An Active Suspension System Design for the Lateral Dynamics of a High Speed Wheel - Rail System" ASME Vol 93 No. 4 1971.
- 26) Sinha P.K., Wormley D.N., Hedrick J.K., "Rail Passenger Vehicle Lateral Dynamic Performance Improvement Through Active Control" ASME Publications 78-WA/DSC-14 1978.
- 27) Celniker G., Hedrick J.K., "Rail Vehicle Active Suspensions for Lateral Ride Quality and Stability Improvement". ASME Vol 104 No. 1, 1982.
- 28) Caudill R.J., Sweet L.M., Oda K., "Magnetic Guidance of Conventional Railroad Vehicles." ASME Vol 104 No. 3, 1982.
- 29) Hauschild W., "Design of a Limit Cycle Controller for the Non linear Wheel Rail System". Vehicle System Dynamics Vol 10 No. 2-3, 1981.
- 30) Jaschinski A., Duffek W., "Evaluation of Bogie Models with respect to Dynamic Curving Performance of Rail Vehicles" Vehicle System Dynamics Vol 12 No. 6 1983.

- 31) Gottzein E., Rogg D., "Status of High Speed Maglev Train Development in FRG" Institution of Mechanical Engineer C407/84 1984.
- 32) Nakamura S., "Development of High Speed Surface Transport (HSST)", IEEE Transactions on Magnetics, Vol MAG-15, No. 6, 1979.
- 33) Masada E., Kitamoto M., Kawashuma M., "Present Status of Maglev Development in Japan and HSST-03 Project". I.Mech.E. Conference C412/84 1984.
- 34) Jayawant B.V., "Dynamical Aspects of Passenger Carrying Vehicles Using Controlled DC Electro-Magnetics" Dynamics of vehicles of Road and Tracks . Swets & Zeitlinger 1978.
- 35) Heidelberg G., Neimitz K., Weinberger H., "The M-Bahn System" I.Mech.E. Conference C413/84 1984.
- 36) Boldea I., et al "Magnibus - The Romanian Linear Inductor (Synchronous) Motor (Passive Guideway) Maglev" I.Mech.E. Conference C401/84 1984.
- 37) Hullender D.A., Wormley D.N., Richardson H.H., "Active Control of Vehicle Air Cushion Suspensions". ASME JDSM & C Vol 93 No. 1 1972.
- 38) Ooi B.T., Banakar M.H., "Passive and Active Damper Winding for the Repulsive Magnetic Levitation System". IEEE Trans on Magnetics, Vol MAG-13 No. 5 1977.
- 39) Baker A., "Anti-Roll Vehicle Suspension with Hydraulic Powered Actuation". Hydraulic/Pneumatic/Mechanical Power Vol 24 No. 281 1978.
- 40) Bell J., "An Active Tilt to a Concept Car" New Scientist 25 Oct 84.

- 41) MacLanin B., "Progress in British Tracked Vehicle Suspension Systems" SAE Paper 830442, 1983.
- 42) Darenbery W., Panik F., Weidenam W., "Automated Guidance Systems for Buses and Trucks" Proc. 1st Int Conf. Automated Guided Vehicles Systems, Stratford-on-Avon 1981.
- 43) Gottzein E., Crämer W., Ossenbergr F., Roche C., "Optimal Control of a Maglev Vehicle". The Dynamics of Vehicles on Roads and Railway Tracks. Swets and Zeitlinger B.V., Amsterdam August 1975.
- 44) Thompson A.G., "Optimal and Suboptimal Linear Active Suspensions for Road Vehicles". Vehicle System Dynamics No. 13 Swets and Zeitlinger 1984.
- 45) Kwakernaak H., and Sivan R., "Linear Optimal Control Theory" Wiley Interscience 1972.
- 46) N.A.G. Subroutine Library, Numerical Algorithm Group, Oxford.
- 47) Pollard M.G. "A Standard Track Roughness Spectral Density" British Rail R & D Division DT2 1969
- 48) "Guide for the Evaluation of Human Exposure to Whole - Body Vibration" International Standards Organisation 1974.
- 49) Pollard M.G., Simons N.J.A., "Passenger Comfort - The Role of Active Suspensions" Railway Engineer, I.Mech.E. Issue 1 1984
- 50) Noton A.R.M. "Variational Methods in Control Engineering" Pergamon 1965.
- 51) MacFarlane A.G.J. "An Eigenvector Solution of the Optimal Linear Regulator Problem" 1964. J Electronics and Control Vol 14 No. 6 1964.
- 52) Potter J.E. "Matrix Quadratic Solutions" Siam J. Appl. Math Vol 14 1966.

- 53) Laub A.J. "A Schur Method of Solving Algebraic Riccati Equations" IEEE Trans Auto Control Vol AC - 24 No. 6 1979.
- 54) Kalman R.E. and Bucy R.S. "New Results in Linear Filtering and Prediction Theory" ASME J of Basic Eng. Sec D. Vol 83 1961.
- 55) Hedrick J.K., Billington G.F., Dreesbach D.A., "Analysis, Design, and Optimisation of High Speed Vehicle Suspensions using State Variable Techniques" ASME JDS M & C, June 1974.
- 56) Hedrick J.K. and Firouztash H, "The Covariance Propagation Equation Including Time-Delayed Inputs" IEEE Trans Auto Control AC-19 No. 5 October 1974.
- 57) Williams R.A., "Electrical Specification for Experimental Active Vertical Suspension on a Mk. III Coach" British Rail R & D Div. IMDOS 144 1984.
- 58) Williams R.A., "Electromagnetic Actuators for Active Suspensions" British Rail R & D Division IMDOS 67 1980.
- 59) Gore P., "The Theory, Design and Testing of an Electromagnetic System for a Vertical Secondary Suspension" British Rail R & D Division TMDOS 86 1981.
- 60) Williams R.A., "An Electromagnetic Active Suspension in Theory and Practice" British Rail R & D Division IMDOS 142 1984.
- 61) Hedrick J.K., Cooperider N.K., Law E.H., "The Application of Quasi-Linearisation to Rail Vehicle Analysis", U.S. Dept, Transport No. FRA/ORD-78-56.
- 62) "General Specification for Electronic Equipment" BRB/RIA Technical Callaboration Committee Specification No. 13: 1976.
- 63) Fisher D.E., "A Novel Non-Contacting Gap Transducer" British Rail R & D Division, TM CONS 1, 1980.

- 64) Fisher D.E., "Circuit Description and Setting Up Procedure of Capacitive Gap Transducer for the Maglev Vehicle", British Rail R & D Division, IM CON 57.
- 65) Pearce T.G., "Comments on a Comparison Between the Ride in Prototype and Production, Mk III Coaches". Unpublished Memorandum 1975.
- 66) Kosieradzki W. "The Influence of Damping Produced by Gangway Connections on the Vertical Oscillations of Coupled Vehicles", British Rail R & D Division IMDA 233, 1975.
- 67) Kuo B.C. "Digital Control Systems" Holt, Rinehart and Wiston 1980.
- 68) Katz P. "Digital Control Using Microprocessors" Prentice Hall International 1981.
- 69) Golden R.M., Kaiser J.F. "Design of Wideband Sampled - Data Filters". The Bell System Technical Journal, July 1964.
- 70) Goodall R.M., "Calculation of the Frequency Responses of Complex Systems Directly From the Physical Parameters" Trans Inst M.C V812 No 3 July-Sept 1981.
- 71) Grubel G., Kreisselmier G., "Systematic Computer Aided Design" from lecture Series 128, Advisory Group for Aerospace Research and Development 1983.
- 72) Luckel J., Kasper R., Jaker G.P., "Application of a New Design Method for Linear Multivariable Controllers to the Active Suspension of Road Vehicles" C.C.G. - Lehrgang V1.12, Munich 1985.



APPENDIX AState Equation Pitch and Bounce Model Section 2.5.3

$$1) \ddot{z} = - \frac{2C}{M} \dot{z} - \frac{2Kz}{M} + \frac{Kz}{M} t_1 + \frac{Kz}{M} t_2$$

$$2) \ddot{\phi} = - \frac{2}{I} \frac{1}{I} C \dot{\phi} - \frac{2}{I} \frac{1}{I} K \phi - \frac{Kl z}{I} t_1 + \frac{Kl z}{I} t_2$$

M	=	16 000	kg
I	=	533 000	kg m <sup>2</sup>
C	=	50	KNs/m
K	=	.300	MN/m
l	=	8	m

## APPENDIX B

MK III COACHSTATE EQUATIONS

$$1) \ddot{Z} = -\frac{2}{M} (K_a + K_s - K_g)Z + \frac{1}{M}(K_a - k_g)Z_{B1} + \frac{1}{M}(K_a - k_g)Z_{B2}$$

$$\frac{K_s Z_1}{M} + \frac{K_s Z_2}{M} + \frac{2g_f(K_a + K_s - K_g)Z_f}{M}$$

$$2) \ddot{\Phi} = -\frac{2I^2}{I} (K_a + K_s - K_g)\Phi - \frac{1}{I}(K_a - K_g)Z_{B1} + \frac{1}{I}(K_a - K_g)Z_{B2}$$

$$-\frac{1K_s Z_1}{I} + \frac{1K_s Z_2}{I}$$

$$3) \ddot{Z}_{B1} = \frac{1}{M_B} (K_a + K_s - K_g)Z - \frac{1}{M_B} (K_a + K_s - K_g)\Phi$$

$$-\frac{1}{M_B} \frac{(2K_d(1_3)(1_1 + 1_3) + 2K_p(1_1 + 1_2)^2 + K_a - k_g)Z_{B1} - K_d(1_1 + 1_3)Z_{P1}}{1_1}$$

$$-\frac{K_d(1_1 + 1_3)Z_{P2} - K_s Z_1}{M_B 1_1} - \frac{g_f(K_a + K_s - K_g)Z_f}{M_B}$$

$$+ \frac{1}{M_B} \frac{(K_d(1_1 + 1_3)^2 + K_p(1_1 + 1_2)^2) Z_{t1} + \frac{1}{M_B} (K_d(1_1 + 1_3)^2 + K_p(1_1 + 1_2)^2) Z_{t2}}{1_1}$$

$$4) \ddot{\Phi}_{B1} = -\frac{2}{I_B} \frac{(K_d(1_3)(a-1_1)a(1_3 + 1_1) + K_p(a + 1_2 + (a-1_1)(1_1 + 1_2)))\Phi_{B1}}{1_1}$$

$$+ \frac{K_d(a)(1_3 + 1_1)Z_{P1} - K_d(a)(1_3 + 1_1)Z_{P2}}{I_B 1_1}$$

$$-\frac{1}{I_B} \frac{(K_p(1_1 + 1_2)(a + 1_2 + (a - 1_1)(1_1 + 1_2)) + K_d a(1_1 + 1_3)^2)Z_{t1}}{1_1}$$

$$+ \frac{1}{I_B} \frac{(K_p(1_1 + 1_2)(a + 1_2 + (a - 1_1)(1_1 + 1_2)) + K_d a(1_1 + 1_3)^2)Z_{t2}}{1_1}$$

$$5) \ddot{Z}_{B2} = \frac{1}{M_B} (K_a + K_s - K_g)Z + \frac{1}{M_B} (K_a + K_s - K_g)\Phi$$

$$-\frac{1}{M_B} \frac{(2K_d(1_3)(1_1 + 1_3) + 2K_p(1_1 + 1_2)^2 + K_a - K_g)Z_{B2} - K_d(1_1 + 1_3)Z_{P3}}{1_1}$$

$$\begin{aligned} & -\frac{K_d}{M_B} \frac{(l_1 + l_3)Z_{p4}}{l_1} - \frac{K_s}{M_B} Z_2 - \frac{g_f(K_a + K_b - K_g)Z_f}{M_B} \\ & + \frac{1}{M_B} (K_d \frac{(l_1 + l_3)^2}{l_1} + K_p \frac{(l_1 + l_2)^2}{l_1}) Z_{t3} + \frac{(K_d \frac{(l_1 + l_3)^2}{l_1} + K_p \frac{(l_1 + l_2)^2}{l_1}) Z_{t4}}{l_1} \end{aligned}$$

$$\begin{aligned} 6) \quad \ddot{\Phi}_{B2} &= -\frac{2}{I_2} (K_d \frac{(l_3)}{l_1} (a - l_1) a \frac{(l_3 + l_1)}{l_1}) + K_p (a + l_2 + (a - l_1) \frac{(l_1 + l_2)^2}{l_1}) \Phi_{B2} \\ & + \frac{K_d}{I_B} \frac{(a)}{l_1} (l_3 + l_1) Z_{p3} - \frac{K_d}{I_B} \frac{(a)}{l_1} (l_3 + l_1) Z_{p4} \\ & - \frac{1}{I_B} (K_p \frac{(l_1 + l_2)}{l_1} (a + l_2 + (a - l_1) \frac{(l_1 + l_2)}{l_1}) + K_d a \frac{(l_1 + l_3)^2}{l_1}) Z_{t3} \\ & + \frac{1}{I_B} (K_p \frac{(l_1 + l_2)}{l_1} (a + l_2 + (a - l_1) \frac{(l_1 + l_2)}{l_1}) + K_d a \frac{(l_1 + l_3)^2}{l_1}) Z_{t4} \end{aligned}$$

$$\begin{aligned} 7) \quad \dot{Z}_{p1} &= \dot{Z}_{B1} - \frac{K_d}{C_p} \frac{(l_3)Z_{B1}}{l_1} - (a + l_3) \dot{\Phi}_{B1} + \frac{K_d(l_3)(a - l_1)\Phi_{B1}}{C_p l_1} \\ & - \frac{K_d}{C_p} Z_{p1} + \frac{K_d}{C_p} \frac{(l_1 + l_3)Z_{t1}}{l_1} \end{aligned}$$

$$\begin{aligned} 8) \quad \dot{Z}_{p2} &= Z_{B1} - \frac{K_d}{C_p} \frac{(l_3)Z_{B1}}{l_1} + (a + l_3) \dot{\Phi}_{B1} - \frac{K_d}{C_p} \frac{(l_3)(a - l_1)\Phi_{B1}}{G} \\ & - \frac{K_d}{C_p} Z_{p2} + \frac{K_d}{C_p} \frac{(l_1 + l_3)Z_{t2}}{l_1} \end{aligned}$$

$$\begin{aligned} 9) \quad \dot{Z}_{p3} &= Z_{B2} - \frac{K_d}{C_p} \frac{(l_3)Z_{B2}}{l_1} - (a + l_3) \dot{\Phi}_{B2} + \frac{K_d}{C_p} \frac{(l_3)(a - l_1)\Phi_{B2}}{G} \\ & - \frac{K_d}{C_p} Z_{p3} + \frac{K_d}{C_p} \frac{(l_1 + l_3)Z_{t3}}{l_1} \end{aligned}$$

$$\begin{aligned} 10) \quad \dot{Z}_{p4} &= Z_{B2} - \frac{K_d}{C_p} \frac{(l_3)Z_{B2}}{l_1} + (a + l_3) \dot{\Phi}_{B2} - \frac{K_d}{C_p} \frac{(l_3)(a - l_1)\Phi_{B2}}{l_1} \\ & - \frac{K_d}{C_p} Z_{p4} + \frac{K_d}{C_p} \frac{(l_1 + l_3)Z_{t4}}{l_1} \end{aligned}$$

$$11) \quad \dot{z}_1 = \frac{K_s Z}{C_s} - \frac{K_s \Phi}{C_s} + \dot{z}_{B1} + \frac{K_r}{C_s} z_{B1} - \frac{1}{C_s} (K_r + K_s) z_1 - g_f \frac{K_s}{C_s} z_f$$

$$12) \quad \dot{z}_2 = \frac{K_s Z}{C_s} + \frac{K_s \Phi}{C_s} + \dot{z}_{B2} + \frac{K_r}{C_s} z_{B2} - \frac{1}{C_s} (K_r + K_s) z_2 - g_f \frac{K_s}{C_s} z_f$$

$$13) \quad \ddot{z}_f = -\frac{2g_f}{M_f} (K_a + K_s - K_I K_g) z - \frac{g_f}{M_f} (K_a - K_I K_g) z_{B1}$$

$$- \frac{g_f}{M_f} (K_a - K_I K_g) z_{B2} - g_f \frac{K_s}{M_f} z_1 - \frac{g_f K_s}{M_f} z_2 - \frac{g_f K_I I_1}{M_f} - \frac{g_f K_I I_2}{M_f}$$

$$- \frac{C_f}{M_f} \dot{z}_f - \frac{g_f^2}{M_f} (K_f + 2(K_a + K_s - K_I K_g)) z_f$$

TABLE B1 PASSIVE SUSPENSION VEHICLE PARAMETERS

		Laden	Tare
Body Mass	M	26 000 kg	21 400 kg
Bogie Mass	$M_B$	2 707 kg	2 707 kg
Body Pitch Inertia	I	927 500 kgm <sup>2</sup>	803 300 kgm <sup>2</sup>
Bogie Pitch Inertia	$I_B$	1 970 kgm <sup>2</sup>	1 970 kgm <sup>2</sup>
Secondary spring stiffness/bogie	$K_s$	1.160 MN/m	.980 MN/m
Reservoir Stiffness/Bogie	$K_r$	.488 MN/m	.412 MN/m
Area Stiffness/Bogie	$K_a$	.420 MN/m	.340 MN/m
Secondary Damping/Bogie	$C_r$	50 kNs/m	42 kNs/m
Primary Stiffness/Axle	$K_p$	.360 MN/m	.360 MN/m
Primary Damping/Axle	$C_p$	8.4 kNs/m	8.4 kNs/m
Primary Damper End Stiffness	$K_c$	5.0 MN/m	5.0 MN/m
Bogie Centre Spacing	2l	16 m	
Bogie Wheel Base	2 a	2.6 m	
Swinging Arm Geometry )	$l_1$	.535 m	
)	$l_2$	.265 m	
)	$l_3$	.505 m	
)			
)			

## APPENDIX C

## MK III COACH ACTIVE SUSPENSION

## STATE EQUATIONS

$$1) \ddot{Z} = -\frac{2}{M} (K_a + K_s - K_g)Z + \frac{1}{M}(K_a - k_g)Z_{B1} + \frac{1}{M}(K_a - k_g)Z_{B2}$$

$$\frac{K_s Z_1}{M} + \frac{K_s Z_2}{M} + \frac{K_I I_1}{M} + \frac{K_I I_2}{M} + \frac{2g_f (K_a + K_s - K_g)Z_f}{M}$$

$$2) \ddot{\Phi} = -\frac{2l^2}{I} (K_a + K_s - K_g)\Phi - \frac{1}{I}(K_a - K_g)Z_{B1} + \frac{1}{I}(K_a - K_g)Z_{B2}$$

$$-\frac{1K_s Z_1}{I} + \frac{1K_s Z_2}{I} - \frac{K_I I_1}{I} + \frac{K_I I_2}{I}$$

$$3) \ddot{Z}_{B1} = \frac{1}{M_B} (K_a + K_s - K_g)Z - \frac{1}{M_B} (K_a + K_s - K_g)\Phi$$

$$- \frac{1}{M_B} (2K_d \frac{(l_3)(l_1 + l_3)}{l_1} + 2K_p \frac{(l_1 + l_2)^2}{l_1} + (K_a - k_g)Z_{B1} - \frac{K_d(l_1 + l_3)Z_{p1}}{M_B l_1}$$

$$- \frac{K_d(l_1 + l_3)Z_{p2}}{M_B l_1} - \frac{K_s Z_1}{M_B} - \frac{K_I I_1}{M_B} - \frac{g_f (K_a + K_s - K_g)Z_f}{M_B}$$

$$+ \frac{1}{M_B} (K_d \frac{(l_1 + l_3)^2}{l_1} + K_p \frac{(l_1 + l_2)^2}{l_1}) Z_{t1} + \frac{1}{M_B} (K_d \frac{(l_1 + l_3)^2}{l_1} + K_p \frac{(l_1 + l_2)^2}{l_1}) Z_{t2}$$

$$4) \ddot{\Phi}_{B1} = -\frac{2}{I_B} (K_d \frac{(l_3)(a-1_1)a(l_3 + l_1)}{l_1} + K_p (a + l_2 + (a-1_1) \frac{(l_1 + l_2)}{l_1})) \Phi_{B1}$$

$$+ \frac{K_d (a)(l_3 + l_1)Z_{p1}}{I_B l_1} - \frac{K_d (a)(l_3 + l_1)Z_{p2}}{I_B l_1}$$

$$- \frac{1}{I_B} (K_p \frac{(l_1 + l_2)(a + l_2 + (a-1_1) \frac{(l_1 + l_2)}{l_1})}{l_1} + K_d a \frac{(l_1 + l_3)^2}{l_1}) Z_{t1}$$

$$+ \frac{1}{I_B} (K_p \frac{(l_1 + l_2)(a + l_2 + (a-1_1) \frac{(l_1 + l_2)}{l_1})}{l_1} + K_d a \frac{(l_1 + l_3)^2}{l_1}) Z_{t2}$$

$$5) \ddot{Z}_{B2} = \frac{1}{M_B} (K_a + K_s - K_g)Z + \frac{1}{M_B} (K_a + K_s - K_g)\Phi$$

$$- \frac{1}{M_B} (2K_d \frac{(l_3)(l_1 + l_3)}{l_1} + 2K_p \frac{(l_1 + l_2)^2}{l_1} + K_a - K_g)Z_{B2} - \frac{K_d(l_1 + l_3)Z_{p3}}{M_B l_1}$$

$$\begin{aligned} & -\frac{K_d}{M_B} \frac{(l_1 + l_3)Z_{p4}}{l_1} - \frac{K_B}{M_B} Z_2 - \frac{K_I}{M_B} I_2 - \frac{g_f(K_a + K_B - K_g)Z_f}{M_B} \\ & + \frac{1}{M_B} \left( K_d \frac{(l_1 + l_3)^2}{l_1} + K_p \frac{(l_1 + l_2)^2}{l_1} \right) Z_{t3} + \left( K_d \frac{(l_1 + l_3)^2}{l_1} + K_p \frac{(l_1 + l_2)^2}{l_1} \right) Z_{t4} \end{aligned}$$

$$\begin{aligned} 6) \quad \ddot{\Phi}_{B2} &= -\frac{2}{I_2} \left( K_d \frac{(l_3)(a-l_1)a(l_3+l_1)}{l_1} + K_p (a+2 + (a-l_1) \frac{(l_1+l_2)^2}{l_1}) \right) \Phi_{B2} \\ & + \frac{K_d}{I_B} \frac{(a)}{l_1} (l_3+l_1) Z_{p3} - \frac{K_d}{I_B} \frac{(a)}{l_1} (l_3+l_1) Z_{p4} \\ & - \frac{1}{I_B} \left( K_p \frac{(l_1+l_2)}{l_1} (a+l_2 + (a-l_1) \frac{(l_1+l_2)}{l_1}) + K_d a \frac{(l_1+l_3)^2}{l_1} \right) Z_{t3} \\ & + \frac{1}{I_B} \left( K_p \frac{(l_1+l_2)}{l_1} (a+l_2 + (a-l_1) \frac{(l_1+l_2)}{l_1}) + K_d a \frac{(l_1+l_3)^2}{l_1} \right) Z_{t4} \end{aligned}$$

$$\begin{aligned} 7) \quad \dot{Z}_{p1} &= \dot{Z}_{B1} - \frac{K_d}{C_p} \frac{(l_3)Z_{B1}}{l_1} - (a+l_3)\dot{\Phi}_{B1} + \frac{K_d(l_3)(a-l_1)\Phi_{B1}}{C_p l_1} \\ & - \frac{K_d}{C_p} Z_{p1} + \frac{K_d}{C_p} \frac{(l_1+l_3)Z_{t1}}{l_1} \end{aligned}$$

$$\begin{aligned} 8) \quad \dot{Z}_{p2} &= Z_{B1} - \frac{K_d}{C_p} \frac{(l_3)Z_{B1}}{l_1} + (a+l_3)\dot{\Phi}_{B1} - \frac{K_d}{C_p} \frac{(l_3)(a-l_1)\Phi_{B1}}{G} \\ & - \frac{K_d}{C_p} Z_{p2} + \frac{K_d}{C_p} \frac{(l_1+l_3)Z_{t2}}{l_1} \end{aligned}$$

$$\begin{aligned} 9) \quad \dot{Z}_{p3} &= Z_{B2} - \frac{K_d}{C_p} \frac{(l_3)Z_{B2}}{l_1} - (a+l_3)\dot{\Phi}_{B2} + \frac{K_d}{C_p} \frac{(l_3)(a-l_1)\Phi_{B2}}{G} \\ & - \frac{K_d}{C_p} Z_{p3} + \frac{K_d}{C_p} \frac{(l_1+l_3)Z_{t3}}{l_1} \end{aligned}$$

$$\begin{aligned} 10) \quad \dot{Z}_{p4} &= Z_{B2} - \frac{K_d}{C_p} \frac{(l_3)Z_{B2}}{l_1} + (a+l_3)\dot{\Phi}_{B2} - \frac{K_d}{C_p} \frac{(l_3)(a-l_1)\Phi_{B2}}{G} \\ & - \frac{K_d}{C_p} Z_{p4} + \frac{K_d}{C_p} \frac{(l_1+l_3)Z_{t4}}{l_1} \end{aligned}$$

$$11) \dot{z}_1 = \frac{K_B Z}{C_B} - \frac{K_B \Phi}{C_B} + \dot{z}_{B1} + \frac{K_I}{C_B} z_{B1} - \frac{1}{C_B} (K_I + K_B) z_1 - g_f \frac{K_B}{C_B} z_f$$

$$12) \dot{z}_2 = \frac{K_B Z}{C_B} + \frac{K_B \Phi}{C_B} + \dot{z}_{B2} + \frac{K_I}{C_B} z_{B2} - \frac{1}{C_B} (K_I + K_B) z_2 - g_f \frac{K_B}{C_B} z_f$$

$$13) \dot{I}_1 = - \frac{L_M K_a \dot{z}}{(L_L + L_M) K_I} + \frac{L_M K_a \dot{\Phi}}{(L_L + L_M) K_I} + \frac{L_M K_a}{(L_L + L_M) K_I} \dot{z}_{B1} - \frac{(R + K_f I G) I_1}{L_L + L_M} \\ + \frac{G}{L_L + L_M} v_{D1} + g_f \frac{L_M K_a}{(L_M + L_L) K_I} \dot{z}_f$$

$$14) \dot{I}_2 = - \frac{L_M K_a \dot{z}}{(L_L + L_M) K_I} - \frac{L_M K_a \dot{\Phi}}{(L_L + L_M) K_I} + \frac{L_M K_a}{(L_L + L_M) K_I} \dot{z}_{B2} - \frac{(R + K_f I G) I_2}{L_L + L_M} \\ + \frac{G}{L_L + L_M} v_{D2} + g_f \frac{L_M K_a}{(L_M + L_L) K_I} \dot{z}_f$$

$$15) \dot{v}_{D1} = - \frac{K_a K_F T_6 \dot{z}}{T_7} - \frac{K_a K_F}{K_I T_7} \dot{z} + \frac{K_a K_F T_6 \dot{\Phi}}{K_I T_7} + \frac{K_a K_F \dot{\Phi}}{K_I T_7} \\ + \frac{K_a K_F T_6 \dot{z}_{B1}}{K_I T_7} + \frac{K_a K_F}{K_I T_7} z_{B1} - \frac{K_F T_6}{T_7} \dot{I}_1 - \frac{K_F I_1}{T_7} + \frac{T_6}{T_7} \epsilon_b + \frac{\epsilon_b}{T_7} \\ - \frac{T_6 \dot{\epsilon}_p}{T_7} - \frac{\epsilon_p}{T_7} + \frac{g_f K_a K_F T_6 \dot{z}_f}{K_I T_7} + g_f \frac{K_a K_F z_f}{K_I T_7} \\ + \frac{T_6 \dot{N}_f}{T_7} + \frac{N_f}{T_7}$$

$$16) \dot{v}_{D2} = - \frac{K_a K_F T_6 \dot{z}}{K_I T_7} - \frac{K_a K_F}{K_I T_7} \dot{z} - \frac{K_a K_F T_6 \dot{\Phi}}{K_I T_7} - \frac{K_a K_F \dot{\Phi}}{K_I T_7} \\ + \frac{K_a K_F T_6 \dot{z}_{B2}}{K_I T_7} + \frac{K_a K_F}{K_I T_7} z_{B2} - \frac{K_F T_6}{T_7} \dot{I}_2 - \frac{K_F I_2}{T_7} + \frac{T_6}{T_7} \epsilon_b + \frac{\epsilon_b}{T_7} \\ + \frac{T_6 \dot{\epsilon}_p}{T_7} + \frac{\epsilon_p}{T_7} + \frac{g_f K_a K_F T_6 \dot{z}_f}{K_I T_7} + g_f \frac{K_a K_F z_f}{K_I T_7} \\ + \frac{T_6 \dot{N}_f}{T_7} + \frac{N_f}{T_7}$$



$$\begin{aligned}
 17) \quad \ddot{\epsilon}_b &= -\frac{G_B T_{2b}}{T_{4b}} \ddot{Z} - \frac{G_B T_{1b}}{T_{4b}} \dot{Z} - \frac{G_B}{T_{4b}} Z + \frac{G_B T_{2b}}{T_{4b}} \ddot{\epsilon}_{bd} \\
 &+ \frac{G_B T_{1b}}{T_{4b}} \dot{\epsilon}_{bd} + \frac{G_B}{T_{4b}} \epsilon_{bd} - \frac{T_{3b}}{T_{4b}} \dot{\epsilon}_b - \frac{\epsilon_b}{T_{4b}} + g_f \frac{G_B T_{2b}}{T_{4b}} \ddot{Z}_f \\
 &+ g_f \frac{G_B T_{1b}}{T_{4b}} \dot{Z}_f + g_f \frac{G_B}{T_{4b}} Z_f
 \end{aligned}$$

$$18) \quad \ddot{\epsilon}_{bd} = \frac{\omega_b^2}{2} Z_{b1} + \frac{\omega_b^2}{2} Z_{b2} - 2\xi \omega_b \dot{\epsilon}_{bd} - \omega_b^2 \epsilon_{bd}$$

$$\begin{aligned}
 19) \quad \ddot{\epsilon}_p &= -\frac{G_p T_{2p}}{T_{4p}} \ddot{\Phi} - \frac{G_p T_{1p}}{T_{4p}} \dot{\Phi} - \frac{G_p}{T_{4p}} \Phi + \frac{G_p T_{2p}}{T_{4p}} \ddot{\epsilon}_{pd} \\
 &+ \frac{G_p T_{1p}}{T_{4p}} \dot{\epsilon}_{pd} + \frac{G_p}{T_{4p}} \epsilon_{pd} - \frac{T_{3p}}{T_{4p}} \dot{\epsilon}_p - \frac{\epsilon_p}{T_{4p}}
 \end{aligned}$$

$$20) \quad \ddot{\epsilon}_{pd} = \frac{\omega_p^2}{21} Z_{p1} + \frac{\omega_p^2}{21} Z_{p2} - 2\xi \omega_p \dot{\epsilon}_{pd} - \omega_p^2 \epsilon_{pd}$$

$$\begin{aligned}
 21) \quad \ddot{Z}_f &= \frac{-2g_f}{M_f} (K_a + K_s - K_I K_g) Z - \frac{g_f}{M_f} (K_a - K_I K_g) Z_{B1} \\
 &- \frac{g_f}{M_f} (K_a - K_I K_g) Z_{B2} - g_f \frac{K_s}{M_f} Z_1 - \frac{g_f K_s}{M_f} Z_2 - \frac{g_f K_I I_1}{M_f} - \frac{g_f K_I I_2}{M_f} \\
 &- \frac{C_f}{M_f} \dot{Z}_f - \frac{g_f^2}{M_f} (K_f + 2(K_a + K_s - K_I K_g)) Z_f
 \end{aligned}$$

$$22) \quad \dot{N}_f = \ddot{\epsilon}_b + \omega_b^2 \epsilon_b - 2\xi \omega_{NF} \dot{N}_f - \omega_{NF}^2 N_f$$

In order to compute the absolute damping response equations 15 and 16 are replaced by equations 15a) and 16a)

$$\begin{aligned}
 15a) \quad \dot{V}_{D1} &= -\frac{T_6}{T_7} G_B \ddot{Z} - \frac{1}{T_7} (G_B + \frac{K_a K_f T_7}{K_I}) \dot{Z} - \frac{K_a K_f}{K_I T_7} Z \\
 &+ \frac{T_6}{T_7} G_p \ddot{\Phi} + \frac{1}{T_7} (G_p + \frac{K_a K_f T_7}{K_I}) \dot{\Phi} + \frac{K_a K_f}{K_I T_7} \Phi \\
 &+ \frac{K_a K_f T_6}{K_I T_7} \dot{Z}_{B1} + \frac{K_a K_f}{K_I T_7} Z_{B1} - \frac{K_f T_6}{T_7} \dot{I}_1 - \frac{K_f I_1}{T_7}
 \end{aligned}$$

$$\begin{aligned}
 16a) \quad \dot{V}_{D2} = & -\frac{T_6}{T_7} G_B \ddot{z} - \frac{1}{T_7} \left( G_B + \frac{K_a K_F T_7}{K_I} \right) \dot{z} - \frac{K_a K_F}{K_I T_7} z \\
 & - \frac{T_6}{T_7} G_P \ddot{\phi} - \frac{1}{T_7} \left( G_P + \frac{K_a K_F T_7}{K_I} \right) \dot{\phi} - \frac{K_a K_F}{K_I T_7} \phi \\
 & + \frac{K_a K_F T_6}{K_I T_7} \dot{z}_{B2} + \frac{K_a K_F}{K_I T_7} z_{B2} - \frac{K_F T_6}{T_7} \dot{I}_2 - \frac{K_F}{T_7} I_2
 \end{aligned}$$

TABLE C1 MAGNETIC ACTUATOR PARAMETERS

Height		350 mm
Diameter		300 mm
Air Gap		30 mm
Peak Force		9 kN
R.M.S. Force		3 kN
Peak Current		50 amps
Continuous Current		20 amps
Armature Resistance (Cold)	R	1.6 ohms
Armature Resistance (Hot)	R	2.25 ohms
Mutual Inductance	$L_m$	.15 H
Leakage Inductance	$L_1$	.10 H

TABLE C2 PASSIVE SUSPENSION VEHICLE PARAMETERS

		Laden	Tare
Body Mass	M	26 000 kg	21 400 kg
Bogie Mass	$M_B$	2 707 kg	2 707 kg
Body Pitch Inertia	I	927 500 kgm <sup>2</sup>	803 300 kgm <sup>2</sup>
Bogie Pitch Inertia	$I_B$	1 970 kgm <sup>2</sup>	1 970 kgm <sup>2</sup>
Secondary spring stiffness/bogie	$K_s$	1.160 MN/m	.980 MN/m
Reservoir Stiffness/Bogie	$K_r$	.488 MN/m	.412 MN/m
Area Stiffness/Bogie	$K_a$	.420 MN/m	.340 MN/m
Secondary Damping/Bogie	$C_r$	50 kNs/m	42 kNs/m
Primary Stiffness/Axle	$K_p$	.360 MN/m	.360 MN/m
Primary Damping/Axle	$C_p$	8.4 kNs/m	8.4 kNs/m
Primary Damper End Stiffness	$K_c$	5.0 MN/m	5.0 MN/m
Bogie Centre Spacing	$2l_1$	16 m	
Bogie Wheel Base	$2a$	2.6 m	
Swinging Arm Geometry )	$l_1$	.535 m	
)	$l_2$	.265 m	
)	$l_3$	.505 m	
)			
)			

TABLE C3 ACTIVE SUSPENSION INNER CONTROL LOOP GAINS

Time Constants	$T_1$	12.5E-3 s
	$T_2$	5E-3 s
	$T_3$	2.s
	$T_4$	2.s
	$T_5$	2.s
	$T_6$	2.s
Feed back gain	$K_F$	.2 V/A
Current Feed Back	$K_{fI}$	.2 V/A
Power Amplifier Gain	$G_a$	30
Linear Force Constant	$K_I$	150 N/A
Negative Stiffness	$K_g$	30 kN/m

TABLE C4 ACTIVE SUSPENSION ABSOLUTE DAMPING GAINS

Bounce Damping Gain	$G_B$	77 V/m/s
Pitch Damping Gain	$G_P$	285 V/rad/s

TABLE C5 ACTIVE SUSPENSION POSITION CONTROL GAINS

Bounce Gain	$G_B$	5000 V/m
Bounce Phase Advance	$T_{1b}$	.077 s
Time Constants	$T_{2b}$	.003 s <sup>2</sup>
	$T_{3b}$	.025 s <sup>2</sup>
	$T_{4b}$	.0003 s
Bounce Notch Filter	$\omega$	68 rad/s
	$\xi$	.5
Bounce Filter	$\omega$	6.3 rad/s
	$\xi$	.7

Pitch Gain	$G_p$	21 000	V/rad
Pitch Phase Advance	$T_{1p}$	.077	s
Time Constants	$T_{2p}$	.003	s <sup>2</sup>
	$T_{3p}$	.025	s <sup>2</sup>
	$T_{4p}$	.0003	s <sup>2</sup>
Pitch Filter	$\omega$	6.3	rad/s
	$\xi$	.7	

## APPENDIX D

## MK III COACH ACTIVE SUSPENSION STATE EQUATIONS

$$1. \quad \ddot{z} = -\frac{2}{M} [K_a + K_s - K_g] z + \frac{1}{M} [K_a - K_g] z_{B1} + \frac{1}{M} [K_a - K_g] z_{B2}$$

$$\frac{K_s}{M} z_1 + \frac{K_s}{M} z_2 + \frac{K_I}{M} I_1 + \frac{K_I}{M} I_2$$

$$2. \quad \ddot{\Phi} = -\frac{2I_1^2}{I} [K_a + K_s - K_g] \Phi - \frac{1}{I} [K_a - K_g] z_{B1} + \frac{1}{I} [K_a - K_g] z_{B2}$$

$$- \frac{1K_2}{I} z_1 + \frac{1K_s}{I} z_2 - \frac{1K_I}{I} I_1 + \frac{1K_I}{I} I_2$$

$$3. \quad \ddot{z}_{B1} = \frac{1}{M_B} [K_a + K_s - K_g] z - \frac{1}{M_B} [K_a + K_s - K_g] \Phi$$

$$- \frac{1}{M_B} \left[ 2 K_d \left( \frac{l_3}{l_1} \right) \left( \frac{l_1 + l_3}{l_1} \right) + 2K_p \left( \frac{l_1 + l_2}{l_1} \right)^2 + K_a - K_g \right] z_{B1}$$

$$- \frac{K_d}{M_B} \left( \frac{l_1 + l_3}{l_1} \right) z_{P1} - \frac{K_d}{M_B} \left( \frac{l_1 + l_3}{l_1} \right) z_{P2} - \frac{K_s}{M_B} z_1 - \frac{K_I}{M_B} I_1$$

$$+ \frac{1}{M_B} \left[ K_d \left( \frac{l_1 + l_3}{l_1} \right)^2 + K_p \left( \frac{l_1 + l_2}{l_1} \right)^2 \right] z_{t1}$$

$$+ \frac{1}{M_B} \left[ K_d \left( \frac{l_1 + l_3}{l_1} \right)^2 + K_p \left( \frac{l_1 + l_2}{l_1} \right)^2 \right] z_{t2}$$

$$4. \quad \ddot{\Phi}_{B1} = -\frac{2}{I_B} \left[ K_d \left( \frac{l_3}{l_1} \right) (a - l_1) a \left( \frac{l_3 + l_1}{l_1} \right) \right.$$

$$\left. + K_p (a + l_2 + (a - l_1) \left( \frac{l_1 + l_2}{l_1} \right)) \right]^2 \Phi_B$$

$$+ \frac{K_d}{I_B} \left( \frac{a}{l_1} \right) (l_3 + l_1) z_{P1} - \frac{K_d}{I_B} \left( \frac{a}{l_1} \right) (l_3 + l_1) z_{P2}$$

$$- \frac{1}{I_B} \left[ K_p \left( \frac{l_1 + l_2}{l_1} \right) (a + l_2 + (a - l_1) \left( \frac{l_1 + l_2}{l_1} \right)) \right]$$

$$+ K_d a \left( \frac{l_1 + l_3}{l_1} \right)^2 \Big] z_{t1} + \frac{1}{I_B} \left[ K_P \left( \frac{l_1 + l_2}{l_1} \right) (a + l_2 + (a - l_1) \left( \frac{l_1 + l_2}{l_1} \right) \right. \\ \left. + K_d a \left( \frac{l_1 + l_3}{l_1} \right)^2 \right] z_{t2}$$

$$5. \ddot{z}_{B2} = \frac{1}{M_B} [K_a + K_s - K_g] z + \frac{1}{M_B} [K_a + K_s - K_g] \Phi \\ - \frac{1}{M_B} \left[ 2 K_d \left( \frac{l_3}{l_1} \right) \left( \frac{l_1 + l_3}{l_1} \right) + 2 K_P \left( \frac{l_1 + l_2}{l_1} \right)^2 + K_a - K_g \right] z_{B2} \\ - \frac{K_d}{M_B} \left( \frac{l_1 + l_3}{l_1} \right) z_{P3} - \frac{K_d}{M_B} \left( \frac{l_1 + l_3}{l_1} \right) z_{P4} - \frac{K_s}{M_B} z_2 - \frac{K_I}{M_B} I_2 \\ + \frac{1}{M_B} \left[ K_d \left( \frac{l_1 + l_3}{l_1} \right)^2 + K_P \left( \frac{l_1 + l_2}{l_1} \right)^2 \right] z_{t3} \\ + \left[ K_d \left( \frac{l_1 + l_3}{l_1} \right)^2 + K_P \left( \frac{l_1 + l_2}{l_1} \right)^2 \right] z_{t4}$$

$$6. \ddot{\Phi}_{B2} = - \frac{2}{I_2} \left[ K_d \left( \frac{l_3}{l_1} \right) (a - l_1) a \left( \frac{l_3 + l_1}{l_1} \right) + \right. \\ \left. + K_P \left( a + l_2 + (a - l_1) \left( \frac{l_1 + l_2}{l_1} \right) \right)^2 \Phi_{B2} + \frac{K_d}{I_B} \left( \frac{a}{l_1} \right) (l_3 + l_1) z_{P3} \right. \\ \left. - \frac{K_d}{I_B} \left( \frac{a}{l_1} \right) (l_3 + l_1) z_{P4} \right. \\ \left. - \frac{I}{I_B} \left[ K_P \left( \frac{l_1 + l_2}{l_1} \right) (a + l_2 + (a - l_1) \left( \frac{l_1 + l_2}{l_1} \right) + K_d a \left( \frac{l_1 + l_3}{l_1} \right)^2 \right] z_{t3} \right. \\ \left. + \frac{1}{I_B} \left[ K_P \left( \frac{l_1 + l_2}{l_1} \right) (a + l_2 + (a - l_1) \left( \frac{l_1 + l_2}{l_1} \right) + K_d a \left( \frac{l_1 + l_3}{l_1} \right)^2 \right] z_{t4} \right]$$

$$7. \dot{z}_{P1} = z_{B1} - \frac{K_d}{C_P} \left( \frac{l_3}{l_1} \right) z_{B1} - (a + l_3) \dot{\Phi}_{B1} + \frac{K_d}{C_P} \left( \frac{l_3}{l_1} \right) (a - l_1) \Phi_{B1} \\ - \frac{K_d}{C_P} z_{P1} + \frac{K_d}{C_P} \left( \frac{l_1 + l_3}{l_1} \right) z_{t1}$$

$$8. \quad \dot{z}_{P2} = \dot{z}_{B1} - \frac{K_d}{C_P} \left( \frac{l_3}{l_1} \right) z_{B1} + (a + l_3) \dot{\Phi}_{B1} - \frac{K_d}{C_P} \left( \frac{l_3}{l_1} \right) (a - l_1) \Phi_{B1} \\ - \frac{K_d}{C_P} z_{P2} + \frac{K_d}{C_P} \left( \frac{l_1 + l_3}{l_1} \right) z_{t2}$$

$$9. \quad \dot{z}_{P3} = \dot{z}_{B2} - \frac{K_d}{C_P} \left( \frac{l_3}{l_1} \right) z_{B2} - (a + l_3) \dot{\Phi}_{B2} + \frac{K_d}{C_P} \left( \frac{l_3}{l_1} \right) (a - l_1) \Phi_{B2} \\ - \frac{K_d}{C_P} z_{P3} + \frac{K_d}{C_P} \left( \frac{l_1 + l_3}{l_1} \right) z_{t3}$$

$$10. \quad \dot{z}_{P4} = \dot{z}_{B2} - \frac{K_d}{C_P} \left( \frac{l_3}{l_1} \right) z_{B2} + (a + l_3) \dot{\Phi}_{B2} - \frac{K_d}{C_P} \left( \frac{l_3}{l_1} \right) (a - l_1) \Phi_{B2} \\ - \frac{K_d}{C_P} z_{P4} + \frac{K_d}{C_P} \frac{l_1 + l_3}{l_1} z_{t4}$$

$$11. \quad \dot{z}_1 = \frac{K_S}{C_S} z + \frac{lK_S}{C_S} \Phi + \dot{z}_{B1} + \frac{K_r}{C_S} z_{B1} - \frac{1}{C_S} (K_r + K_S) z_1$$

$$12. \quad \dot{z}_2 = \frac{K_S}{C_S} z + \frac{lK_S}{C_S} \Phi + \dot{z}_{B2} + \frac{K_r}{C_S} z_{B2} - \frac{1}{C_S} (K_r + K_S) z_2$$

$$13. \quad \dot{I}_1 = - \frac{L_M K_g}{(L_L + L_M)} \frac{\dot{z}}{K_I} + \frac{L_M l K_g}{(L_L + L_M)} \frac{\dot{\Phi}}{K_I} + \frac{L_M K_g}{(L_L + L_M)} \frac{\dot{z}_{B1}}{K_I} - \frac{(R + K_{FI} G)}{(L_L + L_M)} I_1 + u_1$$

$$14. \quad \dot{I}_2 = - \frac{L_M K_g}{(L_L + L_M)} \frac{\dot{z}}{K_I} - \frac{L_M l K_g}{(L_L + L_M)} \frac{\dot{\Phi}}{K_I} + \frac{L_M K_g}{(L_L + L_M)} \frac{\dot{z}_{B2}}{K_I} \\ - \frac{(R + K_{FI} G)}{(L_L + L_M)} I_2 + u_2$$

$$15. \quad \dot{z}_{t1} = - z_{t1} + w(t)$$

$$16. \quad \dot{z}_{t2} = - z_{t2} + w(t + \delta_1)$$

$$17. \quad \dot{z}_{t3} = - z_{t3} + w(t + \delta_2)$$

$$18. \quad \dot{z}_{t4} = - z_{t4} + w(t + \delta_3)$$

$w$  is a white noise track input and  $\delta$  the time delay after the leading wheel set.



## APPENDIX D 2

SMALL REGULATOR MODEL

$$1. \quad \ddot{z} = -\frac{2}{M} (K_a - K_g K_I) z - \frac{K_s}{M} z_1 - \frac{K_s}{M} z_2 + \frac{K_I}{M} I_1 + \frac{K_I}{M} I_2 \\ + \frac{1}{M} (K_a + K_s - K_g K_I) z_{t1} + \frac{1}{M} (K_a + K_s - K_g K_I) z_{t2}$$

$$2. \quad \ddot{\phi} = -\frac{2l^2}{I} (K_a - K_g K_I) \phi + \frac{1}{I} K_s z_1 - \frac{1}{I} K_s z_2 - \frac{1}{I} K_I I_1 \\ + \frac{1}{I} K_I I_2 - \frac{1}{I} (K_a + K_s - K_g K_I) z_{t1} + \frac{1}{I} (K_a + K_s - K_g K_I) z_{t2}$$

$$3. \quad \dot{z}_1 = \dot{z} + \frac{K_r}{C_s} z - l \dot{\phi} - l \frac{K_r}{C_s} \phi - \frac{K_r + K_s}{C_s} z_1 + \frac{K_s}{C_s} z_{t1}$$

$$4. \quad \dot{z}_2 = \dot{z} + \frac{K_r}{C_s} z + l \dot{\phi} + \frac{l K_r}{C_s} \phi - \frac{K_r + K_s}{C_s} z_2 + \frac{K_s}{C_s} z_{t2}$$

$$5. \quad \dot{I}_1 = -\frac{L_m K_g}{L_L + L_m} \dot{z} + \frac{l L_m K_g}{L_L + L_m} \dot{\phi} - \frac{R + K_{IF} G}{L_L + L_m} I_1 + \frac{G u_1}{L_L + L_m}$$

$$6. \quad \dot{I}_2 = -\frac{L_m K_g}{L_L + L_m} \dot{z} - \frac{l L_m K_g}{L_L + L_m} \dot{\phi} - \frac{R + K_{IF} G}{L_L + L_m} I_2 + \frac{G u_2}{L_L + L_m}$$

$$7. \quad \dot{z}_{t1} = -z_{t1} + w(t)$$

$$8. \quad \dot{z}_{t2} = -z_{t2} + w(t + \delta)$$

$w$  is a white noise track input and  $\delta$  the time delay between wheelsets.

TABLE D1

SUSPENSION PARAMETERS

	Laden	Tare
Body Mass	M 26 000 kg	21 400 kg
Bogie Mass	M <sub>B</sub> 2 707 kg	2 707 kg
Body Pitch Inertia	I 927 500 kg m <sup>2</sup>	803 300 kg m <sup>2</sup>
Bogie Pitch Inertia	I <sub>b</sub> 1 970 kg m <sup>2</sup>	1 970 kg m <sup>2</sup>
Secondary Spring Stiffness/Bogie	K <sub>S</sub> 1.16 MN/m	.98 MN/m
Reservoir Stiffness/Bogie	K <sub>r</sub> .488 MN/m	.412 MN/m
Area Stiffness/Bogie	K <sub>a</sub> .420 MN/m	.340 MN/m
Secondary Damping/Bogie	C <sub>r</sub> 50 kN s/m	43 kN s/m
Primary Stiffness/Axle	K <sub>p</sub> .360 MN/m	.360 MN/m
Primary Damping/Axle	C <sub>p</sub> 8.40 kN s/m	8.4 kN s/m
Primary Damper End Stiffness	K <sub>C</sub> 5.0 MN/m	5.0 MN/m
Bogie Centre Spacing	2 16 m	
Bogie Wheel Base	2a 2.6 m	
Swinging Arm Geometry	) l <sub>1</sub> .535 m	
	) l <sub>2</sub> .265 m	
	) l <sub>3</sub> .505 m	
Current Gain Per Actuator	K <sub>I</sub> 150 N/A	
Current Feedback Gain	K <sub>fi</sub> .2 V/A	
Amplifier Gain	G <sub>a</sub> 30 V/V	

## APPENDIX D3

## PADÉ APPROXIMATION

$$1) \quad Z_{t2} = \frac{1 - as + bs^2 - cs^3 + ds^4 - es^5}{1 + as + bs^2 + cs^3 + ds^4 + es^5} Z_{t1}$$

$$2) \quad Z_5 = -Z_4 \frac{d}{e} - Z_3 \frac{c}{e} - Z_2 \frac{b}{e} - Z_1 \frac{a}{e} - \frac{Z_0}{e} + \frac{Z_{t1}}{e}$$

$$3) \quad \dot{Z}_4 = Z_5$$

$$4) \quad \dot{Z}_3 = Z_4$$

$$5) \quad \dot{Z}_2 = Z_3$$

$$6) \quad \dot{Z}_1 = Z_2$$

$$7) \quad \dot{Z}_0 = Z_1$$

$$8) \quad Z_{t2} = -eZ_5 + dZ_4 - cZ_3 + bZ_2 - aZ_1 + Z_0$$

This value of  $Z_{t2}$  is substituted for  $Z_{t2}$  in equations 2 and 4 in Appendix D2.

APPENDIX ETrain ModesState EquationsAdditional Terms in Vehicle Modes

$$1) \quad \ddot{z} = -\frac{2K}{M^c} z + \frac{K}{M^c} z_{g1} + \frac{K}{M^c} z_{g2}$$

$$2) \quad \ddot{\phi} = -\frac{2I^2}{I^c} K_c + \frac{1}{M} K_c z_{g1} - \frac{1}{M} K_c z_{g2}$$

Leading Lab Coach

$$23) \quad \ddot{z}_L = -\left(\frac{2C_L}{M_L} + \frac{C}{M_L} g\right) \dot{z}_L - \frac{2K_L}{M_L} z_L + \frac{C}{M_L} \dot{z}_{L1} + \frac{C}{M_L} \dot{z}_{L2} + \frac{K}{M_L} z_{L1} + \frac{K}{M_L} z_{L2} + \frac{C}{M_L} z_{g1}$$

$$24) \quad \ddot{\phi}_L = -\left(\frac{2I_L^2 C_L}{I_L} + \frac{1}{I_L} C_L g\right) \dot{\phi}_L - \frac{2I_L^2 K_L}{I_L} \phi_L + \frac{1}{I_L} C_L \dot{z}_{L1} - \frac{1}{I_L} C_L \dot{z}_{L2} + \frac{1}{I_L} K_L z_{L1} - \frac{1}{I_L} K_L z_{L2} - \frac{1}{I_L} C_L g z_{g1}$$

$$25) \quad \ddot{z}_{L1} = -\frac{C}{M_{LB}} \dot{z}_{L1} - \left(\frac{K_L + 2K_{PL}}{M_{LB}}\right) z_{L1} + \frac{C}{M_{LB}} \dot{z}_L + \frac{K}{M_{LB}} z_L - \frac{1}{M_{LB}} C_L \phi_L - \frac{1}{M_{LB}} K_{PL} \phi_L + \frac{K_{PL}}{M_{LB}} z_{L1} + \frac{K_{PL}}{M_{LB}} z_{L2}$$

$$26) \quad \ddot{z}_{LZ} = -\frac{C_{ML}}{M_{LB}} \dot{z}_{LZ} - \left( \frac{K_{ML} + 2K_{PL}}{M_{LB}} \right) z_{LZ} + \frac{C_{ML}}{M_{LB}} \dot{z}_L + \frac{K_{ML}}{M_{LB}} z_L \\ + \frac{1}{M_{LB}} C_{ML} \dot{\Phi}_L + \frac{1}{M_{LB}} K_{ML} \Phi_L + \frac{K_{PL}}{M_{LB}} z_{Lt3} + \frac{K_{PL}}{M_{LB}} z_{Lt4}$$

$$27) \quad \dot{z}_{g1} = -\frac{K_c}{C_g} z_{g1} - \frac{K_c}{C_g} z + \frac{1}{C_g} K_c \Phi + \dot{z}_{L1} - l_{CL} \dot{\Phi}_L$$

Trailing Lab Coach

$$28) \quad \ddot{z}_T = -\left( \frac{2C_T + C_g}{M_T} \right) \dot{z}_T - \frac{2K_T}{M_T} z_T + \frac{C_T}{M_T} \dot{z}_{T1} + \frac{C_T}{M_T} \dot{z}_{T2} + \frac{K_T}{M_T} z_{T1} \\ + \frac{K_T}{M_T} z_{T2} + \frac{C_T}{M_T} z_{g2}$$

$$29) \quad \ddot{\Phi}_T = -\left( \frac{2l_T^2 C_T}{I_T} + \frac{l_T^2 C_T C_g}{I_T} \right) \dot{\Phi}_T - \frac{2l_T^2 K_T}{I_T} \Phi_T + \frac{l_T C_T}{I_T} \dot{z}_{T1} \\ - \frac{l_T C_T}{I_T} \dot{z}_{T2} + \frac{l_T K_T}{I_T} z_{T1} - \frac{l_T K_T}{I_T} z_{T2} + \frac{l_T C_T C_g}{I_T} z_{g2}$$

$$30) \quad \ddot{z}_{T1} = -\frac{C_T}{M_{TB}} \dot{z}_{T1} - \left( \frac{K_T + 2K_{PT}}{M_{TB}} \right) z_{T1} + \frac{C_T}{M_{TB}} \dot{z}_T + \frac{K_T}{M_{TB}} z_T \\ - \frac{1}{M_{TB}} C_T \dot{\Phi}_L - \frac{1}{M_{TB}} K_T \Phi_T + \frac{K_{PT}}{M_{TB}} z_{Tt1} + \frac{K_{PT}}{M_{TB}} z_{Tt2}$$

$$31) \quad \ddot{z}_{T2} = - \frac{C_T}{M_{TB}} \dot{z}_{T2} - \left( \frac{K_T + 2K_{PT}}{M_{TB}} \right) z_{T2} + \frac{C_T}{M_{TB}} \dot{z}_T + \frac{K_T}{M_{TB}} z_T + \frac{P_T C_T}{M_{TB}} \dot{\Phi}_T \\ + \frac{l_T K_T}{M_{TB}} \Phi_T + \frac{K_{PT}}{M_{TB}} z_{Tt3} + \frac{K_{PT}}{M_{TB}} z_{Tt4}$$

$$32) \quad \ddot{z}_{g2} = - \frac{K_C}{C_g} \dot{z}_{g2} - \frac{K_C}{C_g} z_{g2} - \frac{l_C K_C}{C_g} \Phi + \dot{z}_T + l_{CT} \dot{\Phi}_T$$

Table E1 Lab Coach Parameters

Body Mass	$M_L M_T$	27 000 kg
Pitch Inertia	$I_L I_T$	842 000 kg m <sup>2</sup>
Bogie Mass	$M_{LB} M_T$	3 000 kg
Sec Dampers per bogie	$C_L C_T$	70 000 kNs/m
Sec Springs	$K_L K_T$	1.4 MN/m
Primary Springs per axle	$K_{PL} K_{PT}$	1.2 MN/m
Gangway End Stiffness	$K_C$	2.5 MN/m
Gangway Damping	$C_g$	100 kNs/m
Bogie Centre Spacing	$l_L l_T$	13.65 m
Wheel Spacing	$2a_L 2a_T$	2.6 m
Lab Coach Centre to Gangway	$l_{CL} l_{CT}$	10.125 m
MkIII Centre to Gangway	$l_c$	11.5 m

## APPENDIX F

## SYSTEM EQUATIONS FOR FREQUENCY RESPONSE PROGRAM

F1 VEHICLE MODEL

$$1) \quad \ddot{Z}_{B1} = \left( \frac{K_a + K_r + 2K_p}{M_B} + (C_p + 2C_r)s \right) Z_{B1}$$

$$+ \left( \frac{K_r + C_r s}{M_B} \right) Z_1 + \frac{K_a Z}{M_B} - \frac{K_a \phi}{M_B} - \frac{F_1}{M_B}$$

$$+ \left( \frac{K_p + C_p s}{M_B} \right) Z_{t1} + \left( \frac{K_p + C_p s}{M_B} \right) Z_{t2}$$

$$2) \quad Z_{B1} = \frac{1}{s^2} \ddot{Z}_{B1}$$

$$3) \quad Z_1 = \frac{(K_r + C_r s) Z_{B1}}{\left( \frac{K_r + C_r s}{M_B} + C_r s \right)} + \frac{K_a Z}{(K_r + K_s) + C_r s} - \frac{K_a \phi}{(K_r + K_s) + C_r s}$$

$$4) \quad \ddot{\phi}_{B1} = -2 \left( \frac{K_p + C_p s}{I_B} \right) a^2 Z_{t1} - \left( \frac{K_p + C_p s}{I_B} \right) a Z_{t1} + \left( \frac{K_p + C_p s}{I_B} \right) a Z_{t2}$$

$$5) \quad \phi_{B1} = \frac{1}{s^2} \ddot{\phi}_{B1}$$

$$6) \quad \ddot{Z} = \frac{K_a}{M} Z_{B1} + \frac{K_s}{M} Z_1 - \frac{2(K_a + K_s)}{M} Z + \frac{K_s}{M} Z_2 + \frac{K_a}{M} Z_{B2}$$

$$+ \frac{F_1}{M} + \frac{F_2}{M}$$

$$7) \quad Z = \frac{1}{s^2} \ddot{Z}$$

$$8) \quad \ddot{\phi} = -\frac{1K_a}{I} Z_{B1} - \frac{1K_s}{I} Z_1 - \frac{2I^2}{I} (K_a + K_s) \phi + \frac{1K_s}{I} Z_2$$

$$9) \quad \phi = \frac{1}{s^2} \ddot{\phi}$$

$$10) \quad \ddot{Z}_{B2} = \frac{K_a}{M_B} Z - \left( \frac{K_a + K_r + 2K_p}{M_B} + (C_r + 2C_p)s \right) Z_{B2}$$

$$+ \left( \frac{K_r + C_r s}{M_B} \right) Z_2 + \frac{K_a I}{M_B} - \frac{F_2}{M_B} + \left( \frac{K_p + C_p s}{M_B} \right) Z_{t3}$$

$$+ \left( \frac{K_p + C_p s}{M_B} \right) Z_{t4}$$

$$11) \quad Z_{B2} = \frac{1}{s} \ddot{Z}_{B2}$$

$$12) \quad Z_2 = \frac{K Z}{(K_r + K_s) + C_r s} + \frac{K \phi}{(K_r + K_s) + C_r s} + \frac{(K_r + C_r s) Z_{B2}}{(K_r + K_s) + C_r s}$$

$$13) \quad \ddot{\phi}_{B2} = \frac{-2(K_p + C_p s)a^2 \phi}{I_B} - \frac{(K_p + C_p s)a Z_{t3}}{I_B} + \frac{(K_p + C_p s)a Z_{t4}}{I_B}$$

$$14) \quad \phi_{B2} = \frac{I_2}{s} \ddot{\phi}_{B2}$$

$$15) \quad Z_{t1}$$

$$16) \quad Z_{t2} = Z_t e^{-2a/V}$$

$$17) \quad Z_{t3} = Z_t e^{-1/V}$$

$$18) \quad Z_{t4} = Z_t e^{-(2a + 1)/V}$$

$$19) \quad Z_1 = Z - 1 \phi$$

$$20) \quad Z_2 = Z + 1 \phi$$

$$21) \quad Z_{R1} = -Z_{B1} + Z - 1 \phi$$

$$22) \quad Z_{R2} = -Z_{B2} + Z + 1 \phi$$

#### F2 Analogue Controller

$$23) \quad F_1 = K_g Z_{R1} + K_I I_1$$

$$24) \quad I_1 = \frac{K}{K_I} \left( \frac{L s}{R + L s} \right) Z_{R1} - \frac{L m s I_1}{R + L s} + \frac{V_1}{R + L s}$$



$$25) \quad V_1 = -\frac{K_f G_a}{K_I} \left( \frac{1 + sT_6}{sT_7} \right) F_1 - K_{fI} G_a I_1 + G_a \left( \frac{1 + sT_6}{sT_7} \right) \varepsilon_b \\ - G_a \left( \frac{1 + sT_6}{sT_7} \right) \varepsilon_p$$

$$26) \quad F_2 = K_g Z_{R2} + K_g I_2$$

$$27) \quad I_2 = \frac{K_g}{K_I} \left( \frac{L s}{R + L s} \right) Z_{R2} - \frac{L s I_2}{R + L s} + \frac{V_2}{R + L s}$$

$$28) \quad V_2 = -\frac{K_f G_a}{K_I} \left( \frac{1 + sT_6}{sT_7} \right) F_2 - K_{fI} G_a I_2 + G_a \left( \frac{1 + sT_6}{sT_7} \right) \varepsilon_b \\ + G_a \left( \frac{1 + sT_6}{sT_7} \right) \varepsilon_p$$

$$29) \quad \varepsilon_b = G_B \left( \frac{1 + sT_{1b} + s^2 T_{2b}}{1 + sT_{3b} + s^2 T_{4b}} \right) \varepsilon'_b$$

$$30) \quad \varepsilon'_b = - \left( \frac{2 \zeta \omega s + s^2}{\omega^2 + 2 \zeta \omega s + s^2} \right) Z_I - \left( \frac{0.5 \omega^2}{\omega^2 + 2 \zeta \omega s + s^2} \right) Z_{R1F} \\ - \left( \frac{0.5 \omega^2}{\omega^2 + 2 \zeta \omega s + s^2} \right) Z_{R2F}$$

$$31) \quad \varepsilon_p = G_P \left( \frac{1 + sT_{1p} + s^2 T_{2p}}{1 + sT_{3p} + s^2 T_{4p}} \right) \varepsilon'_p$$

$$32) \quad \varepsilon'_p = - \left( \frac{2 \zeta \omega s + s^2}{\omega^2 + 2 \zeta \omega s + s^2} \right) \phi_I + \frac{1}{I} \left( \frac{0.5 \omega^2}{\omega^2 + 2 \zeta \omega s + s^2} \right) Z_{R1F} \\ - \frac{1}{I} \left( \frac{0.5 \omega^2}{\omega^2 + 2 \zeta \omega s + s^2} \right) Z_{R2F}$$

$$33) \quad Z_I = \frac{Z}{2s + s^2} - \frac{Z}{2s + s^2}$$

$$34) \quad Z_s = Z_I \left( \frac{1 + 2s}{s} \right)$$

$$35) \quad \phi_I = \frac{\phi}{2s + s^2} - \frac{\phi}{2s + s^2}$$

$$36) \quad \phi_s = \phi_I \left( \frac{1 + 2s}{s} \right)$$

$$37) \quad Z_{R1F} = \frac{s Z_{R1}}{s + 1}$$

$$38) \quad Z_{R2F} = \frac{s Z_{R2}}{s + 1}$$

F3 Digital ControllerAnalogue Interfaces

$$23) \quad F_1 = K_g Z_{R1} + K_I I_1$$

$$24) \quad I_1 = \frac{K_g}{K_I} \left( \frac{Ls}{R + mLs} \right) Z_{R1} - \frac{LsI_1}{R + Ls} + \frac{V_1}{R + Ls}$$

$$25) \quad V_1 = \frac{G_a}{sT} V_{s1} - K_{fI} G_a I_1$$

$$26) \quad F_2 = K_g Z_{R2} + K_I I_2$$

$$27) \quad I_2 = \frac{K_g}{K_I} \left( \frac{Ls}{R + mLs} \right) Z_{R2} - \frac{LsI_2}{R + Ls} + \frac{V_2}{R + Ls}$$

$$28) \quad V_2 = \frac{G_a}{sT} V_{s2} + K_{fI} G_a I_2$$

$$29) \quad Z_{R1F} = \frac{Z_{R1}}{1 + .003s}$$

$$30) \quad Z_{R2F} = \frac{Z_{R2}}{1 + .003s}$$

$$31) \quad Z_F = \frac{Z}{1 + .003s}$$

$$32) \quad \phi_F = \frac{\phi}{1 + .003s}$$

$$33) \quad F_{1F} = \frac{F_1}{1 + .003s}$$

$$34) \quad F_{2F} = \frac{F_2}{1 + .003s}$$

Digital Controller

$$35) \quad V_{s1} = (1 - z^{-1})V_{z1}$$

$$36) \quad V_{s2} = (1 - z^{-1})V_{z2}$$

$$37) \quad V_{z1} = -\frac{K_f}{K_I} \left( \frac{-a_1 + a_2 z}{-b_1 + b_2 z} \right) F_{1F} + \left( \frac{-a_1 + a_2 z}{-b_1 + b_2 z} \right) \epsilon_b$$

$$- \left( \frac{-a_1 + a_2 z}{-b_1 + b_2 z} \right) \epsilon_p$$

- 38)  $V_{z2} = \frac{-K_f}{K_I} \left( \frac{-a_1 + a_2 z}{-b_1 + b_2 z} \right) F_{2F} + \left( \frac{-a_1 + a_2 z}{-b_1 + b_2 z} \right) \epsilon_b$   
 $+ \left( \frac{-a_1 + a_2 z}{-b_1 + b_2 z} \right) \epsilon_p$
- 39)  $\epsilon_b = G_B \left( \frac{\alpha_1 + \alpha_2 z + \alpha_3 z^2}{\beta_1 + \beta_2 z + \beta_3 z^2} \right) \epsilon'_b$
- 40)  $\epsilon'_b = - \left( \frac{\alpha_4 + \alpha_5 z + \alpha_6 z^2}{\beta_4 + \beta_5 z + \beta_6 z^2} \right) Z_I - \frac{1}{2} \left( \frac{1 + 2z + z^2}{\beta_4 + \beta_5 z + \beta_6 z^2} \right) Z_{RF1}$   
 $- \frac{1}{2} \left( \frac{1 + 2z + z^2}{\beta_4 + \beta_5 z + \beta_6 z^2} \right) Z_{RF2}$
- 41)  $\epsilon_p = G_p \left( \frac{\alpha_1 + \alpha_2 z + \alpha_3 z^2}{\beta_1 + \beta_2 z + \beta_3 z^2} \right) \epsilon'_p$
- 42)  $\epsilon'_p = - \left( \frac{\alpha_4 + \alpha_5 z + \alpha_6 z^2}{\beta_4 + \beta_5 z + \beta_6 z^2} \right) \Phi_I - \frac{1}{2} \left( \frac{1 + 2z + z^2}{\beta_4 + \beta_5 z + \beta_6 z^2} \right) Z_{RF1}$   
 $- \frac{1}{2} \left( \frac{1 + 2z + z^2}{\beta_4 + \beta_5 z + \beta_6 z^2} \right) Z_{RF2}$
- 43)  $Z_I = \left( \frac{1 + 2z + z^2}{\delta_1 + \delta_2 z + \delta_3 z^2} \right) Z_F - Z_s$
- 44)  $Z_s = \left( \frac{-\gamma_1 + \gamma_2 z}{-\gamma_4 + \gamma_5 z} \right) Z_I$
- 45)  $\Phi_I = \left( \frac{1 + 2z + z^2}{\gamma_1 + \gamma_2 z + \gamma_3 z^2} \right) \Phi_F - \Phi_s$
- 46)  $\Phi_s = \left( \frac{-\gamma_1 + \gamma_2 z}{-\gamma_4 + \gamma_5 z} \right) \Phi_I$

TABLE F5Digital Control Variables

$$a_1 = 1.5$$

$$a_2 = 3.5$$

$$b_1 = 1$$

$$b_2 = 1$$

$$\alpha_1 = 105.6$$

$$\alpha_2 = -238$$

$$\alpha_3 = 136.4$$

$$\beta_1 = 8$$

$$\beta_2 = -22$$

$$\beta_3 = 18$$

$$\alpha_4 = 956$$

$$\alpha_5 = -2000$$

$$\alpha_6 = 1044$$

$$\beta_4 = 957$$

$$\beta_5 = -1998$$

$$\beta_6 = 1045$$

$$\delta_1 = 39,600$$

$$\delta_2 = 80,000$$

$$\delta_3 = 40,400$$

$$\delta_4 = 200$$

$$\delta_5 = 200$$

$$\gamma_1 = -399$$

$$\gamma_2 = 401$$

TABLE F1 MAGNETIC ACTUATOR PARAMETERS

Height		350 mm
Diameter		300 mm
Air Gap		30 mm
Peak Force		9 kN
RMS Force		3 kN
Peak Current		50 Amps
Continuous Current		20 Amps
Armature Resistance (Cold)	R	1.6 Ohms
Armature Resistance (Hot)	R	2.25 Ohms
Mutual Inductance	$L_m$	.15 H
Leakage Inductance	$L_l$	.10 H

TABLE F2 PASSIVE SUSPENSION VEHICLE PARAMETERS

		Laden	Tare
Body Mass	M	26,000 kg	21,400 kg
Bogie Mass	$M_B$	2,707 kg	2,707 kg
Body Pitch Inertia	$I$	927,500 kgm <sup>2</sup>	803,300 kgm <sup>2</sup>
Bogie Pitch Inertia	$I_B$	1,970 kgm <sup>2</sup>	1,970 kgm <sup>2</sup>
Secondary spring stiffness/bogie	$K_s$	1.160 MN/m	.980 MN/m
Reservoir Stiffness/Bogie	$K_r$	.488 MN/m	.412 MN/m
Area Stiffness/Bogie	$K^a$	.420 MN/m	.340 MN/m
Secondary Damping/Bogie	$C^r$	50 kNs/m	42 kNs/m
Primary Stiffness/Axle	$K^p$	.360 MN/m	.360 MN/m
Primary Damping/Axle	$C^p$	8.4 kNs/m	8.4 kNs/m
Primary Damper End Stiffness	$K^c$	5.0 MN/m	5.0 MN/m
Bogie Centre Spacing	$2l$	16 m	
Bogie Wheel Base	$2a$	2.6 m	
Swinging Arm Geometry	$l_1$	.535 m	
	$l_2$	.265 m	
	$l_3$	.505 m	

TABLE F3 ACTIVE SUSPENSION INNER CONTROL LOOP GAINS

Time Constants	$T_1$	12.5E-3 s
	$T_2$	5E-3 s
	$T_3$	2 s
	$T_4$	2 s
	$T_5$	2 s
	$T_6$	2 s
Feedback gain	$K_F$	.2 V/A
Current Feedback	$K_{fI}$	.2 V/A
Power Amplifier Gain	$G^a$	30
Linear Force Constant	$K^I$	150 N/A
Negative Stiffness	$K_g$	30 kN/m

TABLE F4 ACTIVE SUSPENSION POSITION CONTROL GAINS

Bounce Gain	$G_B$	1250 V/m
Bounce Phase Advance	$T_{1b}$	.077 s <sup>2</sup>
Time Constants	$T_{2b}$	.003 s
	$T_{3b}$	.025 s <sup>2</sup>
	$T_{4b}$	.0003 s
	$\omega^{4b}$	68 rad/s
Bounce Notch Filter	$\xi$	.5
Bounce Filter	$\omega$	6.3 rad/s
	$\xi$	.7
Pitch Gain	$G_P$	5250 V/rad
Pitch Phase Advance	$T_{1p}$	.077 s <sup>2</sup>
Time Constants	$T_{2p}$	.003 s
	$T_{3p}$	.025 s <sup>2</sup>
	$T_{4p}$	.003 s
	$\omega^{4p}$	6.3 rad/s
Pitch Filter	$\xi$	.7

## APPENDIX F4

SMALL REGULATOR MODEL USED FOR DIGITAL REGULATOR

1. 
$$\ddot{Z} = -\frac{2}{M} (K_a - K_g K_I) Z - \frac{K_s}{M} Z_1 - \frac{K_s}{M} Z_2 + \frac{K_I}{M} I_1 + \frac{K_I}{M} I_2$$

$$+ \frac{1}{M} (K_a + K_s - K_g K_I) Z_{t1} + \frac{1}{M} (K_a + K_s - K_g K_I) Z_{t2}$$
2. 
$$\ddot{\phi} = -\frac{2I^2}{I} (K_a - K_g K_I) \phi + \frac{1}{I} K_s Z_1 - \frac{1}{I} K_s Z_2 = \frac{1}{I} K_I I_1$$

$$+ \frac{1}{I} K_I I_2 - \frac{1}{I} (K_a + K_s - K_g K_I) Z_{t1} + \frac{1}{I} (K_a + K_s - K_g K_a) Z_{t2}$$
3. 
$$\dot{Z}_1 = \dot{Z} + \frac{K_r}{C_s} Z - 1\dot{\phi} - 1\frac{K_r}{C_s} \phi - \frac{K_r + K_s}{C_s} Z_1 + \frac{K_s}{C_s} Z_{t1}$$
4. 
$$\dot{Z}_2 = \dot{Z} + \frac{K_r}{C_s} Z + 1\dot{\phi} + \frac{1K_r}{C_s} \phi - \frac{K_r + K_s}{C_s} Z_2 + \frac{K_s}{C_s} Z_{t2}$$
5. 
$$\dot{I}_1 = -\frac{L_m}{L_L + L_m} K_g \dot{Z} + \frac{1L_m}{L_L + L_m} K_g \dot{\phi} - \frac{R + K_{IF}G}{L_L + L_m} I_1 + \frac{G}{L_L + L_m} u_1$$
6. 
$$\dot{I}_2 = -\frac{L_m}{L_L + L_m} K_g \dot{Z} - \frac{1L_m}{L_L + L_m} K_g \dot{\phi} - \frac{R + K_{IF}G}{L_L + L_m} I_2 + \frac{G}{L_L + L_m} u_2$$
7. 
$$Z_{t1} = -Z_{t1} + w(t)$$
8. 
$$Z_{t2} = -Z_{t2} + w(t + \delta)$$

w is a white noise track input and  $\delta$  the time delay between bogie centres.

## APPENDIX G

## THE SYSTEM EQUATIONS

A Matrix Equations

$$1) \quad \ddot{Z} = - \left[ 2(K_a - K_g K_I) \right] \frac{Z}{M} - \frac{K_s}{M} Z_1^1 - \frac{K_s}{M} Z_2^1 + \frac{K_I}{M} I_1 + \frac{K_I}{M} I_2 \\ + \left[ K_a + K_s - K_g K_I \right] \frac{Z_{t1}}{M} + \left[ K_a + K_s - K_g K_I \right] \frac{Z_{t2}}{M}$$

$$2) \quad \dot{Z} = \dot{Z}$$

$$3) \quad \ddot{\phi} = - \left[ 2I^2 (K_a - K_g K_I) \right] \frac{\phi}{I} + \frac{1K_s Z_1^1}{I} - \frac{1K_s Z_2^1}{I} - \frac{1K_I I_1}{I} + \frac{1K_I I_2}{I} \\ - 1 \left[ K_a + K_s - K_g K_I \right] \frac{Z_{t1}}{I} + 1 \left[ K_a + K_s - K_g K_I \right] \frac{Z_{t2}}{I}$$

$$4) \quad \dot{\phi} = \dot{\phi}$$

$$5) \quad \dot{Z}_1 = \dot{Z} - 1 \dot{\phi} + \frac{K_r Z}{C_s} - \frac{1K_r \phi}{C_s} - (K_r + K_s) \frac{Z_1}{C_s} + K_s \frac{Z_{t1}}{C_s}$$

$$6) \quad \dot{Z}_2 = \dot{Z} + 1 \dot{\phi} + \frac{K_r Z}{C_s} + \frac{1K_r \phi}{C_s} - (K_r + K_s) \frac{Z_2}{C_s} + K_s \frac{Z_{t2}}{C_s}$$

$$7) \quad \dot{I}_1 = - \frac{L_m K_g \dot{Z}}{L_L + L_m} + \frac{1L_m K_g \dot{\phi}}{L_L + L_m} - \frac{(R + K_{IF}G) I_1}{L_L + L_m} + \frac{G V_{D1}}{L_L + L_m}$$

$$8) \quad \dot{I}_2 = - \frac{L_m K_g \dot{Z}}{L_L + L_m} - \frac{1L_m K_g \dot{\phi}}{L_L + L_m} - \frac{(R + K_{IF}G) I_2}{L_L + L_m} + \frac{G V_{D2}}{L_L + L_m}$$



A Matrix (Cont'd)

9)  $\dot{z}_{t1} = -z_{t1}$

10)  $\dot{z}_{t2} = -z_{t2}$

$$11) \quad \dot{V}_{D1} = \left[ \frac{K_f T_6 L_m K_g}{T_7 (L_L + L_m)} - \frac{K_g K_f T_6}{T_7} \right] \dot{z} - \frac{K_g K_f}{T_7} z + \left[ \frac{K_g K_f T_6}{T_7} - \frac{K_f T_6 L_m K_g}{T_7 (L_L + L_m)} \right] \dot{\phi}$$

$$+ \frac{K_g K_f}{T_7} \phi + \left[ \frac{K_f T_6 (R + K_{IF} G)}{T_7 (L_L + L_m)} - \frac{K_f}{T_7} \right] I_1 + \frac{K_g K_f}{T_7} z_{t1} - \frac{K_f T_6 G}{T_7 (L_L + L_m)} V_{D1}$$

$$12) \quad \dot{V}_{D2} = \left[ \frac{K_f T_6 L_m}{T_7 (L_L + L_m)} - \frac{K_g K_f T_6}{T_7} \right] \dot{z} - \frac{K_g K_f}{T_7} z - \left[ \frac{K_g K_f T_6}{T_7} - \frac{K_f T_6 L_m}{T_7 (L_m + L_L)} \right] \dot{\phi}$$

$$- \frac{K_g K_f}{T_7} \phi + \left[ \frac{K_f T_6 (R + K_{IF} G)}{T_7 (L_L + L_m)} - \frac{K_f}{T_7} \right] I_2 + \frac{K_g K_f}{T_7} z_{t2} - \frac{K_f T_6 G}{T_7 (L_m + L_L)} V_{D2}$$

B Matrix

11)  $V_{D1} = \frac{u_1}{T_7}$

12)  $V_{D2} = \frac{u_2}{T_7}$

E Matrix

9)  $\dot{z}_{t1} = \dot{z}_{t1}$     10)  $\dot{z}_{t2} = \dot{z}_{t2}$     11)  $\dot{V}_{D1} = \frac{K_g K_f T_6}{T_7} \left( 1 - \left( \frac{L_m}{L_m + L_L} \right) \right) \dot{z}_{t1}$

12)  $\dot{V}_{D2} = \frac{K_g K_f T_6}{T_7} \left( 1 - \left( \frac{L_m}{L_m + L_L} \right) \right) \dot{z}_{t2}$

$$7) \quad \dot{I}_1 = \frac{L_m K}{(L_m + L_L)} \dot{Z}_{t1} \quad 8) \quad \dot{I}_2 = \frac{L_m K}{(L_m + L_L)} \dot{Z}_{t2}$$

### Measured Variables

#### C<sub>M</sub> Matrix

1) Z    2) Z    3) ϕ    4) ϕ    5) Z<sub>1</sub>    6) Z<sub>2</sub>    7) I<sub>1</sub>    8) I<sub>2</sub>

9) Z<sub>t1</sub>    10) Z<sub>t2</sub>

### Controller Equations

#### A<sub>R</sub> Matrix

$$1) \quad \epsilon_b = -\frac{T_{3b}}{T_{4b}} \epsilon_b - \frac{\epsilon_b}{T_{4b}} + \left[ \frac{G_b T_{1b}}{T_{4b}} - \frac{2 G_b T_{2b} \omega_b}{T_{4b}} \right] \epsilon_{db} + \left[ \frac{G_b}{T_{4b}} - \frac{G_b T_{2b} \omega_b^2}{T_{4b}} \right] \epsilon_{db}$$

$$2) \quad \epsilon_b = \epsilon_b$$

$$3) \quad \epsilon_p = -\frac{T_{3p}}{T_{4p}} \epsilon_p - \frac{\epsilon_p}{T_{4p}} + \left[ \frac{G_p T_{1p}}{T_{4p}} - \frac{2 G_p T_{2p} \omega_p}{T_{4p}} \right] \epsilon_{dp} + \left[ \frac{G_p}{T_{4p}} - \frac{G_p T_{2p} \omega_p^2}{T_{4p}} \right] \epsilon_{dp}$$

$$4) \quad \epsilon_p = \epsilon_p$$

$$5) \quad \epsilon_{db} = -2 \omega_b \epsilon_{db} - \omega_b^2 \epsilon_{db}$$

$$6) \quad \epsilon_{db} = \epsilon_{db}$$

$$7) \quad \epsilon_{dp} = -2 \omega_p \epsilon_{dp} - \omega_p^2 \epsilon_{dp}$$

$$8) \quad \epsilon_{dp} = \epsilon_{dp}$$

B<sub>R</sub> Matrix

$$\begin{aligned}
 1) \quad \ddot{\varepsilon}_b = & \left[ \frac{2G_b T_{2b} (K_a - K_g K_I)}{T_{4b} M} - \frac{G_b}{T_{4b}} \right] Z - \frac{G_b T_{1b}}{T_{4b}} \dot{Z} + \frac{G_b T_{2b} K_s}{T_{4b} M} Z^1 \\
 & + \frac{G_b T_{2b} K_s}{T_{4b} M} Z_2 - \frac{G_b T_{2b} K_I}{T_{4b} M} I_1 - \frac{G_b T_{2b} K_I}{T_{4b} M} I_2 \\
 & - \frac{G_b T_{2b}}{T_{4b}} \left( \frac{K_a + K_s - K_g K_I}{M} - \frac{\omega_b^2}{2} \right) Z_{t1} - \frac{G_b T_{2b}}{T_{4b}} \left( \frac{K_a + K_s - K_g K_I}{M} \right) \\
 & - \frac{\omega_b^2}{2} Z_{t2}
 \end{aligned}$$

$$\begin{aligned}
 3) \quad \ddot{\varepsilon}_p = & \left[ \frac{2G_p T_{2p} (K_a - K_g K_I)}{T_{4p} I} - \frac{G_p}{T_{4p}} \right] \phi - \frac{G_p T_{1p}}{T_{4p}} \dot{\phi} - \frac{G_p T_{2p} K_s}{T_{4p} I} Z^1 \\
 & + \frac{G_p T_{2p} K_s}{T_{4p} I} Z_2 + \frac{G_p T_{2p} K_I}{T_{4p} I} I_1 - \frac{G_p T_{2p} K_I}{T_{4p} I} I_2 \\
 & + \frac{G_p T_{2p}}{T_{4p}} \left( \frac{K_a + K_s - K_g K_I}{I} - \frac{\omega_p^2}{2} \right) Z_{t1} - \frac{G_p T_{2p}}{T_{4p}} \left( \frac{K_a + K_s - K_g K_I}{I} \right) \\
 & - \frac{\omega_p^2}{2} Z_{t2}
 \end{aligned}$$

$$5) \quad \ddot{\varepsilon}_{db} = \frac{\omega_b^2}{2} Z_{t1} + \frac{\omega_b^2}{2} Z_{t2}$$

$$7) \quad \ddot{\varepsilon}_{dp} = -\frac{\omega_p^2}{21} Z_{t1} + \frac{\omega_p^2}{21} Z_{t2}$$

Control Signals C<sub>R</sub> Matrix

$$1) \quad u_1 = T_6 \dot{\varepsilon}_b + \varepsilon_b - T_6 \dot{\varepsilon}_p - \varepsilon_p$$

$$2) \quad u_2 = T_6 \dot{\varepsilon}_b + \varepsilon_b + T_6 \dot{\varepsilon}_p + \varepsilon_p$$

### Controller Equations With Free Variables

#### A<sub>R</sub> Matrix

$$1) \quad \ddot{\epsilon}_b = -1.4 \sqrt{T_b} \epsilon_b - T_b \epsilon_b + \left[ \sqrt{\frac{T_b GB}{100}} - \frac{\omega_B GB}{45} \right] \epsilon_{db} \\ + \left[ \frac{GB T_b}{450} - \frac{GB \omega_{2B}}{45} \right] \epsilon_{db}$$

$$2) \quad \dot{\epsilon}_b = \dot{\epsilon}_b$$

$$3) \quad \ddot{\epsilon}_p = -1.4 \sqrt{T_p} \epsilon_p - T_p \epsilon_p + \left[ \sqrt{\frac{T_p GP}{22.4}} - \frac{\omega_p GP}{10} \right] \epsilon_{dp} \\ + \left[ \frac{GP T_p}{100} - \frac{GP \omega_{2P}}{10} \right] \epsilon_{dp}$$

$$4) \quad \dot{\epsilon}_p = \dot{\epsilon}_p$$

$$5) \quad \ddot{\epsilon}_{db} = -\omega_B \epsilon_{db} - \omega_{2B} \epsilon_{db}$$

$$6) \quad \dot{\epsilon}_{db} = \dot{\epsilon}_{db}$$

$$7) \quad \ddot{\epsilon}_{dp} = -\omega_p \epsilon_{dp} - \omega_{2P} \epsilon_{dp}$$

$$8) \quad \dot{\epsilon}_{dp} = \dot{\epsilon}_{dp}$$

#### B<sub>R</sub> Matrix

$$1) \quad \ddot{\epsilon}_b = -\sqrt{\frac{T_b GB}{100}} Z + \left[ \frac{GB}{1.624} - \frac{GB T_b}{450} \right] Z + GB Z_1^1 \\ + GB Z_2 - \frac{GB}{3900} I_1 - \frac{GB}{3900} I_2 - \frac{GB}{90} \left[ 1.3 - \frac{\omega_{2B}}{90} \right] Z_{t1} \\ - G_B \left[ 1.3 - \frac{\omega_{2B}}{90} \right] Z_{t2}$$

B<sub>R</sub> Matrix (Cont'd)

$$3) \quad \epsilon_p = - \sqrt{\frac{T_p GP}{22}} + [5Gp - \frac{GPT_p}{100}]Z - GPZ_1^1$$

$$+ GPZ_2^1 + \frac{GP I_1}{3900} - \frac{GP I_2}{3900} + GP [1.3 - \frac{\omega_{2P}}{160}] Z_{t1}$$

$$- GP [1.3 - \frac{\omega_{2P}}{160}] Z_{t2}$$

$$5) \quad \epsilon_{db} = \frac{\omega_{2B}}{2} Z_{t1} + \frac{\omega_{2B}}{2} Z_{t2}$$

$$7) \quad \epsilon_{dp} = - \frac{\omega_{2P}}{16} Z_{t1} + \frac{\omega_{2P}}{16} Z_{t2}$$

Free Variables

$$\text{Set } T_{4b} = 1/T_b$$

$$\text{Then } T_{1b} = \frac{4.47}{T_b} \quad T_{2b} = \frac{10}{T_b} \quad T_{3b} = \frac{1.4}{T_b}$$

$$\text{and } T_{4p} = 1/T_p$$

$$\text{Then } T_{1p} = \frac{4.47}{T_p} \quad T_{2p} = \frac{10}{T_p} \quad T_{3p} = \frac{1.4}{T_p}$$

$$GB = \frac{10 K_s}{M} G_b = 446$$

$$GP = \frac{10 K_s}{I} G_p = 100 G_p$$

$$\begin{aligned}\omega_B &= 2 \omega_b \\ \omega_{2B} &= \omega_b^2 \\ \omega_P &= 2 \omega_p \\ \omega_{2P} &= \omega_p^2\end{aligned}$$

Starting Values

$$\begin{aligned}T_b &= 3333 \\ T_p &= 3333 \\ GB &= .56E6 \\ GP &= .52E6 \\ \omega_{2B} &= 39 \\ \omega_{2P} &= 39 \\ \omega_B &= 8.7 \\ \omega_P &= 8.7\end{aligned}$$

Design Values

M	26 000 kg
I	927 500 kgm <sup>2</sup>
K <sub>S</sub>	1.16 MN/m
K <sub>r</sub>	.488 MN/m
K <sub>a</sub>	.42 MN/m
KgK <sub>I</sub>	60 kN/m
K <sub>I</sub>	300 N/Amp
l	8 m
C <sub>s</sub>	100 kNs/m
L <sub>L</sub>	.1 H
L <sub>M</sub>	15 H
R	2.25 Ω
G	30 V/V
K <sub>f</sub>	.2 V/Amp
K <sub>IF</sub>	.2 V/Amp
T <sub>6</sub>	.0125 s
T <sub>7</sub>	.005 s

$T_{1b}=T_{1p} =$	.077 s
$T_{2b}=T_{2p} =$	.003 s <sup>2</sup>
$T_{3b}=T_{3p} =$	.025 s
$T_{4b}=T_{4p} =$	.0003 s <sup>2</sup>
$G_b$	1250
$G_p$	5250
$2 \omega_b$	8.7
$\omega_b^2$	39
$2 \omega_p$	8.7
$\omega_p^2$	39

Non-Zero Elements of A Matrix

$A(1,2) = -27.7$	$A(1,5) = -44.6$	$A(1,6) = -44.6$
$A(1,7) = .0115$	$A(1,8) = .0115$	$A(1,9) = 58.5$
$A(1,10) = 58.5$	$A(2,1) = 1.0$	$A(3,4) = -49.7$
$A(3,5) = 10.0$	$A(3,6) = -10.0$	$A(3,7) = -2.6E-3$
$A(3,8) = 2.6 E-3$	$A(3,9) = -13.1$	$A(3,10) = 13.1$
$A(4,3) = 1.0$	$A(5,1) = 1.0$	$A(5,2) = 4.88$
$A(5,3) = -8$	$A(5,4) = -39.0$	$A(5,5) = -16.5$
$A(5,9) = 11.6$	$A(6,1) = 1.0$	$A(6,2) = 4.88$
$A(6,3) = 8$	$A(6,4) = 39.0$	$A(6,6) = -16.5$
$A(6,10) = 11.6$	$A(7,1) = -120$	$A(7,3) = 960$
$A(7,7) = -33$	$A(7,11) = 120$	$A(8,1) = -120$
$A(8,3) = -960$	$A(8,8) = -33$	$A(8,12) = 120$
$A(9,9) = -1$	$A(10,10) = -1$	$A(11,1) = -40$
$A(11,2) = -8000$	$A(11,3) = 320$	$A(11,4) = 64000$
$A(11,7) = -23.5$	$A(11,9) = 8000$	$A(11,11) = -60$
$A(12,1) = -40$	$A(12,2) = -8000$	$A(12,3) = -320$
$A(12,4) = -64000$	$A(12,8) = -23.5$	$A(12,10) = 8000$
$A(12,12) = -60$		

Non-Zero Elements of B Matrix

$$B(11,1) = 200 \quad B(12,1) = 200$$

Non-Zero Elements of E Matrix

$$E(9,1) = 1.0 \quad E(10,2) = 1.0 \quad E(11,1) = 40 \quad E(12,2) = 40$$

$$E(7,1) = 120 \quad E(8,2) = 120$$

Non-Zero Elements of C<sub>M</sub> Matrix

$$C_M(1,1) = 1 \quad C_M(2,2) = 1 \quad C_M(3,3) = 1 \quad C_M(4,4) = 1$$

$$C_M(5,5) = 1 \quad C_M(6,6) = 1 \quad C_M(7,7) = 1 \quad C_M(8,8) = 1$$

$$C_M(9,9) = 1 \quad C_M(10,10) = 1$$

Non-Zero Elements of A<sub>R</sub> Matrix

$$A_R(1,1) = -83.3 \quad A_R(1,2) = -3333.$$

$$A_R(1,5) = .212E6 \quad A_R(1,6) = 3.68E6$$

$$A_R(2,1) = 1.0 \quad A_R(3,3) = -83.3$$

$$A_R(3,4) = -3333. \quad A_R(3,7) = .89E6$$

$$A_R(3,8) = 15.5E6 \quad A_R(4,3) = 1.0$$

$$A_R(5,5) = -8.7 \quad A_R(5,6) = -39.0$$

$$A_R(6,5) = 1.0 \quad A_R(7,7) = -8.7$$

$$A_R(7,8) = -39.0 \quad A_R(8,7) = 1.0$$

Non-Zero Elements of B<sub>R</sub> Matrix

$$B_R(1,1) = -.32E6 \quad B_R(1,2) = -3.82E6$$

$$B_R(1,5) = .55E6 \quad B_R(1,6) = .55E6$$

$$B_R(1,7) = -144 \quad B_R(1,8) = -144.$$

$$B_R(1,9) = -.488E6 \quad B_R(1,10) = -.488E6$$

$$B_R(3,3) = -1.35E6 \quad B_R(3,4) = -14.9E6$$

$$B_R(3,5) = -.53E6 \quad B_R(3,6) = .53E6$$

$$B_R(3,7) = 135.75 \quad B_R(3,8) = -135.75$$



$$B_R(3,9) = .56E6$$

$$B_R(5,9) = 19.5$$

$$B_R(7,9) = -2.44$$

$$B_R(3,10) = -.56E6$$

$$B_R(5,10) = 19.5$$

$$B_R(7,10) = 2.44$$

C<sub>R</sub> Matrix

$$C_R(1,1) = .0125$$

$$C_R(1,3) = -.0125$$

$$C_R(2,1) = .0125$$

$$C_R(2,3) = .0125$$

$$C_R(1,2) = 1.0$$

$$C_R(1,4) = -1.0$$

$$C_R(2,2) = 1.0$$

$$C_R(2,4) = 1.0$$

